UNIVERSITÄT
DUISBURG
ESSEN

Neutrophil biology in Chronic Lymphocytic Leukaemia and infections

Inaugural - Dissertation

zur

Erlangung des Doktorgrades

Dr. rer. nat.

der Fakultät für

Biologie

an der

Universität Duisburg - Essen

vorgelegt von

Nirojah Vijitha

aus Ibbenbüren

Dezember 2018

Die der vorliegenden Arbeit zu Grunde liegenden Experimente wurden am Institut für Experimentelle Immunologie und Bildgebung der Universität Duisburg-Essen von Januar 2015 bis Dezember 2018 durchgeführt.

DOI: 10.17185/duepublico/70048
URN: urn:nbn:de:hbz:464-20210421-091305-8

1. Gutachter: Prof. Dr. rer. nat. Daniel Robert Engel
2. Gutachterin: Prof. Dr. rer. nat. Wiebke Hansen

Vorsitzender des Prüfungsausschusses: Prof. Dr. rer. nat. Ralf Küppers

Tag der mündlichen Prüfung: 12.03.2019

The work described in this thesis was started in January 2015 and completed in December 2018 under the supervision of Prof. Dr. rer. nat. Daniel Robert Engel at the Institute of Experimental Immunology and Imaging of the University Duisburg-Essen.

For அம்மா and அப்பா.

Table of content

1. List of abbreviations

° C	Degree Celsius
3D	Three-dimensional
AF	Alexa Fluor
ANOVA	Analysis of variance
APC	Allophycocyanin (fluorochrome)
APC	Antigen-presenting cell
APC-Cy7	Allophycocyanin conjugated to Cyanine 7 dye
APRIL	A proliferation-inducing ligand
AT	Adoptive transfer
ATM	Ataxia telangiectasia-mutated gene
BAFF	B-cell activating factor
BCL2	B-cell lymphoma 2
BCR	B-cell receptor
BM	Bone marrow
BMSC	Bone marrow-derived stromal cell
BSA	Bovine serum albumin
BV	Brilliant™ Violet
C3b	Complement component 3 b
C57BL/6	Inbred mouse laboratory strain
C5a	Complement component 5 a
CD	Cluster of differentiation
Cdc42	Cell division control protein 42 homolog
CGD	Chronic granulomatous disease
CLL	Chronic lymphocytic leukaemia
CO_2	Carbon dioxide
COX2	Cyclooxygenase 2
CXCL1/2	C-X-C motif chemokine 1/2
CXCR2/4	C-X-C chemokine receptor type 2/4
DAMP	Damage-associated molecular pattern
DAPI	4’,6-Diamidin-2-phenylindol
dl	decilitre
DMSO	Dimethyl sulfoxide
DNA	Deoxyribonucleic acid
dpi	Days post-infection
DUOX1	Dual oxidase 1
EDTA	Ethylenediaminetetraacetic acid
ELISA	Enzyme linked-immunosorbent assay
EpCAM	Epithelial cell adhesion molecule
Erk	Extracellular-signal regulated kinase

FACS	Fluorescence-activated cell sorting
FCS	Foetal calf serum
Fgr	Gardner-Rasheed feline sarcoma viral (v-fgr) oncogene homolog
FITC	Fluorescein isothiocyanate
fMLP	N-Formylmethionyl-leucyl-phenylalanine
FPR	Formyl peptide receptor
FSC	Forward scatter
g	Gram
G	Gauge (syringe needle)
G	G-force (centrifugation)
G-CSF	Granulocyte-colony stimulating factor
G/EBP	CCAAT/enhancer-binding protein
GC	Germinal centre
GDF15	Growth/differentiation factor 15
Gfi-1	Growth factor independent 1 transcription factor
GFP	Green fluorescent protein
GO	Gene ontology
GPCR	G protein-coupled receptor
GTPase	Guanosine triphosphatase
h	hour(s)
H3	Histone 3
Hb	Haemoglobin
Hck	Haematopoietic cell kinase
hIgG	Human immunoglobulin G
Hpi	Hours post-infection
HSC	Haematopoietic stem cell
i.p.	Intraperitoneal
i.v.	Intravenous
ICAM	Intercellular Adhesion Molecule 1
IGHV	Immunoglobulin heavy chain variable region
IHC	immunohistochemistry
IL	Interleukin
IL-8	Interleukin-8
IP_3	Inositol trisphosphate
IVC	Individually ventilated cage
JAM-A	Junctional Adhesion Molecule A
l	Litre
LANUV	Landesamt für Natur, Umwelt und Verbraucherschutz (State Agency for Nature, Environment and Consumer Protection)
LB medium	Lysogeny broth medium
LC-ESI-MS/MS	Liquid chromatography coupled to tandem mass spectrometry via

	electrospray ionization
LDN	Low density neutrophils
LFA1	Lymphocyte function-associated antigen 1
LSP1	Lymphocyte-specific protein 1
Ly6C	lymphocyte antigen 6 complex, locus C1
Ly6G	Lymphocyte antigen 6 complex locus G6D
Lyn	Lck/Yes novel tyrosine kinase
M	Molar
Mac1	Macrophage-1 antigen
MACS	Magnetic activated cell sorting
MACS LS	MACS columns used for positive selection or depletion
MAPK	Mitogen-activated protein kinase
MBL	Monoclonal B-cell lymphocytosis
MEM	Minimal essential medium
MFI	Mean fluorescence intensity
Min	Minute(s)
ml	Millilitre
mM	Millimolar
MMP	Matrix metalloproteinase
MPO	Myeloperoxidase
MPP	Multipotent progenitors
MZ	Marginal zone
NADPH	Nicotinamide adenine dinucleotide phosphate oxidase
NDN	Normal density neutrophils
NET	Neutrophil extracellular trap(s)
NETosis	Process of neutrophils ejecting DNA into the extracellular space
ng	nanogram
NLC	Nurse-like cells
NLR	Nod-like receptor
nm	nanometre
nM	nanomolar
OCT	Optimal cutting temperature
PAD4	Peptidyl arginine deiminase type IV
PAMP	Pathogen-associated molecular pattern
PBS	Phosphate-buffered saline
PBT	Phosphate Buffered Saline and Tween 20
PDL1	Programmed cell death 1 ligand 1
PE	Phycoerythrin
PECAM1	Platelet endothelial cell adhesion molecule
PerCP-Cy5.5	Peridinin-chlorophyll-protein complex conjugated to Cy5.5 dye
PFA	Paraformaldehyde

pg	Picogram
pH	Power of hydrogen
pHrodo®	Bioparticles to track pH-dependent internalization in live cells
PI3K	Phosphoinositide 3-kinase
PIPKIγ661	phosphatidylinositol phosphate kinase isoform-gamma 661
PLCβ	Phospholipase C-β
PLP	Periodate-lysine-paraformaldehyde fixative
PMN	Polymorphonuclear leukocyte(s)
PRR	Pattern-recognition receptor
PSGL-1	P-selectin glycoprotein ligand-1
QIR	Quiescent intracellular reservoirs
Rac	Rho family of GTPases, including Cdc42 and RhoA
RCB	Red cell lysis buffer
RhoA	Ras homolog gene family, member A
RLT	RNA lysis buffer
RNA	Ribonucleic acid
ROS	Reactive oxygen species
rpm	Rounds per minute
RPMI	Roswell Park Memorial Institute
RT	Room temperature
s	Second(s)
SD	Standard deviation
SEM	Standard error of mean
SHM	Somatic hypermutation
SMAC	supramolecular activation cluster
SPF	Specific-pathogen-free zone in the animal facility
Src	Sarcoma tyrosine kinase
SSC	Sideward scatter
SSC	Sideward scatter
Syk	Spleen tyrosine kinase
t.u.	transurethral
TAM	Tumour-associated macrophages
TAN	Tumour-associated neutrophils
TCA	Trifluoroacetic acid
TCL1	T-cell leukaemia protein 1
TGF-ß	Transforming growth factor- ß
TGF-ßRI	Transforming growth factor-ß receptor I
TLR	Toll-like receptor
TNF	Tumour necrosis factor
TP53	Tumour protein p53

UPEC	Uropathogenic *Escherichia coli*
UTI	Urinary tract infection
v/v %	Concentration in volume/volume percent
VLA4	Very late antigen 4
WASp	Wiskott–Aldrich Syndrome protein
WT	Wildtype
YOYO-1™	Tetracationic homodimer of Oxazole Yellow
ZAP70	ζ-chain associated protein kinase 70

2. Index of figures

3. Index of tables

4. Summary

Bacterial infections are the leading cause of morbidity and mortality in patients suffering from Chronic Lymphocytic Leukaemia (CLL). CLL is characterised by accumulation of malignant B-cells in the peripheral blood and neutrophils are crucial to fight off infections. However, the contribution of neutrophils during the antibacterial response in CLL has not been elucidated.

This study has employed a murine adoptive transfer model by intravenously injecting splenocytes from Eμ-TCL1 transgenic mice into syngeneic wildtype mice. We found CLL B-cells in lymphoid as well as non-lymphoid organs, such as the urinary bladder and the lung. Proteome and flow cytometric analysis of neutrophils from CLL mice showed a rather mature and activated phenotype through enhanced frequencies of $CD11b^+$, $CXCR2^+$ and $ICAM1^+$ and decreased frequencies of $CXCR4^+$ and $CD62L^+$. Such aberrant neutrophil phenotype coincided with a severe urinary tract infection (UTI) after inoculating uropathogenic *E.coli* (UPEC). Also in this murine infection model, neutrophils showed an activated and functionally altered neutrophil phenotype in CLL. The phenotype of neutrophils showed enhanced TGF-βRI, CD62L, cKit and CXCR4 frequencies and was immunosuppressed and immature at the site of infection. Moreover, the phagocytic function of neutrophils was diminished during CLL and MPO levels declined in neutrophils of CLL mice. Additionally, neutrophil numbers during UTI inversely correlated with bacterial burden in CLL indicating a recruitment defect. However, migratory defects in neutrophils from CLL were not found in a 3D-*in vitro* migration assay. Finally, phenotypical characterization of neutrophils from untreated CLL patients confirmed the murine findings by showing decreased frequencies of $CD10^+$, $CXCR4^+$ and $CD62L^+$ and increased frequencies of $ICAM1^+$ and $PDL1^+$.

In conclusion, this study provides comprehensive evidence on the functional alterations in the phenotype of neutrophils as well as modulation of the antibacterial response by neutrophils in CLL. Restoration of neutrophil function in CLL might serve as a therapeutic intervention to reduce infection-related morbidity and mortality in CLL patients. Future experiments are required to identify neutrophil-specific targets to improve the antibacterial response during CLL.

Conclusively, these data suggest that neutrophils are functionally aberrant in mice and humans. This study also reveals increased expression of TGF-β and TGF-βRI molecules on neutrophils indicating a potential mechanism for impaired functionality

of neutrophils in CLL. Finally, translational data confirmed the aberrant neutrophil phenotype in human subjects suggesting that therapeutic restoration of the canonical phenotype and function in CLL patients might reduce the risk of severe infections and mortality during CLL.

5. Zusammenfassung

In Patienten mit chronisch lymphatischer Leukämie (CLL) sind bakterielle Infektionen im klinischen Alltag die Hauptursache für Komplikationen und Todesfälle. Charakteristisch für CLL ist die klonale Expansion bösartiger B-Zellen im Knochenmark und ihre Akkumulation in der Zirkulation. Neutrophile Granulozyten sind zentrale Effektorzellen in der Bekämpfung von Infektionen, dennoch wurde ihre Beteiligung an der erhöhten Infektionslast bei CLL-Patienten nicht erforscht.

Die vorliegende Studie hat ein murines adaptives Transfermodell verwendet, bei dem Splenozyten aus Eμ-TCL1 Mäusen intravenös in syngene Kontroll-Mäuse appliziert wurden. CLL B-Zellen konnten sowohl in den lymphoiden wie auch in nicht-lymphoiden Organen, wie der Harnblase und der Lunge, gefunden werden. Proteomische und durchflusszytometrische Analysen haben gezeigt, dass CLL Neutrophile im Vergleich zu Wildtyp Neutrophilen einen reiferen und aktivierteren Phänotypen anhand der höheren Anteile von $CD11b^+$, $CXCR2^+$ und $ICAM^+$ Zellen und der verminderten Anteile von $CXCR4^+$ und $CD62L^+$ Zellen aufweisen. Dieser ungewöhnliche Phänotyp ging einher mit einer starken Blaseninfektion, induziert durch die Inokulation uropathogener *E.coli* (UPEC). Dieses Infektionsmodell konnte den aktivierteren Phänotyp der Neutrophilen reproduzieren und zusätzlich eine geringere Funktionalität der Neutrophilen in CLL-Bedingungen zeigen. Phänotypisch gab es höhere Anteile von $TGF\text{-}\beta RI^+$, $CD62L^+$, $cKit^+$ und $CXCR4^+$ Neutrophilen, die am Infektionsherd einen immunsupprimierteren und unreiferen Phänotypen zeigen. Des Weiteren war die Phagozytose Leistung und die MPO Produktion der Neutrophilen in CLL reduziert. Die negative Korrelation der Neutrophilenanzahl mit der Bakterienlast im Harnwegsinfektionsmodell, weist auf einen Rekrutierungsdefekt in der CLL hin. In einem 3D-*in vitro* Migration Assay konnte jedoch gezeigt werden, dass die Migration der CLL Neutrophilen nicht verändert war.

Die phänotypische Charakterisierung von humanen CLL-Neutrophilen konnte den bisherigen Phänotypen aus der murinen Studie anhand der verringerten Anteile von $CD10^+$, $CXCR4^+$ und $CD62L^+$ und der erhöhten Anteile von $ICAM^+$ und PDL^+ bestätigen.

Zusammenfassend ergibt diese Studie, das sowohl murine wie auch humane Neutrophile in CLL funktional von gesunden Neutrophilen abweichen. Darüber hinaus verweist die erhöhte Expression von TGF-β und TGF-βRI auf Neutrophilen, auf einen möglichen Mechanismus, welcher die verminderte Funktionalität der

Neutrophilen in CLL vermittelt. Diese translationalen Daten, aus dem klinischen Alltag, und der Grundlagenforschung an Mäusen, bestätigen den abweichenden Phänotyp der Neutrophilen ebenfalls in der humanen CLL Situation und identifizieren die medikamentöse Restoration des normalen Phänotypen als potentielles therapeutisches Target, um schwerwiegende Infektionen und die damit einhergehende erhöhte Sterberate in CLL-Patienten zu vermindern.

6. Aims of this study

This study concentrates on the neutrophil function in bacterial infections during CLL. In CLL, more than 75% of patients are affected by infections during the course of their disease progression [1, 2]. Notably, more than 50% of CLL patients develop and succumb to infections [3, 4]. According to our Comprehensive Cancer Centre at the University Hospital Essen, recurrent infections are the main reason for the referral to a clinic and often lead to the diagnosis of CLL. Most of these infections originate from bacterial pathogens, *Uropathogenic Escherichia coli* (UPEC) amongst others, and affect the urinary tract [5]. Using various infection models, neutrophils have been demonstrated to be the first responders of host defence. Hence, the plethora of antibacterial activities of neutrophils might be compromised during CLL causing an increased risk of infections. Thus, the rationale of this study is to identify whether and how the CLL microenvironment modulates neutrophil effector functions during urinary tract infections caused by UPEC.

7. Introduction

7.1. Neutrophil biology

7.1.1. The history of neutrophils and their physiological functions

Neutrophils have been depicted in the early research literature as one of many white blood cell types in the 19th century by Ehrlich using acid and basic dyes that allows labelling of granulocytes [6]. Initially, “polymorphous nucleus” was proposed to name this particular granulocyte subset based on the neutral staining property [7]. Up to this point, nothing was revealed about the cell’s functions. In 1893, Metchnikoff observed phagocyte recruitment as a response to injury in starfish embryo [6]. The newly described activity and the distinctly segmented nucleus in neutrophils led to a renaming and neutrophils were termed as polymorphonuclear leukocytes (PMN), a name that is still synonymous for neutrophils.

Neutrophils constitute the largest white blood cell population in the peripheral blood (PB). In detail, neutrophils account for 20-30% in mice and 50-70% of all white blood cells in human circulation [8, 9]. These cells play a significant role during the onset of antimicrobial immune responses by being among the first effector cells at the site of infection [10]. Consequently, neutropenic patients are at a high risk for severe and life-threatening infections [11]. Neutrophils fight invaded pathogens directly as well as

initiate further steps of the immune response and orchestrate inflammation by secreting cytokines [12]. Their migratory capacity and granular content are vital during antimicrobial killing and have extensively been studied [11]. NETosis, the ability of neutrophils to eject their DNA to trap microorganisms, has been identified as an additional, distinct and novel neutrophil activity only 15 years ago [13, 14]. These functions highlight the essential range of functionality and complexity of these cells to protect the host from any invaders. The release of neutrophils into the circulation, migration, antimicrobial killing, NETosis and their impact on B-lymphocyte maturation will be described in more detail in sections 7.1.3 to 7.1.7.

As widely stated in the literature, neutrophils are reported to have a short half-life unless their life span extends upon recruitment to the site of infection and do not remain alive in culture for more than a couple of hours [15]. Notably, the exact *in vivo* lifespan of neutrophils has not been clearly elucidated. The textbook knowledge defines a timespan of few hours while new reports range from hours to several days [7, 12, 16, 17]. Since some studies allowed neutrophil tracing upon *ex vivo* labelling, concerns were raised as to whether this approach aptly reflects the *in vivo* situation [16, 18]. In another experiment, neutrophils were observed to remain in the murine circulation for more than 12 hours during homeostatic conditions [16]. The lifespan of human neutrophils is still uncertain due to unspecific labelling, however, there is a consensus that circulating neutrophils may survive for days [19, 20]. In spite of these uncertainties, it is widely accepted that these leukocytes have a prolonged lifespan upon activation via inflammation [15, 21, 22]. With respect to proliferation, another study and our own observations suggest that neutrophils do have a proliferative capacity post-stimulation via PAMPs in other tissues than the bone marrow, supporting the notion of neutrophil longevity in infected tissues [23]. On one hand, neutrophils might have more time to perform their effector functions and properly induce adaptive immunity, on the other hand continuous presence of neutrophils might contribute to host tissue damage [24].

7.1.2. The development of neutrophils

The development of erythrocytes and vascular systems occurs early during embryogenesis shortly after 3 weeks of human gestation [25, 26]. Initially, the foetal liver is the site for haematopoiesis around 6 weeks of gestation. Subsequently the bone marrow becomes the major site of haematopoiesis in all vertebrates but fish

[27]. Then the bone marrow takes over as the major production site. Neutrophils originate from haematopoietic stem cells (HSC). Retention within the bone marrow is accomplished through stem cell factor 1 (SCF1) and stromal-derived factor 1 (SDF1) or CXCL12 that bind to c-Kit and CXCR4, respectively [24, 28, 29]. In addition, CXCL1 and CXCL2 are being constitutively produced by osteoblasts and endothelial cells in the bone marrow for CXCR2, which in turn is responsible for the egress [11]. Only a few HSC proliferate in the bone marrow and induce myelopoiesis on a large scale [30]. First, HSC differentiate into multipotent progenitors (MPP) inducing the development of different hematopoietic lineages (Figure 1).

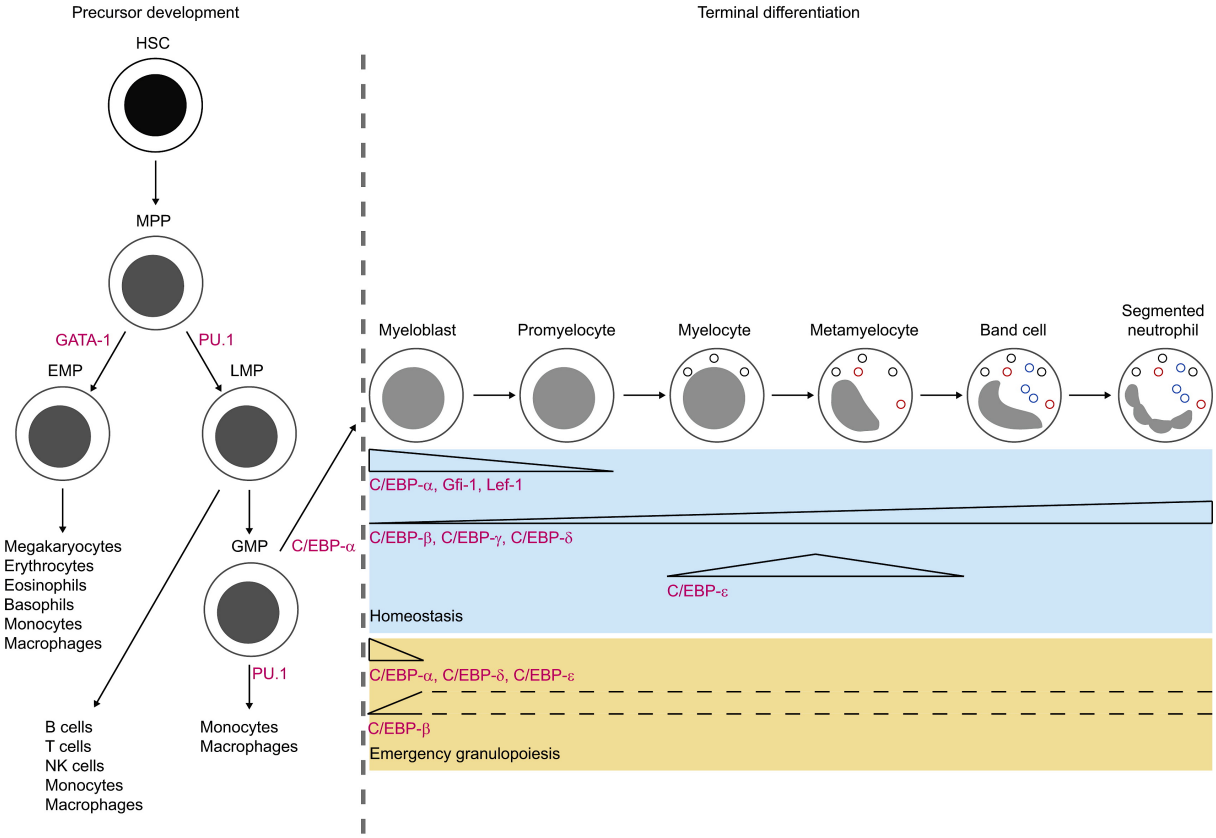

Figure 1. The development of neutrophils from HSC.

Neutrophils are terminally differentiated cells developing from HSC in the bone marrow. This figure depicts progenitors and essential transcription factors (pink) leading to the production of segmented polymorphonuclear leukocytes. HSC give rise to multipotent precursors (MPP) which in turn enable the development of erythromyeloid (EMP) and lymphomyeloid lineage (LMP). LMP develop into granulocyte-macrophage precursors (GMP). The expression of PU.1 leads to monocyte and macrophage development, whereas the expression of C/EBP-α is responsible for the neutrophil commitment. Myeloblasts are the first cells to emerge during terminal differentiation. The gradual disappearance of C/EBP-α, Gfi-1 and Lef-1 occurs during the granulopoiesis, Simultaneously, the expression of other C/EBPs take over. Myeloblasts give rise to promyelocytes and myelocytes. The production of granular proteins begins. Subsequently, metamyelocytes and band cells are formed. Finally, the characteristic segmented nucleus is formed, and the terminal differentiation is completed. The figure has been adapted from [30].

The current notion is that MPP give rise to lymphomyeloid and erythromyeloid precursors [31]. Whether one or the other lineage will be chosen, depends on the ratio of the antagonistic transcription factors GATA-1 and PU.1 [30, 32]. Neutrophils develop from the lymphomyeloid lineage and depend mainly on the PU.1 expression [33]. Subsequently, the commitment of lymphomyeloid precursors to develop into granulocyte/monocyte progenitors (GMP) depends on the C/EBP-α, Gfi-1 and Lef-1 coordinating the differentiation into neutrophil precursors [30]. More than 60% of the haematopoiesis gives rise to monocytes and granulocytes [34]. The turnover rate of neutrophils can be specifically increased during infections through granulocyte colony stimulating factor (G-CSF), but neutrophil production does not solely depend on G-CSF secretion. This underlines the ultimate necessity of these cells for the host defence [35].

Declining levels of G/EBP-α and Gfi-1 and increasing levels of G/EBP-β, -γ and -δ enable the development of neutrophil progenitors initially into myeloblasts, but the transcription factors will be expressed until the terminal differentiation (Figure 1). Up to this point, neutrophil progenitor cells do not contain granules. Later, these cells differentiate into promyelocytes. Next, myelocytes are formed, give rise to metamyelocytes initially, then into segmented band cells before terminally differentiating into neutrophils [30, 34]. Only during the short span of myelocyte and metamyelocyte stage, G/EBP-ε, another transcription factor, starts appearing and expression slowly fades when differentiation continues [36, 37]. The transcription factors that are implicated during neutrophil development are different to the ones required for neutrophil recruitment. As illustrated in Figure 1, neutrophils mature by expressing granules that are required for their effector functions. Azurophilic granules start appearing in promyelocytes, while myelocytes and segmented band cells produce specific and gelatinase granules, respectively [7]. The remaining group of granules, secretory vesicles, are generated during the terminal differentiation of neutrophils [34, 38]. In fact, granular protein composition varies among neutrophils and highly depends on the gene expression profile which in turn is based on the biological stimuli during maturation [30, 39]. Neutrophilic granules are essential during fighting off *S. aureus, P. aeruginosa* and *Klebsiella pneumoniae*, as patients with a C/EBP-ε mutation suffer from neutrophil-specific granule deficiency [40]. At the same time, these insufficiencies are not only associated to neutrophils, as monocytes and macrophages are also affected [40]. Throughout the maturation process,

receptors mediating captivity in the bone marrow slowly fade on the neutrophil surface [15].

7.1.3. Release of neutrophils from the bone marrow into the circulation

Neutrophils have to transmigrate through endothelial vessels and reach the site of infection where pathogens have to be fought via various effector mechanisms [39, 41]. A recent study by Wang has described the entire life circle of neutrophils, starting with the release from the bone marrow, reaching the lung and spleen before homing back to the bone marrow during sterile injury [42]. For such migratory events, neutrophils have to exit the peripheral bloodstream and enter tissues and vice versa [41]. Neutrophil extravasation follows a multistep process and has been investigated extensively. The chemokine receptors, CXCR4 and CXCR2, both expressed on neutrophils antagonistically mediate retention and release from the bone marrow, respectively [43, 44]. As a result to inflammatory stimuli during sterile injury or infection, various chemokines may bind to their corresponding receptor on neutrophils, orchestrating the migration into the bloodstream through postcapillary blood vessels in the bone (Table 1) [11, 34, 45]. Additionally, PAMPs by pathogens, DAMPs by sterile injury, complement factors and/or proinflammatory cytokines, such as IL-1β, TNFα and IL-17, from resident immune cells have the potential to activate neutrophil recruitment [46, 47].

Table 1. Human and murine chemoattractants and corresponding receptor expression on neutrophils.

Chemoattractant			Receptor	
Chemokines				
Systematic	**Human**	**Murine**	**Human PMN**	**Murine PMN**
CXCL1	GROα	KC	CXCR2	CXCR2
CXCL2	GROβ	MIP-2	CXCR2	CXCR2
CXCL3	GROγ	n/a	CXCR2	n/a
CXCL5	ENA-78	LIX	CXCR2	CXCR2
CXCL6	GCP-2	n/a	CXCR1/CXCR2	n/a
CXCL7	NAP-2	NAP-2	CXCR1/CXCR2	CXCR2
CXCL8	IL-8	n/a	CXCR1/CXCR2	CXCR2
CCL3	MIP-1α	MIP-1α	n/a	CCR1
CCL5	RANTES	RANTES	n/a	CCR1
CCL6	(MPIF-1)	C10	n/a	CCR1
CCL7	MCP-3	MARC	n/a	CCR1
CCL9	(HCC-2)	MIP-1γ	n/a	CCR1
CXCL12	SDF-1α	SDF-1α	CXCR4	CXCR4
Peptides/Cytokines				
C5a			C5aR	
C3a			C3aR	
Formylated peptides (e.g. fMLF)			FPR1	
Pro-Gly-Pro (PGP)			CXCR2	
LL37			FPR2	
MIF			CXCR2	
Eicosanoids				
Leukotriene B_4 (LTB_4)			BLT1	
Platelet activating factor (PAF)			PAFR	

Typically, the extravasation consists of five distinct patterns: tethering, rolling, adhesion, crawling and transmigration as illustrated in Figure 2 [23].

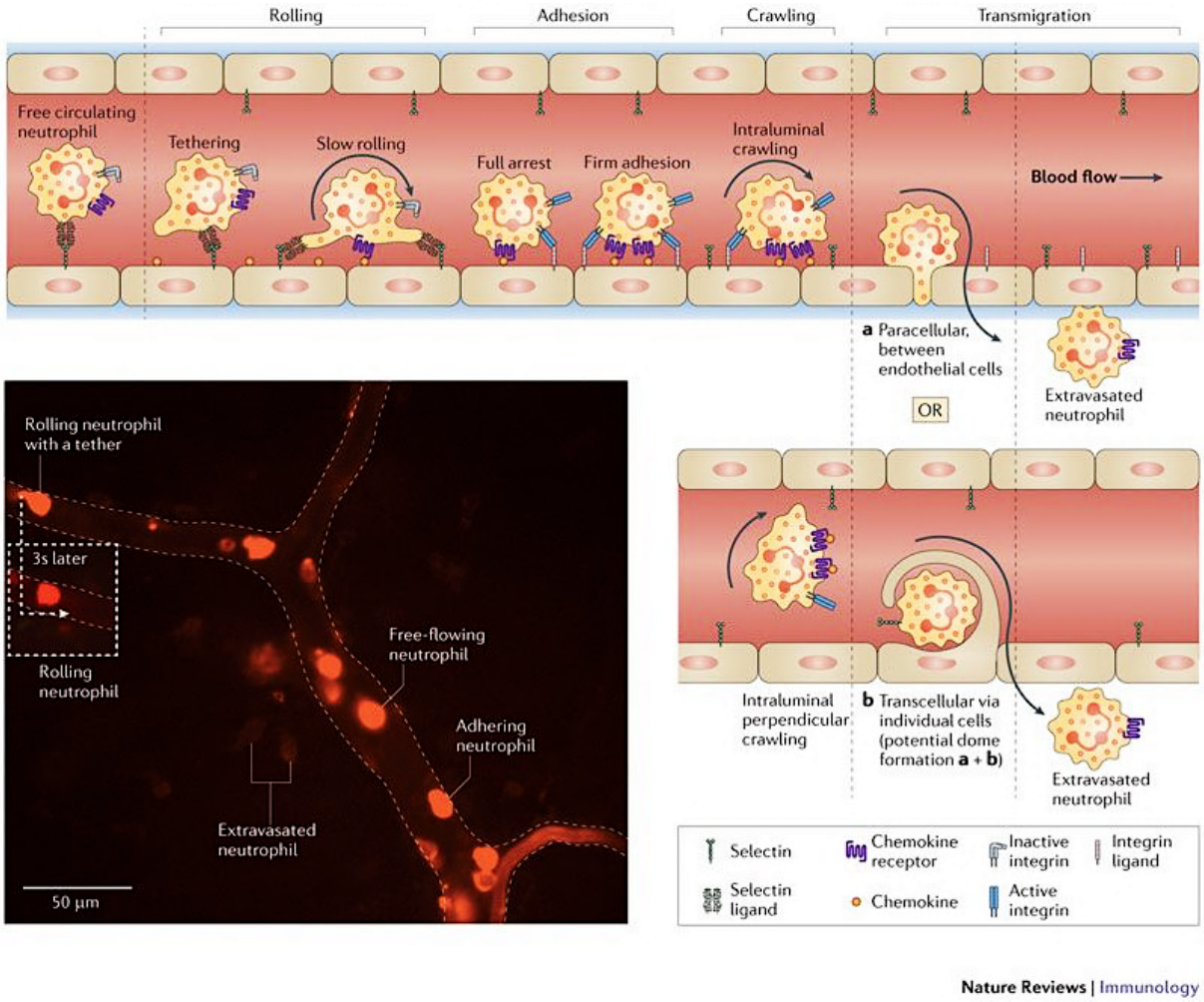

Figure 2. The neutrophil recruitment cascade.

The consecutive events during neutrophil recruitment from the vasculature are illustrated. Tethering, rolling, adhesion, crawling and transmigration are the specific steps during the recruitment cascade. Essential surface molecules involved in adhesion are listed in the box. In summary, the entire process depends on selectins and integrins. Chemokines on the luminal side of the endothelium stimulate neutrophils, leading to cytoskeleton changes required for the upcoming transmigration. Neutrophils follow the chemokine gradient along the endothelium to opt for an appropriate site for transmigration. Two hypotheses for transmigration are depicted: Neutrophils squeeze through endothelial cells (a) or enter the peripheral tissue by migrating through endothelial cells (b). The intravital image reveals a capillary venule with neutrophils labelled with PE 2 h post-infection of murine skin with S. aureus. Neutrophils have been captured at different points during the recruitment cascade. This figure has been adapted from [23].

In addition to the changes to neutrophil receptor expression, the endothelium surface is also altered in order to improve recognition of pathogens and proinflammatory stimuli, such as histamine, leukotrienes and cytokines from resident white blood cells when encountering a pathogen [48-50]. The luminal side of the endothelium upregulates the expression of P- and E-selectin within 2 hours of activation to bind P-selectin glycoprotein ligand 1 (PSGL1) and L-selectin on neutrophils [48, 51]. During

this process, the constitutive expression of these surface molecules on circulating neutrophils allows tethering to endothelial cells [50]. Following this, PSGL-1 and L-selectin (CD62L) set a kinase cascade in motion, in which Syk, PI3K and p38 MAPK convey the signal to initiate antimicrobial defence [48, 52, 53]. In particular, CD62L is an adhesion molecule on the surface of neutrophils, amongst other leukocytes, that binds to endothelial cell ligands and facilitates tethering and rolling, initiating the first step of the recruitment cascade [54]. The “rolling” of neutrophils induces integrin activation and leads to leukocyte attachment to the endothelium [7, 55]. The rotation of neutrophils along the endothelium takes place when the P-selectin-PSGL1 binding detaches at the rear and attaches at the front in the direction of circulatory movement [56, 57]. Notably, neutrophils perform selectin-mediated rolling by rapidly enhancing tethering to meet the increasing wall shear stress [56, 58].

Adhesion is mediated by chemokine signalling to CXCR2 through CXCL8 in humans and its corresponding murine chemokines, e.g. CXCL1, CXCL2 and CXCL5 [59]. Similarly, Duffy antigen receptor on venule endothelial cells stabilizes neutrophil adhesion through chemokines [60, 61]. On top of this, the activation of neutrophil GPCRs modulates the structure of integrins leading to a higher binding efficiency to immunoglobulin-like cell adhesion molecules (CAMs) [23]. Constitutively expressed β2-integrins, such as LFA-1 (α1β2; β2 integrin CD11a:CD18) and Mac-1 (αMβ2; CD11b:CD18), retain neutrophils at one spatial point [62]. While being attached, further activation of neutrophils by chemoattractants, cytokines, selectins and PAMPs leads to an increased expression and aggregation of intracellularly stored β2-integrins in neutrophils [7, 48]. Next, neutrophils crawl along the luminal side of the endothelium slightly detaching from their spot of firm adhesion before transmigration occurs [23]. Once neutrophils firmly adhere, ICAM1 and ICAM2 on the endothelium reinforce arrest which also holds true for neutrophil transmigration across the blood-brain barrier [7, 63]. This involves cytoskeleton rearrangements as neutrophils are required to adjust through the gaps along the endothelium preparing for cell motility mediated via integrin clustering [48, 64-66].

In fact, neutrophils preferably remain in the vasculature until they reach the centre of inflammation [67]. A specific site for extravasation will be chosen based on the intercellular junctions between endothelial cells, breach between pericytes and low matrix protein deposition [23, 68]. Neutrophil diapedesis consists of two distinct steps. The first process involves the transition of the endothelium for almost 5

minutes. This is followed by integrin-, ICAM1-, ICAM2-, VCAM1- mediated transversion. Crossing of the basement membrane also involves endothelial and epithelial adhesion molecules, such as PECAM1 and EpCAM, respectively, and neutrophil proteases, like MMP9, MMP2 or neutrophil elastase [69]. This highly organised crossing requires another 5 – 15 minutes [23, 48, 49]. The basement membrane is a matrix scaffold enriched by laminins and collagens, requiring active digestion and degranulation although no study has observed this process directly so far [7]. As already suggested in Figure 2, once neutrophils are firmly adhered, there are two transmigratory pathways: paracellular, the most preferred option for neutrophils or the time-consuming transcellular pathway. The paracellular path requires the dissociation of VE-cadherin, intercellular junctions, for endothelial cells to detach from each other and to facilitate transmigration [55]. In contrast, endothelial cells generate dome-like structures engulfing neutrophils during transcellular diapedesis [70, 71]. This process is enabled by the involvement of ICAM1 and VCAM1 on the dome-like structures and LFA1 and VLA4 enriched on arrested neutrophils [72]. The dome-formations require LSP1 for actin remodelling upon stimulation of the endothelium [73]. Full dome formations have not been verified *in vivo*, nevertheless, this process has been observed *in vitro* and is distinct from phagocytosis as there is no fusion of neutrophils into intracellular compartments of endothelial cells [71, 73-75].

There are also a few exceptions to the previously described extravasation which most probably arose due to the anatomical structure of the tissue. Neutrophil diapedesis has been visualised by intravital microscopy revealing more information (reviewed in [23]). Neutrophils in the liver sinusoidal capillaries do not follow the events during neutrophil extravasation as previously described [76, 77]. Depending on whether proinflammatory mediators are released in response to sterile injury or infection, neutrophils may attach to the endothelium via Mac1:ICAM1 bonds, while hyaluronan on endothelial cells may bind to CD44 on neutrophils without any contribution by integrins, respectively [78]. Interestingly, IL-10 mediates the integrin-independent hyaluronan:CD44 ligation during neutrophil adhesion in the inflamed liver, particularly during systemic infection [78, 79]. This observation might be restricted to neutrophil recruitment in the liver [78]. Similarly, neutrophils in the lung and brain seem to transmigrate differently which emphasizes the need to adjust to tissue requirements [23, 80]. However, it should be mentioned that the expression of

CD44 on neutrophil and their ligation to hyaluronan on endothelial cells regulate cell trafficking and modulate inflammatory responses during health and diseases. These ligations might result in inhibitory as well as activating effects during inflammation [81, 82].

7.1.4. From incoming signals to neutrophil polarization and migration

Neutrophil motility depends on the proper navigation through tissues and is coordinated by the pseudopod at the front and uropod as the tailing edge. Simultaneously, they have to integrate a complex cascade of activation, effector functions, extravasation, transmigration and chemotaxis. This is reflected in the 30 different receptors that regulates these processes, including pattern recognition receptors (PRR), F_c receptors, chemokine receptors and GPCRs [41]. GPCR, a seven transmembrane protein, responds to chemoattractants of various kinds, reactive oxygen species (ROS) and granules and are of high importance in regard to the early phase of chemotactic migration in mice [83]. Chemoattractants mediate their signal via pertussis toxin-sensitive heterotrimeric G-proteins. Upon stimulation, the $G\alpha$ subunit detaches from the $G\beta\gamma$ formation and several signalling pathways are activated [84]. Neutrophil motility includes signal transduction via biphasic Ca^{2+}, phosphoinositide 3-kinase (PI3K) and tyrosine kinases. Neutrophil activation through bacteria- or mitochondria-derived fMLP binds to the corresponding receptors FPR1, FPR2 and FPR3 [85-87]. Other initial stimuli during early chemotaxis include intracellular calcium ions derived from tissue injury, chemokines and lipid mediators, some of which are listed in Table 1[88, 89].

The classical biphasic calcium signalling includes an early phase where calcium is released intracellularly and inositol triphosphate (IP_3) is produced by phospholipase $C\beta$ ($PLC\beta$) [84]. Similar to $PLC\beta$ signalling, $PI3K\gamma$ signal transduction is also activated through $G\beta\gamma$ [90]. In regard to tyrosine kinases, neutrophils express Hck, Fgr and Lyn within the Src kinase group [84]. In detail, Src family kinases are H_2O_2-sensitive and initiate chemotaxis of human, murine and zebrafish neutrophils *in vitro* [91-93]. Mostly, dual oxidase 1 (DUOX1) in the epithelium generates hydrogen peroxide post-injury [93]. After direct recognition of H_2O_2, phosphorylation of Src family kinase Lyn initiates Erk signalling [91]. Further downstream signalling has not been elucidated yet, but most probably Rac and Erk are involved in neutrophil motility [41]. Mostly, the incoming cues synergize, and common intracellular signal transduction occurs

through PI3Kγ, PLCβ, Rac and Erk. Detailed studies on the *in vivo* neutrophil migration in zebrafish have demonstrated that Rac signalling and calcium flux at the front guides cell motility [94, 95].

The localization of downstream signalling molecules at the front of activated neutrophils enables gradient recognition stimulated by chemoattractants [96-98]. In detail, actin dynamics is mediated by Rac and Cdc42, both performing distinct tasks at the leading edge, while high actomyosin contractility is regulated by RhoA at the tailing edge during chemotaxis [94, 99-101]. Notably, Cdc42 is reported to be involved in the navigation the cells [101]. Importantly, Rho GTPase activity regulates the actin polymerization within the cell. Effector molecules, such as PIP_3 and PI3K, accumulate at the front of neutrophils and signal via a Rac-dependent positive feedback loop with Rac to generate protrusions and facilitate neutrophil migration [94, 102-105]. Even though Cdc42 is dispensable for PIP_3 deposition, it is essential for guiding a single protrusion towards the chemogradient [101, 106]. Moreover, as illustrated in Figure 3, Cdc42 impedes RhoA activity at the leading edge [107]. Simultaneously, Rac activity is inhibited by RhoA signalling at the tailing edge. Furthermore, PIPKIγ661 mediates detachment of the uropod while key RhoA regulators decreases myosin II-dependent contractility and activates RhoA during cell motility [105, 108]. Additionally, ezrin/radixin/moesin (ERM) proteins are implicated in the polarization process by impeding Rac activity and controlling protrusion formation at the tailing edge of the cell [109].

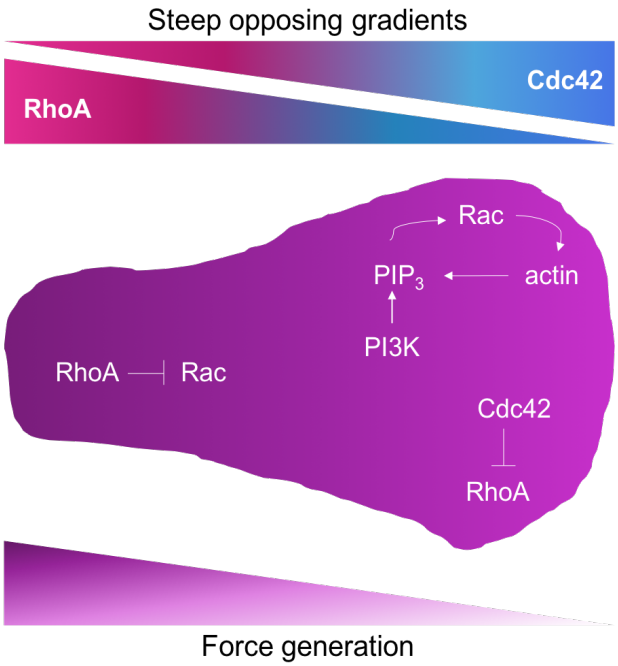

Figure 3. Neutrophil pseudopod and uropod signalling during migration.

Antagonizing gradients of RhoA and Cdc42 signalling controls neutrophil polarization and generation force during cell motility. At the pseudopod, a positive feedback loop is established to accumulate PIP3, while Cdc42 inhibits RhoA activity. Simultaneously, RhoA inhibits Rac signalling leading to an asymmetric generation of force at the rear (created based on [107]).

Besides, Cdc42 is also implied in myosin contraction at the uropod by realigning WASp, which in turns regulates CD11b clustering [110, 111]. This process is essential for stabilizing the uropod. As already mentioned earlier, a defining character of uropods is the ability to detach quickly to maintain during cell motility and extravasation [112]. Functional detachment during cell motility is facilitated by decreased affinity of LFA1 at the uropod [113]. In addition, the ability of neutrophils to detach their tailing edge is also mediated through JAM-A-mediated decreased integrin expression at the uropod [114].

However, it has been shown that there are differences in neutrophil motility between 2D and 3D study systems. It has been reported that neutrophil migration must not be mediated through integrin-dependent adhesion [115]. In contrast, neutrophil motility and attachment to the endothelium is integrin-dependent which resembles a 2D-migration system *in vivo* [107]. Nevertheless, neutrophils require integrins, specifically β_1 and β_2, to maintain the force generation in order to push the cell forward. Conclusively, neutrophils use force generation at the tailing edge of the cell to migrate, while at the same time the uropod detaches from the migrating surface [113].

7.1.5. Antibacterial response by neutrophils

After being recruited, neutrophils embark on a path to reach the site of inflammation or injury. Neutrophil action is amplified through continuous recognition of danger signals. There is a sophisticated system of PRRs on the cell surface and in the cytoplasm to detect PAMPs, DAMPs, stress or sterile injury and instruct an antimicrobial manoeuvre. The sophistication is based on integrating information about which cellular component of the microbe is sensed and its location. If the same pathogen is recognized extracellularly, mainly toll-like receptors (TLR) activation occurs, whereas intracellular sensing leads to nod-like receptor (NLR) activation [116, 117]. Consequently, extracellular pathogens stimulate cytokine production and phagocytosis whereas the serious threat of intracellular pathogens would ultimately switch on programmed cell death to control dissemination [117]. Additionally, dectin-1 receptors serve to detect fungi [118]. In addition to direct pathogen recognition, neutrophils are also be prepared for the engulfment of microbes through opsonisation which in turn is mediated by antibodies, complements or soluble factors, e.g. pentraxins or collectins [119]. Phagocytosis is the one of the neutrophil effector mechanisms to kill microbes and pick up the debris [7]. Pathogens are engulfed by membrane protrusions that fuse with the neutrophilic vacuole and granules forming a phagolysosome [120]. As an example, the entire process of IgG-coated microbe phagocytosis by neutrophils just takes about 20 seconds [121]. During this process, ROS and intracellular granules will be exposed to pathogens leading to the professional killing [15, 122]. Although macrophages are able to generate ROS as well, ROS-mediated killing is much stronger in neutrophils [119]. As illustrated in Figure 4, ROS generation is dependent on the NADPH oxidase complex assembly [123]. The NADPH oxidase complex is an enzyme, consisting of five oxidase subunits:

- the catalytic unit: flavocytochrome b protein consisting of $gp91^{phox}$ and $p22^{phox}$,
- the cytosolic portion: $p47^{phox}$ and $p67^{phox}$ and
- $p40^{phox}$.

Furthermore, two small GTPases Rac1 and Rac2 are involved in the formation of the NADPH oxidase complex [124-126]. During homeostasis, the NADPH oxidase complex is inactivated. Activation occurs upon PAMP recognition and through secretion of proinflammatory cytokines [127]. The following process during

phagocytosis is described as the respiratory burst in neutrophils and is distinct from the mitochondrial respiration [128]. First, superoxide is converted from extracellular oxygen by NADPH oxidase: NADPH + O_2 → $NADP^+$ + H^+ + O_2^- [129]. Superoxide is a weak one-electron oxidant. Radicals quickly react with other radicals, enabling superoxide being catalysed into hydrogen peroxide [130]. Simultaneously, neutrophil granules fuse with the phagosomal membrane to secrete proteases, antimicrobial peptides and peroxidases. Hydrogen peroxide serves as a substrate for peroxidases, such as myeloperoxidase (MPO) which makes up a fifth of the total granule protein content [128, 131]. At this point, MPO converts hydrogen peroxide into hypochlorous acid in the presence of chloride ions [30]. This step is not restricted to chloride ions, hydrogen peroxide-dependent oxidation can occur in presence of other halides to form toxic hypohalous acids [128]. After fusion of granules with the neutrophil phagosome, further NADPH oxidase can be activated, amplifying the ROS catalysation [132, 133]. During this process, electron transport across the phagosomal membrane is essential for the production of ROS. Electron transport is facilitated by the activation of the cytosolic portions of the NADPH oxidase complex, $p47^{phox}$ and $p67^{phox}$, and Rac2 [128]. Subsequently, they translocate to the $gp91^{phox}$, also known as the electron transferase, where protons are transported across the phagosomal membrane. At this point, protons are accepted by free oxygen radicals facilitating the generation of hydrogen peroxide [134].

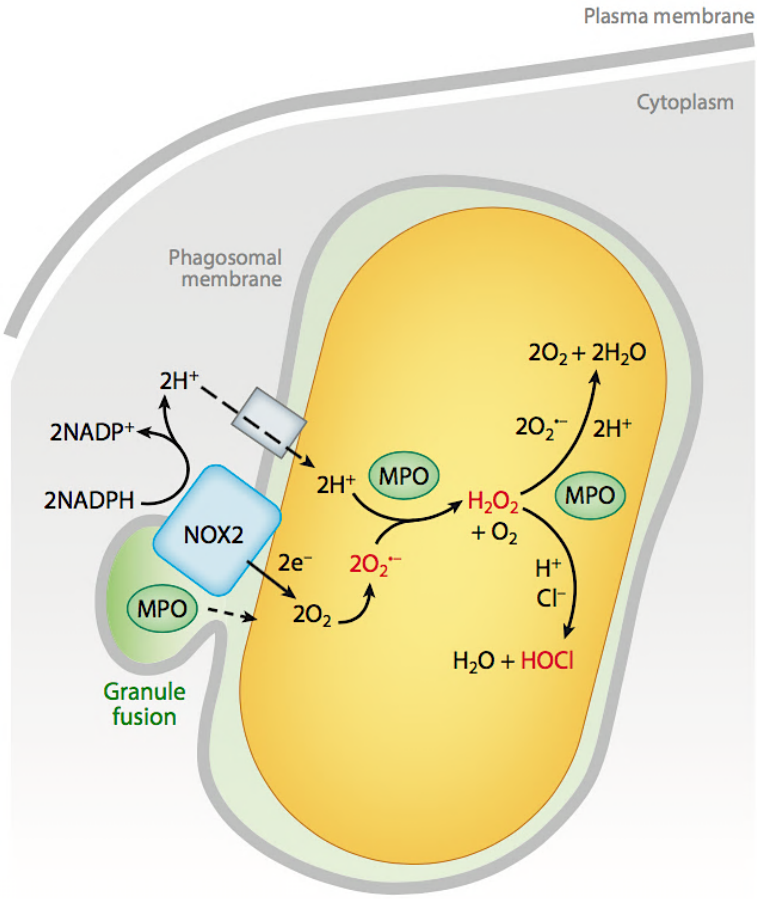

Figure 4. The production of ROS via NADPH oxidase in the phagosome.

The picture illustrates a partial view of neutrophil phagocytosing a bacterium (yellow) in a phagosome, activated NOX2 on the phagosomal membrane and the fusion of the granule (green) (adapted from [123]). The central redox reactions are visualised. Oxygen radicals are ejected into the gap between the bacterium and the phagosomal membrane. Simultaneously, protons are released through proton channels. The catalysation of superoxide by MPO leads to hydrogen peroxide generation. Additionally, chloride ions and superoxide form hypochlorous acid (HOCl) subsequently leading to the killing of the bacterium.

The essential role of ROS is to exert antimicrobial activity. Throughout this process, many antimicrobial peptides and proteins are produced with varying killing capacities, such as superoxide, hydrogen peroxide and hypochlorous acid [123]. Only limited microbicidal action has been attributed to superoxide by its inhibition via superoxide dismutase during bacterial ingestion and it is definitely less potent than hypochlorous acid [135]. In contrast, only adequate levels of hydrogen peroxide make it a potent biocide [123]. Bacterial toxicity depends on the intracellular iron release and reactive radical generation [136]. The cellular levels of hypochlorous acid in isolated neutrophils has been shown to act on a plethora of bacteria efficiently [137]. In line with these findings, neutrophils reveal diminishing hypochlorous acid production and antibacterial action when exposed to low chloride concentrations [138, 139]. The

exact killing mechanism of hypochlorous acid has not been completely elucidated. But studies imply that the oxidation of methionine of bacteria by hypochlorous acid leads to bacterial destruction [140]. Moreover, it has been described that ROS amplifies the antimicrobial activity of neutrophils by activating granule release, NETosis and secretion of proinflammatory cytokines [38, 141, 142]. Hence it is proposed that the induction of further neutrophil action is more antimicrobial than direct ROS-mediated killing [143].

The failure of the correct assembly of NADPH oxidase subunits due to a missense mutation in Chronic granulomatous disease (CGD) patients inhibits ROS production leading to an impairment in oxidative killing [24]. Thus, CGD patients require chronic antibiotic treatment in order to prevent severe microbial infections [144]. After phagocytosis, azurophilic granules synergize with MPO to be secreted into the phagosome and lead to the formation of hypochlorous acid from H_2O_2 and chloride (Figure 4). Notably, hypochlorous acid acts as an antimicrobial agent itself making MPO contributing to the neutrophil effector function [145]. Human neutrophils from patients with MPO mutations show delayed phagocytic response although they seem relatively healthy in contrast to CGD patients [30]. Furthermore, NE, cathepsin G and defensins facilitate the antimicrobial defence in neutrophils as it has been shown *in vitro* [30]. Neutrophilic granules are essential during fighting off *S. aureus, P. aeruginosa* and *Klebsiella pneumoniae*, as patients with a C/EBP-ε mutation suffer from neutrophil-specific granule deficiency [40]. At the same time, these insufficiencies are not only associated to neutrophils, as monocytes and macrophages are also affected [40].

7.1.6. Neutrophil extracellular traps (NETs)

The most recent discovery to be added to the functional plethora of neutrophils is certainly the ability to eject neutrophilic DNA into the extracellular space. However, the initial description of NETosis was considered as an additional cell death mechanism that is distinct from apoptosis and necrosis [146, 147]. The ability to release NETs was found to contribute to the antibacterial defence in a later study. In an *in vitro* approach, PMA- or IL-8-stimulation of neutrophils leads to DNA ejection enriched with histone proteins and neutrophil elastase which in turn killed bacteria [13]. Several experiments were performed to decipher the signalling cascade leading to NET formation. Nevertheless, it is still unclear to what extent certain neutrophil

enzymes and components contribute to the induction of NETs. However, more than 20 proteins have been associated to NETs through mass spectrometry [148]. In detail, neutrophils from CGD patients disclose the involvement of NADPH oxidase during NETosis. However, it seems that neutrophils of CGD patients are capable of releasing NETs through NADPH oxidase-independent mechanisms [14, 149-152]. The exact mechanism behind this NADPH oxidase-independent manner has not been elucidated. It has been reported that MPO and ROS induce NE-mediated NETosis [147, 153]. During NETosis, NE disintegrates histones and affiliates with MPO to dissolve chromatin [153]. Up to this date, the distinct mechanism leading to NETosis is also not unfolded. Only partial information is available: The chromatin dissolvement through H3 citrullination by PAD4 in mature human neutrophils [154]. Additionally, calprotectin, a major neutrophil cell component, has been identified as the essential NET part contributing to Candida defence [148, 155]. Trapping of *Staphylococcus aureus* has been observed for *in vitro* experiments where pathogens attached to NETs directly [156]. *In vivo* imaging revealed attachment of *Klebsiella pneumoniae* in NETs during intratracheal infection of mice [153]. Another study showed LFA1-mediated NETosis in liver sinusoids trapping *E.coli* and significantly controlling the infection [157]. More evidence for NETs controlling infection has been demonstrated as bacteraemia was reported in the absence of NETs [158]. Containment of viral dissemination and antiviral activity during NETosis have been observed during HIV infection [159, 160]. Direct bactericidal evidence is derived from protease-, antimicrobial peptide- and histone-enriched DNA [147, 161]. These observations emphasize that NETosis is an universal effector function during antimicrobial defence, as this capacity is maintained even during pharmacological inhibition of phagocytosis [13].

7.1.7. Neutrophils regulate B-lymphocyte maturation and activation in the spleen

Neutrophils are considered as classical effector cells, but they also have the capacity to orchestrate the adaptive immunity. Non-Germinal Centre (GC) marginal zone (MZ) B-lymphocytes near the splenic sinus are responsible for the antibody secretion in response to pathogens into the circulation [15]. In this context, neutrophils remain in the regions close to the MZ with quick access to blood vessels and MZ B-lymphocytes [162]. During infection, neutrophils pick up pathogens from the blood and migrate to the MZ to the B-lymphocytes [163]. Subsequently, activated

neutrophils secrete BAFF and APRIL which in turn contribute to activate MZ B-lymphocytes in a T-cell-independent manner in humans [15, 164-166]. Activation of MZ B-lymphocytes only has been shown to be facilitated via BAFF, APRIL and IL21 from splenic neutrophils leading to antibody synthesis and class switching in mice [15, 166]. *In vitro* approaches have confirmed these observations. In addition, patients with impaired neutrophil maturation show healthy levels of B-lymphocytes in circulation but show decreased numbers of MZ B-lymphocytes and antibody titres to T-lymphocyte-independent antigens [166]. Conclusively, these data show a neutrophil-dependent mechanism to initiate B-cell responses after encountering pathogens in the circulation.

7.2. Chronic lymphocytic leukaemia

7.2.1. Clinical and genetic presentation of CLL

Chronic lymphocytic leukaemia is an incurable and indolent disease of B-lymphocytes and its progenitors. The disease is characterised through the massive outgrowth of mature B-cells expressing CD5+ on their surface accumulating in lymphoid organs, in the blood and bone marrow [167]. The accumulation in lymphoid organs causes them to enlarge in size and result in clinical features like hepatosplenomegaly and lymphadenopathy [168]. Most importantly, recurrent infections play a pivotal role, mostly leading up to the initial diagnosis of CLL. Thus, CLL patients experience an asymptomatic course with unspecific features like fatigue, fever and infections [169]. In addition to structural changes in the affected organs, the clonal expansion of B-cells also affects functions of other immune cells and leads to an immunocompromised state of the patient [170].

CLL is the most prevalent form of leukaemia occurring in the elderly population, predominantly in males. In fact, it accounts for almost a third of all leukaemia in European and North American countries [171]. The median age of diagnosis varies between 60-70 years depending on the patient's ethnicity [172]. Another major reason for a late diagnosis in CLL might be due to its asymptomatic progression. Notably, a decrease in the median age of diagnosis has been observed recently because of increased routine healthcare procedures and revised blood tests. As a result, up to 10% of all CLL patients are aged below 55 years with a tendency to increase in the coming years.

Although the pathogenesis of CLL may be heterogeneous and will be up for later discussion, the homogeneity of the immunophenotype of the disease is remarkable. In addition to CD5, other antigenic surface structures such as CD19, low CD20 expression, CD38, ZAP70 and CD23 (FcεRII) constitute an immunophenotype that is specific for CLL and differs from other haematological malignancies [173, 174]. The surface immunoglobulins IgM and IgD were considered for diagnosis prior of having a complete understanding of the CLL immunophenotype [175, 176].

Haematological neoplasms can be usually traced back to a specific chromosomal abnormality, such as the Philadelphia translocation in Chronic Myeloid Leukaemia [177]. In CLL, there is no single hallmark genetic aberration that defines the pathogenesis of this disease. There are several genetic factors that play a role in CLL. A commonly found deletion in band 13q14 affecting microRNAs *mir15a* and *mir16-1* contributes to the development of CLL [178]. Deletions in 11q23 are associated with an accelerated progression and frequently found in the later stages of CLL. Ataxia telangiectasia-mutated gene (*ATM*) can be found in this particular chromosomal location and in nearly 15% of patients [179]. *ATM* is responsible to initiate counteractions upon DNA damage, such as cell cycle checkpoint activation and apoptosis. It is currently not elucidated which exact genes in the 11q23 band region contribute to the CLL pathogenesis [180]. Similarly, it is not clear which genes contribute to the development of CLL in regard to trisomy 12. There is also no clear link between the disease outcome and this chromosomal mutation [181]. Deletion in 17p13 and *TP53* inactivation usually occur simultaneously and account for almost 10% of CLL cases [180, 182]. This genotype is associated with a poor outcome as it predisposes to a variety of clinical complications [178]. In addition, epigenetic modifications have also been reported in CLL, such as hypomethylation of *BCL2*, *TCL1* and other differently methylated genes account for up to 8% of all samples [183]. *BCL2* might contribute to the pathogenesis in two distinct ways. On one hand, it may lose its anti-apoptotic function and cause disease development directly. On the other hand, *BCL2* can be upregulated through *mir15a* and *mir16-1* and confer apoptotic resistance to CLL cells [184].

The prognosis for CLL patients depends on many prognostic factors, e.g. genetic lesions, immunophenotype, lymphocyte count, IGHV mutation status (will be discussed in 7.2.2), areas of enlarged lymph nodes (lymphadenopathy), serum markers (β_2-microglobulin), anaemia and thrombocytopenia. Based on these clinical

features, clinicians refer to either one of the two staging systems, the Rai or Binet staging system, in order to stratify CLL progression and risk [182]. The former is primarily used in the USA, while the latter is more commonly used in Europe [185].
In regard to the Binet system, there are three stages which include the areas and numbers of palpable lymph nodes, haemoglobin (Hb) and thrombocyte levels (Table 2) [167, 186]:

Table 2. Binet staging system for CLL risk stratification.

Stage	**Areas of lymphadenopathy**	**Clinical features**	**Median survival / years**
A	< 3	No anaemia (Hb ≥10 g/dl) and no thrombocytopenia (platelets ≥100,000/µl)	13
B	> 3		8
C	irrelevant	Cytopenia (Hb <10 g/dl; platelets <100,000/µl)	2

7.2.2. IGHV status and the pathogenesis of CLL

Interestingly, monoclonal B-cell lymphocytosis (MBL) has often been described as an indolent preceding condition leading up to CLL [187]. Despite the fact that only 1-2% of MBL cases develop CLL, there is a strong link between MBL and CLL [188]. Chromosomal mutations that occur in CLL and the slightly increased incidence rate of MBL in family members of CLL patients strengthen the notion of MBL being a predecessor of CLL [189, 190]. Mutations in the immunoglobulin heavy variable region (IGHV), deletion of 13q14 or trisomy 12 are commonly reported in both, MBL and CLL. But what precedes MBL is not clear in terms of CLL pathogenesis. The exact answer to the origin of the malignant B-cell clone can be found if CLL is subdivided according to the mutational status of IGHV: mutated and unmutated IGHV-CLL. In order to understand the biology and clinical relevance of the IGHV status, the B-cell response through its B-cell receptor (BCR) will be shortly described. Upon antigenic activation, immunoglobulins on B-cells recognize the pathogen and convey an adaptive response via clonal expansion and antibody secretion. A specific BCR consists of different combinations of V, D and J segments for the heavy chain of Ig and of V and J segments for its light chain [191]. The resulting number of combinations and the process of somatic hypermutation (SHM) through T-cell dependent or independent stimuli lead to a vast variety of antigens being covered

[192]. In the context of CLL, the level of SHM status of the IGHV determines a patient's disease outcome, response to therapy and might identify the cellular progenitor of CLL [193]. Approximately 40% of all CLL cases have an unmutated IGHV (IGHV-UM) status with a poor prognosis and typically harbour mutations with an unfavourable disease outcome. Clonal expansion is more severe in IGHV-UM cases [169]. Additionally, BCR of a significant portion of CLL B-cells in IGHV-UM patients respond to neo-autoantigens in a low affinity manner probably due to the fact that their expansion has been selectively driven by only a few antigens [194]. In contrast, mutated IGHV (IGHV-M) CLL harbours high affinity monoreactive BCRs. Less clonal expansion and some distinct genetic mutations that define this subcategory are linked to favourable prognosis and higher overall survival rates [195].

As a result, a single cell theory as the pathogenesis of CLL could not explain the origin of this heterogeneous disease. In fact, a lot of concepts and theories are still being established and for different types of CLL different hypotheses exist. As illustrated in Figure 5, genetic or epigenetic lesions occurring in one HSC are the initial events that result in CLL. The resulting cell in turn acts as a skewed cell that gives rise to further progenitors in the B-cell lineage. This line of argument is supported by a xenotransplantation study performed by Kikushige, Ishikawa [196]. HSC from CLL patients gave rise to further B cell clones in immunodeficient mice [169]. Diverging routes create foundations for different forms of CLL dependent (TD) or independent (TI) of T-cells during the mature phase of the B-cell development. Particularly, naïve B-lymphocytes can differentiate into $CD5^{+}CD27^{-}$ cells without undergoing the germinal centre (GC) process as proposed by Fabbri and Dalla-Favera [169]. Further genetic and epigenetic mutations might drive transformation of these cells leading to MBL and culminate in IGHV-UM CLL. B-cells give up their polyreactivity as genetic lesions drive the clonal selection. A study performed by Damle, Ghiotto [197] describes B-cells in IGHV-UM CLL as activated, supporting the idea that these cells may originate from antigen-stimulated B-cells. However, a more profound understanding for the cellular origin was proposed in a recent study by Seifert and Kuppers [198]. Post-GC B-cells were identified as the cellular origin for a previously unknown $CD5^{+}CD27^{+}$ B-cell subset in IGHV-M CLL, while pre-GC naïve $CD5^{+}CD27^{-}$ B-cells were proposed to be the cellular basis for IGHV-UM based on similarities on gene expression profiles [198].

Alternatively, antigen-driven B-cells may experience genetic and epigenetic modifications after their GC reaction in a T-lymphocyte-dependent manner. Mature B-lymphocytes are being saved from apoptotic signals and start accumulating leading to MBL and ultimately to IGHV-M CLL. The cellular origin of these CLL cells derives from $CD5^{+}CD27^{+}$ B-cells as it is reviewed by Fabbri and Dalla-Favera [169].

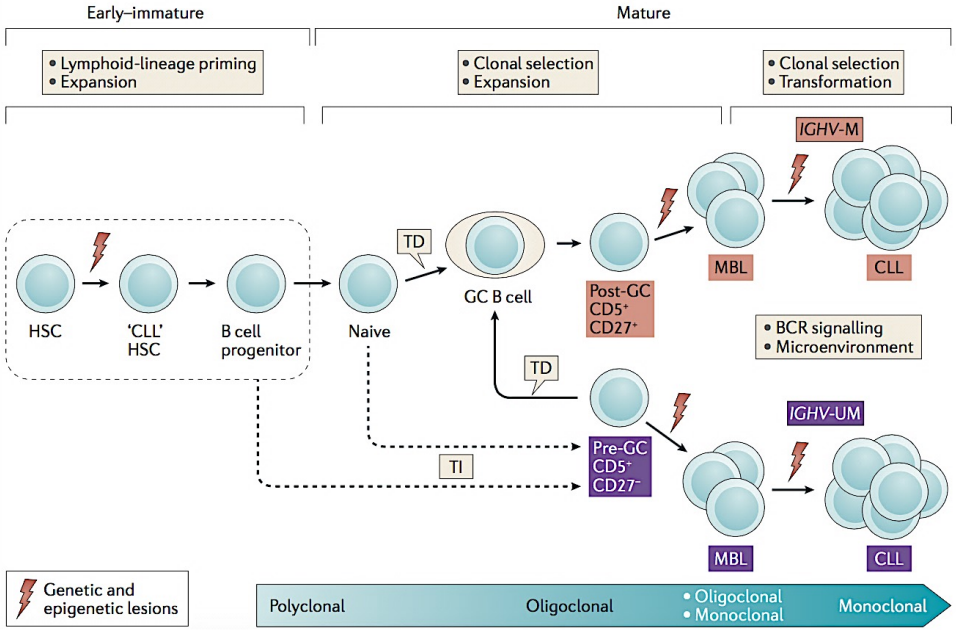

Figure 5. The pathogenesis of chronic lymphocytic leukaemia.

Although the exact pathogenesis of CLL is still elusive, the proposed mechanisms are summarised and illustrated in this figure. The early genetic and epigenetic modifications experienced by the HSC is believed to be the first event in the progression of the disease. Depending on T-cell interactions, the B-cell progenitor gives rise to clonal expansion with clones resembling a post- (IGHV-M) or pre-GC B-cell phenotype (IGHV-UM). Further genetic lesions and promoting microenvironment lead to an apoptotic resistance, enhanced survival and accumulation of B-cell clones in CLL (adapted from [169]).

As a conclusion, the current general hypothesis for the molecular pathogenesis of CLL cells is based on skewed HSC, which harbour an unknown genetic or epigenetic lesion. From here, CLL B-cell progenitors can differentiate into IGHV-M or IGHV-UM CLL depending on their involvement with T-cells dependent or independent reaction in the GC reaction, respectively.

7.2.3. CLL microenvironment

As reported widely, most of the CLL cells are likely to be arrested in G0/G1 phase and reveal little or no proliferating capacity, prolonged life span and deficiencies in the apoptosis machinery [180]. In other words, CLL cells accumulation of CLL cells in lymphoid organs does not seem to involve local proliferation. Accordingly, once

genetic and epigenetic lesions have occurred in CLL cells, there must be an anti-apoptotic micromilieu that supports the hoarding of malignant B-cells in the secondary lymphoid organs. Microenvironmental factors play a major role in the apoptotic resistance of CLL B-lymphocytes as demonstrated in an attempt to culture malignant B-cells *ex vivo*. CLL B-cells cannot remain alive *in vitro* unless bone marrow-derived stromal cells (BMSC), nurse-like cells (NLC) or cytokines are added to the culture [199-201]. These experiments highlight the importance and dependency on external factors that nurture CLL B-cell survival *in vivo.* In addition to BMSC and NLC, T-cells, follicular dendritic cells, endothelial cells and NK cells constitute the architecture of CLL microenvironment. The soluble factors secreted by these cells and the crosstalk through ligation with CLL cells provides an anti-apoptotic and therapy-resistant microenvironment for malignant B-cells.

NLC and BMSC are key mediators providing a supportive micromilieu for malignant B-cells in the CLL microenvironment. NLC are classified as a subset of tumour-associated macrophages (TAM) of monocytic origin and reported to have a M2-phenotype.

7.2.4. Perturbations of the immune system during CLL

Despite of routine blood tests, most of the patients are diagnosed with CLL because of recurrent infections or serious infectious complications by common microbes, mainly in the respiratory or urinary tract [170]. Almost all CLL patients suffer from recurrent infections and more than 50% of these patients succumb to secondary complications from the infection [1, 202]. The understanding of which immune perturbations predispose CLL patients to an increased infection risk is highly relevant for pre- and post-therapy options. Similar to other haematological malignancies, there are number of inherent defects in the immune system. The aetiology of increased infection risk is often linked to hypogammaglobulinemia, T-cell dysfunction or complement impairment [203]. The impact of hypogammaglobulinemia on the predisposition of CLL patients to infections has been established already over 50 years ago [204]. The production of Ig-producing $CD95^+$ plasma B-cells is inhibited by neoplastic B-lymphocytes and impaired functions of T- and non-CLL B cells are some of the underlying factors that have been implicated for hypogammaglobulinemia for almost all CLL patients [3, 205]. Decreased levels of serum IgG, IgA and salivary IgM are another clinical feature during early stages of CLL [1, 206, 207]. Notably, not all

immunoglobulins correlate with a survival outcome, do not restore upon treatment and the condition mostly worsens over the course of the disease without a clear correlation between serum levels and infection risk [4, 202]. Nevertheless, there are also CLL patients suffering from persistent infections with healthy levels of immunoglobulins which points at a functional impairment of antibodies [1]. Furthermore, vaccination against infections in CLL is not likely to trigger functional immune responses indicating a greater B-cell defect than the hypogammaglobulinemia itself [208]. In regard to the IGHV status on infection risk, there are two major studies that analysed survival outcomes for both CLL groups. In one study, no quantitative variations in serum levels of immunoglobulins, vaccination responses to *Haemophilus influenzae B*, or morbidity rates in IGHV-UM CLL or IGHV-M CLL patients were found [209]. Another study reports that the time to the initial major infection is shorter and infection-related mortality is decreased in IGHV-M CLL compared to IGHV-UM CLL despite of equal levels of immunoglobulins in a retrospective review with over 200 CLL patients [202]. In IGHV-UM CLL, the specificity of antigen receptors in a major portion of neoplastic B-cells might be limited to a few antigens which in turn dampens the ability to mount an efficient immune response to pathogens [194, 210]. The antimicrobial response is further impacted due to dysfunctional $CD4^+$ T-cell responses, altered CD4/CD8 ratios and elevated levels of T-regulatory cells especially towards the advanced stage in CLL patients [211-213]. Gene expression profiles of T-cells reveal aberrations associated with cytotoxicity and actin cytoskeleton [214]. In particular, the formation of the supramolecular activation complex by T-lymphocytes and APC is perturbed in CLL patients which translates into an impaired T-cell signalling and secretion of effector molecules [215]. This report also shows that even healthy allogeneic T-cells fail to form an immunological synapse once they have been bound by malignant B-cells. The release of immunosuppressive cytokines, such as IL-10 or TGF-ß, by malignant B-cells has an impact on responsive immune cells in CLL. Additionally, IL-2 receptor is secreted into the circulation by malignant B-cells, binds to IL-2 and thus hinders the activation of T-cell proliferation [2].

Quantitative reduction in certain complements, especially in the opsonizing agent C3b, is another underlying factor for immunosuppression in CLL [216], and restricts the treatment outcome of monoclonal antibodies as their functioning is based on complement-mediated killing [217]. The alternative pathway of the complement

cascade is stimulated by IgA and subject to properdin function [218]. In a two-year monitoring of CLL patients, serum complement protein concentrations were measured. The most common finding was diminished levels of properdin which was linked to late-stage CLL [219]. In the same way, another study reports how lower levels of components from the classical complement pathway at the early stage of disease corresponds with compromised survival outcome [220]. Impaired immune responses can be traced back to the inherent dysfunctions of specific cell subsets or acquired treatment-related abnormalities. Unlike other diseases, CLL patients experience a state of immunosuppression which predisposes them to an increased risk for infections before and after treatment [3].

The spectrum of infections includes bacteria, viruses and fungi. Two thirds of untreated CLL cases are affected by bacterial infections, one quarter by viruses and fungi account for almost 10% [2, 5]. *Staphylococcus aureus* and *Streptococcus pneumoniae* are responsible for lung infections and uropathogenic *Escherichia coli* are common pathogens in bladder infections of CLL patients [5].

7.2.5. Neutrophil function in CLL

As discussed above, neutrophils are the primary cells to fight off bacterial infections and a significant proportion of infections in CLL patients at various stages of disease progression are of bacterial origin. The inability to mount an efficient antibacterial response rises questions of whether neutrophils are affected by inherent defects and how the immunosuppressive CLL microenvironment modulates granulocyte functions. Initial studies have examined the neutrophil activity in CLL patients, but there is no comprehensive study that explains the mechanism of diminished neutrophil responses to bacterial infections.

Despite of the widespread notion of neutropenia in CLL patients, the total numbers of neutrophils in PB does not decrease significantly in untreated CLL patients [1]. Hence, the proportional decrease is attributed to the massive accumulation of neoplastic B-lymphocytes in the PB prior to treatment. Neutropenia develops during more advanced stages of disease or post-chemotherapy where patients become immunosuppressed with an even higher risk of opportunistic infection [221]. In regard to inherent defects, there are conflicting and incomplete analyses of whether neutrophil function is altered before chemotherapy. One study reports undirected migration, and C5a- or fMLP-mediated chemotaxis was clearly diminished in CLL

patients with infections which was compared to healthy donors or CLL patients not suffering from an infection. At the same time, phagocytic defects were not detected in CLL patients [206]. A study from the 1960s supports this finding, claiming that no abnormalities in neutrophil responses were detected in CLL patients [222]. However, impaired bactericidal enzymes, such as ß-glucuronidase, lysozyme and myeloperoxidase, were detected and found to be restored in a minor cohort of CLL patients during remission [223]. Similarly, antibacterial but not antifungal responses were decreased in non-neutropenic CLL patients [224]. In addition, the NETosis capacity of neutrophils in CLL patients is higher compared to healthy donors, presumably due to the chronic stimulation of the CLL microenvironment through increased cytokine release [225]. No differences in antimicrobial enzymes, such as elastase, myeloperoxidase or ROS synthesis were detected in this particular study. In a different approach, neutrophils were described as tumour-associated neutrophils where they exhibited a B-cell helper phenotype in the spleen providing survival signals for malignant CLL cells [226]. In this particular study, Ly6G antibody depletion was used to show decelerated CLL development.

Given these points, neutrophil deficiencies seem to have been observed similar to other affected components of the innate or adaptive immunity during CLL. Although the CLL microenvironment provides a particular survival niche for neoplastic B-lymphocytes, it most probably has an impact on other immune cells as they share identical anatomical sites for their development and maturation. Notably, the spleen also serves as a residence site for immature neutrophils where effector cells can be quickly recruited upon infection, and thus contributes to the impact of CLL on neutrophil function [227].

7.3. CLL mouse models

7.3.1. Currently available CLL mouse models

Based on different mutant drivers of the disease, there are several CLL mouse models available ranging from indolent to aggressive disease severity (Table 3) [228]. The aim of this study demanded the investigation of the innate immune response in an *in vivo* model, but an *in vitro* system was used wherever possible, especially for NETosis or migration of neutrophils. Even then, neutrophils were harvested from the blood or bone marrow (BM) of laboratory bred mice. Despite of a wide range of *in vitro* assays available to examine the phagocytic function, other

effector functions of neutrophils, the complex composition of the CLL microenvironment and an infectious setting cannot be mimicked in one culture model. Furthermore, immortalized neutrophil lines do not reflect neutrophil properties from an *in vivo* setting during physiology or disease. Consequently, results from such cell lines should be interpreted carefully and hence were not utilized in this study.

Table 3. CLL mouse models.

Model	Mutant gene /driver	B cell phenotype	CLL subtype
Eμ-TCL1 transgenic	T cell leukaemia protein 1A (*TCL1*)	$CD5^+IgM^+B220^+CD19^+$ Unmutated stereotypic CDR3	Aggressive
TRAF2DN/BCL-2 transgenic	TNR receptor ass. factor 2 (*TRAF2*) and *BCL-2*	$CD5^+IgM^{high}IgD^{low/-}$ $B220^{moderate}CD23^-CD21^{low/-}$ $CD11b^{low}$	N/A
Irf4$^{-/-}$*Vh11*	Interferon regulatory factor 4 (IRF4) deficiency	$CD5^+IgM^+CD19^+IgD^{low}$ $B220^{low/-}CD23^-CD21^-$ $CD1d^{int}$	MBL, indolent and aggressive
TNFSF13/APRIL transgenic	A proliferation-inducing ligand (APRIL)	$IgM^+CD5^+B220^+$	Indolent
Altered microRNA	Deletion of *DLEU2/miR-15a/16-1* cluster of transgenic miR-29a	$IgM^+CD5^+B220^+$	Indolent
New Zealand Black	Age-associated	$IgM^+B220^{dim}CD5^{dim}$	Indolent, familial

7.3.2. Eμ-TCL1 mouse model and the adoptive transfer approach

In the Eμ-TCL1 transgenic line, the human *TCL1* gene is expressed under the V_H of immunoglobulin-promoter and *Eμ*-enhancer leading to a progressive accumulation of $CD5^+IgM^+CD19^+$ B-lymphocytes [229]. In this aggressive model, the onset of CLL occurs approximately after 12 months of age with clonal expansion of monoclonal B-lymphocytes [229]. Malignant B-cells can be detected starting from 2 to 6 months in the PB. $CD5^+$ CLL B-cells localize in the PB, spleen, bone marrow and peritoneal cavity [229, 230]. In fact, the Eμ-TCL1 transgenic line was the first CLL mouse model and is commonly used to investigate the disease origin and to evaluate

chemotherapies [230]. Aberrant expression of *TCL1* was found in many CLL patients [231]. However, it is linked to poor disease outcome and the BCRs on the CLL B-cells are associated to the IGHV-UM CLL [231]. Hence it is commonly accepted that the Eμ-TCL1 transgenic line reflects the aggressive and therapy-resistant human CLL [230]. In contrast to the human disease progression, there is no precedence of a MBL phase in Eμ-TCL1 mice [230]. Similarities between the CLL phenotype in humans and mice comprise switching of T-cells from naïve to memory subsets, rising T-cells in the circulation, deficient signal cascade during immunological synapse and epigenetic modifications amongst others [232-234].

As previously described, nurse-like cells contribute to the anti-apoptotic machinery of malignant B-cells through BAFF and APRIL, members of the TNF cytokine family [235-237]. As a matter of fact, immunosuppression was described in Eμ-TCL1 mice through IL10-producing neoplastic B-lymphocytes in regard to B-cell regulatory functions, disease outcome and resistance to therapy [238]. But the impact of this regulatory micromilieu on other immune cells by CLL B-cells has not been deciphered at all. The microenvironment consisting of the previously described cytokines has also been found in CLL patients, again verifying the potential of the Eμ-TCL1 transgenic mouse line. The late onset of disease has been conquered by allograft and xenograft models to accelerate CLL progression into syngeneic immunocompetent or immunodeficient mice [239-243]. The advantage of these transplantation models is that any scientific question can be addressed by inducing CLL in various mouse models within a much shorter span of time. Also, transplantation into syngeneic immunocompetent mice eases the study of infections during CLL.

7.4. Urinary tract infections

7.4.1. UTI pathogenesis

The renal system consists of the urethra, urinary bladder, kidneys and ureters with only the urethra being exposed to uropathogenic bacteria [244]. The host defence is based on recruited and resident innate immune cells which will be explained in the next section. Anatomical barriers, such as the epithelium, also contributes to the protection from bacterial invaders. Uroplakin is a deposition of mucus on the top of epithelial cells which is enriched with antimicrobial properties [245]. At the same time, uropathogenic microbes harbour virulence factors to adhere and cause an infection

in the urinary tract that might spread to the upper renal system due to immunocompromised host factors.

UTIs are considered to be community and nosocomial acquired infections contributing to the international health burden. In detail, more than 150 million individuals suffer from an UTI worldwide [246].

While most of the UTIs can be self-resolving, some infections can progress to a recurrent and severe state. Infectious complications, such as acute pyelonephritis, bacteraemia and septic shock has also been described in CLL patients during the most progressive stages [1, 4].

Most of the UTIs originate from uropathogenic *Escherichia coli* (UPEC), but might be caused by other bacteria and fungi as well, such as *Klebsiella pneumoniae, Pseudomonas aeruginosa, Staphylococcus aureus* and *Candida spp.* [246-248].

Urinary tract infections (UTIs) affect females more than males due to the shorter urethra which facilitates bacterial adherence and colonization [249]. UTI patients usually show the same clinical features as in other infections, such as increases in C-reactive protein and neutrophil levels at the site of infection and in the circulation, and fever. Infrequent pain during urination and neutrophils and bacteria in the urine are some of the clinical manifestations during UTI [249].

As illustrated in Figure 6, UTI will be described based on UPEC infection, the most common causative UTI agent. Gut-resident UPEC migrate into the urethra and move forward to the urinary bladder where migration and adhesion occurs in a flagella-, adhesin- and pili-dependent manner, respectively [246]. In particular, UPEC feature adhesins with varying preferences for different compartments in the renal system [250]. Moreover, UPEC have a wide variety of pili increasing their chances to adhere, colonize and remain to and in different epithelial linings within the urinary tract [251]. Epithelial cells are activated by UPEC-specific pili leading to cytoskeletal rearrangements and engulfment of bacteria [252]. Furthermore, UPEC-derived toxins and proteases ease epithelium cell invasion to derive nutrients for their own expansion [246]. Specifically, iron scavenging is of utmost importance for survival through UPEC-derived toxin α-haemolysin [246]. Mucosal immunoglobulin IgA cannot reach the site of infection as UPEC-derived PapG inhibits the immunoglobulin carrier required for the transport across epithelial layers [253]. Infected epithelial cells are shed with plaques of bacteria. Nevertheless, some bacteria are able to evade the host immune defence and expulsion by forming quiescent intracellular reservoirs

(QIR) in the underlying epithelial layers [246, 254, 255]. Recurrent infections may occur due to reactivation of bacteria from the QIR [256]. Once the host innate response can be evaded by UPEC, bacteria begin to ascend to the kidneys, specifically through the absence of IgA, and are able to enter the circulation [246, 253, 257].

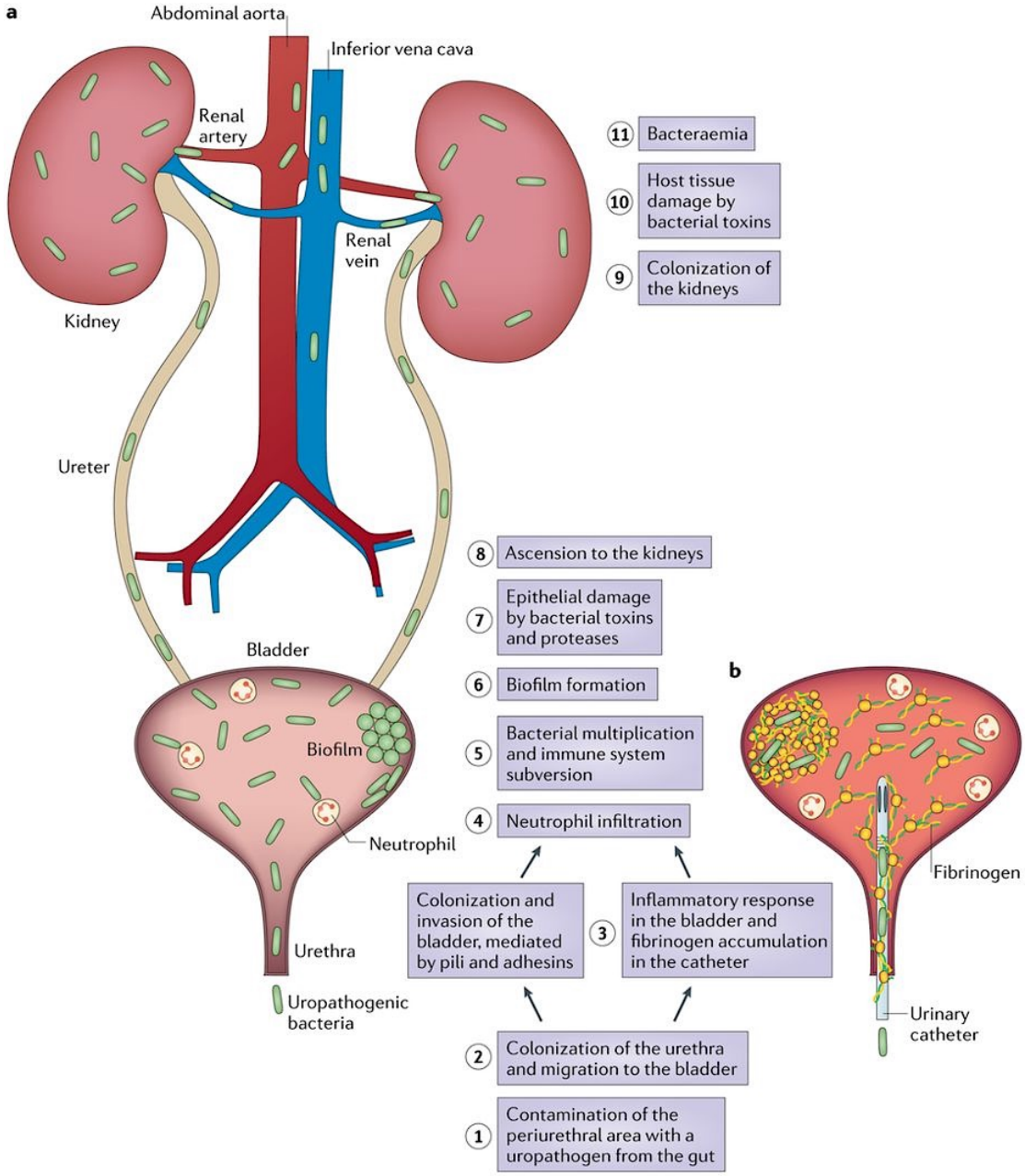

Figure 6. Pathogenesis of UTIs with two different outcomes.

Self-resolving UTI originate from uropathogenic microbes finding their way into the urinary bladder through the urethra. Bacterial pili and adhesins facilitate colonization and initiate immune responses leading to neutrophil infiltration. Biofilm synthesis on the mucosal bladder lining enhances bacterial invasion into the ureter and ascension into the kidneys that could lead to pyelonephritis and bacteraemia during immunosuppression (a). During the nosocomial-acquired infections, pathogens are introduced to the bladder via a catheter. Fibrinogen

deposits on the catheter enables bacterial colonization and invasion into the upper urinary tract affecting kidneys and having the possibility to cause sepsis (b) (adapted from [246]).

7.4.2. Neutrophil anti-bacterial response during UPEC infection

The antimicrobial response by innate cells is crucial for the progression of the UPEC infection. More importantly, the efficacy of the initial clearance determines whether recurrent infections may occur [255]. Once bacterial components are recognised through TLRs on the luminal layer of epithelial cells, mast cells, resident macrophages and Ly6C$^-$ macrophages beneath the mucosa, CXCL1, tumour necrosis factor (TNF) and antimicrobial peptides are secreted to initiate an immune response against invading UPEC [69, 244, 258, 259].

In order to reach the lumen, the site of infection, neutrophils have to transverse several sheaths of epithelial cells [260]. They are the first cells to reach the site of urinary tract infection, already 2 hours post-infection, and are crucial for the clearance of UPEC [260, 261]. For this, neutrophils have to reach the site of infection by crossing the epithelial layer and its collagen IV-rich basement membrane in a MMP9-dependent manner [69, 262]. MMP9 release is induced by CXCL2 secretion from Ly6C$^-$ macrophages [263]. In detail, Ly6C$^+$ macrophages produce TNF, which in turn enables CXCL2 secretion by resident macrophages [69]. Hence, CXCL2 does not act as a chemoattractant to recruit neutrophils to the site of infection. It rather promotes the epithelial crossing of neutrophils. Other CXCR2 ligands, specifically, CXCL1 promote neutrophil migration. After crossing the epithelial basement membrane, neutrophils are able to fight off UPEC infection. In addition, neutrophil levels rise in response to bacterial burden [264]. We have demonstrated that neutrophils are able to phagocytose almost 90 % of fluorescently-labelled UPEC in the first 6 hpi [263]. Thus, neutrophils are the main effector cells during UTI.

Consequently, it is established that neutrophils fight the infection through the orchestration of resident macrophages and Ly6C$^-$ macrophages with the help of cytokines, antimicrobial peptides and enzymes. After antimicrobial action, neutrophils are disposed in the urine in order to prevent any excessive host damage [265]. Consequently, host tissue damage may occur from profuse neutrophil responses, mediated via ROS and COX2, which in turn contribute to the risk of recurrent infections [266].

8. Materials and methods

8.1. Materials

8.1.1. Mice

All mice were bred and kept under SPF conditions in the central animal facility at the University Hospital Essen. Female C57BL/6 mice aged 6-8 weeks were purchased from Janvier Labs and Charles River Laboratories. Catchup mice had been backcrossed more than 10 times to the C57BL/6 background [267]. All experimental procedures were conducted according to the guidelines for the care and use of laboratory animals and were approved by the LANUV Gelsenkirchen.

Table 4: Mouse strains used in this study.

Mouse strain	Manufacturer	Description
C57BL/6	Janvier, France Charles River, USA	Inbred wildtype laboratory mouse strain
Catchup (Gt(ROSA)26Sor(CAG-tdTomato): fl/fl x Ly6g(cre-tdTomato): +/ki)	Anja Hasenberg, Matthias Gunzer, University Duisburg-Essen and University Hospital Essen, Germany	Reporter mouse line for Ly6G expressing cells on C57BL/6 background, heterozygous for Ly6G expression of tdTomato under the endogenous Ly6G locus [267].
Eμ-TCL1	Molecular Genetics, German Cancer Research Centre, Heidelberg, Germany	Mutant TCL1 under the B-cell specific IGHV promoter leads to extensive B-cell proliferation in PB and lymphoid organs. This model reflects an aggressive type of CLL [229].

8.1.2. Chemicals / Reagents

Table 5: List of chemicals and reagents used in this study.

Chemical / reagent	Manufacturer
Bovine serum albumin (BSA) Fraction V	Sigma-Aldrich, Munich
Calibrite APC beads	BD Biosciences, Heidelberg
Collagenase D	Sigma-Aldrich, Munich
Complete Protease Inhibitor Mix	Roche, Karlsruhe
D-Sucrose	Carl Roth, Karlsruhe

Dimethyl sulfoxide (DMSO)	PanReac, AppliChem, Darmstadt
Disodium phosphate (0.2 M; Na_2HPO_4)	Sigma-Aldrich, Munich
DNase I	Sigma-Aldrich, Munich
Ethanol, ≥ 99,5 %	Carl Roth, Karlsruhe
Ethanol, 70 %	Carl Roth, Karlsruhe
Ethylenediaminetetraacetic acid disodium salt (EDTA)	Carl Roth, Karlsruhe
Foetal calf serum (FCS)	Biochrome, Berlin
Forene 100 % (Isoflurane)	Abbott GmbH & CoKG, Wiesbaden
Immu Mount	Sakura Finetek, USA
Ketamine 10 %	Bela-pharm, Vechta
L-Glutamine solution	Sigma-Aldrich, Munich
L-Lysine monohydrochloride	Sigma-Aldrich, Munich
LB medium	Carl Roth, Karlsruhe
Minimal essential medium (MEM)	ThermoFisher Scientific, USA
N-Hexane	Carl Roth, Karlsruhe
OneComp eBeads	ThermoFisher Scientific, USA
Paraformaldehyde 95 % (PFA)	Sigma-Aldrich, Munich
PBS tablet	Life Technologies, Darmstadt
Penicillin/Streptomycin	PAA Laboratories GmbH, Austria
Pierce Amino Acid Standard	ThermoFisher Scientific, USA
Polymorphprep™	Axis Shield, UK
Privigen hIgG 100 mg/ml (10 %)	CSL Behring, Marburg
Protease Inhibitor Mix	Roche, Mannheim
PureCol I®, Type I Collagen Solution (3.1 mg/ml)	Advanced BioMatrix, USA
RPMI 1640	Life Technologies, USA
Sodium azide (NaN_3)	Carl Roth, Karlsruhe
Sodium dihydrogen phosphate (0.2 M; NaH_2PO_4)	Sigma-Aldrich, Munich
Sodium hydrogen carbonate	ThermoFisher Scientific, USA
Sodium hydroxide (NaOH)	Carl Roth, Karlsruhe
Sodium periodate ($NaIO_4$)	Carl Roth, Karlsruhe
Solvent A	ThermoFisher Scientific, USA
Solvent B	ThermoFisher Scientific, USA
TissueTek OCT Compound	Sakura Finetek, USA
Triton-X 100	Carl Roth, Karlsruhe
Trypan blue solution	Sigma-Aldrich, Munich
Water with 0.1 % Trifluoroacetic acid (TFA)	Sigma-Aldrich, Munich

hypergrade for LC-MS/MS	
Xylazine 2 %	Ceva, France

8.1.3. Antibodies / Dyes / Fluorochromes

Table 6. Antibodies and dyes used to stain murine blood and tissues via FC.

Antibody	Clone	Fluorochrome	Dilution	Manufacturer
CD115	AFS98	APC	1:200	eBioscience, USA
CD117	2B8	PerCP-Cy5.5	1:200	BioLegend, Fell
CD11b	M1/70	APC, APC-Cy7	1:200	BioLegend, Fell
CD11c	HL3	APC	1:200	BD Biosciences, USA
CD19	6D5	BV605, FITC, PE, AF647	1:200	BioLegend, Fell
CD3e	145-2C11	APC	1:200	BD Biosciences, USA
CD45	30-F11	PE, BV421, APC-Fire	1:200	BioLegend, Fell
CD5	53-7.3	PerCP-Cy5.5	1:200	BioLegend, Fell
CD62L	MEL-14	BV605	1:200	BioLegend, Fell
CXCR2	SA044G4	APC	1:200	BioLegend, Fell
CXCR4	L276F12	BV421	1:200	BioLegend, Fell
F4/80	BM8.1	APC, PE	1:200	Tonbo Biosciences, USA
F4/80	T45-2342	BV510	1:200	BD Biosciences, USA
ICAM1	YN1/1.7.4	FITC	1:200	BioLegend, Fell
Ly6G	1A8	BV421, PE, FITC, PE-Cy7	1:200	BioLegend, Fell
MPO	8F4	Biotinylated	1:200	Hycult Biotech, Netherlands
NK1.1	PK136	APC	1:200	BioLegend, Fell
Streptavidin		AF647	1:400	ThermoFisher Scientific, USA
TGF-βRI	141231	PE	1:200	R&D Systems, USA

Table 7. Antibodies used for IHC of murine urinary bladder section.

Antibody	Clone	Fluorochrome	Dilution	Manufacturer
CD19	6D5	PE, AF647	1:200	BioLegend, Fell
Anti-GFP		AF488	1:1000	ThermoFisher Scientific, USA
DAPI			1:5000	ThermoFisher Scientific, USA
Ly6G	1A8	PE, AF647	1:200	BioLegend, Fell

Table 8. Antibodies used for neutrophil phenotyping in human whole blood.

Antibody	Clone	Fluorochrome	Dilution	Manufacturer
CD10	HI10a	APC	1:10	BioLegend, Fell
CD11b	ICRF44	APC-Cy7	1:20	BD Biosciences, USA
CD16	3G8	PE-Cy7	1:100	BD Biosciences, USA
CD45	5B1	VioGreen	1:100	Miltenyi Biotec, Bergisch Gladbach
CD62L	DREG-56	V450	1:20	BD Biosciences, USA
CD66b	80H3	FITC	1:50	Beckman Coulter, USA
CXCR2	5E8-C7-F10	PerCP-eFluor 710	1:20	ThermoFisher Scientific, USA
CXCR4	12G5	PE	1:10	BioLegend, Fell
HLA-DR	G46-6	APC	1:20	BD Biosciences, USA
ICAM1	HA58	APC	1:50	ThermoFisher Scientific, USA
PD-L1	MIH1	PerCP-eFluor 710	1:100	ThermoFisher Scientific, USA

Table 9. Isotype controls used for neutrophil phenotyping in human whole blood.

Isotype	Clone	Flurochrome	Corresponding human Antibody	Dilution	Manufacturer
mIgG1	MOPC-1	APC	CD10 APC	1:10	BioLegend, Fell
mIgG1	MOPC-1	V450	CD62L V450	1:80	BD Bioscience,
mIgG1	MOPC-1	APC	ICAM1 APC	1:50	BioLegend, Fell
mIgG1	MOPC-1	PE-Cy7	CD16 PE-Cy7	1:100	ThermoFisher Scientific,
mIgG1	MOPC-1	PerCP-eFluor 710	PDL1 PerCP-eFluor710	1:100	ThermoFisher Scientific,
mIgG1	MOPC-1	PerCP-eFluor 710	CXCR2 PerCP-eFluor710	1:80	ThermoFisher Scientific,
mIgG2a	G155-178	APC	HLA-DR APC	1:20	BD Bioscience
mIgG2b	G155-178	PE	CXCR4 PE	1:10	BD Bioscience

Table 10. Antibody and dye used for the NETosis assay.

Antibody/dye	Clone	Fluorochrome	Dilution	Company
CD66b	G10F5	PE	1:200	BioLegend, Fell
YOYO®-1 Iodide			1:10000	ThermoFisher Scientific, USA

Table 11. Fluorochromes and their corresponding absorption and emission spectra.

Flurochrome	Definition	Excitation laser / nm	Excitation $_{max}$ / nm	Emission $_{max}$ / nm
AF488	Alexa Fluor 488	488	496	516
AF647	Alexa Fluor 647	633	649	668
APC	Allophycocyanin	633	652	660
APC-Cy7	Allophycocyanin conjugated to Cyanine 7 dye	633	652	778
BV421	Brilliant Violet ™ 421	405	408	421
BV510	Brilliant Violet ™ 510	405	405	510
BV605	Brilliant Violet ™ 605	405	405	603
DAPI	4’,6-Diamidin-2-	405	358	461

	phenylindol			
FITC	Fluorescein isothiocyanate	488	490	517
PE	Phycoerythrin	488	565	575
PE-Cy7	Phycoerythrin conjugated to Cyanine 7 dye	488	565	778
PerCP-Cy5.5	Peridinin-chlorophyll-protein complex conjugated to Cyanine 5.5 dye	488	482	690
PerCP-eFluor710	Peridinin-chlorophyll-protein complex conjugated to eFluor710 dye	488	633	710
V450	BD Horizon™ Violet reagent 450	405	405	448
VioGreen	Vio® Dye Green	405	388	520
YOYO-1	Monomethine cyanine dye	488	491	509

8.1.4. Solutions / Buffers / Media

Table 12. List of solutions, buffers and media used during the study and their composition.

Solution/buffer	Preparation	Storage
20 % Paraformaldehyde (PFA)	20 g PFA	-20 °C
	80 ml PBS, heat to max. 70 °C, add NaOH until solution is transparent, fill up to 10 ml with PBS (adjust to pH=7.4)	
30% Sucrose	60 g D-Sucrose	-20 °C
	0.2 l P buffer	
Anaesthesia	8 ml 1x PBS (sterile)	4 °C
	1 ml Ketamine 10 %	
	1 ml Xylazine 2 %	
Blocking buffer (FC)	FACS	4 °C
	1:66 hIgG	
Blocking buffer (IHC)	1 % BSA in PBT	4 °C

Culture medium	RPMI 1640	4 °C, sterile
	10 % heat-inactivated FCS	
	1 % L-Glutamine	
	1 % Penicillin/Streptomycin	
Digestion medium	RPMI 1640	4 °C, sterile
	10 % heat-inactivated FCS	
	1 % L-Glutamine	
	1 % Penicillin/Streptomycin	
	100 µg/ml DNase I	
	0.5 mg/ml Collagenase	
FACS buffer	1 x PBS	4 °C
	0.2 % FCS	
	0.1 % NaN_3	
L-Lysine solution (0.2 M)	6.59 g L-Lysine monohydrate in 200 ml P-buffer (pH=7.4)	-20 °C
MACS buffer	1 x PBS	4 °C, sterile
	2 mM EDTA	
	0.6 % FCS	
Na_2HPO_4 (0.2 M)	28.4 g Na_2HPO_4 in 1 l dH_2O	RT
NaH_2PO_4 (0.2 M)	12.48 g NaH_2PO_4 in 1 l dH_2O	RT
P-buffer	243 ml Na_2HPO_4	-20 °C
	57 ml NaH_2PO_4	
	300 ml autoclaved dH2O (adjust pH=7.4)	
PBS (free of Ca^{2+} & Mg^{2+})	0.5 l deionized water	4 °C, autoclaved
	1 PBS tablet (5 g)	
PBT	0.05 % Triton-X 100 in 1 x PBS	4 °C
PLP-buffer	12.5 ml PFA 4 % in 50 ml (adjust pH=7.4)	4 °C, prepared freshly prior to use
	18.75 ml L-Lysine	
	18.75 ml P-buffer	
	0.106 g $NaIO_4$	
Protease Inhibitor Mix	1 tablet cOmplete Protease inhibitor cocktail	4 °C, prepared freshly prior to use
	10 ml sterile PBS	
RCB buffer	pH=7.3	4 °C, sterile filtered (0.2 µm)
	155 mM NH_4Cl	
	10 mM $KHCO_3$	

	0.1 mM EDTA	
Solvent A	0.1 % formic acid	RT, dark
Solvent B	0.1 % formic acid	RT, dark
	84 % acetonitrile	

8.1.5. Kits/Assays

Table 13. List of kits used during this study including the manufacturer.

Kits	**Company**
Affymetrix Clariom™ S mouse array	Affymetrix, USA
Bio-Plex Pro™ TGF-β Assay	Bio-Rad, USA
CD19 MicroBeads	Miltenyi Biotec, Bergisch Gladbach
CellROX™ Deep Red Flow Cytometry Assay Kit	ThermoFisher Scientific, USA
Genechip 3' IVT Express Kit	Affymetrix, USA
Fixation/Permeabilization Solution Kit	BD Biosciences, USA
Live/Dead® Fixable Near-IR Dead Cell Stain kit, for 633 or 635 nm excitation	Life Technologies, Darmstadt
Mouse Quantikine G-CSF ELISA kit	R&D Systems, USA
Neutrophil Isolation kit	Miltenyi Biotec, Bergisch Gladbach
pHrodo ® Green E. coli BioParticles® Conjugate for Phagocytosis	ThermoFisher Scientific, USA
RNase-Free DNase Set	Qiagen, Hilden
RNeasy® Micro Kit	Qiagen, Hilden

8.1.6. Machines / Equipment

Table 14. List of machines and equipment used during this study including the manufacturer.

Machine / Equipment	**Type**	**Company**
Autoclave	VX-150	Systec-Linden
Automated electrophoresis system	Agilent 2100 Bioanalyzer	Agilent Technologies, USA
Cell sorter	BD Aria III	BD Biosciences, USA
Centrifuge	5424R 5819R	Eppendorf, Hamburg
Cryostat	CM1950	Leica, Wetzler
Epifluorescence microscope	Axio Observer.Z1 and Apotome	Zeiss, Oberkochen

Flow cytometer	LSR Fortessa	BD Biosciences, USA
Fridge/Freezer	+4 °C -20 °C -80 °C	Liebherr, Biberach a.d. Riß
Heating block	Thermomixer R	Eppendorf, Hamburg
Homogenizer	ULTRA-TURRAX T10	IKA, Staufen
Ice machine	AF 100	Scotsman Ice-System, USA
Isoflurane anaesthetic device		UNO, Netherlands
IVC mouse cages	SealSafe PLUS	Tecniplast, Hohenpeißenberg
Laboratory Counter		BD Biosciences, USA
Laminar flow cabinet	Safe2020	ThermoFisher Scientific, US
LC-MS/MS	Orbitrap Elite mass spectrometer coupled to an Ultimate 3000 RSLCnano system	Dionex, Idstein ThermoFisher Scientific, USA
Microarray system	Affymetrix GeneChip Scanner-3000	Affymetrix, USA
Microplate reader	FLx-800 LB 90 Mithra	BioTex, Bad Friedrichshall Berthold Technologies, Bad Wildbad
Multichannel pipette	Pipet-Lite XLS	Mettler Toledo, Gießen
Multiplex Reader	Bio-Plex System 100	Bio-Rad, USA
NanoDrop	ND-1000	PeqLab, Erlangen
Neubauer counting chamber	Neubauer improved	Hecht-Assistant, Sondheim
Optical microscope	DMIL	Leica, Wetzler
Pipettes		Eppendorf, Hamburg
Shaker	MTS2/4	IKA, Staufen
Thermostat Cabinet		Aqualytic, Dortmund
Ultra-Performance Liquid Chromatography	ACQUITY-UPLC coupled to AccQ Tag Ultra-UPLC column	Waters, Eschbach
Vortexer	Vortex-Genie 2	Scientific Industries Inc., USA
Waterbath	TW12	Julabo, Seelbach

8.1.7. Consumables

Table 15. List of consumables used during this study including the manufacturer.

Consumables	**Company**
6-, 12-well plate	TPP, Switzerland
Centrifuge tube	Greiner Bio One, Nürtingen
ChromID™ CPS® Elite agar plates	Biomérieux, France
Coverslips 40x24mm	Oehmen Labortechnik, Essen
Cryomolds	Weckert Labortechnik, Kitzingen
Disposal bag	Oehmen Labortechnik, Essen
Eppendorf tube (0.2, 0.5, 1.5, 2.0 ml)	Sarstedt, Nürnbrecht
Falcon cell strainer 40 µm	BD Biosciences, USA
Falcon cell strainer 70 µm	BD Biosciences, USA
Flow cytometer tube	Sarstedt, Nürnbrecht
Gloves	B Braun, Melsungen
Heparinised capillary tubes	Brand, Wertheim
Hydrophobic pen	Dako, USA
Hypodermic needle 23G 0.6 x 25 mm	BD Biosciences, USA
Hypodermic needle 26G 0.45 x 23 mm	BD Biosciences, USA
Hypodermic needle 27G 0.4 x 13 mm	BD Biosciences, USA
Hypodermic needle 30G 0.3 x 13 mm	BD Biosciences, USA
Insulin syringe U-100	BD Biosciences, USA
Leukosilk	BSN Medical, Hamburg
MACS LS Columns	Miltenyi Biotec, Bergisch Gladbach
Multichannel pipette reservoir	Brand, Wertheim
Nylon net 100 µm	Oehmen Labortechnik, Essen
Petri dish 94 x 16 mm	VWR International, Radnor, USA
Pipette filter tip 0.2 – 10 µl	Greiner Bio One, Nürtingen
Pipette filter tip 100 – 1000 µl	Greiner Bio One, Nürtingen
Pipette filter tip 20 – 200 µl	Greiner Bio One, Nürtingen
Pipette tip (10, 200, 1000, 5000 µl)	Greiner Bio One, Nürtingen
Serological pipette (5, 10, 25 ml)	Greiner Bio One, Nürtingen
Silicone isolators	Science Services, Munich
Super Frost glass slides	SuboLab GmbH, Pfinztal-Söllingen
Syringe 1 ml	BD Biosciences, USA
Syringe 5 ml	BD Biosciences, USA

8.1.8. Software / open source platforms

Table 16. Software and open source platforms used to perform data analysis and illustration.

Software	**Company**
Adobe Illustrator CS5	Adobe, USA
Affymetrix Transcriptome Analysis Console Software	Affymetrix, USA
Bio Plex Manager 4.1.1.	Bio-Rad, USA
Cytoscape	Institute of Systems Biology, USA
Endnote X9	Thomson Reuters, USA
FACSDiva 6.0	BD Biosciences, USA
FlowJo 10	FlowJo LLC, USA
GraphPad Prism6	GraphPad, USA
ImageJ	NIH, USA
Imaris 7.6.5	Bitplane, United Kingdom
Mascot search engine	Darryl Pappin and Alan Bleasby, UK
Microsoft Office 2016	Microsoft Corporation, USA
Progenesis LC−MS software	Nonlinear Dynamics Ltd., UK
Proteome Discoverer Software	ThermoFisher Scientific, USA
R – programming language	R Development Core Team, New Zealand
UniProtKB/Swiss-Prot database	UniProt Consortium, UK, Swiss, USA
Zen blue	Zeiss, Oberkochen

8.2. Methods

8.2.1. Syngeneic adoptive transfer of CLL splenocytes into immunocompetent mice

Primary splenocytes were harvested from the transgenic Eμ-TCL1 mice that were kept at germ-free conditions at the animal facilities of the German Cancer Research Centre (Heidelberg) until they reached a tumour load exceeding 95 % in the PB [240]. For the adoptive transfer model, 2 x 10^7 primary or secondary Eμ-TCL1 splenocytes were transplanted intravenously into 8-12-week old female C57BL/6 mice.

8.2.2. Preparation of PB samples and *ex vivo* functional analyses

8.2.2.1. Blood isolation from mice ex vivo and in vivo

For FC staining, peripheral blood was collected from the tail vein of mice with heparinized capillaries. For plasma preparation, venous blood was harvested by sacrificing mice via CO_2 inhalation and puncturing the right heart chamber with a syringe containing 5-10 µl 0.5 M EDTA.

8.2.2.2. Preparation of single cell suspension from peripheral blood

Single cell suspensions were obtained by lysing erythrocytes of 20 µl PB samples with the red cell lysis buffer (RCB, 37 °C). Subsequently, samples were incubated for 5 min at room temperature (RT). Erylysis was then stopped with 2 ml cold FACS buffer. The cells were pelleted by centrifugation (5 min, 300 g, 4 °C) and supernatants were discarded.

8.2.2.3. Phagocytosis assay ex vivo

Each whole blood sample was incubated with 0.01 mg/ml pHrodo® Green *E. coli* BioParticles® Conjugate for Phagocytosis for 15 min at 37 °C. Controls were generated by incubating whole blood samples for 15 min at 4 °C with pHrodo® particles. The incubation was stopped by placing the samples on ice and adding 1 ml ice-cold FACS buffer. Samples were centrifuged (300 g, 5 min, 4 °C) and the supernatants were discarded. Erylysis was performed as described above (refer to 8.2.2.2) and centrifuged to obtain leukocyte cell pellets. Subsequently, extracellular molecules were stained for flow cytometry analysis.

8.2.3. Murine UPEC infection model and tissue digestion

8.2.3.1. Transurethral UPEC infection in vivo

Uropathogenic *E. coli* strain 536 (O6:K15:H31) were cultured for 3 h at 37 °C in LB medium. Bacteria were collected by centrifugation (1200 g, 20 min, RT) and re-suspended in 1 ml of sterile PBS. Female mice older than 8 weeks and with a tumour burden higher than 40% were anaesthetized with Xylazine and Ketamine injection (concentration: 10/80 mg/kg, i.p.). Subsequently, direct inoculation of 5 x 10^8 *E. coli* 536 (in PBS; 0.1 ml) into the bladder was performed using a soft polyethylene catheter.

8.2.3.2. Preparation of single cell suspension from bladders

Infected mice were sacrificed 18-21 h post-UPEC infection and bladders were harvested. Single cell suspensions from bladders were obtained by initial mechanical disruption with a scalpel and subsequent enzymatic digestion in RPMI1640 which was supplemented with 10 % heat-inactivated FCS, 1 mM L-Glutamine, 100 µg/mL Penicillin/Streptomycin, 0,5 mg/ml collagenase and 100 µg/ml DNase I (45 min, 150 g, 37 °C). After enzymatic digestion, cell suspensions were filtered through a 100 µm nylon mesh and subsequently washed with FACS buffer.

8.2.3.3. Preparation of single cell suspension from blood, BM, spleen and lung for phenotyping

Uninfected mice were sacrificed after a mean tumour load of at least 70 % was detected in the circulation. Tissues were harvested. The harvest of single cell suspensions from blood, BM and bladder have been described in 8.2.2, 8.2.7 and 8.2.3 respectively. Single cell suspensions from lung and spleen were obtained by initial mechanical disruption with a scalpel and subsequent enzymatic digestion in RPMI1640 which was supplemented with 10 % heat-inactivated FCS, 1 mM L-Glutamine, 100 µg/mL Penicillin/Streptomycin, 0,5 mg/ml collagenase and 100 µg/ml DNase I (45 min for lung and 15 min for spleen at 37 °C). After enzymatic digestion, cell suspensions were filtered through a 100 µm nylon mesh and subsequently washed with FACS buffer.

8.2.4. Flow cytometry (FC) staining

8.2.4.1. FC staining of murine samples

Flow cytometric visualisation is performed by analysing size (FSC), granularity (SSC) and molecule-bound fluorochromes. Additionally, cell surface and intracellular molecules can be detected by fluorochrome-coupled antibodies. For cell surface staining, single cell suspensions were subjected to incubation for 20 min at 4 °C in the dark with a staining volume of 100 µl of fluorochrome-conjugated antibodies and 1.5 mg/ml human immunoglobulins diluted in FACS buffer. For intracellular staining, single cell suspensions were fixed with 4 % PFA for 10 min at 4 °C and incubated with permeabilization buffer for 15 min at 4 °C. Flurochrome-conjugated antibodies were diluted in a staining volume of 100 µl of permeabilization buffer and stained for 20 min at 4 °C in the dark.

Antibodies bind their corresponding epitopes and help to retrieve the signal through their tagged fluorochromes in a specific channel. Apart from the direct approach using fluorochrome conjugated antibodies, an indirect approach available may also be performed. This method involves two staining steps as it uses a primary, unlabelled antibody binding to the corresponding antigen and a second antibody conjugated to a fluorophore which binds to the primary one. An advantage of the indirect approach is that fluorescent signals can be amplified as several secondary antibodies may bind to the primary antibody. In this study, both methods were used. Human immunoglobulins reduced unspecific F_c-receptor binding during the incubation. For a list of antibodies, please refer to Table 6. In order to distinguish between live and dead cells, the Live/Dead Fixable Dead Cell stain kit was used in conjunction with antibodies. Total cell numbers were obtained by adding a specific number of Calibrite APC beads prior to flow cytometric analysis. Finally, flow cytometric measurement was executed on a BD LSR Fortessa II or BD Aria III and data was analysed with FlowJo 10 software.

Total number of cell subsets were calculated according to the following formula:

$$Cell\ subset\ in\ 1\ ml \text{ or } organ = \frac{measured\ cell\ subset\ in\ numbers\ \times\ 10{,}000\ beads\ \times\ factor}{measured\ beads\ in\ numbers}$$

The factor depends on the amount of sample used for the FC staining. For example, if only 20 µl of PB was processed for FC staining, the factor 50 was used to obtain the numerical cell subset value in 1 ml of PB. Furthermore, protein expression was quantified by using the geometric mean of fluorescence intensity which will be termed as mean fluorescence intensity (MFI) in this study.

8.2.4.2. FC staining of human whole blood samples

In regard to human samples, the ethics committee of UK Essen was consulted, and ethics approval was issued under 14-6080-BO. In order to minimize any neutrophil stimulation through EDTA, human blood samples from untreated CLL patients were collected in citrate vacutainers by Prof. Dürig at the Clinic of Haematology at the University Hospital Essen.

50 µl were used for the whole blood neutrophil staining for flow cytometric analysis. The whole blood was stained for 20 min at 4 °C with a plethora of surface markers

elucidating the maturation and activation levels of neutrophils (Table 8 and Table 9). In addition, corresponding isotype antibodies were used for later background signal subtraction. The staining process was stopped, and erythrocytes were depleted by adding erylysis buffer. After an incubation of 5 min at RT, samples were centrifuged (300 g, 5 min, RT) and 10,000 APC beads for quantification purposes were added subsequently. Samples were measured on the BD LSR Fortessa.

8.2.5. Histological analyses of infected murine urinary bladder sections

8.2.5.1. Fixation of organs and immunohistochemistry (IHC)

For visualization of neutrophils during CLL and UTI in the murine urinary bladder, immunohistochemistry was performed on bladder sections. To this end, infected mice were sacrificed 21 h post-UPEC infection. Bladders were harvested and fixed to conserve the organs by immersing organs in PLP-buffer (>12 h, shaking, 4 °C). In order to remove the fixative agent, bladders were washed twice with P-buffer and were then placed in 30 % sucrose solution (>12 h, shaking, 4 °C). After cryoprotection with sucrose, urinary bladders were embedded in OCT and were frozen in n-hexane cooled with dry ice and subsequently stored at -80 °C. This freezing procedure enables a gentle approach to maintain tissue structures.

Consecutive sections of 10 µm were cut on a cryostat at -20 °C, placed onto Super Frost Plus glass slides followed by heat-fixation (10 min, 70 °C). Next, sections were rehydrated with 0.5 ml PBT per slide for 5 min. Murine urinary bladder sections were treated with blocking buffer to avoid unspecific staining (0.5 ml/slide, 1h, RT). A hydrophobic pen marked the tissue section in order to concentrate the antibody staining solution to the staining region. The antibody staining allows visualisation of certain cell types via distinct epitopes by fluorescence microscopy.

Murine urinary bladder sections could only be labelled with a limited number of fluorochromes due to the microscopic set up. Thus, consecutive sections were used to retrieve as many biological information as possible. The antibodies that were used for staining can be found in Table 7. Antibodies were diluted in 200 µl blocking buffer per section and incubated for 1 h in the dark (RT). After each staining step, three washing steps were performed (5 min in PBT). Subsequently, DAPI was diluted 1:5000 and incubated for 5 min. When the staining was completed, the sections were embedded in ImmuMount and sealed with a cover slip. Once dried, urinary bladder sections were imaged with either a 10x, 20x or 40x magnification by the Zeiss Axio

Observer.Z1 and Apotome at the Imaging Centre Essen and images were acquired using the Orca Flash camera.

8.2.5.2. Image acquisition and processing

As a tiling approach was performed to record the entire bladder in high resolution, the obtained images were stitched and analysed by the ZEN Software and ImageJ. The exact procedures include stitching, image processing, mask generation, conversion into point maps and border drawing. A short summary of the steps will be provided here. After stitching, all channels of an image were adjusted for colour balance. Subsequently, a segmentation of subcompartments within the murine urinary bladder was performed by drawing a defined border for lumen, epithelium, connective tissue and muscle. Binary masks of each fluorescent channel were generated and converted into point maps. Additionally, point maps were stacked onto the segmented areas to represent the spatial distribution of each cell subset. An ImageJ output allows the final quantification of cells in different areas of the bladder, cellular neighbours and distance to the lumen analysis. The entire image processing was a semi-automatic process performed with the help of R, the programming language. The script has been gradually developed by Julia K. Volke, Jenny K. Bottek, Anthony Squire and Camille Soun.

8.2.6. Murine cytokine analyses

8.2.6.1. Murine blood plasma preparation

Blood was obtained by cardiac puncture as described above (8.2.2.1). The EDTA-treated blood was centrifuged (10 min, 13,000 rpm, 4 °C) and the supernatant was transferred into a cryovial and supplemented with 10 % (v/v %) complete protease inhibitor mix to prevent cytokine degradation. Samples were then processed immediately or frozen in liquid nitrogen.

8.2.6.2. Urinary bladder homogenate preparation

Murine bladders were harvested from mice 18 h post-infection and mechanically disrupted in 0.5 ml 1x sterile PBS supplemented with complete protease inhibitor mix for 30 s by using an ULTRA-TURRAX®. The homogenized samples were centrifuged (10 min, 13,000 rpm, 4 °C) and supernatants were isolated. Supernatants were shock frozen with liquid nitrogen and stored at -80 °C.

8.2.6.3. TGF-β cytokine analysis

TGF-β1, TGF-β2 and TGF-β3 levels were measured in murine blood plasma on the Bio-Plex System 100 by using the flow cytometry-based beads assay Bio-Plex Pro™ TGF-β Assay using the standardised protocol provided.

8.2.6.4. G-CSF Enzyme-linked immunosorbent Assay (ELISA)

Murine bladder homogenates and murine blood plasma were obtained as described above. Both, bladder supernatants and blood plasma were analysed through the Mouse G-CSF Quantikine ELISA Kit according to the manufacturer's protocol.

8.2.7. Neutrophil isolation and proteomics workflow

8.2.7.1. Neutrophil cell isolation from circulation and bone marrow from control and CLL mice

A proteomic analysis was performed on murine neutrophils from control and CLL conditions. As neutrophils are generated in the bone marrow and enter the circulation upon maturation and for antimicrobial defence, both, bone marrow and circulating neutrophils were isolated in a two-step approach [24]. For this study, neutrophils from steady state conditions were isolated. First, cells were negatively isolated via magnetic cell separation (MACS). In this negative isolation method, all cell subsets except for target cells are magnetically labelled. Once the cell suspension is passed through a magnetic field, the cell population of interest passes through due to the lack of magnetic labelling and all other cells are retained [268]. In order to yield a high purity of neutrophils, the negative neutrophil isolation was paired with a CD19 depletion to increase the magnetic labelling of CLL B-cells. In general, the number of murine neutrophils in the PB is low compared to the human levels.

Isolated populations were stained with PerCP-Cy5.5 conjugated anti-CD5 and BV605™ conjugated anti-CD19 antibodies to visualise any remaining CLL B-cells. Additionally, BV421™ conjugated Ly6G antibody, a murine neutrophil marker, was used to perform a positive neutrophil isolation during FACS [269]. The cell sorting strategy has been illustrated in Figure 7. Neutrophils were centrifuged (10 min, 300 g, 4 °C) and the entire supernatant was discarded. Cell pellets were shock frozen in liquid nitrogen and stored in -80 °C. Finally, samples were processed for proteomic

analysis. The total numbers of isolated neutrophil were sufficient to perform proteomic analysis and are listed in Table 18.

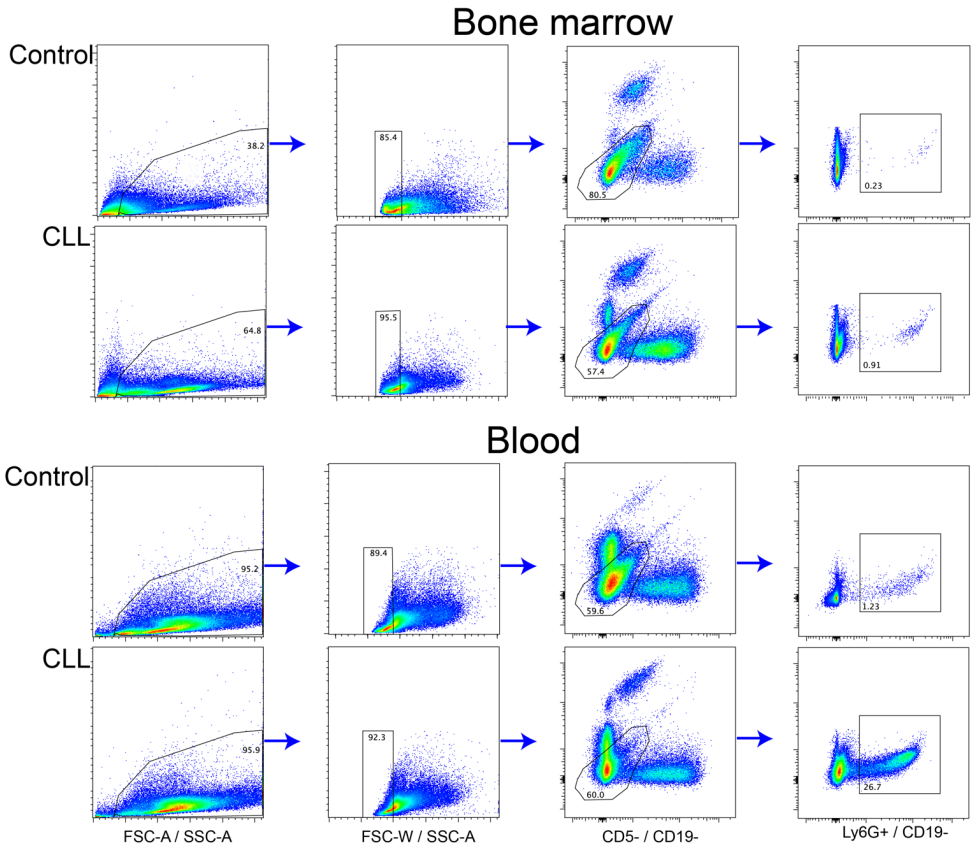

Figure 7. The gating strategy for neutrophil isolation from BM and blood from control and CLL mice.

CLL induction was performed through i.v. injection of primary CLL splenocytes into syngeneic WT mice. Neutrophils were collected from the BM and blood through CD19 depletion in a negative neutrophil MACS isolation approach. After MACS isolation, cells were stained for CD5, CD19 and Ly6G. First, cells were gated for live cells and subsequently for single cells. Next, cells were gated for $CD5^{-}CD19^{-}$ and then gated for positively selected for $Ly6G^{+}$ isolation through FACS.

8.2.7.2. Proteomics workflow

The proteome of a cell describes all proteins expressed on the surface and within a cell at a given time. The plasticity of the proteome differs from cell to cell and changes during any condition. Consequently, the proteome might reveal any underlying molecular differences. The abundance of each protein on and within the cell was measured by liquid chromatography coupled to tandem mass spectrometry via electrospray ionization (LC-ESI-MS/MS) at the Medical Proteomics Centre, Ruhr-University Bochum. While the sample generation and preparation were performed by me, the entire workflow for the proteomics was performed in Bochum. Birgit Korte and Thilo Bracht performed protein digestion and label-free analysis, while protein

identification, quantification and data analysis was performed by Thilo Bracht. Additional pathway and enrichment analysis was performed by me.

8.2.7.3. Peptide quantification and digestion

As described above, the analyses were conducted on positively isolated neutrophils (Figure 7). As more neutrophils were retrieved from the BM as needed, spare samples were generated for peptide quantification. Approximately, 100,000 neutrophils in the replicates yielded a sufficient protein content between 1.5 – 2 µg. This was determined precisely through quantitative amino acid analysis performed on an ACQUITY-UPLC equipped with AccQ Tag Ultra-UPLC column and calibrated with Pierce Amino Acid Standard as described by [270]. For the main study, neutrophil samples were alkylated with 15 mM iodoacetamide, digested with 50 ng trypsin overnight and subsequently treated with 0.5 % TFA at 37°C for acidification as described in [271]. Then, peptides were dried through vacuum centrifugation and dissolved in 0.1% TFA.

8.2.7.4. Peptide quantification and digestion

350 ng peptides in a volume of 15 µl 0.1 % TFA were loaded onto an Orbitrap Elite mass spectrometer coupled to an Ultimate 3000 RSLCnano system for label-free analysis. The peptides were preconcentrated for 7 min on a trap column (Acclaim PepMap 100, 300 µm x 5 mm, C18, 100 Å, flow rate 30 µl/min). Next, peptides were separated on an analytical column (Acclaim PepMap RSLC, 75 µm x 50 cm, nano Viper, C18, 2 µm, 100 Å) by a gradient from 5 % to 40 % solvent B over 98 min (flow rate 400 nl/min; column oven temperature 60 °C). Through a data-dependent acquisition mode, full MS scan spectra were obtained in the Orbitrap analyser. The most abundant peptides were then selected for MS/MS analysis. Tandem spectra were analysed in the linear ion trap post peptide fragmentation by collision-induced dissociation. These methods and MS operating settings have been previously described [272].

8.2.7.5. Protein identification and quantification

Peptides were identified using Proteome Discoverer Software. The mass spectra were searched against UniProtKB/Swiss-Prot database restricted to *mus musculus* using the Mascot search engine. Search parameters have been previously described

[271]. Ion intensity-based label-free quantification was conducted by using Progenesis LC−MS software. All runs were aligned to a reference run automatically chosen by the software, and a master list of features considering *m/z* values and retention times was generated. Peptide identifications were exported from Proteome Discoverer and imported in Progenesis LC−MS to be matched to the respective features. Peptide counts with a minimum of two peptides, a false-discovery rate (FDR)-adjusted p- value ≤ 0.05, and an absolute fold change ≥ 1.5 were considered to be significantly differentially expressed and used for further evaluation.

8.2.7.6. Statistical rationale and pathway analysis

Statistical analysis was performed using R. In total, data sets from four groups were available. Notably, only results from the following groups will be analysed in this study to identify alterations in neutrophils by CLL: “BM CLL vs. control” and “Blood CLL vs. control”. These data were tested for statistical significance using the Mann-Whitney *U* test. The resulting p-values were adjusted to control the FDR.

Comparisons of differently abundant proteins in neutrophils were achieved by employing bioinformatics analyses, such as principal component analyses, volcano plotting, unsupervised hierarchical clustering and molecular network approaches through Cytoscape. Possible target molecules were assessed by integrating results from the different bioinformatics analyses. By integrating and ranking the results from the different network approaches, the predictive potential of candidate molecules can be assessed with respect to their antibacterial function, regulation of neutrophil responses and immunosuppressive signalling.

8.2.8. 3D-migration assay of BM neutrophils from control and CLL mice

8.2.8.1. Neutrophil isolation from bone marrow

After sacrificing mice, tibia and femur were collected. Their ends were cut open and the bone marrow was flushed with a 26 G needle fitted to a syringe with 5-10 ml sterile PBS into a petri dish. By pipetting the bone marrow suspension up and down a single cell suspension was generated and passed through a 70 µm filter mesh. Next, cells were centrifuged (10 min, 300 g, 4 °C) and the supernatant was discarded. In order to purify leukocytes, samples were erylysed with RCB buffer (2 min, RT). Erylysis was stopped by adding 1 ml PBS followed by centrifugation (10 min, 300 g,

4 °C). The supernatant was discarded, and cell pellets were processed for the Neutrophil Isolation Kit and isolated via MACS™ Technology.

8.2.8.2. Embedding of neutrophils in 3D-migration assays

In order to generate 3D-migration chambers, modified silicone isolators were pressed on a glass slide and covered with coverslips (Figure 8). This process must be performed sterile, without any dust inclusion so that all migration chambers are tightly pressed to the cover slip and glass slide. The collagen gel formula was prepared according to the protocol described in Table 17.

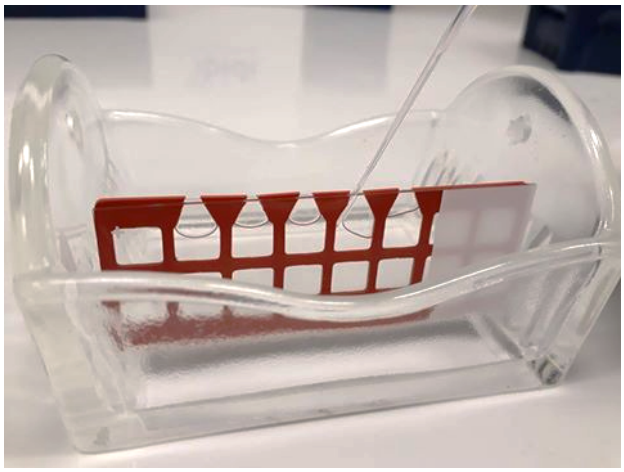

Figure 8. 3D-migration assay chambers.

Neutrophils were harvested from the BM and isolated via MACS technology. Subsequent embedding into a 3D-collagen scaffold was possible by generation migration chambers with silicone isolators. The silicone isolator (red) was placed on a glass slide and pressed to ensure air-tight sealing. One side of the silicone isolator was cut to leave triangular openings. These openings formed filling pockets for the gel. In total, five migration chambers were created this way. A cover glass was placed on top of the silicone isolator. After insertion of the gel as shown through the capillary tip, the opening of the silicone isolators was topped up with dental wax to keep the migration chamber air-tight and protected.

Next, 30 µl of the gel was filled into each chamber by using pre-cooled capillary tips. All components and steps to generate 3D-collagen matrix were prepared and performed on ice. The glass slides were then placed into an appropriate rack (Figure 8) facing an upright position and an incubation time of 45 min at 37 °C and 5 % CO_2 was set for gel polymerization. The polymerized gel was topped up with medium supplemented with 200 ng/ml CXCL2 or just plain medium (control). Dental wax was heated and used to seal the top of all migration chambers.

Table 17. The collagen gel composition for the 3D-collagen matrix.

Component	Final concentration	Volume / µl
$NaHCO_3$	(v/v %) 7,5 %	13
MEM	(v/v %) 12,5 %	22
PureCol I	3,1 mg/ml	140
Cell suspension	$7{,}7x10^6$ cells/ml	65

Time-lapse imaging was started 40 min post-chemokine addition and recording was performed every 30 s for a total time span of 30 min with a 100x magnification on the Zeiss Axio Observer.Z1. In order to enable 3D-visualisation, a z-stack (range: 40 µm; step size: 8 µm) was acquired. The field of view was chosen to be in the centre of the gel in close proximity to the medium edge as shown in Figure 9.

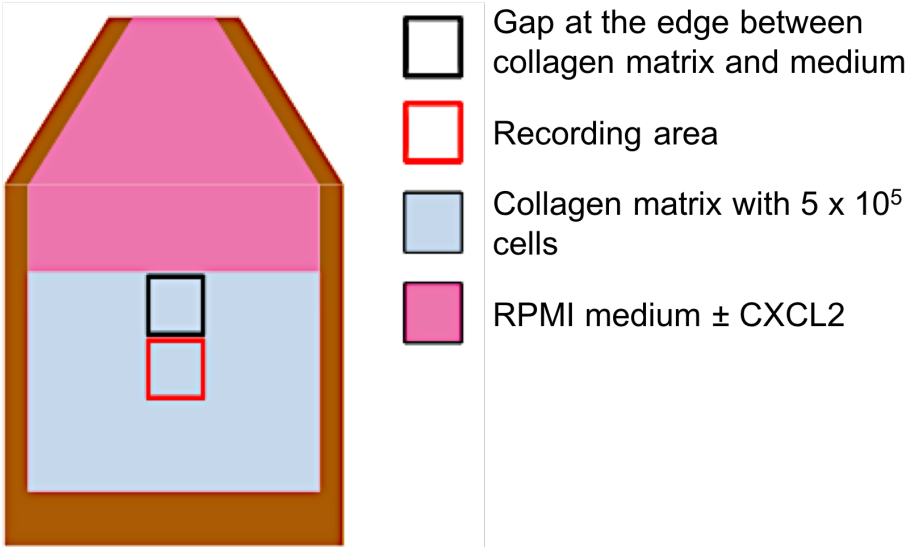

Figure 9. Recording area for the 3D-migration assay.

In order to perform a reproducible 3D-migration assay, a consistent recording area for all 3D-migration assays was chosen as illustrated in this figure. The gap between the collagen matrix and medium (±CXCL2) was always chosen to be a field of view during a 100x magnification.

For analysis, videos were compromised in size and subsequently subject to a Gaussian Blur Filter with a sigma radius of 3.0 on ImageJ. The contrast was optimised for ideal individual cell visualisation. Finally, cell migration was quantified through the ImageJ Plugin TrackMate. The evaluation and experiments were performed with Elena de Dios Panal under my supervision.

8.2.9. Modification of the NETosis assay with human neutrophils and plasma

Neutrophils have the capacity to induce NETosis in addition to phagocytosis and degranulation [23]. Their ability to form NETs was investigated in this approach. Human plasmas were freshly isolated from untreated CLL and healthy donors via Polymorphprep™ gradient centrifugation. The neutrophil isolation from the healthy donor blood started not later than 5 h after blood collection and was performed at RT, if not stated otherwise. The PBS used during this NETosis assay is free of any Ca^{2+} and Mg^{2+} ions. Gradient centrifugation was performed in a 15 ml falcon tube by carefully layering 3-5 ml peripheral blood from an EDTA-Vacutainer on top of 5 ml of Polymorphprep™. For successful neutrophil isolation, the phase interphase must be clear with little or no turbulences. Gradients were obtained by centrifugation (30 min, 450 g, without a brake), in which six phases have formed. The human plasma (top phase) was transferred into a cryovial and instantly frozen at -80 °C. Neutrophils were carefully collected into a new tube from the corresponding phase (90-95 % neutrophil purity; Figure 10) and subsequently washed with 10 ml PBS. Next, cells were pelleted (5 min, 200 g) and erylysed for 4 min with RCB Buffer. After stopping erylysis with 10 ml PBS, cells were centrifuged again and counted after resuspension in pre-heated RPMI medium in a Neubauer chamber.

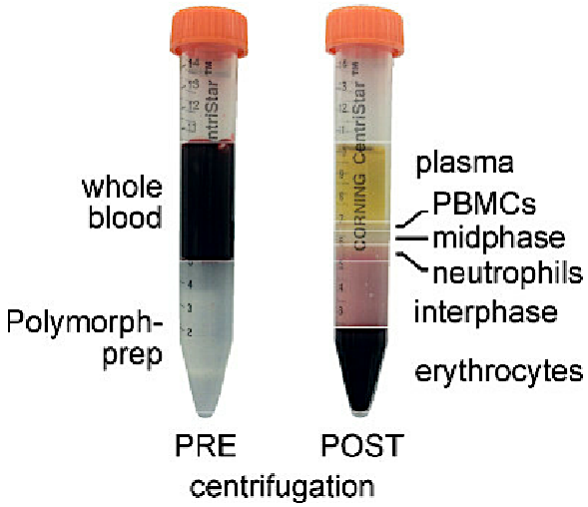

Figure 10. Human blood prior and after gradient centrifugation with Polymorphprep™

After gradient centrifugation at 450 g for 30 min without brake, plasma and neutrophils were isolated from the indicated phases. Erythrocytes form the bottom phase, followed by an interphase of Polymorphprep™ and then a neutrophil phase would top up the interphase. The top phase forms the human plasma (adapted from [273]).

A perforated plate was prepared with round cover slips (diameter: 12 mm). The final volume of 0.5 ml per well consists of 2 x 10^5 cells, human plasma and a final concentration of 25 nM PMA for stimulated samples. In order to investigate the role

of human plasma on the NETosis capacity of neutrophils, 5 µl of human plasma was added per well. The plasma was derived from a healthy donor or a CLL patient as described before. The NETosis assay was performed by incubating the cells for 3 h at 37 °C and 5 % CO_2. Next, the samples were fixed with 0.2 ml 4 % PFA for 10 min. All subsequent steps were performed at RT, not sterile and carefully treated to prevent disruption of NETs. In detail, all buffers and solutions were never added directly onto the cover slips. After incubation with PFA, cells were washed three times with PBS for 5 min each. Subsequently, samples were treated with blocking buffer for 20 min at 37 °C. Finally, samples were stained for 1 h with 0.2 ml PBS supplemented with CD66b conjugated to PE and YOYO-1. Cover slips were placed onto a glass slide and mounted with mounting medium. An overview was constructed with a 100x magnification while zoom-ins were generated with a 400x magnification.
The quantitative NETosis analysis using a DNA mask, was based on the images from the 100x magnification. The area of NETs was determined by including signals larger than 10 pixels. Taking into account that a perfect circle would have a value of 1.0, all cell signals with a circularity value larger than 0.4 were not considered for the analysis. The NETosis assay and analysis were performed with Elena de Dios Panal as part of her master thesis under my supervision.

8.2.10. Statistical analysis

Comparisons were based on using non-parametric Mann-Whitney *U* test, Kruskal-Wallis tests or two-way ANOVA with Bonferroni post-hoc. Linear correlation analyses were performed by F-test. The confidence of regression lines was assessed through R^2 and p values. These tests were performed by GraphPad Prism 6. Data distribution was not tested for *in vivo* studies due to the limited sample size. For migration assays, appropriate assumptions of data (normal distribution or similar variation between experimental groups) were examined by D'Agostino and Pearson omnibus normality test before statistical tests were conducted. Results are expressed as mean, if not indicated otherwise ± standard deviation (SD; *p ≤ 0.05; **p ≤ 0.01; ***p ≤ 0.001 and **** p ≤ 0.0001).

9. Results

To establish an apt CLL model to study neutrophils, littermate mice were injected with primary CLL splenocytes from leukemic Eμ-TCL1 donor animals. As different clone batches were used for the induction of CLL, the degree of the CLL induction will be described through the proportion of tumour load of CLL malignant B-cells ($CD5^+CD19^+$) in the bloodstream. In order to maintain the reproducibility of the studies, infection experiments were performed after a certain frequency of CLL malignant B-cells was reached in the circulation.

9.1. CLL induction

9.1.1. CLL induction and immune cells during disease progression

In order to quantify CLL, neutrophil and monocyte levels post-CLL induction, a kinetic study has been performed (Figure 11). In order to evaluate the findings statistically, a two-way ANOVA with Bonferroni post-hoc was calculated as previously described (8.2.10). The transplantation of cells was engrafted and the body weight of mice has increased (Figure 11A). Weight differences became apparent on 56 days post-induction of CLL and the gap between control and CLL-induced mice continued to rise until the end of the study. Simultaneously, CLL cells gradually rose in the peripheral circulation with first signs of variation becoming apparent at 28 days post CLL induction (Figure 11B). In contrast, initial fluctuations have been observed throughout the study for neutrophil numbers in circulation, mostly being similar in numbers with a slight tendency to rise during the final phase of the study (Figure 11C). Furthermore, monocyte levels were measured throughout the study and were gradually increasing with a steep rise towards the end of the kinetic (Figure 11D). Both immune cell levels are subject to higher fluctuations during CLL progression. Subsequent experiments were based on the percentage of CLL malignant B-cells ($CD5^+CD19^+$) in the circulation.

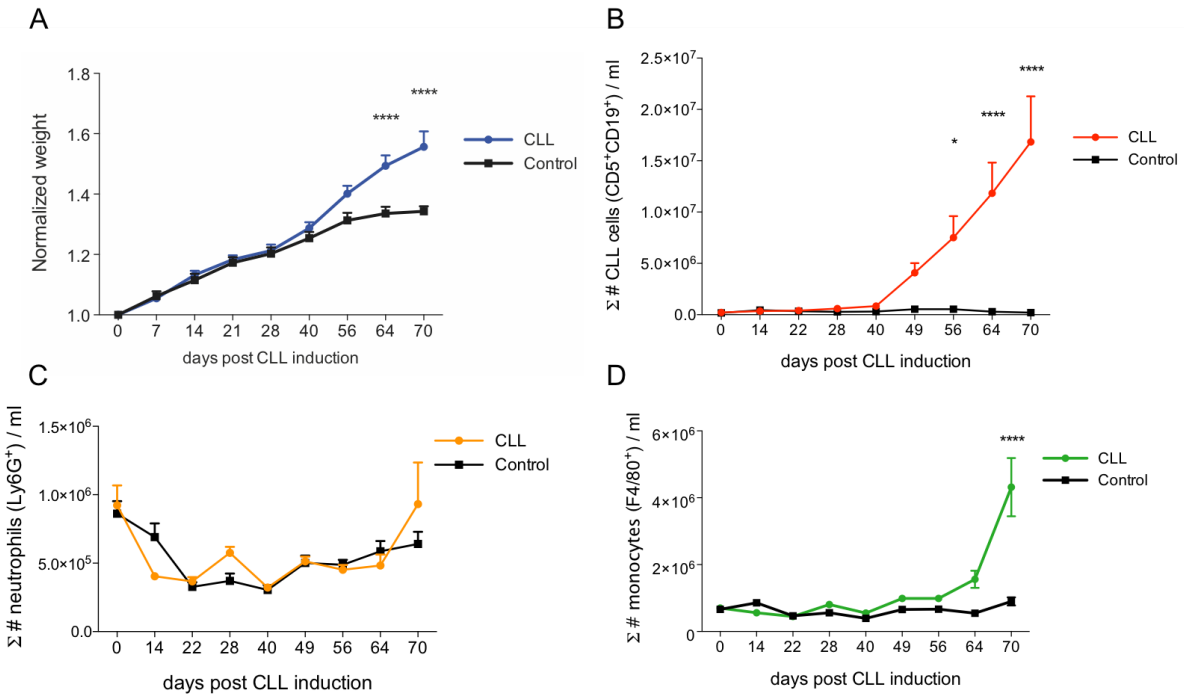

Figure 11. Secondary CLL in immunocompetent C57BL/6 wildtype mice.

CLL induction was performed as previously described. Weight was recorded and blood was withdrawn at various time points. Subsequent flow cytometric analysis allowed quantification of immune subsets. (A) Normalized weight curves for control and CLL mice. (B) Kinetics of $CD5^+CD19^+$ cells in CLL-induced mice. (C) Neutrophil kinetics and (D) monocyte levels per ml blood post CLL induction (Control n=10; CLL n=10)). Statistical test: Two-way ANOVA with Bonferroni post-hoc.

In Figure 12, the splenomegaly in CLL-induced mice is shown in bottom panel, while control spleens are shown in the top. Both, control and CLL-induced mice gradually increased their weight compared to their initial weight at the beginning of the study.

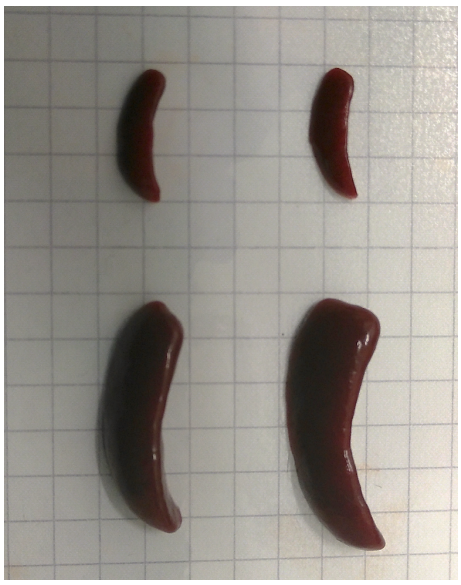

Figure 12. Splenomegaly in CLL mice.

CLL induction was performed as previously described and spleens were harvested 70 days post CLL induction. Murine spleens from control (top; n=2) and CLL (bottom; n=2) mice are shown. Splenomegaly is one of the clinical features during CLL progression. In summary, CLL spleens are increased in size and weight and contribute to the weight gain in CLL mice.

9.1.2. CLL load in organs

The presence of malignant B-lymphocytes in non-lymphoid organs has not been described yet. In order to identify the precise localisation of the CLL microenvironment, the presence of malignant B-lymphocytes in other organs outside the lymphatic system was tested via flow cytometric analysis of the peripheral blood, BM, spleen, lung and bladder (Figure 13A). The Kruskal-Wallis test was used to determine if there are statistically significant differences among the groups.

For this, CLL mice were injected with CLL splenocytes from primary CLL-induced donor animals. CLL cells were found in the organs that were tested (Figure 13B). In this study, the presence of neoplastic B-lymphocytes in the lung and bladder have been observed for the first time with a mean value of 63.7 % and 56.6 % of $CD45^+$ cells, respectively. In contrast, only 7.2 % and 19.5 % of $CD45^+$ cells in the lung and bladder were $CD5^+CD19^+$. The highest mean value was observed for the circulation. Specifically, 76.23 % of cells are CLL B-cells in the blood. Only 9.7 % of cells were $CD5^+CD19^+$ in control mice. The second highest mean CLL percentage was observed in the spleen. In detail, 73.6 % of $CD45^+$ cells are CLL cells in CLL mice, while only 7.8 % were $CD5^+CD19^+$ in control mice. The lowest mean percentages of neoplastic B-cells were found in the bone marrow of control and CLL mice (Control:

2.6 %; CLL: 14.3 %). Furthermore, frequency of CLL cells in the BM were increased in CLL animals, but lower than in other organs. In short, $CD5^+CD19^+$ CLL B-cells were found in the blood, BM, lung, spleen and bladder. Altogether, this study shows the presence of malignant $CD5^+CD19^+$ B-cells in lymphoid as well as non-lymphoid organs and specifically in the lung and bladder, for the first time.

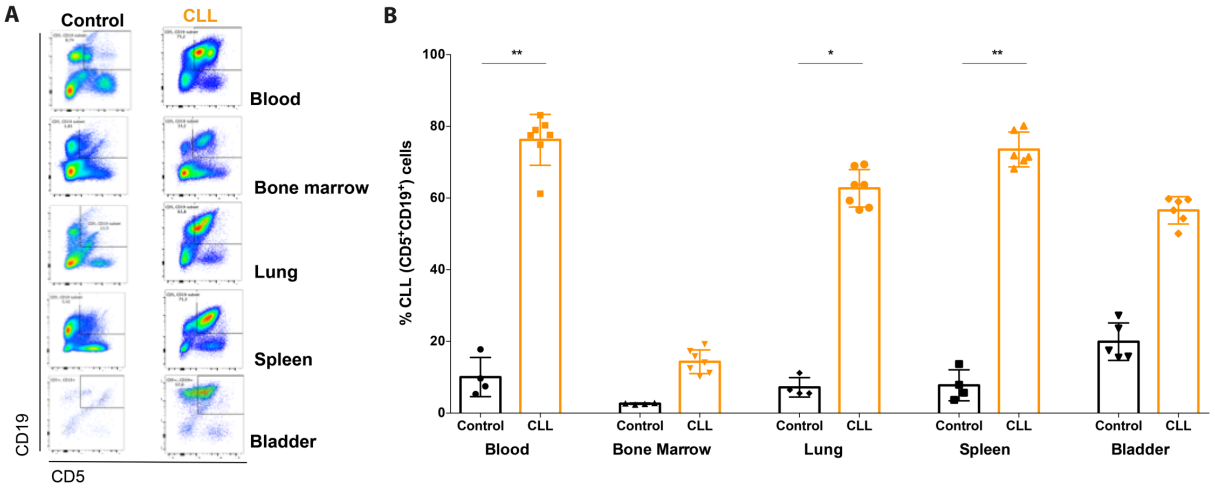

Figure 13. CLL cell infiltration into lymphoid and non-lymphoid organs.

The presence of CLL cells was verified in various murine lymphoid and non-lymphoid tissues (Control n=4; CLL n=7). (A) Flow cytometry graphs visualise malignant B-cells through typical CLL surface marker co-expression of $CD5^+$ and $CD19^+$, in circulating cells, bone marrow, lung, spleen and bladder. (B) The bar graph shows average percentages of CLL ($CD5^+CD19^+$) cells in the blood, bone marrow, lung, spleen and bladder. For blood and bone marrow, the percentages are proportions from singlets, whereas the CLL % represent $CD45^+$cells. Statistical testing: Kruskal-Wallis test.

9.2. Phenotypical characterisation of neutrophils

9.2.1. Phenotyping of circulating neutrophils

In order to characterise neutrophils in CLL, several surface markers were measured. For the statistical analysis, a nonparametric test was chosen based on the assumption that the data distribution is not normal and sample sizes were small to test distribution. The Mann-Whitney *U* test was conducted for the comparison of neutrophil subsets from control and CLL mice.

In detail, CD11b, CXCR2, CXCR4, cKit, CD62L and ICAM1 describe the maturation and activation status (Figure 14). In general, the neutrophil phenotype in CLL is dynamic. Frequencies illustrate the proportion of marker-specific subsets of all neutrophils in the blood.

The percentage of $CD11b^+$ neutrophils was higher in CLL (CLL: 93.6 %, SD: ± 3.2) than in control mice (Control: 83.2 %, SD: ±2.4). Furthermore, $CXCR4^+$ neutrophils are increased in the circulation of control mice with a mean value of 12.3 % (SD: ±14.6). In CLL mice, the frequency of $CXCR4^+$ neutrophils was only 1.1 % of the entire neutrophil population (SD: ±0.5). Another maturation marker, cKit, also known as CD117, was quantified. The proportion of $cKit^+$ neutrophils was declining to an average of 4.4 % in the circulation of CLL mice (SD: ±1.8), whereas 6.5 % of circulating neutrophils were $cKit^+$ in control animals (SD: ±1.2). Moreover, 87.7 % of neutrophils in the circulation of control mice were $CD62L^+$ (SD: ±3.2), while only 56.3 % of Neutrophils were positive for L-selectin (SD: ±27.7). The scattering L-selectin positive neutrophils was higher in CLL compared to controls. In contrast, standard deviation was low for CXCR2 and ICAM1 expression on both, control and CLL neutrophils. A mean value of 98.3 % $CXCR2^+$ neutrophils was reached in the CLL setting (SD: ±0.5), while 93.9 % of circulating neutrophils expressed CXCR2 in control mice (SD: ±0.6). Similar trends were observed for ICAM1 expression. Circulating $ICAM1^+$ neutrophils in CLL mice were higher than in control mice (Control: 0.7 %, SD: ±0.1; CLL: 4.7 %, SD: ±1.1). The differences for CD11b, CXCR2, CXCR4, CD62L and ICAM1 were significant.

In brief, CLL neutrophils in circulation showed a mixed phenotype in regard to their maturation and activation. The proportion of CD11b, $CXCR2^+$ and $ICAM1^+$ neutrophils are increased, while $CXCR4^+$, $CD62L^+$ and $cKit^+$ percentages decline in CLL mice. Thus, neutrophil population in the circulation of CLL mice showed a rather mature and activated phenotype than in control animals.

a

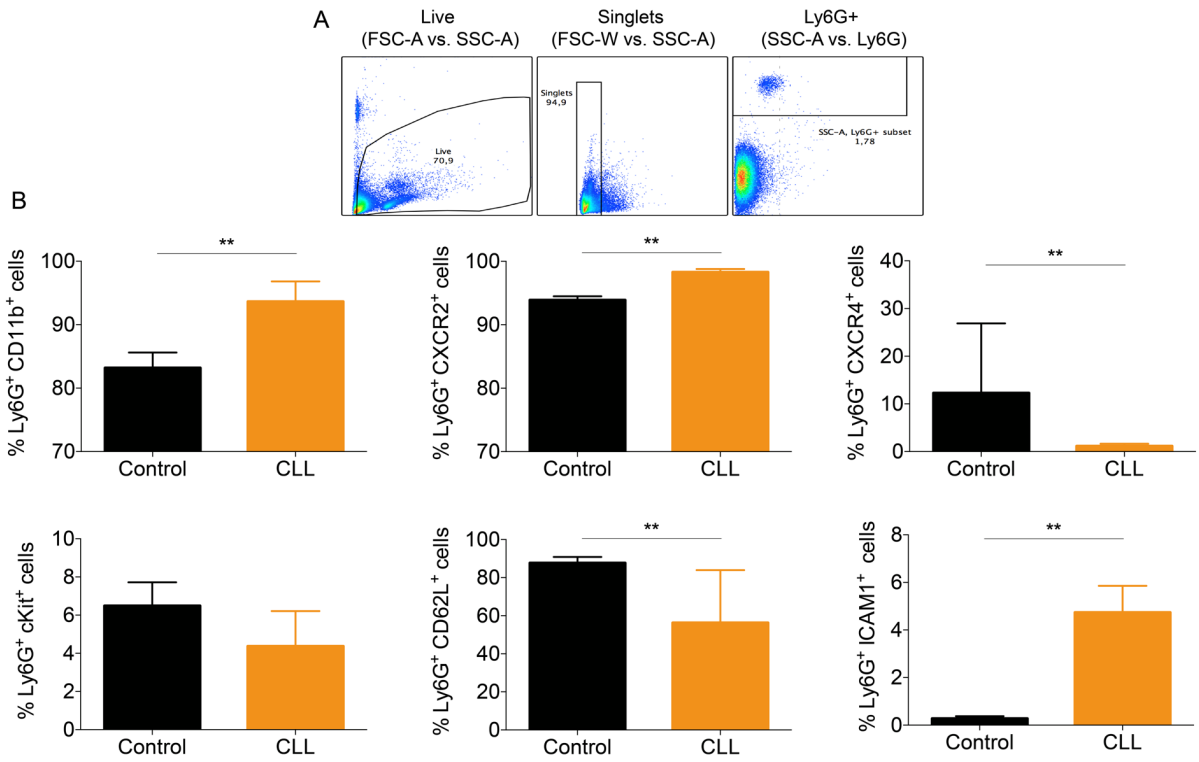

Figure 14. Phenotyping of murine neutrophils in the blood during CLL.

Circulating neutrophils were stained and analysed by FC for various surface markers in regard to their maturation and activation status (Control n=4; CLL n=7). (A) Flow cytometry graphs of Ly6G$^+$ gating strategy. Neutrophils were gated from alive and singlets cells with no limitation to their granularity (SSC). (B) The bar graphs show frequencies of circulating neutrophil subsets with CD11b, CXCR2, CXCR4, cKit, CD62L and ICAM1 expression from control and CLL mice. Statistical testing: Mann-Whitney U test.

In order to specify the expression of each surface marker, the MFI was measured for each neutrophil subset (Figure 15). For statistical analysis, the Mann-Whitney *U* test was chosen.

In detail, CD11b expression on neutrophils of control and CLL mice were equal (Control: 1193, SD: ±163.8; CLL: 1152, SD: ±175.1). CXCR2 expression was decreased on circulating CLL neutrophils (Mean: 5701, SD: ±996.0) compared to control neutrophils (Mean: 7311, SD: 457.7). In contrast, CXCR4 was increased on CLL neutrophils compared to their corresponding controls (Control: 3057, SD: ±332.8; CLL: 440, SD: ±645.0). Reduced cKit (Control: 885, SD: ±57.9; CLL: 1082, SD: ±135.0) and CD62L expression (Control: 16919, SD: ±3003; CLL: 4796, SD: ±986.6) was observed on neutrophils from CLL. The changes in expression of CXCR2, CXCR4, cKit and CD62L were statistically significant. In regard to ICAM1, expression was decreased but statistically not relevant (Control: 925.2, SD: ±480.2; CLL: 400.8, SD: ±45.3).

In brief, the expression of CXCR4 and cKit were increased and CXCR2, CD62L and ICAM1 expression decreased on blood neutrophils in CLL animals. By combining these findings with the frequencies, CXCR4$^+$ and cKit$^+$ neutrophil subsets declined in frequency but enhanced the expression of their surface marker. Vice versa, frequencies of CXCR2$^+$ and ICAM1$^+$ neutrophils increased in the circulation of CLL mice, but the expression of these surface markers decreased. Consequently, neutrophil surface marker expression was inversely correlated to its frequency in the circulation, e.g. for CXCR2, CXCR4, ICAM1 and cKit neutrophil subsets in CLL. Simultaneously, the frequency of CD62L$^+$ neutrophils and CD62L expression declined.

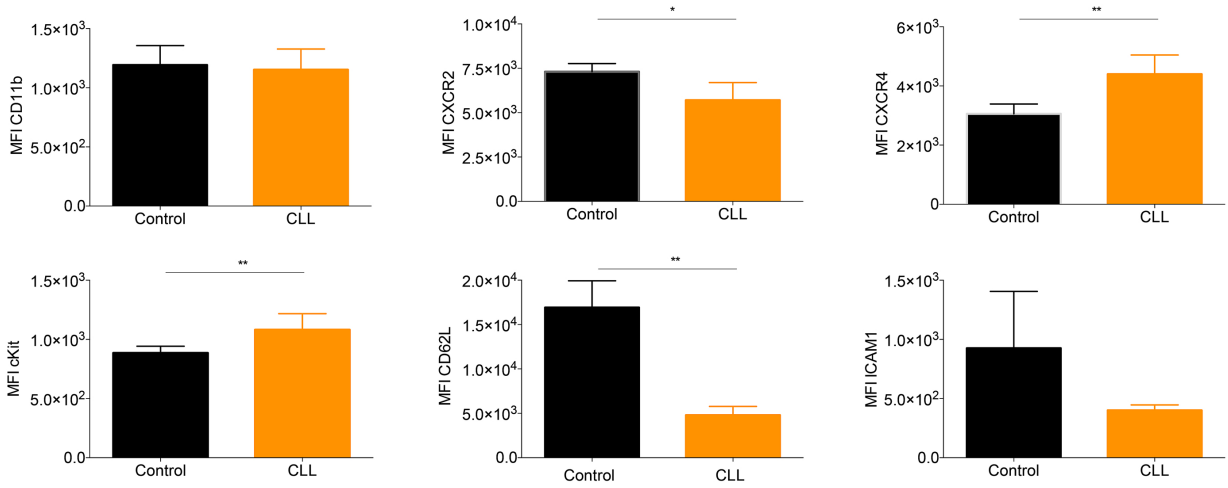

Figure 15. Phenotyping of murine neutrophils in the blood during CLL.

Circulating neutrophils were stained and analysed by FC for various surface markers (Control n=4; CLL n=7). Neutrophils were gated as previously described. The bar graphs show expression patterns on blood neutrophils of control and CLL mice. Statistical testing: Mann-Whitney U test.

9.2.2. Phenotyping of neutrophils in the blood post-UPEC infection

In order to define the impact of CLL on neutrophils during UPEC infection, phenotyping and intracellular MPO staining were performed on circulating neutrophils 21 hpi. Dashed lines indicate the frequency of uninfected control and CLL animals. The black dashed line refers to the corresponding subset in control mice and the orange line visualises the threshold value for the CLL condition. Statistical relevance was tested through Mann-Whitney *U* test.

Blood phenotyping was performed after a mean CLL load of 77.0 % (SD: ±7.6) was reached in the circulation. In control mice, only an average of 5.7 % (SD: ±1.6) of cells co-expressed CD5 and CD19 (Figure 16A). In detail, intracellular MPO (B) and

extracellular TGF-βRI (C), CD62L (D), ICAM1 (E), cKit (F) and CXCR4 (G) were analysed. As shown in Figure 40, MPO levels were decreased in circulating neutrophils of CLL mice. The difference in MPO levels between control and CLL neutrophils were bigger during UTI infection (Figure 16B). Specifically, 97.7 % (SD: ±0.6) of control neutrophils express MPO intracellularly, while only 79.8 % (SD: ±12.6) of circulating CLL neutrophils are MPO^+. Control neutrophils maintained their MPO levels, while the MPO^+ population in CLL neutrophils declined. In regard to TGF-βRI on neutrophils, the frequency of this particular subset diminished in control mice to an average of 0.7 % (SD: 0.3; Figure 16C). CLL neutrophils maintained their TGF-βRI^+ proportion with a mean value of 3.0 % (SD: ±4.6). Furthermore, the percentage of L-selectin$^+$ neutrophils declined in CLL mice but increased to 96.7 % (SD: ±2.6) upon UPEC infection. Similarly, the proportion of $CD62L^+$ control neutrophils also increased after infection to an average of 99.3 % (SD: ±0.3; Figure 16D). At the same time, the $CD62L^+$CLL neutrophil population was significantly decreased compared to the $CD62L^+$ control subset. In addition, almost no changes were recorded for $ICAM1^+$ neutrophil frequencies in the circulation for control and CLL after UPEC infection (Figure 16E). Percentages of this particular subset were similar to levels in the uninfected situation as indicated by the dashed lines. The mean frequency of 0.6 % (SD: ± 0.3) was maintained by control neutrophils, whereas a significant increase was observed for CLL neutrophils (Mean: 4.5 %; SD: ±0.8). Additionally, the cKit neutrophil population was increased to an average of 7.5 % (SD: ±1.2) in CLL and 6.7 % (SD: ±2.1) after UPEC infection (Figure 16F). Moreover, CXCR4 frequencies mounted up to an average of 40.0 % (SD: ± 4.0) in control and 44.4 % (SD: ± 7.9) in CLL mice during UTI.

Altogether, the phenotype of circulating neutrophils changes upon infection in control as well as CLL mice. Particularly, CD62L and MPO frequencies increased and ICAM1 proportion decreased significantly in CLL mice 21 hpi in the bloodstream.

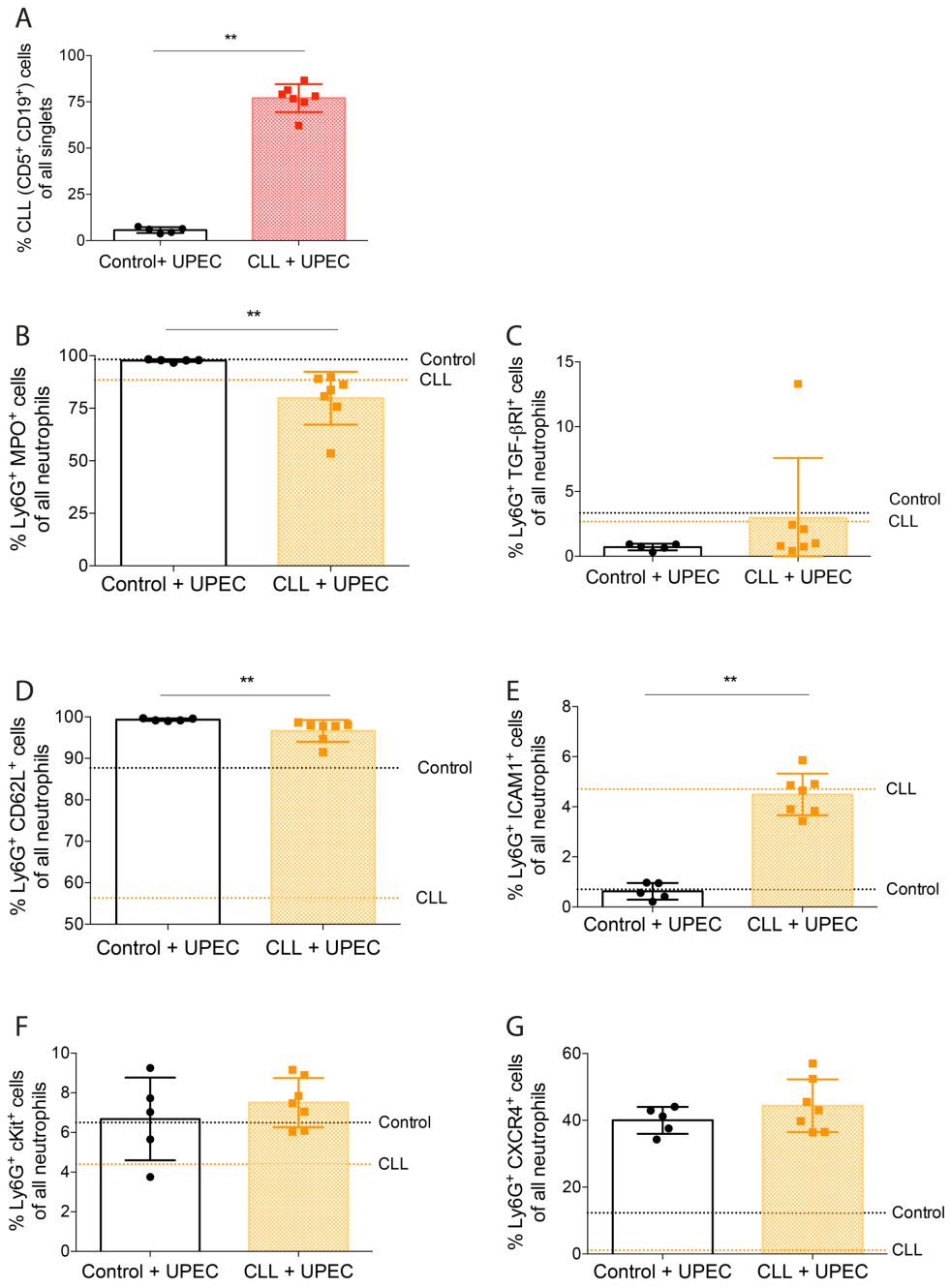

Figure 16. Frequencies of circulating neutrophil subsets after UPEC-infection.

Circulating neutrophils were stained for various surface markers and intracellular MPO 21 hpi (Control + UPEC n=5; CLL + UPEC n=7). Neutrophils were gated as shown in Figure 14. The bar graphs show the CLL load (A) and expression patterns on circulating neutrophils from UPEC-infected control and CLL mice. Significant differences in the expression are present in CD62L, ICAM1 and intracellular MPO expression. Dashed lines indicate values of molecule expression in control (black) and CLL mice (orange) without infection. Statistical testing: Mann-Whitney U test.

In order to measure the expression of surface markers and intracellular MPO, mean fluorescence intensities were quantified on circulating neutrophils 21 hpi (Figure 17). Dashed lines indicate the expression values in uninfected control and CLL animals.

The black dashed line refers to the corresponding subset in control mice and the orange line visualises the expression value for the CLL condition. As previously described, the Mann-Whitney *U* test was used to test for statistical significance.

In detail, a decline in intracellular MPO was observed on circulating CLL neutrophils post-UPEC infection (Control: 7945, SD: ±968.6; CLL: 4773, SD: ±454.6, Figure 17A). While this change was statistically relevant, both MPO levels were decreased to half of its initial mean value. Next, TGF-βRI expression levels rose post-infection but were similar in both groups (Control: 2015, SD: ±3063; CLL: 1064, SD: ±1002, Figure 17B). Furthermore, CD62L expression did not differ from pre-infection conditions, but expression levels still declined in CLL (Control: 16171, SD: ±3960; CLL: 5763, SD: ±1871, Figure 17C). Subsequent surface marker analyses did not reveal any statistically relevant changes. In regard to ICAM1, expression was similar on both, control and CLL subsets (Control: 616.4, SD: ±172.3; CLL: 528.0, SD: ±37.6, Figure 17D). While ICAM1 expression increased for control, it decreased for CLL neutrophils post-UPEC infection. Moreover, cKIT expression declined for both neutrophil populations after UTI to similar levels (Control: 846.4, SD: ±48.0; CLL: 909.1, SD: ±60.6, Figure 17E). Likewise, CXCR4 expression was decreased overall post-UPEC infection, but reached equal levels in both groups (Control: 1028, SD: ±54.7; CLL: 1029, SD: ±111.1, Figure 17F).

To conclude, intracellular MPO declined significantly in neutrophils in the blood of CLL animals 21 hpi. Notably, MPO expression was two-times higher without infection in both, control and CLL animals. Similarly, CD62L expression was decreased in neutrophils in the bloodstream of CLL animals post-UPEC infection. Nevertheless, CD62L expression on neutrophils was only different in the bloodstream of CLL mice. CD62L expression were similar in the circulation of control mice before and after UPEC infection. In brief, these findings indicate an activated but functionally altered neutrophil phenotype in the bloodstream 21 hpi.

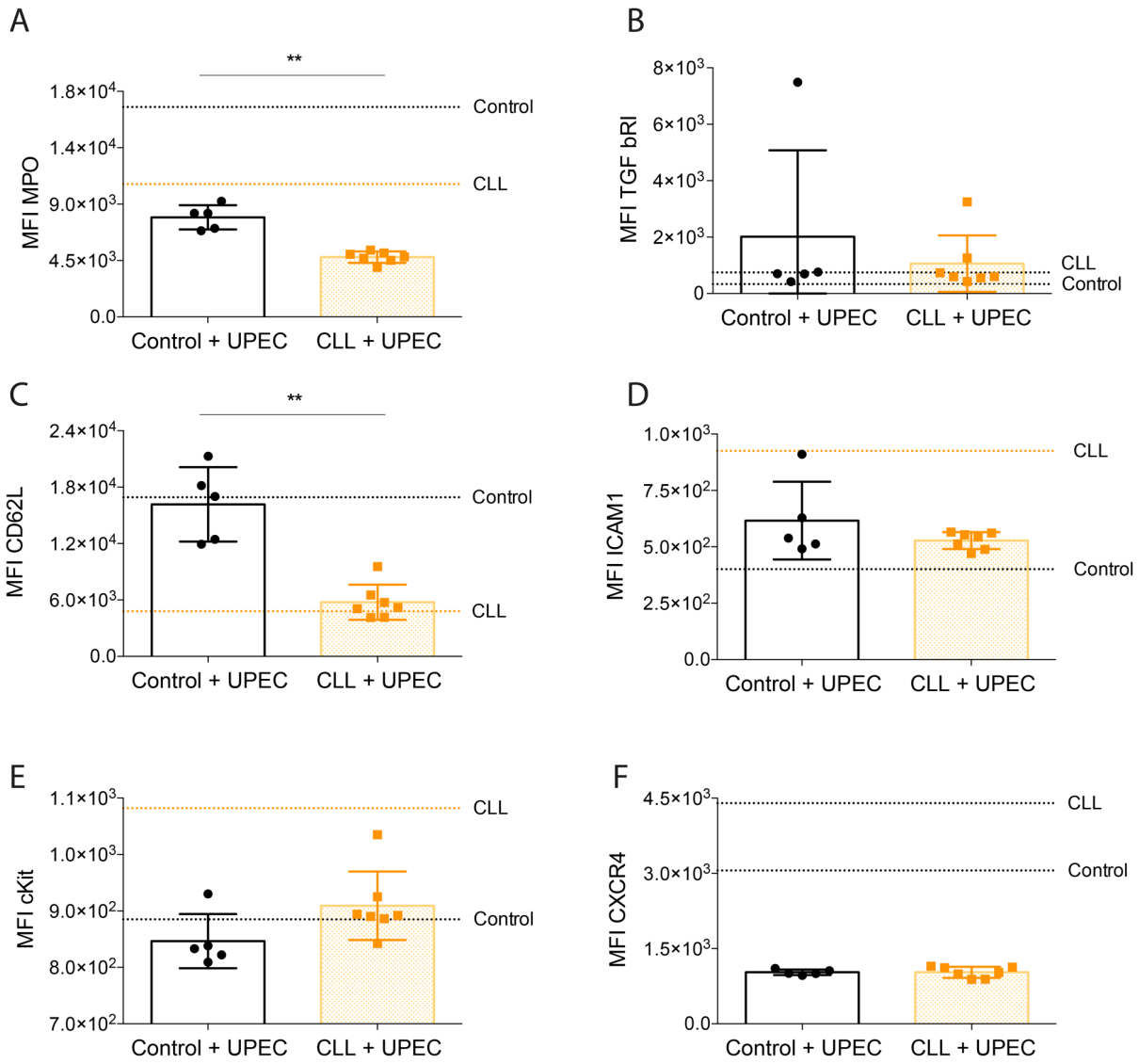

Figure 17. Mean fluorescence intensities of surface markers and intracellular MPO on neutrophil subsets post-UPEC infection.

Circulating neutrophils were stained for various surface markers and intracellular MPO 21 hpi (Control + UPEC n=5; CLL + UPEC n=7). Gating was performed as described previously. Significant differences in the expression were observed for CD62L and intracellular MPO. Expression patterns are shown by MFI for each subset. Dashed lines indicate expression values in uninfected control (black) and CLL mice (orange). Statistical testing: Mann-Whitney U test.

9.2.3. Phenotyping of neutrophils in the bladder post-UPEC infection

In order to define the impact of the CLL on neutrophils at the site of UPEC infection, phenotyping and intracellular MPO staining were performed on neutrophils in the bladder. Here, the Mann-Whitney *U* test was used as a nonparametric statistical test. As described in before, leukaemia was induced with secondary CLL splenocytes. Blood phenotyping was performed after a mean CLL load of 77.0 % was reached in

the circulation. In the bladder, 43.2 % of $CD45^+$ cells were malignant B-cells in CLL mice, whereas only an average of 1.8 % of $CD45^+$ cells constituted the CLL B-cell subset in control mice (Figure 18A).

In regard to neutrophils, intracellular MPO, extracellular TGF-βRI, CD62L, ICAM1, cKit and CXCR4 were analysed. Both MPO^+ neutrophil subsets, from control as well as CLL mice, reached equal levels with the lowest SD after UPEC infection (Control: 99.0 %, SD: ±0.6; CLL: 97.2 %, SD: ±2.8; Figure 18C). However, the frequency of TGF-βRI^+ neutrophils was higher in infected CLL bladders with an average of 7.6 % (SD: ±1.6) compared to 3.8 % (SD: ±3.0) in infected control bladders (Figure 18C). In regard to CD62L, an elevated percentage of $CD62L^+$ neutrophil subset was observed for CLL in comparison to control (Control: 51.7 %, SD: ±4.5; CLL: 64.1 %, SD: ±5.8; Figure 18D). This particular change was statistically significant. In addition, the proportions of $ICAM1^+$ neutrophils were not altered with a mean value of 73.6 % (SD: ±4.0) in control and 79.8 % (SD: ±6.9) in CLL (Figure 18E). Despite, $cKit^+$ and $CXCR4^+$ neutrophil subsets were significantly increased in UPEC-infected CLL bladders (Figure 18F and G). In UPEC-infected control bladders, 9.3 % of neutrophils expressed cKit (SD: ±2.6), while more than 15 % (SD: ±5.1) were $cKit^+$ neutrophils in CLL bladders. Similarly, the frequency of $CXCR4^+$ neutrophils mounted from 58.9 % (SD: ±5.1) in infected control bladders to 71.4 % (SD: ±8.1) in the CLL condition.

Due to the absence of sufficient neutrophil numbers in the bladder during the uninfected situation, threshold values could not be obtained for intracellular and extracellular markers. Conclusively, the phenotype of bladder neutrophils differed from blood neutrophils in control as well as CLL mice during UPEC infection.

In brief, the phenotype of neutrophils at the site of infection is distinct from neutrophils in the bloodstream after UPEC infection. Particularly, significant increases were observed for neutrophil subsets expressing TGF-βRI which hints at an increased immunosuppressive state, while CD62L indicates activation. Furthermore, increased frequencies of $CXCR4^+$ and $cKit^+$ neutrophils refer to an immature phenotype in the bladder of infected CLL mice 21 hpi.

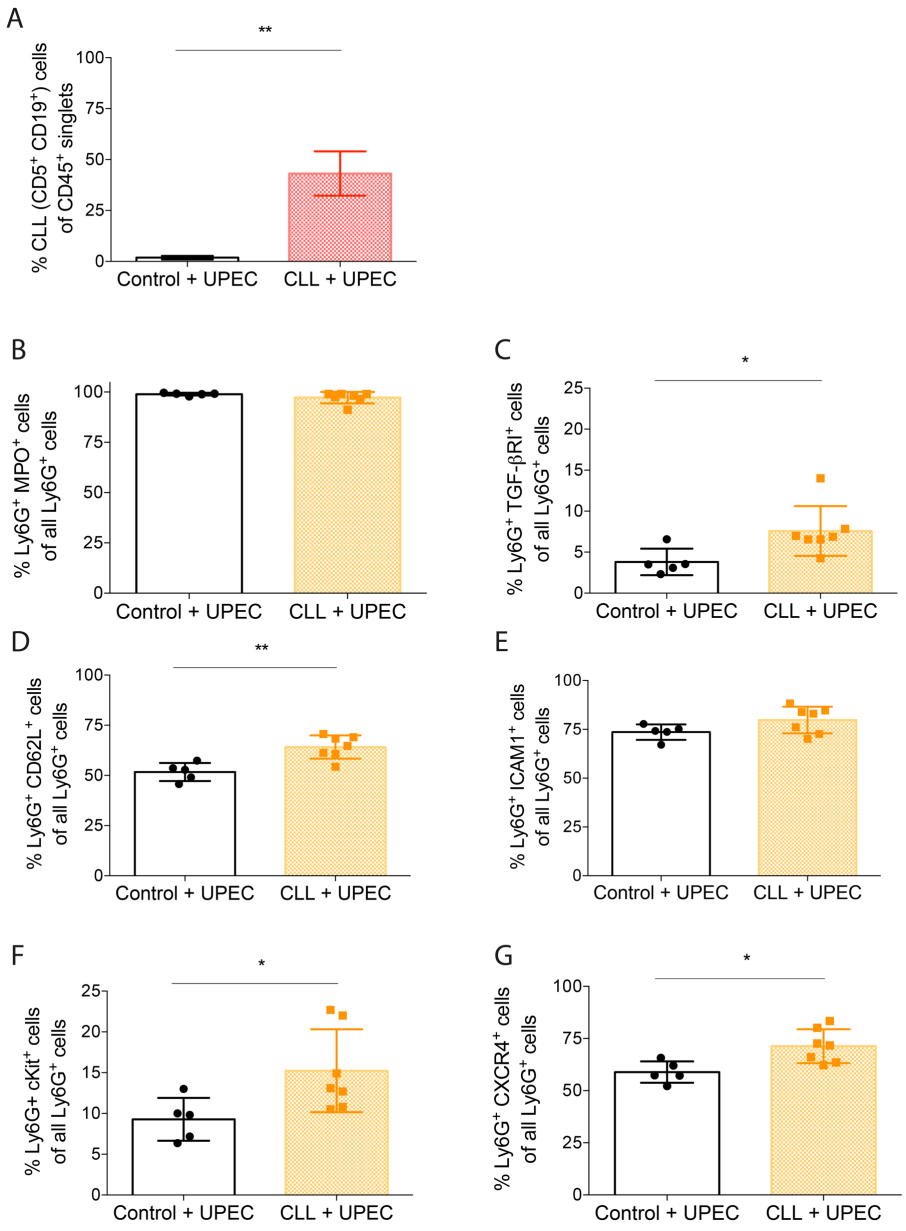

Figure 18. Frequencies of neutrophil subsets in the bladder during UTI in CLL.

Bladder neutrophils were stained after UPEC infection (21 hpi) for various surface markers and intracellular MPO and analysed by FC (Control + UPEC n=5; CLL + UPEC n=7). Neutrophils were gated from alive, single and CD45⁺ cells with no limitation to their granularity (SSC). The bar graphs show expression patterns on circulating neutrophils from UPEC-infected control and CLL mice. Significant differences in the expression are present in TGF-βRI, CD62L, CXCR4 and cKit expression. Dashed lines indicate threshold values of molecule expression in control (black) and CLL mice (orange). Statistical testing: Mann-Whitney U test.

In order to quantify the expression patterns of surface markers and intracellular MPO, MFI of each marker were quantified on circulating neutrophils 21 hpi (Figure 19). The Mann-Whitney *U* test was conducted to test for statistical relevance.

In detail, intracellular MPO levels were similar on bladder CLL neutrophils post-UPEC infection (Control: 3833, SD: ±2208 CLL: 3264, SD: ±1641, Figure 19A). Similarly,

TGF-βRI expression on bladder neutrophils reached equal levels in both groups post-infection (Control: 573.6, SD: ±79.7; CLL: 744, SD: ±254.4; Figure 19B). Furthermore, a rise in CD62L expression was observed in CLL (Control: 1900, SD: ±238.4; CLL: 2280, SD: ±347; Figure 19C). This increment was statistically relevant. In addition, ICAM1 expression was also significantly increased in CLL subsets (Control: 1598, SD: ±80.6; CLL: 2047, SD: ±102.8; Figure 19D). Likewise, cKIT expression rose slightly on CLL neutrophils after UTI (Control: 2298, SD: ±555.7; CLL: 2439, SD: ±551.9; Figure 19E). However, this change was not statistically relevant. In addition, CXCR4 expression was also increased on CLL neutrophils post-UPEC infection (Control: 1037, SD: ±161.8; CLL: 1406, SD: ±293.6; Figure 19F). This particular change in expression was significant.

In brief, intracellular MPO and surface marker expression changed from upon infection, however only CD62L, ICAM1 and CXCR4 expression on bladder CLL neutrophils differed from their corresponding controls.

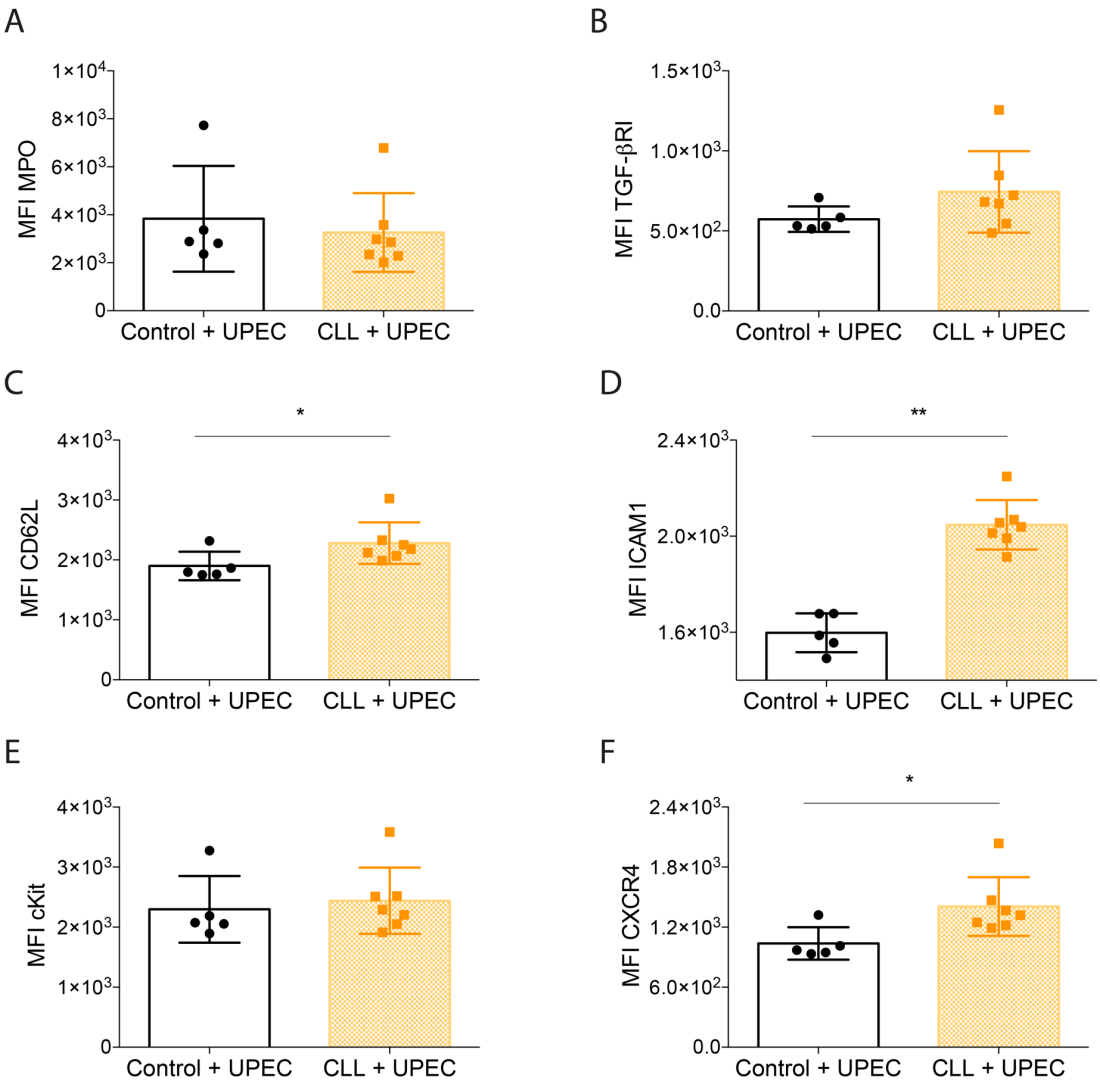

Figure 19. Expression patterns of neutrophil subsets in the bladder after UPEC infection.

Bladder neutrophils were stained for various surface markers and intracellular MPO analysed by FC 21 hpi. Neutrophils were gated as described previously. The bar graphs show expression patterns on circulating neutrophils from UPEC-infected control (n=5) and CLL mice (n=7). Significant differences in the expression were present in CD62L, ICAM1 and CXCR4 expression. Statistical testing: Mann-Whitney U test.

9.2.4. Phenotyping of neutrophils from untreated CLL patients

Blood neutrophils were characterised before and after UPEC infection in the murine model. Additionally, phenotyping was performed on neutrophils from the bladder, the site of infection. In order to translate the findings from the murine model into the clinical situation, surface marker expression was measured on neutrophils from the peripheral circulation of untreated CLL patients (Figure 20 and Figure 21). Staining for flow cytometric analyses was performed on whole blood samples as described in 8.2.4.2. The gating strategy has been illustrated in the top panel of Figure 20. After

live and single cell gating, only $CD45^+$ and $CD16^-$ cells were chosen as a pre-gate for the final $CD66b^+$ selection. CD16 was used to differentiate neutrophils from eosinophils which express CD16 [274]. Isotype controls were used to identify positive staining for each surface marker and thus allows quantification of specific antibody signal (Figure 20).

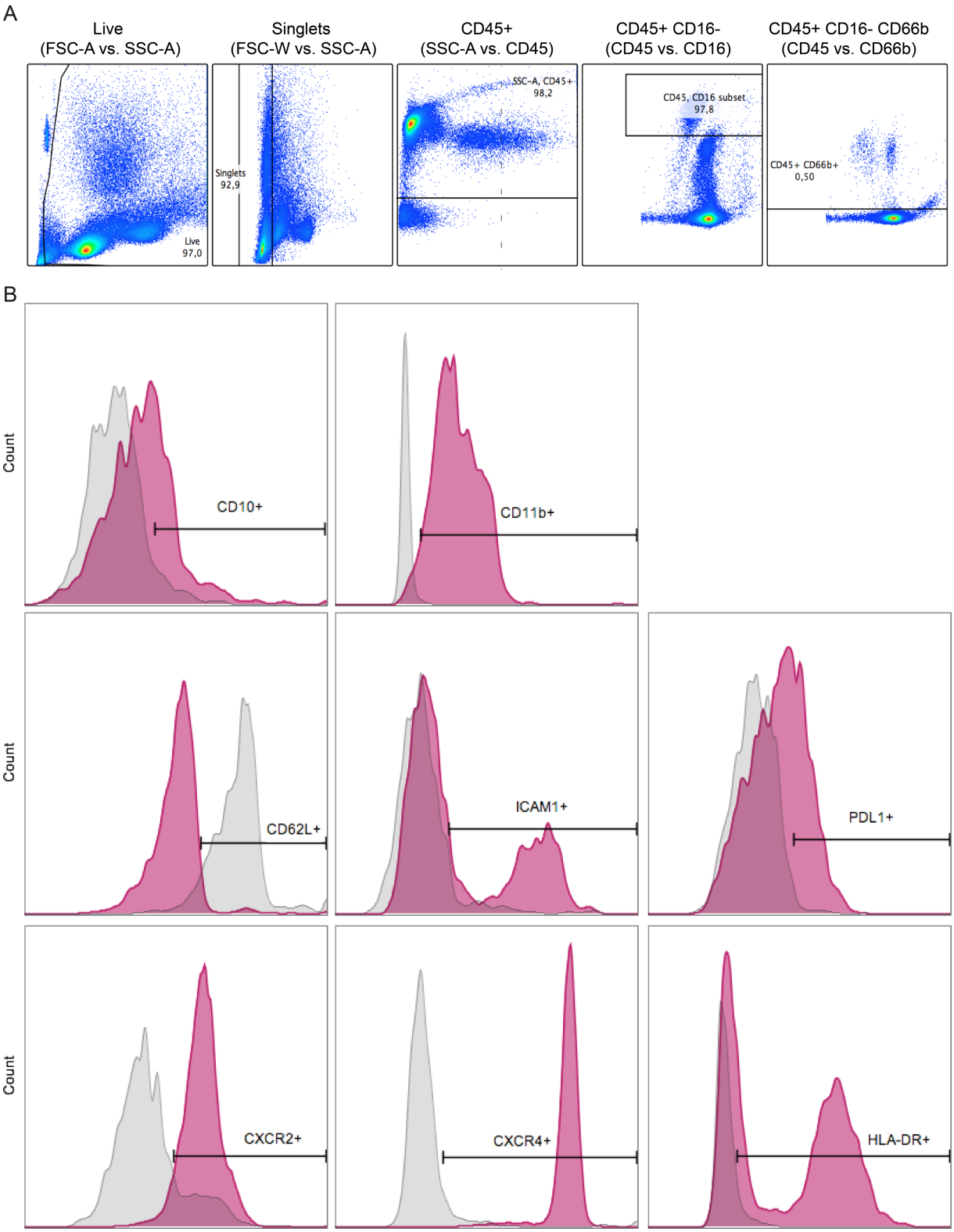

Figure 20. Phenotyping of neutrophil in untreated CLL patients.

The phenotyping on human neutrophils was performed in whole blood samples from five untreated CLL patients. As depicted in the top panel, neutrophils were gated from alive, single, CD45^{+} and CD16^{-} cells. The staining panel included markers defining the maturation, e.g. CD10 and CD11b. Activation markers were CD62L, ICAM1 and PDL1. In addition, chemokine receptors, such as CXCR2, CXCR4 and HLA-DR were measured. Representative histograms were derived from FC analyses and visualise isotype matched controls for each antibody.

Reports showed that the risk of infection increases during CLL progression [4]. Thus, lymphocyte counts in the circulation, which is equal to the CLL load, were used to correlate frequencies of neutrophil subsets (Figure 21). The range varied from 3.5 x 10^4 to 1.7 x 10^5 lymphocytes in 1 µl of peripheral blood. In addition, the Binet staging information was received. No other information regarding disease-related adverse prognostic factors, such as chromosomal or genetic lesions or IGHV status, are known. Two patients were classified to be in Binet stage A, while three CLL patients were in Binet stage B at the point of the study. Statistical relevance was derived from two factors: R^2 and F-test. For correlation analyses, the goodness of fit was analysed by the R^2 value which may range from -1 to 0 to +1. The co-efficient of determination, R^2, reveals the variation of one data point based on another data point. The regression line helps to understand the frequency of variation which is derived from the data. In other words, the most perfect linear correlation would yield a R^2 value of ±1. A value bigger than +0.5 means that the data points are closer to the linear regression line. If R^2 is smaller than +0.5 and between 0, then there is less association between the variables. Values smaller than 0 are negatively associated and strong negative linear association occurs if R^2 approaches -1. For a correlation between frequency of neutrophil subset and lymphocyte count to imply confidence, the R^2 value was considered to be greater than +0.5. In addition, the p-value derived from the F-test reveals whether the results are significant. The statistical testing was conducted as described in 8.2.10.

Albeit many reports on neutropenia in CLL patients, there was no correlation detected in the frequency of neutrophil in the peripheral blood of untreated CLL patients (R^2=0.03; p-value=0.78; Figure 21A). Neutrophil proportions from $CD45^+CD16^-$ cells range from 0.32 to 1.1 % with an average of 0.68 % in the circulation. Percentages of the $CD10^+$ neutrophil subset gradually increase with increasing lymphocyte counts. The data points for the $CD10^+$ neutrophil frequencies created a R^2 value of 0.64 which in turns means that the variation predicts large positive linear association (p-value=0.10; Figure 21B). Similar negative trends were observed for the $CD11b^+$ subset, however, there is only a small negative linear association, reflected in the R^2 value of 0.18 (p-value=0.48; Figure 21C).

In Figure 21D, another strong negative linear association is illustrated. With increasing lymphocytes in circulation, the frequency of the $CD62L^+$ neutrophil subset decreases (p-value=0.06). The $CD62L^+$ neutrophil frequencies almost perfectly

aligned with the regression line, between 50 % and 88.8 % with a mean value of 63.7 %. Furthermore, small positive linear correlation was observed for both, ICAM1 and PDL1 neutrophil percentages and increasing lymphocyte counts in blood. The R^2 value were 0.32 and 0.33 for $ICAM1^+$ and $PDL1^+$ subsets, respectively (p-value=0.32 and 0.33). In detail, the mean frequency of the $ICAM1^+$ neutrophil subset was 26.3 %, while the average for the $PDL1^+$ subset is 10.5 % (Figure 21E and F). The chemokine subsets with CXCR2 and CXCR4 expression, showed negative linear association. The average value of $CXCR2^+$ neutrophils is 80.5 %. For CXCR2, the neutrophil subset was weakly correlated to increasing lymphocytes in the circulation (R^2=0.16; p-value=0.5; Figure 21G). In regard to CXCR4, the average frequency was 86.9 %. Here, a strong negative association was detected for $CXCR4^+$ neutrophil proportions and lymphocyte counts. The R^2 value mounted to 0.77, while the p-value was 0.05, almost reaching significance. There was no linear association observed for the HLA-DR subset and lymphocyte counts in circulation (Figure 21I). Consequently, R^2 was 0.0, the lowest among the entire study with an p-value of 0.9. The average frequency for $HLA\text{-}DR^+$ neutrophils was 44.6 %.

In brief, neutrophils of untreated CLL patients did not show any correlation with increasing tumour load in the circulation. Furthermore, there was a strong negative association found for $CD10^+$, $CD62L^+$ and $CXCR4^+$ neutrophils and increasing CLL load in the blood. A weak but positive correlation was detected for $ICAM1^+$ and $PDL1^+$ neutrophil population with increasing tumour load.

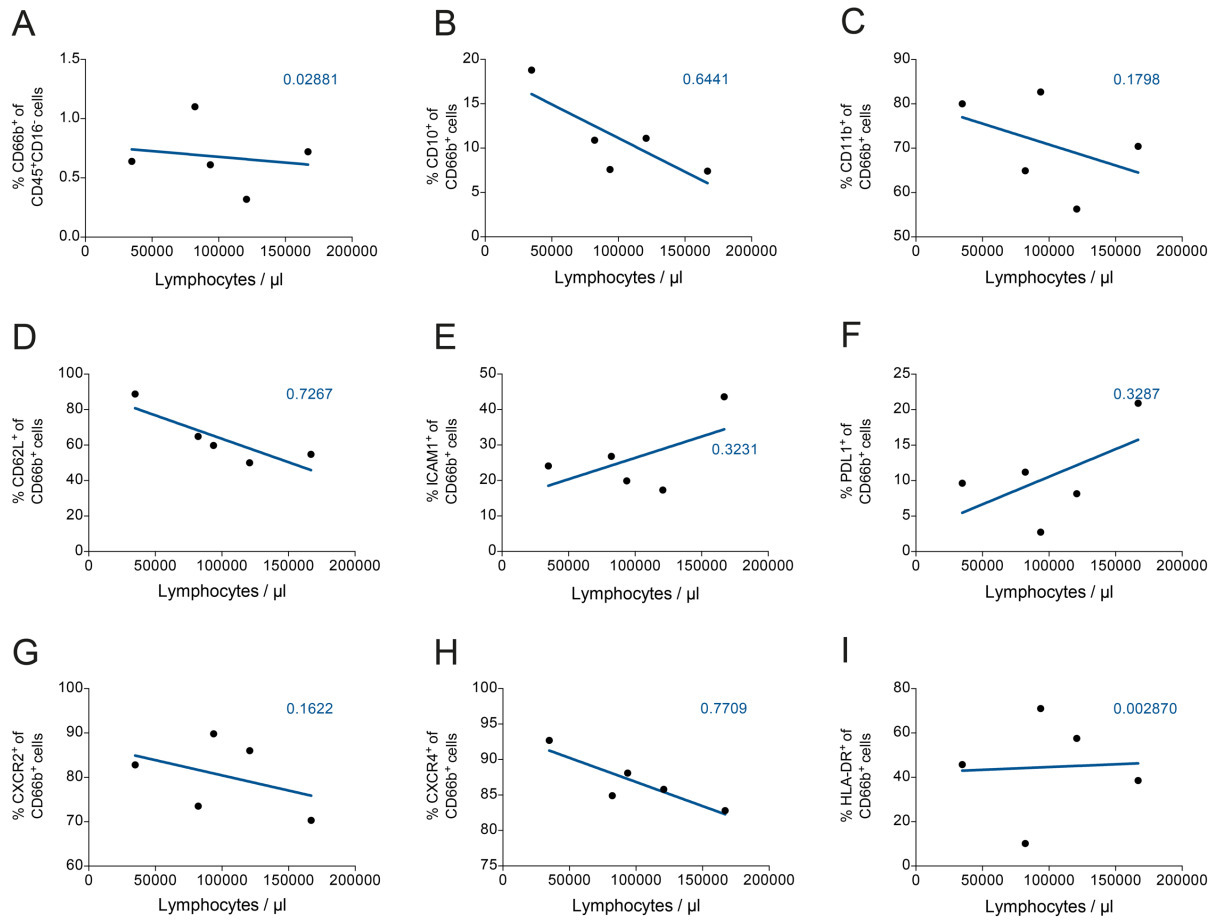

Figure 21. Correlation of neutrophil frequencies and lymphocyte counts in untreated CLL blood samples.

The phenotyping on human neutrophils was performed in whole blood samples from five untreated CLL patients. Maturation (CD10 and CD11b), activation markers (CD62L, ICAM1 and PDL1) and chemokine receptors (CXCR2, CXCR4 and HLA-DR) were measured. In this study, correlation analyses were performed based on the cell frequencies and CLL load (lymphocyte count) in the circulation. Statistical testing: F-test.

9.3. Proteome analysis of neutrophils in CLL

9.3.1. Neutrophil isolation from BM and blood

As previously mentioned, neutrophil frequencies in murine blood are not as high as in the human circulation during homeostasis. For the proteomic analysis, the maximum neutrophil number had to be obtained. Post-MACS isolation and sorting, neutrophils from the bone marrow and blood were obtained from control and CLL mice. The following table summarizes the final numbers of neutrophils that were processed for the proteome analysis by LC-MS/MS (Table 18).

Table 18. Neutrophil numbers isolated from BM and blood of control and CLL mice.

#	Group	Tumour load (% $CD5^+CD19^+$)	Σ no. PMN (BM)	Σ no. PMN (blood)
1	Control	4	**9,47E+05**	**7,46E+04**
2	Control	6	**1,22E+06**	**1,02E+05**
3	Control	4	**1,53E+06**	**9,60E+03**
4	Control	3	**9,41E+05**	**6,70E+04**
5	Control	1	**1,34E+06**	**5,59E+04**
6	Control	3	**1,53E+06**	**6,78E+04**
7	Control	5	**6,09E+05**	**1,27E+05**
8	Control	6	**1,41E+06**	**1,34E+05**
9	Control	5	**1,05E+06**	**4,08E+04**
10	CLL	69	**1,11E+06**	**3,96E+05**
11	CLL	59	**1,88E+06**	**1,15E+05**
12	CLL	42	**9,96E+05**	**1,79E+05**
13	CLL	69	**9,95E+05**	**3,58E+05**
14	CLL	67	**5,07E+05**	**3,15E+05**
15	CLL	59	**1,25E+06**	**2,98E+05**
16	CLL	59	**3,35E+05**	**3,29E+05**
17	CLL	64	**7,89E+05**	**3,38E+05**
18	CLL	43	**1,44E+06**	**3,03E+05**
19	CLL	69	**7,71E+05**	**1,01E+06**
20	CLL	80	**2,22E+05**	**1,14E+06**
21	CLL	75	**1,29E+06**	**3,12E+05**
22	CLL	47	**1,51E+06**	**4,83E+05**

9.3.2. LC-MS/MS analysis and proteomic data

On average, 29,562 tandem MS spectra were obtained for each analysis of three biological replicates from $5x10^4$ isolated BM neutrophils (Figure 22). Approximately 1500 protein groups were identified per sample. With respect to reproducibility, 1374 proteins were quantified using a label-free ion intensity-based approach.

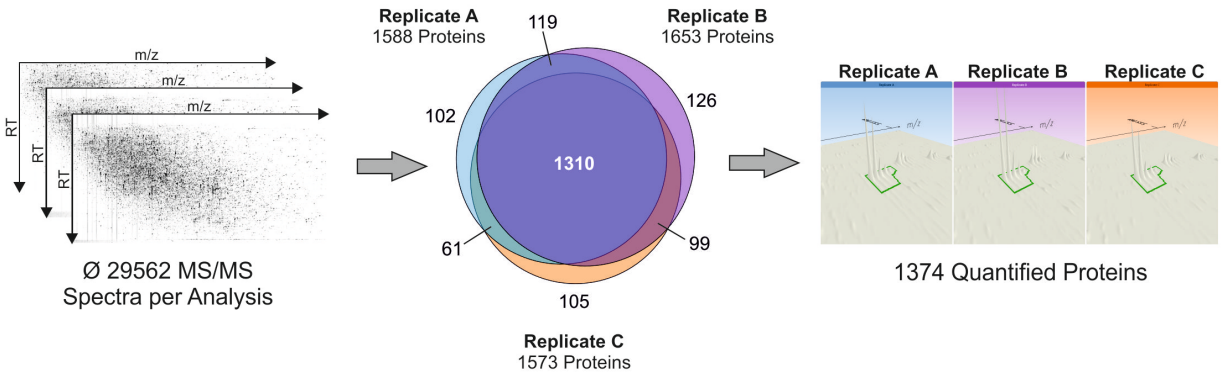

Figure 22. Reproducibility of sample measurement on the LC-MS/MS.

Representative LC-ESI-MS/MS analysis of three biological replicates of 50,000 isolated neutrophils from bone marrow. An average number of 29,562 tandem MS spectra was acquired per analysis and lead to the identification of about 1500 protein groups per sample. 1374 proteins could be quantified reproducibly using a label-free ion intensity-based approach.

Differentially expressed proteins were identified based on the minimum of two peptides, a p-value equal or lesser than 0.05 and a fold change of greater than 1.5.

Figure 23 depicts a heat map of the 243 differentially abundant proteins in neutrophils isolated from the bone marrow of control and CLL mice. This heat map is the result of an unsupervised hierarchical clustering analysis in which differentially expressed proteins of BM neutrophils from 13 CLL and 9 control animals were organised into groups based on a clustering algorithm that recognizes similarities among samples. The association is represented by a tree with branches revealing the degree of similarity between samples. The height of the join indicates the distance between each branching. On the vertical side, the unsupervised clustering led to two major group formations, each associated with a side colour, blue for control and red for CLL samples. In other words, the unsupervised hierarchical clustering of the proteome led to perfect segregation of control and CLL into the two major branches of the dendrogram. On the horizontal side, the dendrogram depicts differentially expressed proteins (Figure 23). Remarkably, the heatmap reveals that there are larger variations in protein expression within the CLL group compared to the control samples. Additionally, there are more upregulated protein signatures for the entity of CLL BM neutrophils when compared to their control counterparts.

In brief, the variation among both groups and within the CLL sample group suggests that CLL has a considerable impact on the protein expression of BM neutrophils.

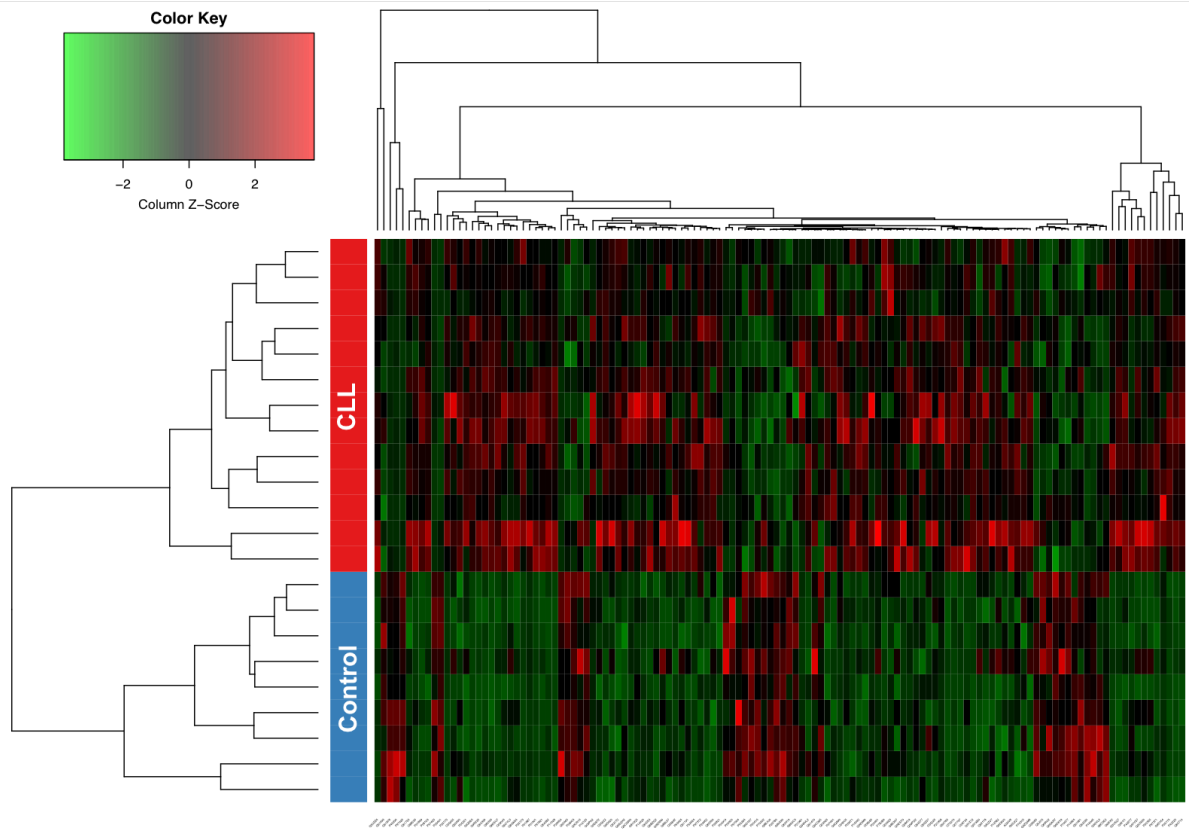

Figure 23. Heatmap and dendogram overview of the unsupervised hierarchical clustering analysis of differentially expressed neutrophil proteins.

Proteome analysis was conducted for isolated BM neutrophils from control (n=9) and CLL animals (n=13) by LC-MS/MS. An unsupervised hierarchical clustering has been performed with R. The heat map indicates relative abundance of 243 proteins through colour-coding. Higher protein abundance is illustrated in red, while green refers to lower abundant proteins. The dendrograms display hierarchical clustering of samples and proteins based on their Euclidian distance.

In order to visualise the proteomic results, volcano plots were generated for differentially expressed neutrophil proteins in the bone marrow and blood (Figure 24 and Figure 25). Volcano plots illustrate $\log_2$ transformed fold changes of mean normalized abundances of the quantified proteins for the comparisons of BM neutrophils (90 proteins, Figure 24) and neutrophils from the blood (62 proteins, Figure 25) against the $\log_{10}$ transformed FDR-adjusted p-values. Dashed lines represent the applied significance cut-offs (FDR-adjusted p-value ≤ 0.05 and fold change >1.5). Differentially abundant proteins are visualised as red dots with corresponding gene annotations. The grey area shows proteins that did not pass the significance threshold.

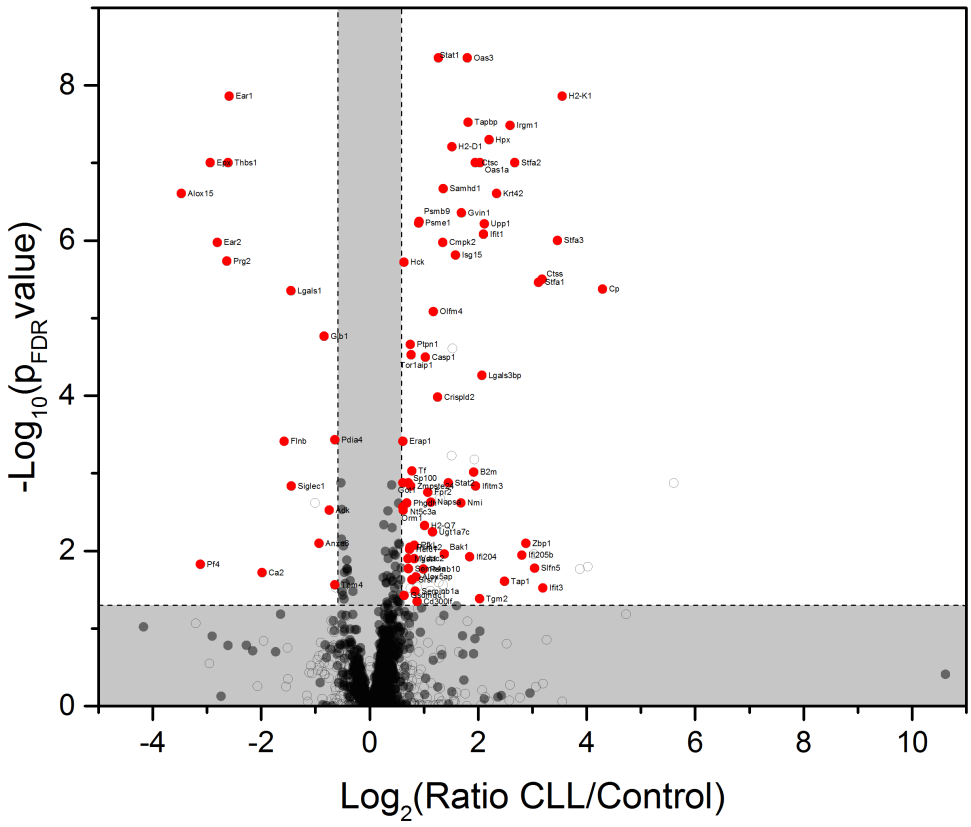

Figure 24. Volcano plot illustrating differential expression of BM neutrophils.

Ratios of means are displayed log_2 transformed, ANOVA p-values are presented $-log_{10}$ transformed. Dashed lines represent the applied thresholds (p-value ≤ 0.05 and fold change ≥ 1.5) and proteins passing this threshold are highlighted in red. Proteins displayed as full black circle in the grey background did not pass the significance threshold. The gene names are given for the top ranked proteins based on their Euclidian distance.

In total, 75 proteins were higher abundant on circulating neutrophils of CLL mice and 15 proteins were lesser abundant (Figure 24). In regard to BM neutrophils, 47 proteins showed higher abundance in CLL neutrophils and 15 proteins showed lower abundance compared to their corresponding controls (Figure 25). As already mentioned, the number of increased abundant proteins is greater than the number of lesser abundant proteins in CLL BM and blood neutrophils.

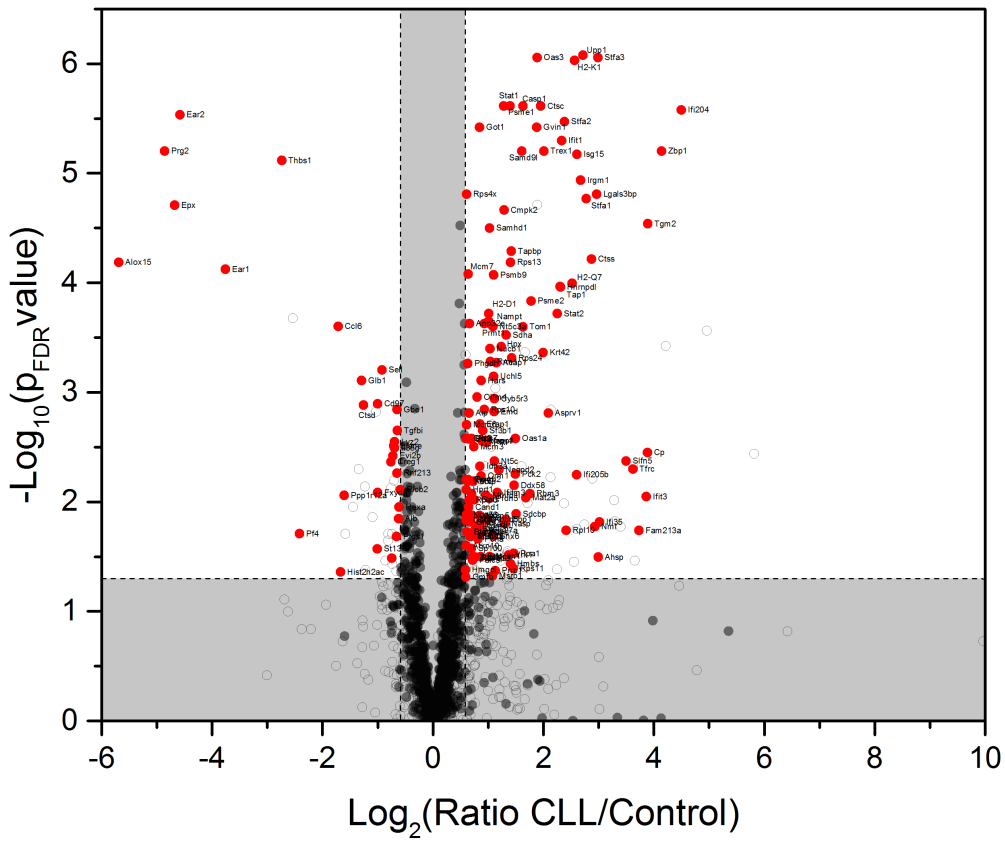

Figure 25. Volcano plot illustrating differential expression of blood neutrophils.

Ratios of means are displayed log_2 transformed, FDR-adjusted p-values are presented $-log_{10}$ transformed. Dashed lines represent the applied thresholds (FDR-adjusted p-value ≤ 0.05, fold change ≥ 1.5) and proteins passing this threshold are highlighted in red. Proteins displayed as full black circle in the grey background did not pass the significance threshold. The gene names are given for the top ranked proteins based on their Euclidian distance.

A Pearson's correlation analysis was performed to study the association of mutually differentially abundant proteins that are significant in both comparison "BM CLL vs. control " and "Blood CLL vs. control" (Figure 26, red dots). A strong positive correlation was found for proteins highlighted as red dots with a coefficient of determination of 0.87 and a slope of 1.2. In other words, a protein increases 0.87-fold in CLL BM and it increases by 1.2-fold in CLL blood. Thus, protein expressions are consistently increased in CLL blood than in CLL bone marrow. The biological significance of differentially abundant proteins was studied by analysing their classification within gene ontology (GO) domains illustrated with the ClueGO plug-in of Cytoscape (9.3.4).

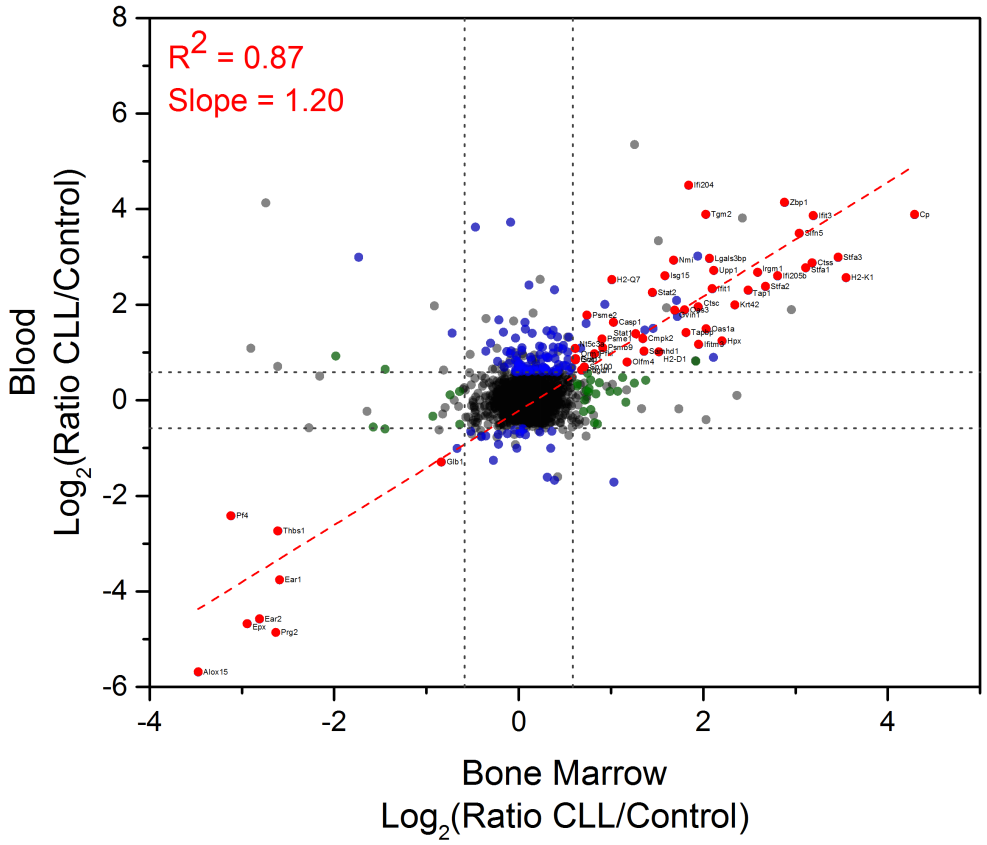

Figure 26. Correlation of differentially abundant proteins significant in both BM and blood conditions (CLL vs. control).

R^2, the correlation coefficient, and the slope of the regression line. Dashed lines visualise the fold change cut-off (>2). Red dots represent proteins that are significant in both comparisons, while the ones in grey are not significant in any comparison. Proteins that are only significant in the CLL bone marrow compared to control bone marrow are blue (n=62), green dots illustrate exclusive significance in the CLL blood vs. control blood (n=90).

9.3.3. Ranking of protein targets on neutrophils in CLL

After peptide quantification and protein identification, further information regarding fold changes and statistical tests were obtained. As this study focusses on the modulation of neutrophil phenotype and function by CLL, ratios of mean expression values were calculated (Table 19 and Table 20).

9.3.3.1. Bone marrow: CLL vs. control

In Table 19, the top ranked higher and lesser abundant proteins have been summarised. The ranking has been based on the highest positive and negative fold changes for CLL BM neutrophils. Interestingly, two out of five higher abundant proteins in CLL BM neutrophils are linked to antigen processing and presentation (*HA2Q, HA1B*), while other proteins are associated with the interferon signalling (*IIGP1*), GTPase activator activity and cadherin binding (*TBD2A*), and ceruloplasmin

(*CERU*) being reported to be an inhibitor of MPO [275]. Furthermore, lesser abundant proteins in CLL BM neutrophils include bactericidal proteins from eosinophils (*PERE*, *ECP2*), ankyrin (*ANK1*) linked to neutrophil bactericidal activity, *PLF4* activates neutrophils and its chemotaxis, as well as arachidonate 15-lipoxygenase (*LOX15*) contributing to neutrophil recruitment in disease settings [276-278].

In brief, the top ranked differentially abundant proteins in CLL BM neutrophils depict different neutrophil effector functions with a majority of them being involved in the antimicrobial response.

Table 19. Fold-change ranked list of higher and lesser abundant proteins in CLL BM neutrophils.

Accession ID	Unique peptides	Description	FDR-adjusted p-value	Fold change (CLL/Control)
Q9QZ85	1	Interferon-inducible GTPase 1 OS=Mus musculus GN=Iigp1 PE=1 SV=2 - [IIGP1_MOUSE]	0,001	48,70
Q61147	2	Ceruloplasmin OS=Mus musculus GN=Cp PE=1 SV=2 - [CERU_MOUSE]	4,21E-06	19,57
P04227	1	\H-2 class II histocompatibility antigen, A-Q alpha chain (Fragment) OS=Mus musculus GN=H2-Aa PE=2 SV=1 - [HA2Q_MOUSE]\""	0,02	16,120
B1AVH7	1	TBC1 domain family member 2A OS=Mus musculus GN=Tbc1d2 PE=2 SV=1 - [TBD2A_MOUSE]	0,02	14,63
P01901	3	\H-2 class I histocompatibility antigen, K-B alpha chain OS=Mus musculus GN=H2-K1 PE=1 SV=1 - [HA1B_MOUSE]\""	1,38E-08	11,70
Q02357	4	Arachidonate 15-lipoxygenase OS=Mus musculus GN=Alox15 PE=1 SV=4 - [LOX15_MOUSE]	2,47E-07	-11,11
P39654	12	Platelet factor 4 OS=Mus musculus GN=Pf4 PE=2 SV=1 - [PLF4_MOUSE]	0,01	-8,68
P43430	1	Eosinophil peroxidase OS=Mus musculus GN=Epx PE=1 SV=2 - [PERE_MOUSE]	9,95E-08	-7,68
Q9Z126	2	Eosinophil cationic protein 2 OS=Mus musculus GN=Ear2 PE=2 SV=1 - [ECP2_MOUSE]	1,06E-06	-7,01
P49222	1	Bone marrow proteoglycan OS=Mus musculus GN=Prg2 PE=1 SV=1 - [PRG2_MOUSE]	1,84E-06	-6,20

9.3.3.2. Blood: CLL vs. control

Interestingly, most differentially abundant proteins in circulating neutrophils (Table 20) from CLL have been top targets in CLL BM neutrophils, such as interferon-

related signalling (*GBP2*, here: *IFI4*) or ceruloplasmin. In addition, *ZBP1* is an interferon-induced immune sensor that was higher abundant in CLL blood neutrophils [279]. Furthermore, transglutaminase 2 was observed among the higher abundant proteins and has been reported to play a role in neutrophil maturation (*TGM2*) [280]. Simultaneously, eosinophil-related proteins (*PERE*, *ECP2*, here: *ECP1*) and arachidonate 15-lipoxygenase were included in the group of lesser abundant proteins. Additionally, proteoglycan (*PRG2*) was a lesser abundant protein in CLL blood neutrophils and has been reported to be involved in neutrophil activation [281]. In short, the top ranked differentially abundant proteins in circulating CLL neutrophils are involved in the neutrophil activation, differentiation, interferon signalling and neutrophil recruitment.

Table 20. Fold-change ranked list of higher and lesser abundant proteins in blood CLL neutrophils.

Accession ID	Unique peptides	Description	FDR-adjusted p-value	Fold change (CLL/Control)
P15092	2	Interferon-activable protein 204 OS=Mus musculus GN=Ifi204 PE=1 SV=2 - [IFI4_MOUSE]	2,65E-06	22,64
Q9QY24	3	Z-DNA-binding protein 1 OS=Mus musculus GN=Zbp1 PE=1 SV=1 - [ZBP1_MOUSE]	6,28E-06	17,63
Q9Z0E6	4	Interferon-induced guanylate-binding protein 2 OS=Mus musculus GN=Gbp2 PE=1 SV=1 - [GBP2_MOUSE]	2,90E-05	17,59
P21981	2	Protein-glutamine gamma-glutamyltransferase 2 OS=Mus musculus GN=Tgm2 PE=1 SV=4 - [TGM2_MOUSE]	0,003	14,84
Q61147	2	Ceruloplasmin OS=Mus musculus GN=Cp PE=1 SV=2 - [CERU_MOUSE]	0,009	14,80
P39654	12	Arachidonate 15-lipoxygenase OS=Mus musculus GN=Alox15 PE=1 SV=4 - [LOX15_MOUSE]	6,50E-05	-51,55
Q61878	5	Bone marrow proteoglycan OS=Mus musculus GN=Prg2 PE=1 SV=1 - [PRG2_MOUSE]	6,28E-06	-29,00
P49290	17	Eosinophil peroxidase OS=Mus musculus GN=Epx PE=1 SV=2 - [PERE_MOUSE]	1,96E-05	-25,55
P97425	2	Eosinophil cationic protein 2 OS=Mus musculus GN=Ear2 PE=2 SV=1 - [ECP2_MOUSE]	2,93E-06	-23,87
P97426	4	Eosinophil cationic protein 1 OS=Mus musculus GN=Ear1 PE=2 SV=1 - [ECP1_MOUSE]	7,53E-05	-13,54

9.3.4. Cytoscape network analysis

Cytoscape is an open source platform which helps to illustrate and analyse biological networks, such as protein-protein, protein-DNA or genetic interactions of different species [282]. Cytoscape analysis was performed for significantly differentially abundant proteins from “BM CLL vs. control” and “Blood CLL vs. control”. Proteins were analysed for three GO domains, biological process, cellular component and molecular function, in order to determine novel potential molecules involved in the altered neutrophil response in CLL. This way the entire context of a target protein can be elucidated, visualised and analysed.

Firstly, biological process refers to the bigger functional context of a particular protein. Secondly, cellular component reveals the cellular localization in which the protein carries out their functional purpose. Finally, molecular function indicates the operation at molecular level carried out by the protein [283]. In the following sections, ClueGO, a Cytoscape plug-in, has been used for data interpretation from the previously mentioned GO terms. In the network analysis by ClueGO, each node refers to a biological process, while the edges refer to connections between the biological processes. Additionally, the distance between edges illustrates the relationship between two processes. Functional terms in the Cytoscape network originate from the comparison of “BM CLL vs. control” or “Blood CLL vs. control”. Only the most significant interactions for biological process, cellular component and molecular function are shown. Moreover, the size of the node reflects the enrichment significance of the GO terms. For every grouping, there is a separate node colour. Nodes with composite colours represents several groups.

9.3.4.1. Bone marrow: CLL vs. control

Biological process

The ClueGO network was visualised for differentially abundant proteins in “BM CLL vs. control” in regard to the GO term Biological process (Figure 27). The biggest node family with 19 nodes belongs to antigen processing and presentation of endogenous peptide antigen via MHC class I (red). This is followed by 10 individual nodes belonging to the response to interferon-β (pink). Similarly, 2 mixed nodes indicated by orange/pink nodes equally refer to another 8 nodes of defence response to virus (orange) and response to type I interferon grouping. Next, positive regulation of leukocyte chemotaxis with 4 nodes (blue) is in close proximity to the orange

clustering. Subsequently, metanephric tubule development (turquoise) and apoptotic clearance (green) were enriched with two nodes each, respectively. Another small but individual node belongs to cellular response to mechanical stimulus. These results were illustrated in the pie chart and in the table (Figure 28 and Table 21). The ClueGO pie chart reveals biological process functions that are associated to the 51-node cluster from Figure 27. Redundancy was reduced by reporting functions with the highest numbers of related genes. Only significant associations between the nodes in the ClueGO cluster are shown. Table 21 shows the top 10 pathways according to the number of genes found in the proteome analysis as well as the percentage of associated genes.

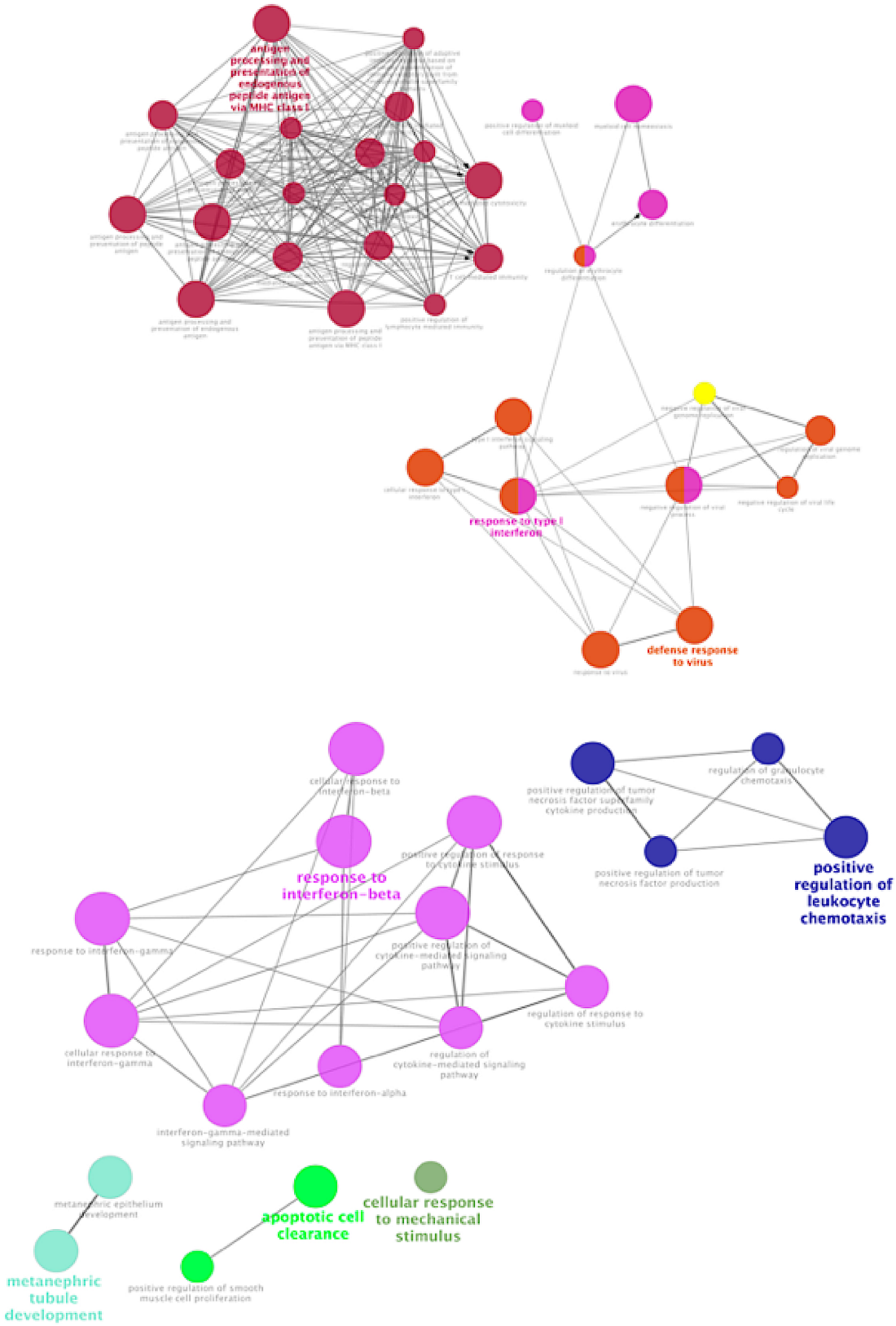

Figure 27. Enriched GO Biological process network groups using ClueGO for differentially abundant proteins in "BM CLL vs. control".

Biological processes (GO category) of the identified higher and lower abundant proteins (n=62, 58 recognized) in our experimental dataset were visualized with ClueGO as a functional grouped network and only the most significant interactions are shown (51 nodes). Ungrouped terms are not shown.

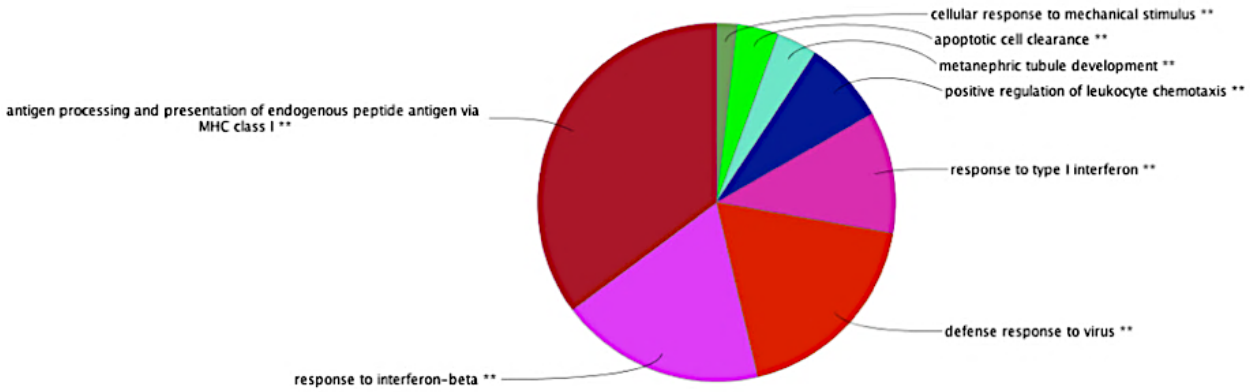

Figure 28. ClueGO pie chart of Biological process (GO term) related functions associated to the 51-node cluster.

*In order to avoid redundancy, functions reported in the pie chart are those with the highest numbers of related genes. **Indicates significant association between the 51-node cluster and represented GO terms (p-value≤0.05).*

Table 21. Top 10 enriched GO Biological process in "BM CLL vs. control".

GO Term	% associated genes	No. genes	Associated genes found
antigen processing and presentation of endogenous peptide antigen via MHC class I	55,56	5,00	[B2m, H2-D1, H2-K1, Tap1, Tapbp]
antigen processing and presentation of endogenous peptide antigen	45,45	5,00	[B2m, H2-D1, H2-K1, Tap1, Tapbp]
antigen processing and presentation of endogenous antigen	38,46	5,00	[B2m, H2-D1, H2-K1, Tap1, Tapbp]
antigen processing and presentation of peptide antigen via MHC class I	25,00	6,00	[B2m, H2-D1, H2-K1, H2-Q7, Tap1, Tapbp]
antigen processing and presentation of peptide antigen	17,07	7,00	[B2m, Ctss, H2-D1, H2-K1, H2-Q7, Tap1, Tapbp]
cellular response to interferon-beta	16,67	5,00	[Gbp2, Ifit1, Ifit3, Irgm1, Stat1]
response to interferon-beta	15,79	6,00	[Gbp2, Ifit1, Ifit3, Ifitm3, Irgm1, Stat1]
positive regulation of T cell mediated cytotoxicity	15,79	3,00	[B2m, H2-D1, H2-K1]
antigen processing and presentation of exogenous peptide antigen	15,00	3,00	[B2m, H2-K1, Tapbp]
response to type I interferon	14,71	5,00	[Ifitm3, Isg15, Stat1, Stat2, Zbp1]

Cellular Components

The ClueGO network visualised differentially abundant proteins in "BM CLL vs. control" in regard to the GO term Cellular component (Figure 29). The biggest node

family with 10 nodes belongs to symbiont-containing vacuole membrane (fluorescent green). This is followed by 9 individual nodes belonging to the phagocytic vesicle membrane (green). Another individual node belongs to endocytic vesicle membrane. These results were visualised in order to show the frequencies in the pie chart (Figure 30Figure 28). The ClueGO pie chart refers to functions associated to cellular component which in turn belonged to the 20-node network. Notably, only two major functions were proposed. Redundancy was reduced by reporting functions with the highest numbers of related genes. Only significant associations between the nodes in the ClueGO cluster are shown. Furthermore, the top 10 enriched cellular component functions in “BM CLL vs. control” were based on the frequency of associated genes found in the list of differentially abundant proteins. In contrast to Figure 30 and Figure 31, the data summarised in Table 22 reveals more information about individual network annotations. Interestingly, differentially abundant proteins from this particular comparison were enriched for MHC class I protein complex, golgi medial cisterna, various endoplasmic reticulum components and the phagocytic and endocytic vesicle membrane. These results partially reflect the information from the ClueGO network and pie chart.

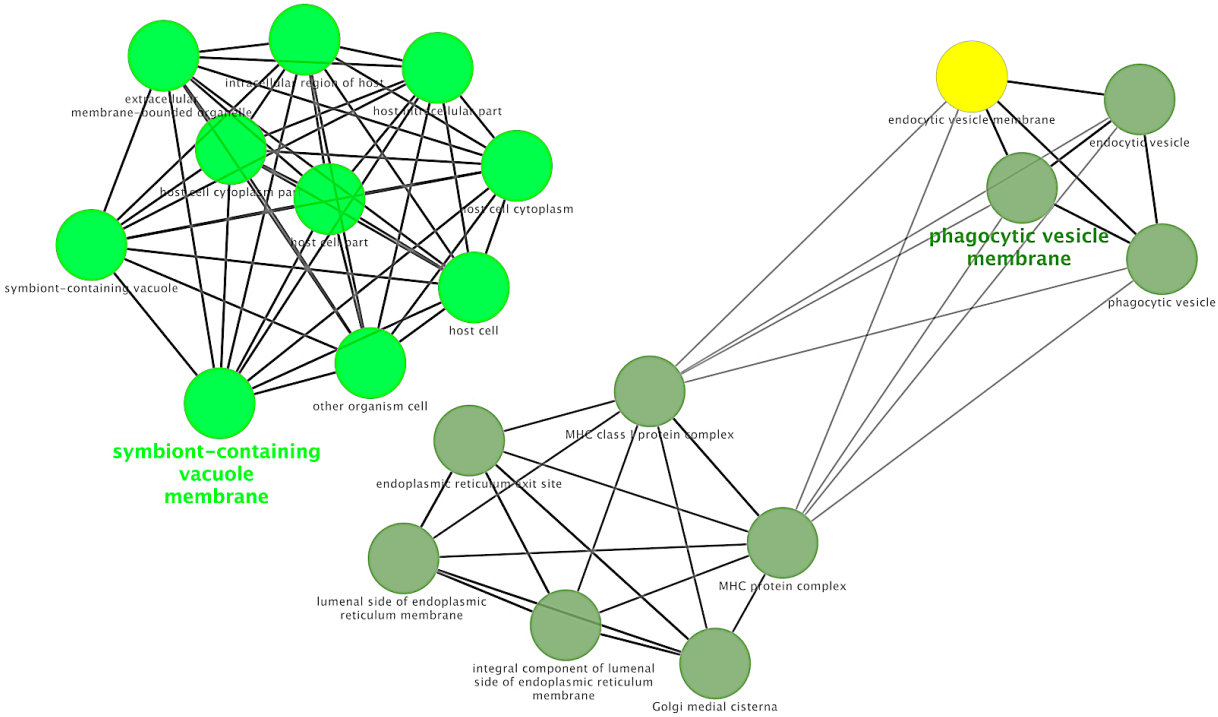

Figure 29. Enriched GO Cellular component network groups using ClueGO for differentially abundant proteins in "BM CLL vs. control".

Cellular component (GO category) of the identified higher and lower abundant proteins (n=62, 58 recognized) in our experimental dataset were visualized with ClueGO as a functional grouped network and only the most significant interactions are shown (20 nodes). Ungrouped terms are not shown.

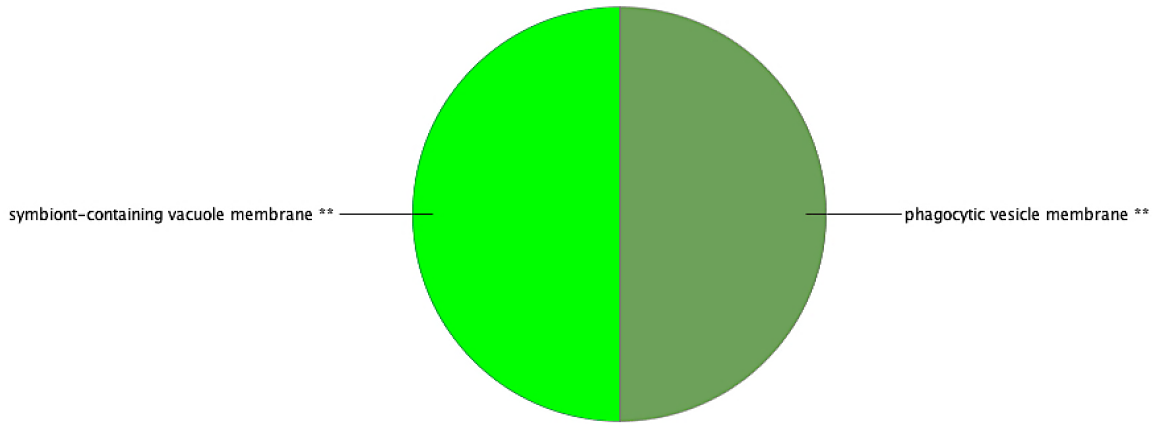

Figure 30. ClueGO pie chart of Cellular component (GO term) functions associated to the 20-node cluster.

*In order to avoid redundancy, functions reported in the pie chart are those with the highest numbers of related genes. **Indicates significant association between the 20-node cluster and represented GO terms (p-value≤0.05).*

Table 22. Top 10 enriched GO Cellular component in "BM CLL vs. control".

GO Term	% associated genes	No. genes	Associated genes found
MHC class I protein complex	25,00	3,00	[H2-D1, H2-K1, H2-Q7]
Golgi medial cisterna	23,08	3,00	[H2-D1, H2-K1, H2-Q7]
endoplasmic reticulum exit site	17,65	3,00	[H2-D1, H2-K1, H2-Q7]
lumenal side of endoplasmic reticulum membrane	17,65	3,00	[H2-D1, H2-K1, H2-Q7]
integral component of lumenal side of endoplasmic reticulum membrane	17,65	3,00	[H2-D1, H2-K1, H2-Q7]
MHC protein complex	15,00	3,00	[H2-D1, H2-K1, H2-Q7]
phagocytic vesicle membrane	11,76	6,00	[H2-D1, H2-K1, H2-Q7, Irgm1, Tap1, Tapbp]
endocytic vesicle membrane	9,09	6,00	[H2-D1, H2-K1, H2-Q7, Irgm1, Tap1, Tapbp]
phagocytic vesicle	7,69	6,00	[H2-D1, H2-K1, H2-Q7, Irgm1, Tap1, Tapbp]
cytosolic small ribosomal subunit	6,52	3,00	[Rps11, Rps13, Rps24]

Molecular function

The ClueGO network visualised differentially abundant proteins in "BM CLL vs. control" in regard to the GO term Molecular function (Figure 31). The biggest node family with 4 nodes belongs to TAP binding (blue). This is followed by 3 individual nodes, each belonging to double-stranded RNA binding (dark green), cysteine-type endopeptidase inhibitor activity (fluorescent green) and laminin binding (turquoise). These results were visualised in order to show the frequencies in the pie chart (Figure 32Figure 28). The ClueGO pie chart refers to functions associated to cellular component which in turn belonged to the 7-node network. Redundancy was reduced by reporting functions with the highest numbers of related genes. Only significant associations between the nodes in the ClueGO cluster are shown. Furthermore, only 7 enriched molecular functions were found for "BM CLL vs. control" and summarised in Table 23. Interestingly, differentially abundant proteins from this particular

comparison were enriched for TAP binding, β2-microglobulin binding, T-cell receptor binding, peptide antigen binding, laminin binding, cysteine-type endopeptidase inhibitor activity and double-stranded RNA binding. These results partially reflect the information from the ClueGO network and pie chart.

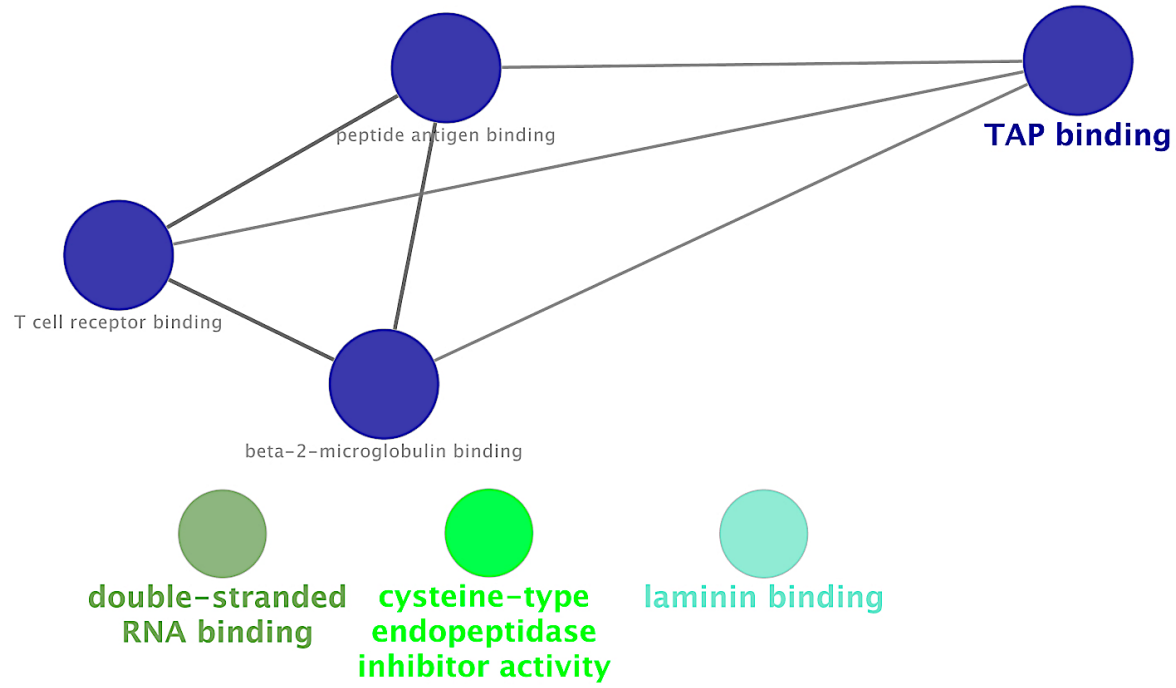

Figure 31. Enriched GO Molecular function network groups using ClueGO for differentially abundant proteins in "BM CLL vs. control".

Molecular function (GO category) of the identified higher and lower abundant proteins (n=62, 58 recognized) in our experimental dataset were visualized with ClueGO as a functional grouped network and only the most significant interactions are shown (7 nodes). Ungrouped terms are not shown.

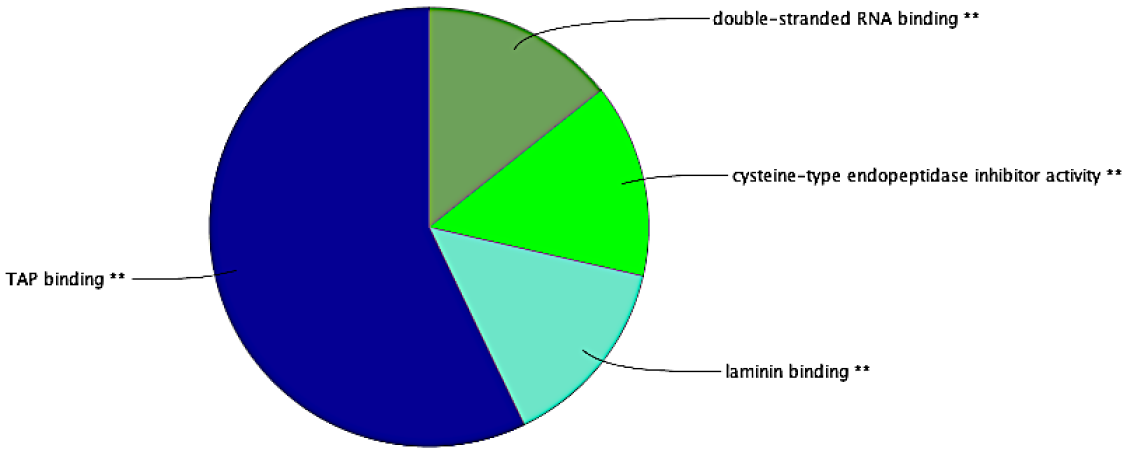

Figure 32. ClueGO pie chart of Molecular function (GO term) functions associated to the 7-node cluster.

*In order to avoid redundancy, functions reported in the pie chart are those with the highest numbers of related genes. **Indicates significant association between the 7-node cluster and represented GO terms (p-value≤0.05).*

Table 23. Top 7 enriched GO Molecular function in "BM CLL vs. control".

GO Term	% associated genes	No. genes	Associated genes found
TAP binding	62,50	5,00	[H2-D1, H2-K1, H2-Q7, Tap1, Tapbp]
beta-2-microglobulin binding	30,00	3,00	[H2-D1, H2-K1, H2-Q7]
T cell receptor binding	25,00	3,00	[H2-D1, H2-K1, H2-Q7]
peptide antigen binding	20,00	3,00	[H2-D1, H2-K1, H2-Q7]
laminin binding	10,00	3,00	[Ctss, Lgals1, Thbs1]
cysteine-type endopeptidase inhibitor activity	4,92	3,00	[Stfa1, Stfa2, Stfa3]
double-stranded RNA binding	4,35	3,00	[Ddx58, Oas1a, Oas3]

9.3.4.2. Blood: CLL vs. control

Biological process

The ClueGO network visualised or differentially abundant proteins in "Blood CLL vs. control" in regard to the GO term Biological process (Figure 33). The biggest node family with 11 nodes belongs to antigen processing and presentation of peptide antigen (pink). This is followed by 10 individual nodes belonging to the response to interferon-γ (orange). Next, defence response to virus with 9 nodes (blue) is in close proximity to the turquoise clustering with 7 nodes belonging to the deoxyribonucleotide metabolic process. Subsequently, the response to interferon-β (green) was enriched with three nodes each, respectively. In addition, two individual nodes belong to positive regulation of smooth muscle cell proliferation and apoptotic cell clearance. These results were illustrated in the pie chart (Figure 34). The ClueGO pie chart reveals biological process functions that are associated to the 42-node cluster. Redundancy was reduced by reporting functions with the highest numbers of related genes. Only significant associations between the nodes in the ClueGO cluster are shown. Furthermore, the top 10 enriched biological process functions in "Blood CLL vs. control" were summarised in Table 24. Interestingly,

differentially abundant proteins from this particular comparison were enriched for various antigen processing and presentation functions, responses to interferon-β and deoxyribonucleotide metabolic process. These results partially reflect the information from the ClueGO network and pie chart.

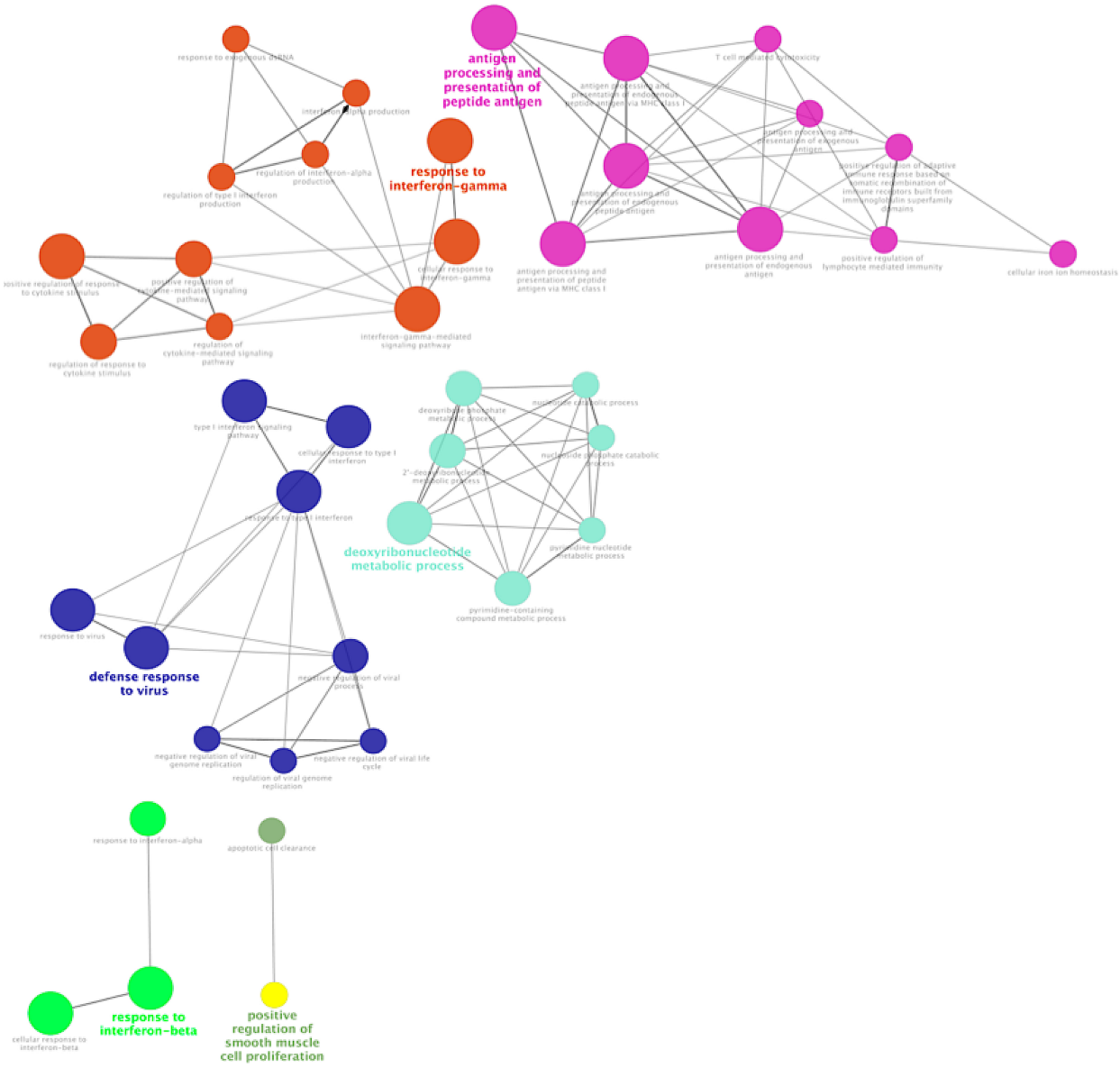

Figure 33. Enriched GO Biological process network groups using ClueGO for differentially abundant proteins in "Blood CLL vs. control".

Biological processes (GO category) of the identified higher and lower abundant proteins (n=90, 86 recognized) in our experimental dataset were visualized with ClueGO as a functional grouped network and only the most significant interactions are shown (42 nodes). Ungrouped terms are not shown.

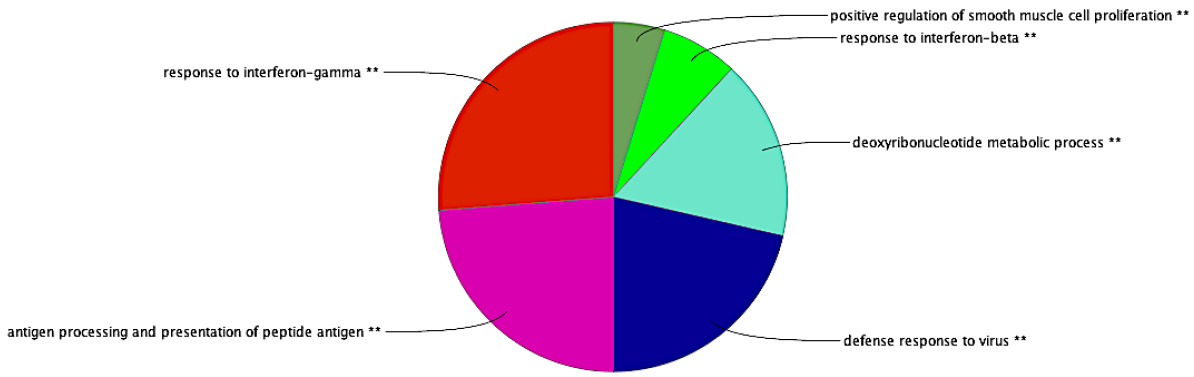

Figure 34. ClueGO pie chart of Biological process (GO term) functions associated to the 42-node cluster.

*In order to avoid redundancy, functions reported in the pie chart are those with the highest numbers of related genes. **Indicates significant association between the 42-node cluster and represented GO terms (p-value≤0.05).*

Table 24. Top 10 enriched GO Biological process in "Blood CLL vs. control".

GO Term	% associated genes	No. genes	Associated genes found
antigen processing and presentation of endogenous peptide antigen via MHC class I	44,44	4,00	[H2-D1, H2-K1, Tap1, Tapbp]
antigen processing and presentation of endogenous peptide antigen	36,36	4,00	[H2-D1, H2-K1, Tap1, Tapbp]
antigen processing and presentation of endogenous antigen	30,77	4,00	[H2-D1, H2-K1, Tap1, Tapbp]
antigen processing and presentation of peptide antigen via MHC class I	20,83	5,00	[H2-D1, H2-K1, H2-Q7, Tap1, Tapbp]
cellular response to interferon-beta	20,00	6,00	[Gbp2, Ifit1, Ifit3, Irgm1, Stat1, Trex1]
response to interferon-beta	18,42	7,00	[Gbp2, Ifit1, Ifit3, Ifitm3, Irgm1, Stat1, Trex1]
interferon-gamma-mediated signalling pathway	18,18	4,00	[Hpx, Irgm1, Nmi, Stat1]
deoxyribonucleotide metabolic process	17,39	4,00	[Cmpk2, Nt5c, Rrm1, Samhd1]
2'-deoxyribonucleotide metabolic process	16,67	3,00	[Cmpk2, Nt5c, Samhd1]
response to type I interferon	14,71	5,00	[Ifitm3, Isg15, Stat1, Stat2, Zbp1]

Cellular Components

The ClueGO network visualised differentially abundant proteins in "Blood CLL vs. control" in regard to the GO term Cellular component (Figure 35). The biggest node family with 11 nodes belongs to phagocytic vesicle membrane (turquoise). This is followed by 2 nodes belonging to the endopeptidase complex (dark green). Two

individual nodes belong to small ribosomal subunit (fluorescent green) and cytosolic small ribosomal subunit (yellow), respectively. These results were visualised in order to show the frequencies in the pie chart (Figure 36Figure 28). The ClueGO pie chart refers to functions associated to cellular component which in turn belonged to the 9-node network. Redundancy was reduced by reporting functions with the highest numbers of related genes. Only significant associations between the nodes in the ClueGO cluster are shown. Furthermore, the top 10 enriched cellular component functions in “Blood CLL vs. control” were summarised in Table 25. Interestingly, differentially abundant proteins from this particular comparison were enriched for MHC class I protein complex, golgi medial cisterna, various endoplasmic reticulum components and the phagocytic and endocytic vesicle membrane. These results partially reflect the information from the ClueGO network and pie chart.

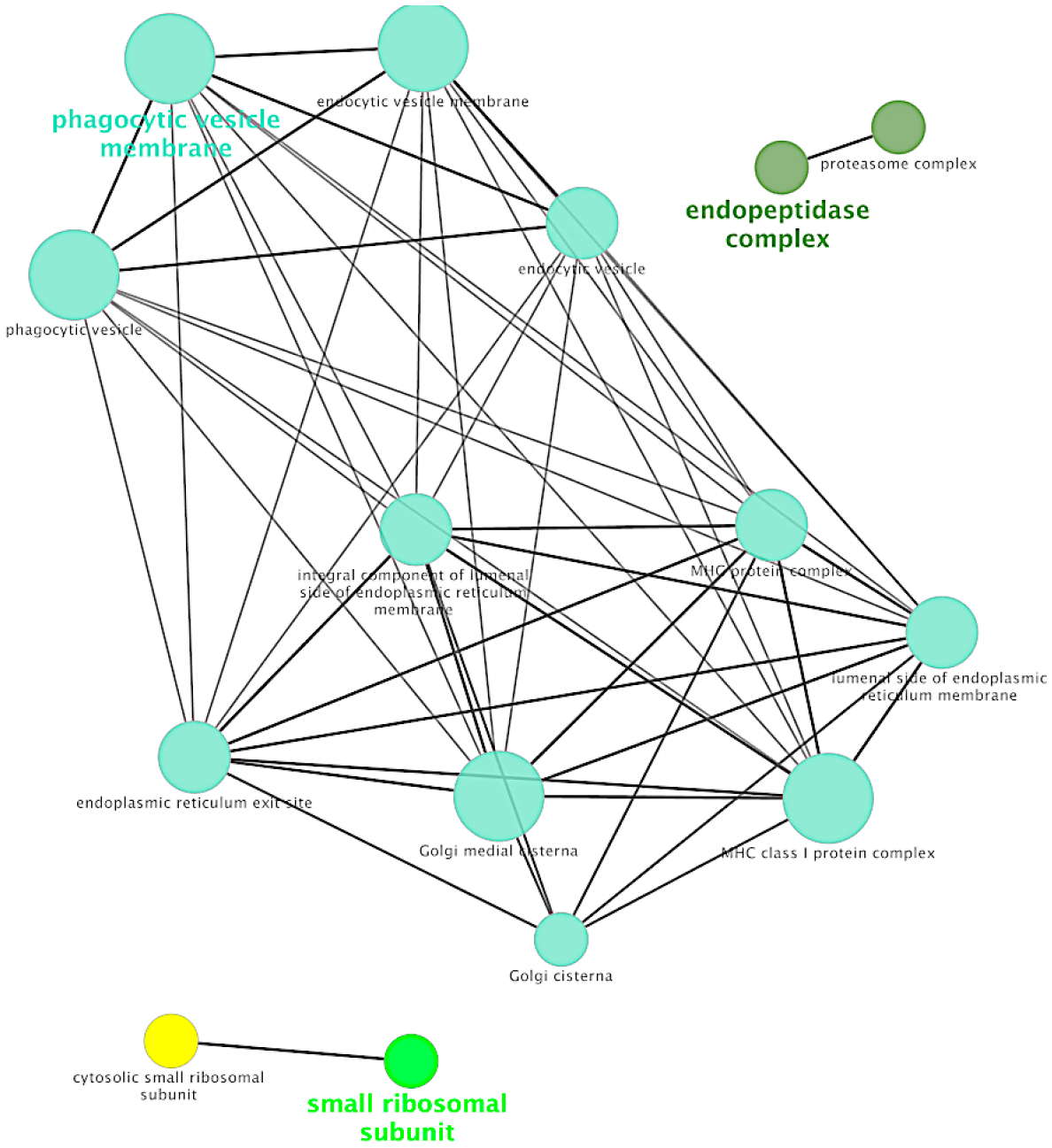

Figure 35. Enriched GO Cellular components network groups using ClueGO for differentially abundant proteins in "Blood CLL vs. control".

Cellular component (GO category) of the identified higher and lower abundant proteins (n=90, 86 recognized) in our experimental dataset were visualized with ClueGO as a functional grouped network and only the most significant interactions are shown (15 nodes). Ungrouped terms are not shown.

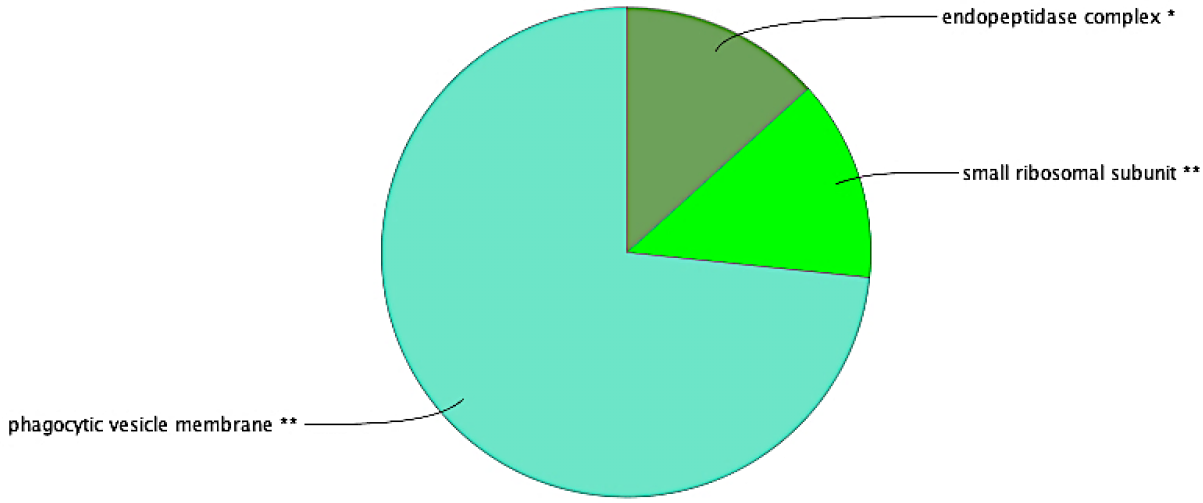

Figure 36. ClueGO pie chart of Cellular component (GO term) functions associated to the 15-node cluster.

*In order to avoid redundancy, functions reported in the pie chart are those with the highest numbers of related genes. **Indicates significant association between the 15-node cluster and represented GO terms (p-value≤0.05).*

Table 25. Top 10 enriched GO Cellular component in "Blood CLL vs. control".

GO Term	% associated genes	No. genes	Associated genes found
MHC class I protein complex	25,00	3,00	[H2-D1, H2-K1, H2-Q7]
Golgi medial cisterna	23,08	3,00	[H2-D1, H2-K1, H2-Q7]
endoplasmic reticulum exit site	17,65	3,00	[H2-D1, H2-K1, H2-Q7]
lumenal side of endoplasmic reticulum membrane	17,65	3,00	[H2-D1, H2-K1, H2-Q7]
integral component of lumenal side of endoplasmic reticulum membrane	17,65	3,00	[H2-D1, H2-K1, H2-Q7]
MHC protein complex	15,00	3,00	[H2-D1, H2-K1, H2-Q7]
phagocytic vesicle membrane	11,76	6,00	[H2-D1, H2-K1, H2-Q7, Irgm1, Tap1, Tapbp]
endocytic vesicle membrane	9,09	6,00	[H2-D1, H2-K1, H2-Q7, Irgm1, Tap1, Tapbp]
phagocytic vesicle	7,69	6,00	[H2-D1, H2-K1, H2-Q7, Irgm1, Tap1, Tapbp]
cytosolic small ribosomal subunit	6,52	3,00	[Rps11, Rps13, Rps24]

Molecular function

The ClueGO network visualised differentially abundant proteins in “Blood CLL vs. control” in regard to the GO term Molecular function (Figure 37). The biggest node family with 4 nodes belongs to TAP binding (pink). Subsequently, two nodes refer to purine deoxyribonucleotide binding (blue). This is followed by 3 individual nodes, each belonging to rRNA binding (turquoise), double-stranded RNA binding (dark green) and cysteine-type endopeptidase inhibitor activity (fluorescent green). These results were visualised in order to show the frequencies in the pie chart (Figure 38Figure 28). The ClueGO pie chart refers to functions associated to cellular component which in turn belonged to the 9-node network. Redundancy was reduced by reporting functions with the highest numbers of related genes. Only significant associations between the nodes in the ClueGO cluster are shown. Notably, only 9 enriched molecular functions were found for “Blood CLL vs. control” and thus ranked and summarised in Table 26. These results completely reflect the information from the ClueGO network and pie chart.

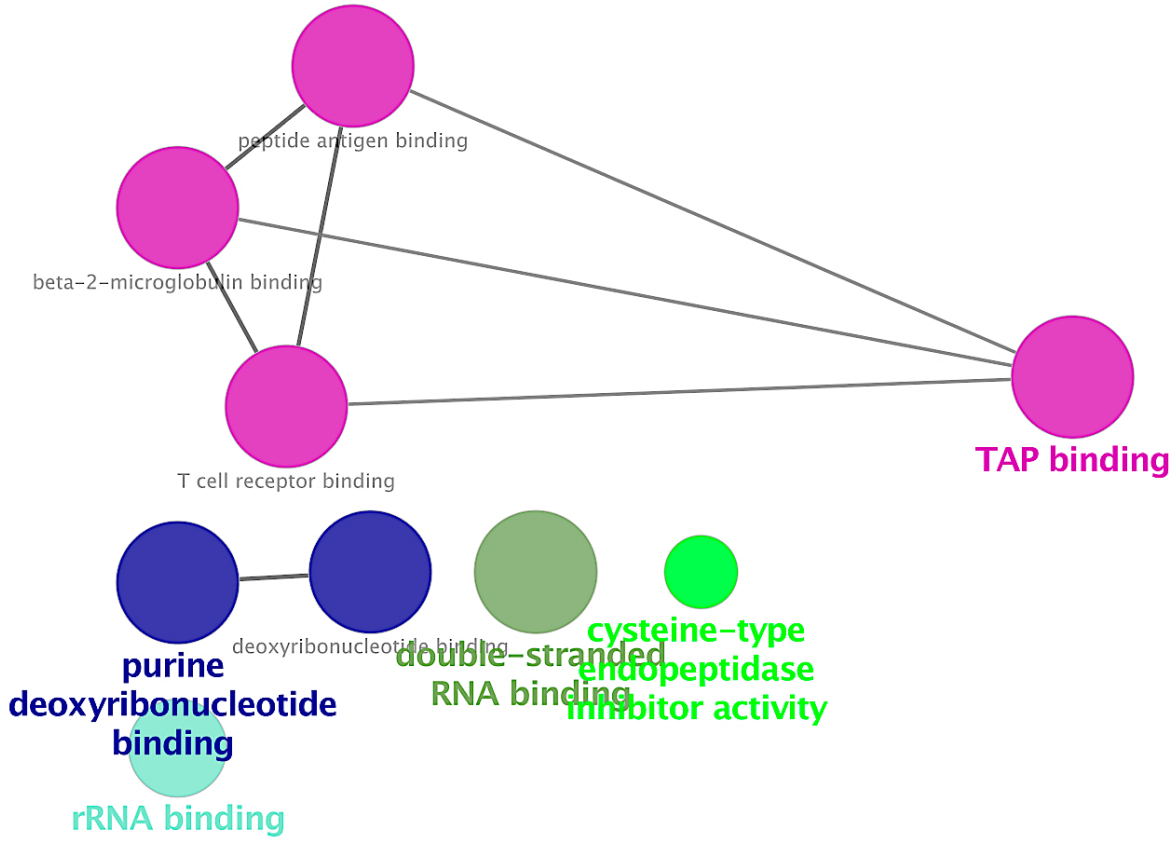

Figure 37. Enriched GO Molecular function network groups using ClueGO for differentially abundant proteins in "Blood CLL vs. control".

Molecular function (GO category) of the identified higher and lower abundant proteins (n=90, 86 recognized) in our experimental dataset were visualized with ClueGO as a functional grouped network and only the most significant interactions are shown (9 nodes). Ungrouped terms are not shown.

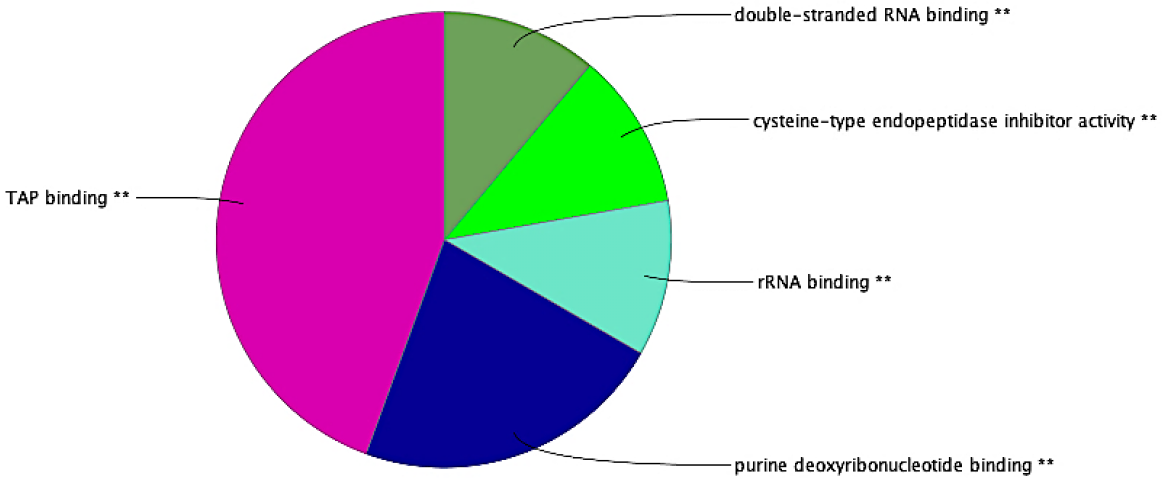

Figure 38. ClueGO pie chart of Molecular function (GO term) functions associated to the 9-node cluster.

*In order to avoid redundancy, functions reported in the pie chart are those with the highest numbers of related genes. **Indicates significant association between the 9-node cluster and represented GO terms (p-value≤0.05).*

Table 26. Top 9 enriched GO Molecular function in "Blood CLL vs. control".

GO Term	% associated genes	No. genes	Associated genes found
TAP binding	62,50	5,00	[H2-D1, H2-K1, H2-Q7, Tap1, Tapbp]
purine deoxyribonucleotide binding	60,00	3,00	[Samhd1, St13, Trex1]
deoxyribonucleotide binding	50,00	3,00	[Samhd1, St13, Trex1]
beta-2-microglobulin binding	30,00	3,00	[H2-D1, H2-K1, H2-Q7]
T cell receptor binding	25,00	3,00	[H2-D1, H2-K1, H2-Q7]
peptide antigen binding	20,00	3,00	[H2-D1, H2-K1, H2-Q7]
double-stranded RNA binding	7,25	5,00	[Ddx21, Ddx58, Oas1a, Oas3, Tfrc]
cysteine-type endopeptidase inhibitor activity	4,92	3,00	[Stfa1, Stfa2, Stfa3]
rRNA binding	4,84	3,00	[Ddx21, Rps11, Rps13]

9.4. Antibacterial response by neutrophils in CLL

9.4.1. Decreased phagocytosis and MPO levels in neutrophils from CLL

To investigate whether neutrophil function is altered during CLL, the phagocytic capacity of blood neutrophils was tested *ex vivo* and intracellular MPO levels were measured after CLL induction. Here, a two-way ANOVA with Bonferroni post-hoc was calculated to compare the mean differences between control and CLL over time. In detail, ingestion of pH-sensitive fluorochrome-conjugated *E. coli* has led to a gradual decline in the proportion of phagocytically active neutrophils during CLL progression (Figure 39). Neutrophils of control and CLL mice have equal phagocytic capacities 14 days after CLL induction (Control mean: 77.8 %; CLL mean: 77.6 %). At this point, the average tumour load ($CD5^+CD19^+$) mounted up to 28.6 % in the peripheral blood of CLL mice. The first difference in the phagocytic activity was observed 21 days post CLL induction with levels dropping to 74.9 % in CLL animals, while 77.8 % of neutrophils retained their phagocytosis activity in control mice. As the phagocytic activity decreased in CLL mice, the CLL load rose to 35.9 % in circulation gradually. After 28 days of disease induction, CLL mice bared an average tumour load of 40.1 % in their circulation. At the same time, the *ex vivo* phagocytic capacity

of neutrophils has decreased significantly to 70.9 % in CLL compared to 84.5 % in control.

In summary, the *ex vivo* phagocytic capacity of circulating neutrophils decreased during progressive CLL B-cell accumulation in the blood.

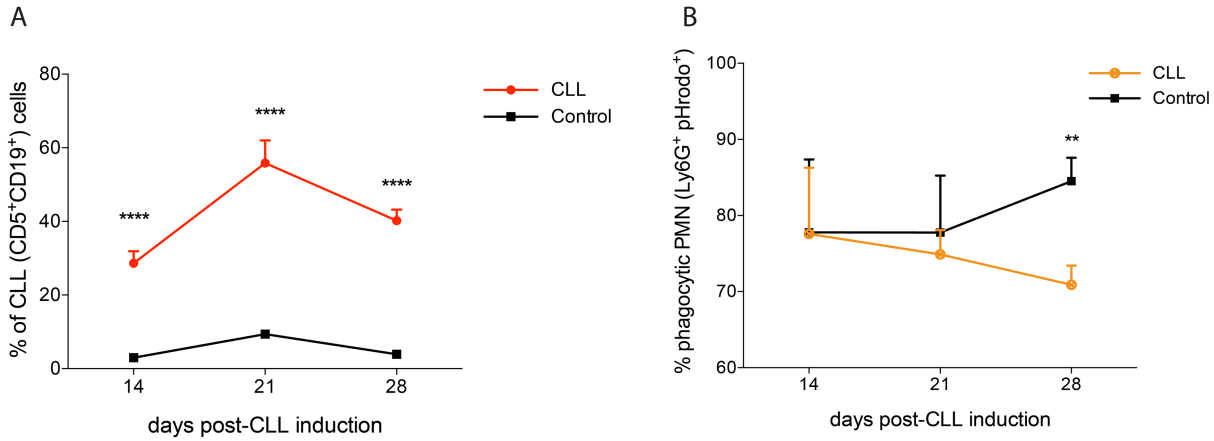

Figure 39. Decreased ex vivo phagocytic activity in circulating neutrophils derived from CLL-induced mice.

CLL was induced and blood was withdrawn from the tail vein at various timepoints. The phagocytic activity was tested ex vivo and quantified in control (n=9) and CLL mice (n=8) by FC. (A) *CLL load was measured 14, 21 and 28 days post-CLL induction. (B) Ex vivo phagocytosis assay of blood neutrophils incubated with pH-sensitive fluorochrome-conjugated E. coli Bioparticles. Statistical testing: Two-way ANOVA with Bonferroni post-hoc.*

Next, intracellular MPO levels were measured by flow cytometry. Based on the assumption that the data distribution is not normal, the Mann-Whitney *U* test was chosen to test for statistical relevance. While CLL levels reached an average of 73.0 % in CLL mice, the threshold value was 10.2 % on average in control animals (Figure 40A). Simultaneously, MPO^+ percentages were quantified in neutrophils (Figure 40B). Almost all neutrophils in control animals expressed MPO. In CLL, the frequency of MPO^+ cells was significantly decreased compared to control mice (Control mean: 96.6 %; CLL mean: 88.4 %; Figure 40B).

Consequently, neutrophil phagocytic function diminished during CLL progression and MPO levels declined in neutrophils of CLL mice with a high load of CLL B-cells in the blood.

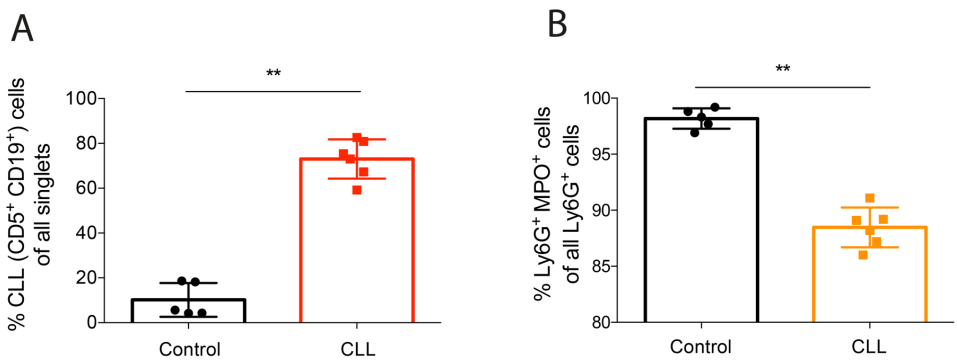

Figure 40. Decreased levels of MPO in neutrophil subsets in circulation.

CLL was induced and blood was withdrawn from the tail vein at various timepoints. Intracellular MPO levels were quantified in control (n=5) and CLL mice (n=6) by FC. (A) Mice were induced with CLL and the tumour burden was measured 28 days post CLL induction. (B) At the same time point, the percentage of MPO⁺ neutrophils was detected in the blood. Statistical testing: Mann-Whitney U test.

9.4.2. Increased bacterial burden in CLL

To investigate whether the antibacterial response is altered *in vivo*, CLL mice were infected with GFP-UPEC and bladder sections were stained with anti-GFP and DAPI (8.2.3.1). Subsequently, the GFP⁺ infection area which correlated with the bacterial burden was quantified through semi-automated analysis (Figure 41). The top panel shows representative images of uninfected bladders. Images in the middle refer to infected bladders of control mice, while the bottom panel illustrates murine bladder sections from infected CLL mice. In uninfected mice, the bladder did not show any GFP-UPEC signals. In contrast, GFP signals were retrieved for UPEC-infected control mice. As shown in the zoom, the bacterial burden was limited to a few spots on the luminal side of the uroepithelium in infected control mice. Furthermore, UPEC clusters and dispersion predominantly on the luminal surface of the uroepithelium was observed in infected CLL mice. The detailed image shows UPEC invasion into the epithelial layer of the urinary bladder.

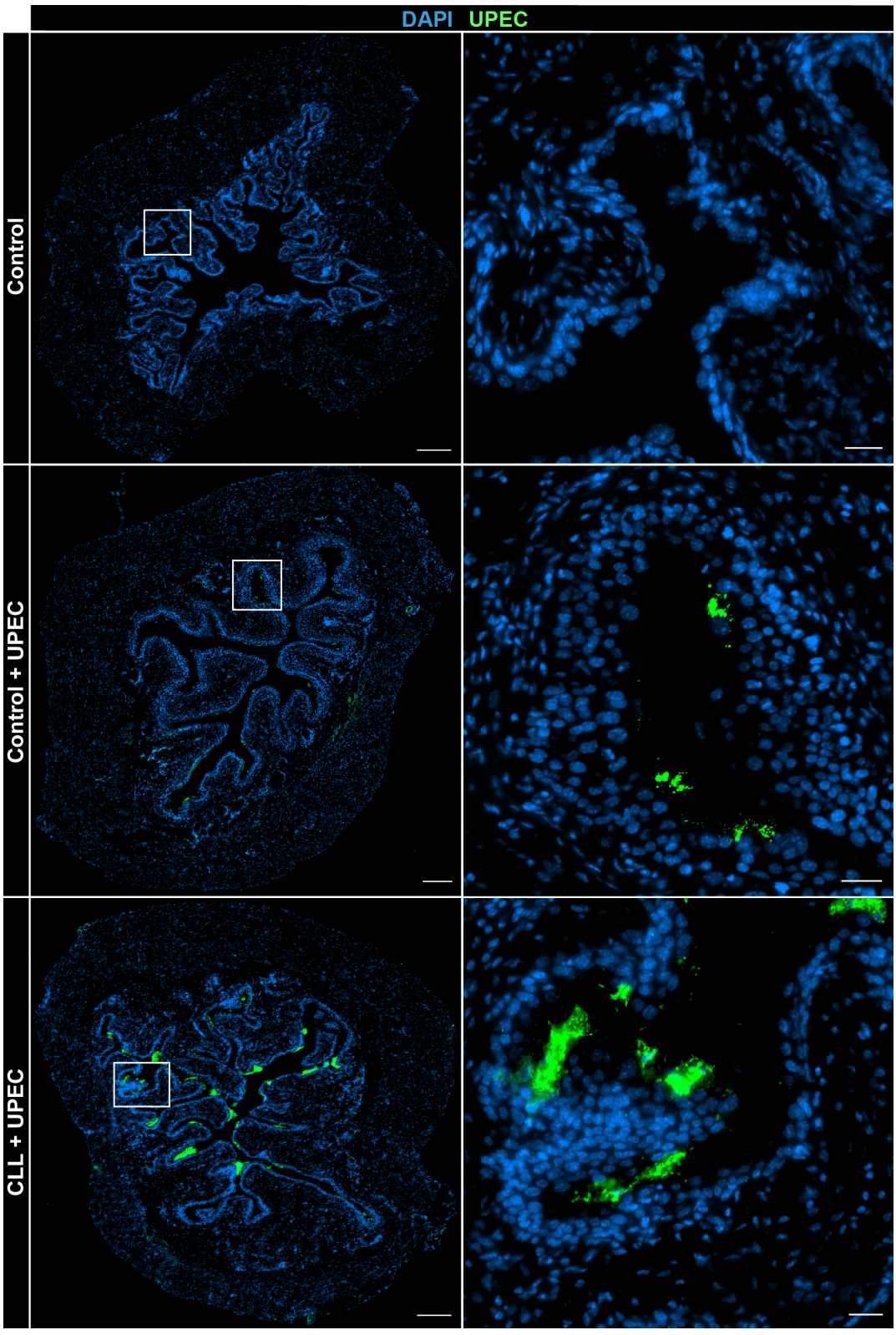

Figure 41. Increased bacterial burden in CLL mice.

Control and CLL mice were infected (t.u.) with GFP-UPEC and bladders were harvested 21hpi. After fixation and cryo-embedding, bladders were cut into 10 µm thick sections and stained with anti-GFP and DAPI. Representative images show composites of DAPI (blue) and GFP-UPEC (green) signals in uninfected (top; n=2), infected control (middle; n=6) and infected CLL bladder (low; n=6). Overview images are on the left, while detailed images are shown on the right. Scale bars: overview 200 µm, zoom 30 µm.

Next, the UPEC burden was quantified by a semi-automated analysis (Figure 42). In regard to statistical testing, the Mann-Whitney *U* test was performed for the comparison of infection areas in UPEC-infected control and CLL mice, while the two-way ANOVA with Bonferroni post-hoc was calculated to compare means of UPEC invasion for various tissue compartments of control and CLL mice. Notably, bacterial burden was not detected in the muscle and thus this particular compartment has not been included in the quantification shown in Figure 42.

The infection area was significantly increased in UPEC-infected CLL mice compared to UPEC-infected control mice (Figure 42A). In detail, 9.0 % (SD: ± 6.6) of the total murine bladder area was covered by UPEC in CLL. In comparison, the average percentage of the infected area mounted up to only 0.9 % (SD: ± 0.6) of the total bladder area in control animals. In order to visualise UPEC invasion, bacterial burden was quantified in various bladder compartments (Figure 42B). The urinary bladder consists of the lumen in the centre. The epithelial layer is the first cellular barrier which is surrounded by the connective tissue [244]. Thus, any bacterial invasion beyond this spatial barrier could serve as a parameter for the severity of infection. Finally, the bladder muscle forms the outermost layer.

The highest UPEC burden was observed in the lumen of UPEC-infected CLL mice with an average of 6.8 %. In contrast, only 0.3 % of the lumen was covered by UPEC in control mice. Subsequently, the degree of UPEC invasion into the uroepithelium was analysed. In detail, 6.8 % of the epithelium of infected CLL mice was invaded by UPEC, while only 0.2 % of the epithelium in UPEC-infected control mice was affected by bacterial invasion. The changes in UPEC invasion in both, the lumen and epithelium, were significantly increased in CLL mice. Furthermore, UPEC invasion was lower in the connective tissue compared to other bladder compartments in both infected groups. Despite, a tenfold increase in the UPEC invasion into the urinary connective tissue was observed in infected CLL mice (Control: 0.01 %; CLL: 0.11 %). This particular increase shows a non-significant trend.

In summary, these data indicate a tenfold increase of UPEC burden in the lumen and a 22.7-fold increase of bacterial burden in the uroepithelium of infected CLL bladders.

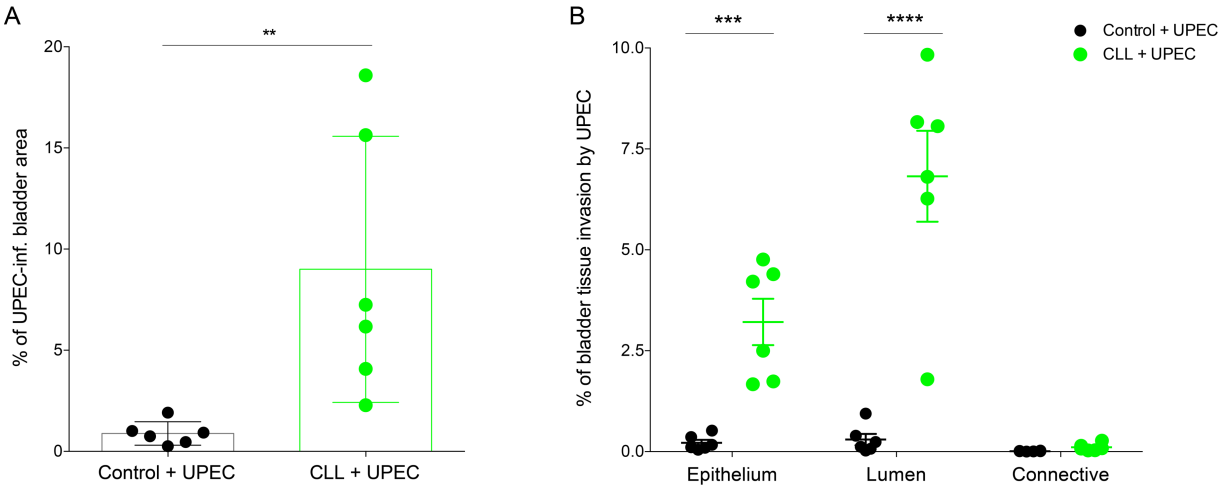

Figure 42. Increased UPEC burden in the epithelium and lumen of bladder during UTI in CLL mice.

Semi-automated quantification was performed on murine bladder sections which were stained with anti-GFP and DAPI. Subsequently, UPEC invasion in general and in various bladder compartments was quantified (Control + UPEC n=6; CLL + UPEC n=6). (A) The bacterial burden was measured for infected control and CLL mice. (B) UPEC invasion was detected in the epithelium, lumen and connective tissue of infected control and CLL mice. Statistical testing: (A) Mann-Whitney U test; (B) Two-way ANOVA with Bonferroni post-hoc.

9.4.3. The role of neutrophils during UTI in CLL

To investigate the role of neutrophils in UTI during CLL *in vivo*, bladder sections of UPEC-infected control and CLL animals were stained for Ly6G, anti-GFP and DAPI (Figure 43). The left panel shows overview images of urinary bladder sections, the right panel refers to corresponding detailed images. The upper row of images refers to uninfected control murine bladders, while infected control bladders sections are illustrated in the middle row. The lower panel of images shows murine bladder sections of UPEC-infected CLL mice. In the uninfected situation, only few neutrophil signals co-localised with DAPI in compartments of the urinary bladder. Neutrophil levels elevated after UPEC infection in control and rose once again during UTI in CLL mice (Figure 43). In detail, individual neutrophils were observed in every bladder compartment, predominantly in the uroepithelium followed by the connective tissue in infected control mice. An increased number of neutrophils were detected around endothelial cells which were located in close proximity to the uroepithelium of UPEC-infected control mice. In contrast to the infected control bladders, neutrophils aggregated into clusters in UPEC-infected CLL bladders. Large cell clusters were particularly found in the uroepithelium, followed by individual or paired cells in the

connective tissue. Strikingly, the images show that the total number of neutrophils is elevated in UPEC-infected bladder.

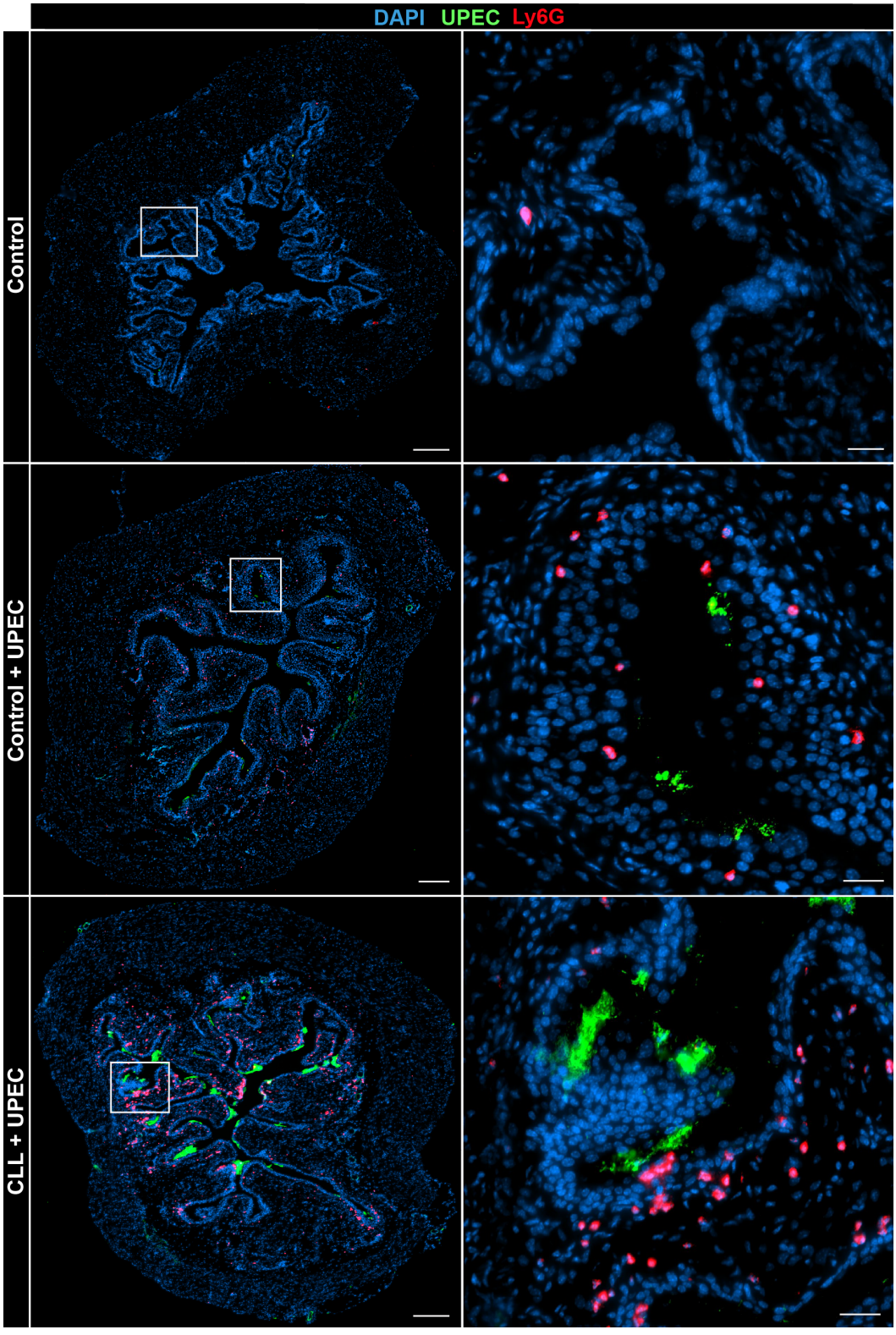

Figure 43. Neutrophil infiltration into the uroepithelium and lumen is stronger during UTI in CLL.

Control and CLL mice were infected (t.u.) with GFP-UPEC and bladders were harvested 21hpi. Representative images show composites of DAPI (blue), GFP-UPEC (green) and Ly6G (red) signals in control (top; n=2), control- (middle; n=6) and CLL-inf. bladder (low; n=6) sections. Scale bars: overview (left) 200 µm, zoom (right) 30 µm.

As illustrated in Figure 44A, neutrophil numbers per mm^2 were measured in the uroepithelium, lumen, connective tissue and muscle of UPEC-infected control and CLL mice. Notably, the average area of murine urinary bladders is between 3-4 mm^2 based on our own observations. The two-way ANOVA with Bonferroni post-hoc was conducted for multiple comparisons in Figure 44A, while the Mann-Whitney *U* test was chosen as a statistical test to compare the distance of neutrophils in UPEC-infected control and CLL mice.

In general, neutrophil numbers were relatively low in the absence of UTI. Only three neutrophils were detected on average in the connective tissue and muscle of uninfected mice. The lumen and uroepithelium contained approximately four neutrophils per mm^2. Hence, the distance analyses illustrated in Figure 44B and C were not performed for uninfected urinary bladders based on the low levels of neutrophil numbers.

Regardless, neutrophil densities were higher for infected urinary bladders of both, control and CLL mice. In detail, neutrophil density mounted up to 1016 cells in the CLL group, while UPEC-infected control mice had an average of 601 neutrophils in the uroepithelium. There is a significant increase in neutrophils in the lumen of UPEC-infected CLL mice 21 hpi (Control: 159; CLL: 318). For other bladder compartments, neutrophil densities were similar. Specifically, 392 and 314 neutrophils were found in the connective tissue, while 43 and 36 neutrophils were localised in the bladder muscle of infected control and CLL mice (Figure 44A). The distribution of neutrophils was concentrated at the focus of the infection, in the uroepithelium and lumen of UPEC-infected CLL mice. In order to visualise the distribution of neutrophils in CLL, the distance to lumen was quantified for neutrophils of one biological sample of each group (Figure 44B). For this, 944 neutrophils from one UPEC-infected control and 1126 neutrophils from one UPEC-infected CLL bladder were taken into consideration. Interestingly, CLL neutrophils were observed to be located closer to the lumen, the site of infection. The median value for neutrophils from CLL mice is 52.0 µm. In contrast, the median distance of neutrophils from UPEC-infected control mice to the lumen increased significantly to 189.5 µm. Next, the biological samples of both groups were analysed and the overall mean distances of neutrophils from infected control and CLL bladders were compared (Figure 44C). The mean distance of neutrophils to the lumen mounted up to 122.5 µm in UPEC-infected control and declined to 66.0 µm in UPEC-infected CLL

mice. The difference in distance to the site of infection was significantly decreased in the CLL group (Figure 44C). However, the decreased distance of neutrophils to the site of infection does not explain the increased UPEC burden in CLL animals.

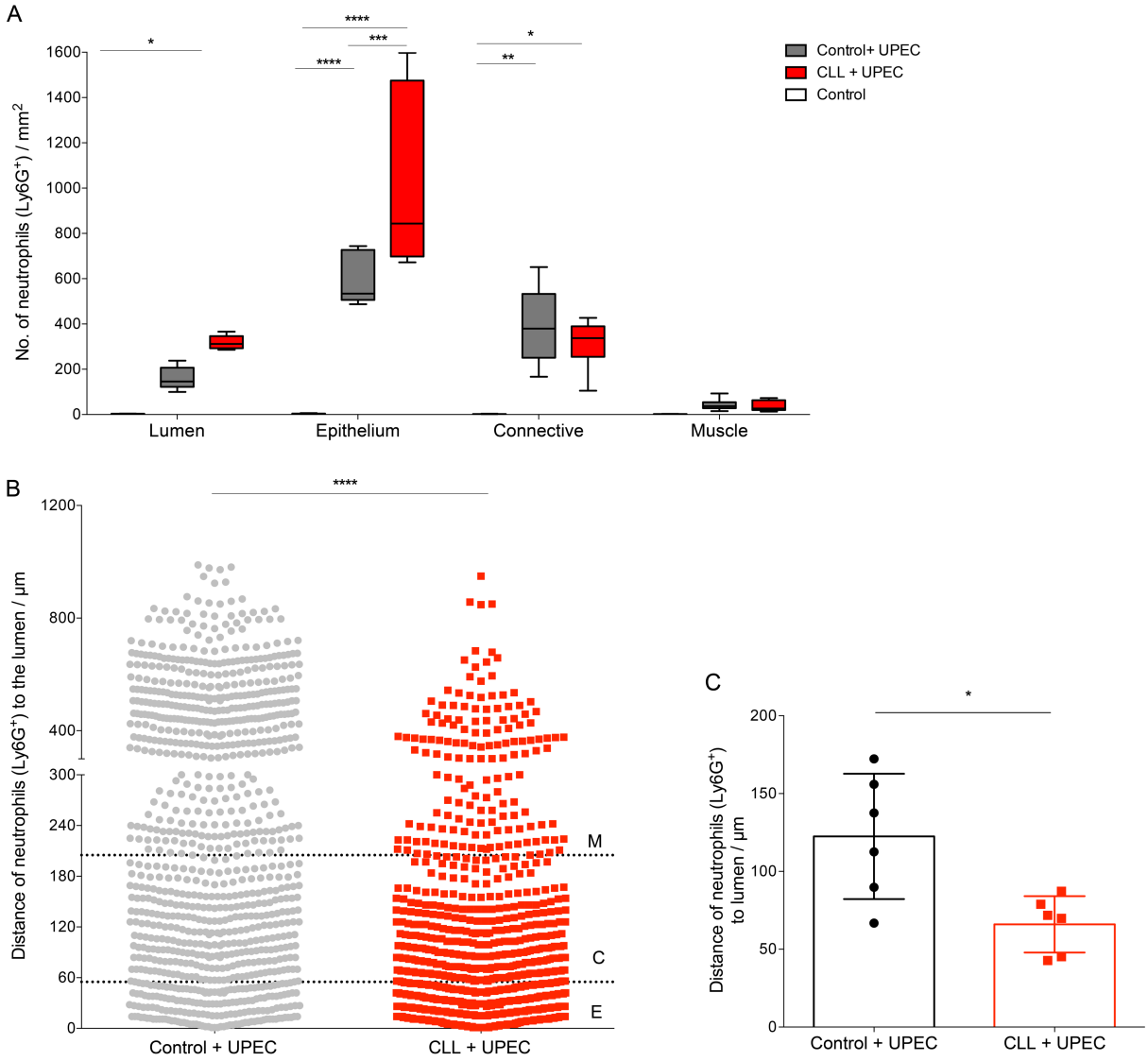

Figure 44. Increased neutrophil numbers and shortened distance to the site of infection in CLL.

Quantification was performed on murine bladder. Sections were stained with anti-GFP, DAPI and Ly6G. Neutrophils levels in various bladder compartments and the distance to lumen of neutrophils from murine bladder sections were quantified (Control + UPEC n=6; CLL + UPEC n=6). (A) The whisker plot illustrates neutrophil levels in various bladder compartments. Particularly, neutrophils were increased in the uroepithelium and lumen of UPEC-infected CLL bladders. (B) The distance to lumen was analysed for neutrophils from one murine bladder sections of UPEC-infected control (PMN=944) and one CLL (PMN=1126). The distance to lumen was decreased in neutrophils from the UPEC-infected CLL mice. Dashed lines indicate bladder compartments (E=epithelium, C=connective tissue, M=muscle). (C) The mean values of distance to lumen were compared for UPEC-infected control and CLL bladders. Statistical testing: (A) Two-way ANOVA with Bonferroni post-hoc; (B and C) Mann-Whitney U test.

In order to correlate the infection burden to neutrophil numbers in CLL, mean neutrophil levels were plotted against the corresponding infection area (Figure 45). To assume association between the infection area and number of neutrophils, correlation analyses were performed. Specifically, the coefficient of determination and slope of the linear regression were used to indicate correlation.

Notably, there is a weak positive correlation for the infection area and neutrophil numbers in UPEC-infected control bladders (R^2=0.17). Surprisingly, there is a stronger inverse correlation for the infection area and neutrophil numbers in UPEC-infected CLL bladders (R^2=0.56). In other words, although the numbers of neutrophils were elevated after UPEC infection in CLL, the numbers did not increase with bacterial burden. Hence, neutrophil density decreased with bacterial burden in CLL mice.

Conclusively, elevated neutrophil levels were present in the lumen and uroepithelium of UPEC-infected CLL bladders. At the same time, neutrophils localised closer to the site of infection. Furthermore, neutrophil numbers did not increase with increased bacterial burden in UPEC-infected CLL mice. Altogether, these data show that neutrophil recruitment is enhanced during UPEC infection in CLL, while the UPEC burden is not controlled.

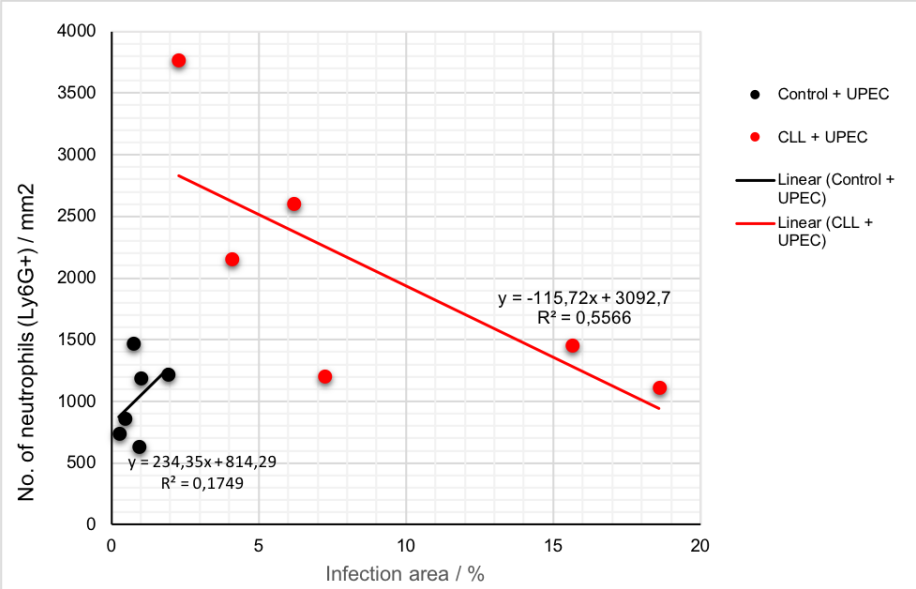

Figure 45. Correlation of bacterial burden and neutrophil numbers in the infected bladder.

Bladder sections were stained and analysed for infection area and neutrophil numbers as described before. Correlation analyses were performed for "Control + UPEC" (black; n=6) and "CLL + UPEC" (red; n=6). The coefficient of determination reveals a weak positive correlation for infection area and neutrophil numbers in control mice (R^2=0.17; slope =234.35). In contrast, there is an inverse correlation for infection area and neutrophil numbers in CLL mice (R^2=0.56; slope=-115.72). Statistical test: F-test.

9.4.4. B-cell infiltration into UPEC-infected bladders of CLL mice

In order to define the role of CLL cells during UTI *in vivo*, the presence of B-cells was determined in infected murine bladder sections. Adaptive immune responses, specifically B-cell responses, are very limited during UTI, B-cell accumulation do not occur until several days after infection and reports about IgA-producing plasma cells in the murine bladder are scarce [244, 284]. Furthermore, there are only These murine bladder sections were generated 21 hpi and thus no B-cell signals were expected. Hence, the presence of any B-cells would be derived from CLL cell infiltration as already shown by FC analysis (Figure 13). CLL B-cells were also detected in UPEC-infected CLL murine bladders 21 hpi (Figure 46). In the illustration, representative composite images are shown with CD19, DAPI and GFP-UPEC signals. The upper panel shows uninfected bladder sections, while the middle row refers to an infected murine bladder with only one B-cell signal in the detailed image. In contrast, several B-lymphocytes were detected arranged in clusters in UPEC-infected CLL bladders. B-lymphocytes mostly localised in the connective tissue in close proximity to the uroepithelium. The exact localisation has been quantified in the following section.

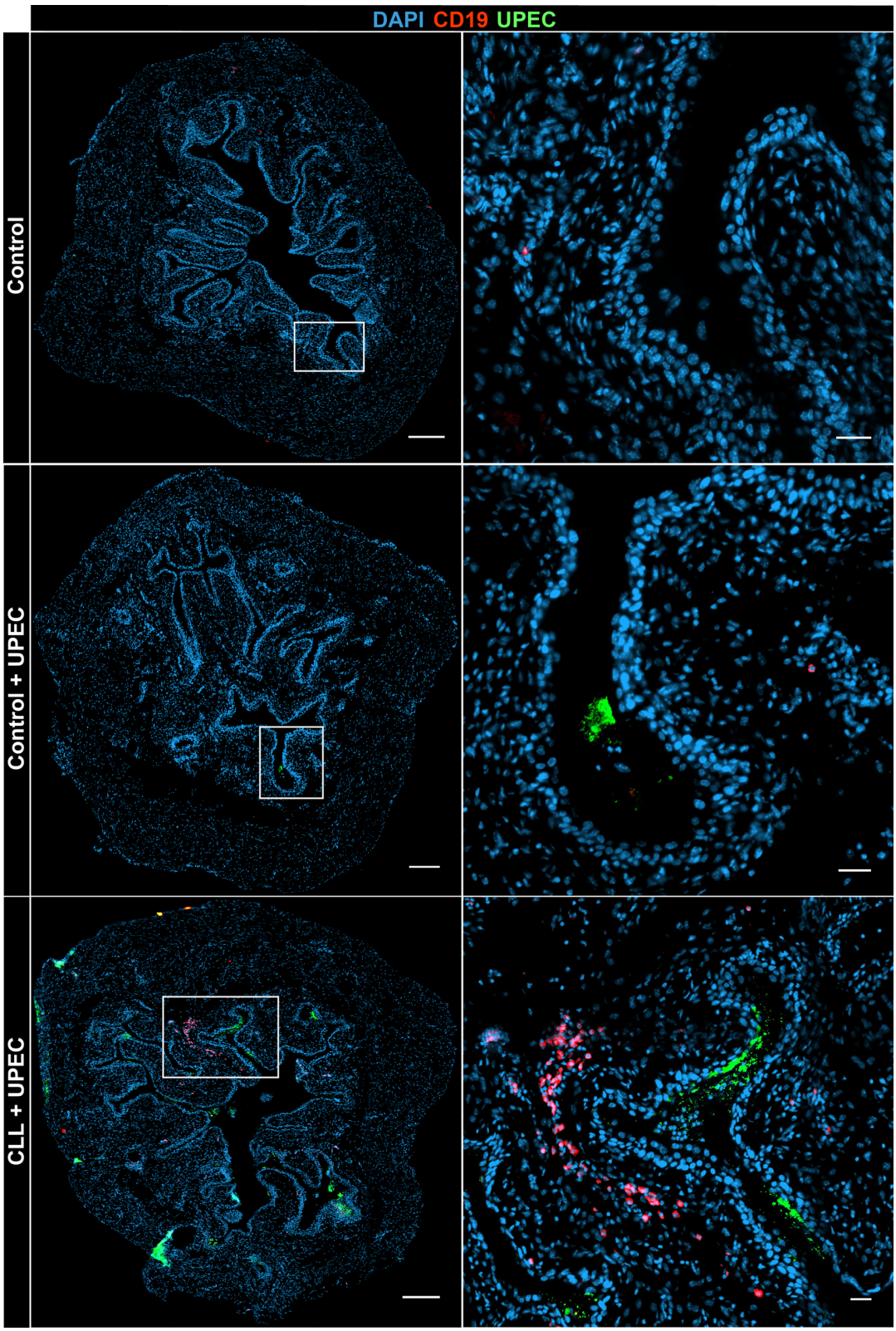

Figure 46. B-lymphocyte infiltration into infected-CLL murine bladder.

Murine bladder sections were stained for CD19 (red), DAPI (blue) and GFP-UPEC (green). Pictures are representative composite images. Overview images are illustrated on the left, while detailed images are shown on the right. Uninfected bladder sections (n=2) are in the top row, while an infected bladder of a control mouse is shown in the middle row (n=6). The bottom panel corresponds to infected bladders of CLL mice (n=6). Scale bars: overview 200 µm, detailed image 30 µm.

As illustrated in Figure 47A, B-cell numbers were measured in various bladder compartments of the urinary bladder in control, UPEC-infected control and CLL mice. Statistical relevance was tested through two-way ANOVA with Bonferroni post-hoc (Figure 47A) and the Mann-Whitney *U* test (Figure 47B). In general, control bladders did not contain any cells in the lumen, epithelium or muscle. An average of three B-cells were detected for the connective tissue of uninfected bladders. In contrast, more B-lymphocytes were detected in the infected bladders. B-cell densities were relatively low in the lumen and muscle and elevated in the epithelium and connective tissue of infected control and CLL bladders. Specifically, three B-lymphocytes were found on average in the lumen of both, infected control and CLL bladders. The muscle of infected control bladders contained one B-cell, while infected CLL bladders harboured two cells per section. However, B-cell counts rose to 37 per mm^2 in the uroepithelium of UPEC-infected CLL bladders, while the UPEC-infected control mean value was maintained at one cell per mm^2. For the connective tissue, B-cell densities increased and reached the maximum of 79 cells per mm^2 in the infected CLL bladder. In infected control bladders, only four B-lymphocytes on average were located in the connective tissue. Next, the mean distances of B-cells to the focus of infection was quantified (Figure 47B). The mean distances were similar and not statistically significant for infected control and CLL bladders (Control: 207.1 µm, SD: ±28.5; CLL: 148.8 µm, SD: ±49.7). To conclude, increased B-cell densities were found in the uroepithelium and connective tissue of UPEC-infected CLL bladders. Moreover, B-cells were localised in slightly closer to the site of infection in one infected CLL bladder.

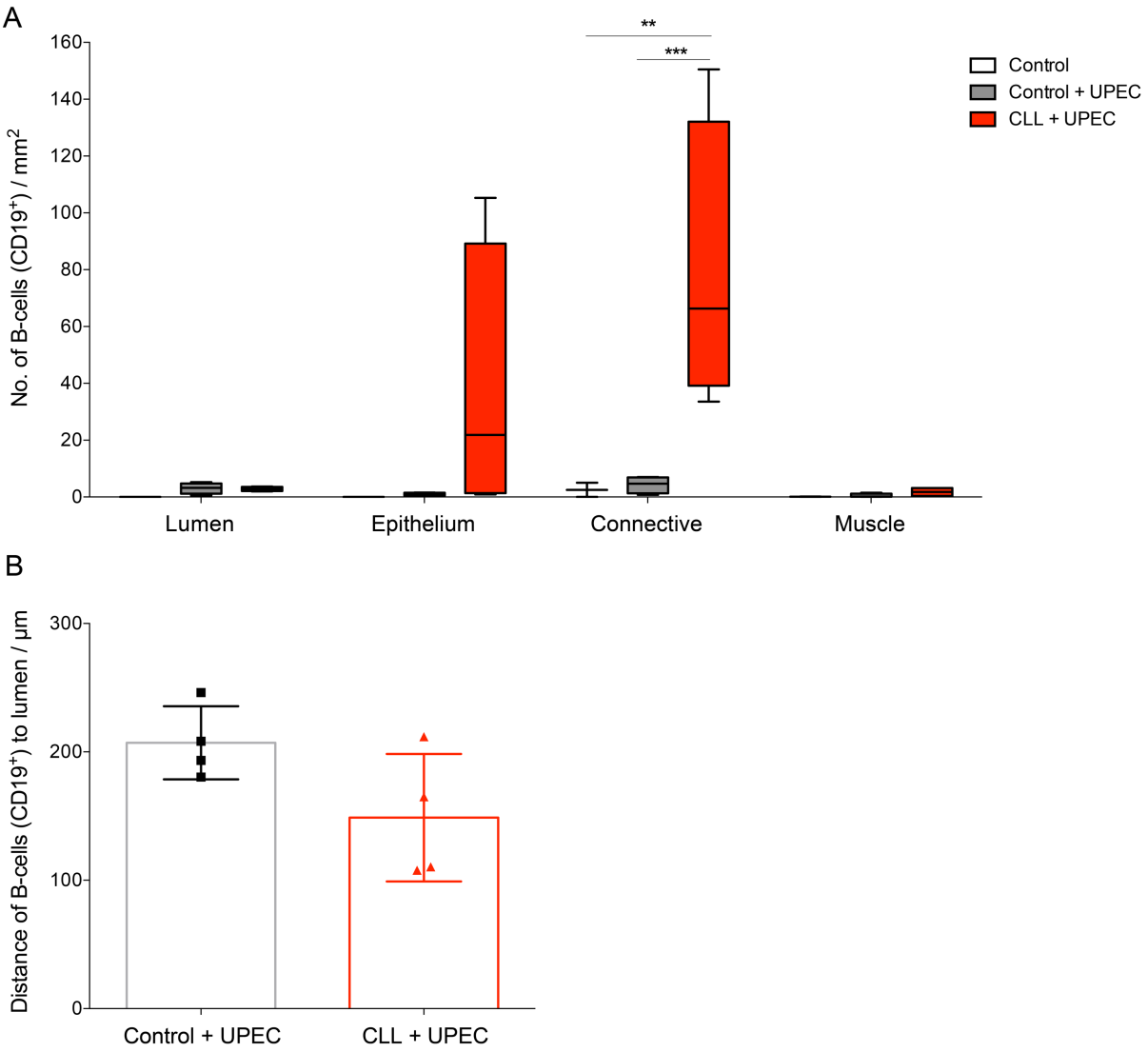

Figure 47. B-cell infiltration into UPEC-infected CLL bladder.

Semi-automated analysis was performed on murine bladder sections to quantify B-cell levels in various bladder compartments and the distance to lumen (Control + UPEC n=6; CLL + UPEC n=6). (A) The box plot illustrates B-lymphocyte levels which were increased in the uroepithelium and connective tissue of UPEC-infected CLL bladders. (B) The means for B-cell distance to the lumen was non-significantly decreased in UPEC-infected CLL bladders. Statistical testing: (A) Two-way ANOVA with Bonferroni post-hoc; (B) Mann-Whitney U test.

9.5. Cytokine analysis

9.5.1. The role of TGF-β signalling during CLL

Non-responsiveness to TGF-β signalling has been described as one of the survival strategies employed by CLL B-cells [285, 286]. Nevertheless, we hypothesized that other immune cells might be affected by TGF-β signalling. In order to identify the mechanism of immunosuppression, the role of TGF-β was investigated during infections in CLL. The Mann-Whitney *U* test has been conducted to test the statistical

relevance. As illustrated in Figure 13, there is a large population of malignant B-cells in the circulation. First, TGF-β levels were quantified in the circulation (Figure 48). To this end, murine plasma was harvested from control and CLL mice 35 days post CLL induction and measured by multiplex analysis. The mean concentration of TGF-β1 was equal in the murine plasma of both groups. The concentration was down to 109.13 pg/ml in the control plasma, while TGF-β1 concentration was 142.68 pg/ml in CLL. However, the mean values for both analytes, TGF-β1 and TGF-β2, were subject to high standard deviation. Specifically, the standard deviation scattered around ±88.28 and ±140.2 for TGF-β1 concentration in control and CLL murine plasma, respectively. Notably, the standard deviation was ±6.18 and ±177.2 for TGF-β2 levels in control and CLL murine plasma. Despite, the mean value for TGF-β2 in murine blood plasma was increased significantly in CLL mice compared to control mice (Control: 10.11 pg/ml, CLL: 130.61 pg/ml).

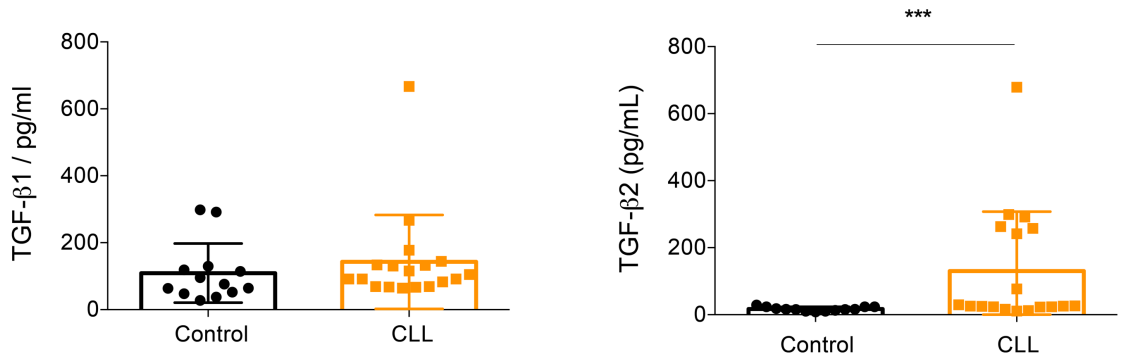

Figure 48. TGF-β levels in the murine blood plasma of control and CLL mice.

CLL was induced and blood via cardiac puncture was harvested 35 days post CLL induction from uninfected control (n=13) and CLL mice (n=18). By centrifuging blood samples, plasma was collected, supplemented with proteinase inhibitor and frozen in liquid nitrogen. Samples were thawed and processed for Bio-Plex Pro™ TGF-β assays. TGF-β1 and TGF-β2 levels were quantified via multiplex analysis. The mean TGF-β1 value for control murine plasma is 109.13 pg/ml (SD: ±88.3), while mean TGF-β1 mounted to 142.68 pg/ml (SD: ±140.2). In regard to TGF-β2, the average concentration in CLL murine plasma of 130.61 pg/ml (SD: ±177.2) was significantly increased compared to the control mean of 10.11 pg/ml (SD: ±6.2). Statistical testing: Mann-Whitney U test.

9.5.2. G-CSF concentration in the murine plasma and bladder supernatant

CLL patients receive prophylactic G-CSF shots in case of neutropenia to promote neutrophil release from the BM into the circulation. In order to evaluate the role of G-CSF during CLL for neutrophils suppression, the level of G-CSF were quantified in the plasma of uninfected mice and in the bladder supernatant of infected mice

(Figure 49). Generally, G-CSF levels were elevated in CLL murine plasma and in the bladder supernatant of UPEC-infected CLL mice. In regard to plasma values, mean concentrations were 0.2018 pg/ml (SD: ± $3.5x10^{-4}$) for control mice. G-CSF mean concentration increased significantly to 0.2023 pg/ml (SD: ± $8.3x10^{-4}$). Subsequently G-CSF levels were measured in the supernatants from UPEC-infected control and CLL urinary bladders. In detail, 0.2013 pg/ml (SD: ± $4.1x10^{-4}$) and 0.2029 pg/ml (SD: ± $1.4x10^{-3}$) were the mean G-CSF concentrations of control and CLL mice, respectively. This difference was not statistically significant.

In summary, the expression of G-CSF during CLL was even enhanced in CLL indicating that the immunosuppression of neutrophils is G-CSF independent.

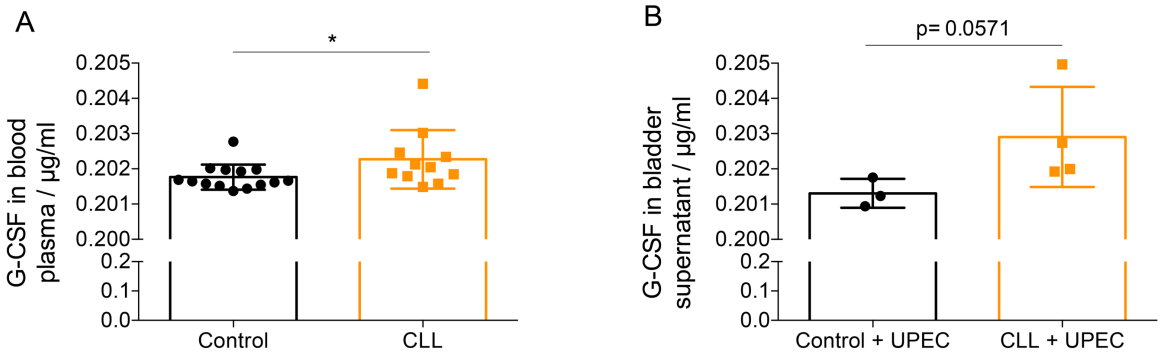

Figure 49. G-CSF levels in murine plasma and infected bladders were increased in CLL mice.

G-CSF levels were quantified in the murine blood plasma of control and CLL mice. Additionally, G-CSF concentrations were quantified in the bladder supernatant of UPEC-infected control and CLL mice. The mean G-CSF concentration for control murine plasma was 0.2018 pg/ml (SD: ± $3.5x10^{-4}$), while the average of G-CSF mounted to 0.2023 pg/ml (SD: ± $8.3x10^{-4}$) in CLL mice. Furthermore, average concentrations of G-CSF were 0.2013 pg/ml (SD: ± $4.1x10^{-4}$) and 0.2029 pg/ml (SD: ± $1.4x10^{-3}$) in bladder supernatant pf infected control and CLL mice. Statistical testing: Mann-Whitney U test.

9.6. 3D-migration capacity of *ex vivo* BM neutrophils

9.6.1. Optimisation of CXCL2 concentration for 3D-migration assay

The 3D-migration was set up by our master student Karen Fischer under my supervision. Polymerization timings, different type of collagens and collagen concentrations were tested. However, the chemokine concentration was yet to be determined. In order to optimise the chemoattractant gradient, various concentrations were tested by supplementing RPMI medium with 20, 75, 10, 200 ng/ml CXCL2 (Figure 50). The migration was recorded for 30 minutes and analysed via ImageJ and Excel. The most adequate CXCL2 concentration was chosen based on the highest velocity of neutrophils. The box plot shows the mean of about 250-350 individual cell

tracks for every concentration tested. After the addition of plain RPMI medium without any chemokine supplementation, the velocity of neutrophils mounts up to 5.3 µm/min. The velocity rose significantly to 6.5 µm/min during migration in medium supplemented 200 ng/ml. When chemotaxis was measured with 20 and 100 ng/ml CXCL2, the velocity did not change, whereas CXCL2 concentration of 75 ng/ml led to a decreased in velocity (4.4 µm/min).

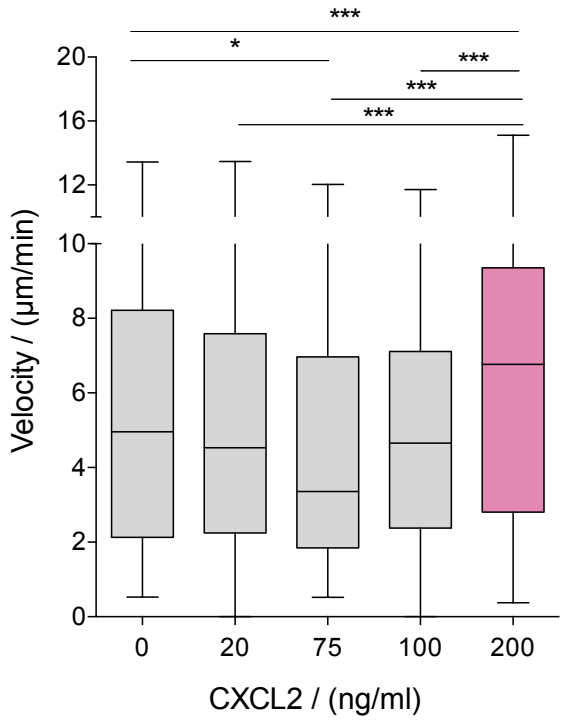

Figure 50. Optimisation of CXCL2 concentration for 3D-migration assay.

BM neutrophils were embedded in a 3D-migration assay and time-lapse imaging was performed for 30 min. Next, the velocity of neutrophils in various CXCL2 concentrations was measured. For this, the average speed of 250-350 tracks of each concentration was determined (n=1). The following values were mean velocities and SD for each concentration: 0 ng/ml CXCL2: mean= 5.3 µm/min, SD= 3.4 µm/min; 20 ng/ml CXCL2 mean = 5.1 µm/min, SD = 3.1 µm/min; 75 ng/ml CXCL2: mean = 4,4 µm/min, SD = 3.1 µm/min; 100 ng/ml CXCL2: mean = 4.9 µm/min, SD = 2.8 µm/min; 200 ng/ml CXCL2: mean = 6.5 µm/min, SD = 3.7 µm/min. Statistical test: Kruskal-Wallis.

9.6.2. Analyses of migratory parameters of bone marrow neutrophils

The migratory behaviour of murine bone marrow neutrophils from control and CLL mice was analysed in regard to parameters of directed, such as the chemotactic index and directed distance, as well as random migration, such as track displacement and velocity (Figure 51). The script to study chemotaxis was developed under my supervision by Elena de Dios Panal, another master student supervision.

9.6.2.1. Directed migration

In order to quantify the migratory capacity towards the chemoattractant gradient, a script was developed, and a fictive target point was defined. Any movement towards this target point has been considered to be directed migration.

Chemotactic index

The chemotactic index is a defining feature to determine the power of a chemoattractant to recruit the cell towards the gradient. Supposedly, the chemotactic index is 1, the entire cell population is attracted by the chemoattractant and migrate directly towards it. In contrast, a chemotactic index of -1 defines maximal repelling indicating a direct migration into the opposite direction of the chemokine. Incubation with plain medium leads to mean values of 0.06 and 0.07 for control and CLL neutrophils, respectively (Figure 51A). The supplementation with 200 ng/ml CXCL2 increases the chemotactic index slightly, but not significantly. The mean CI values are 0.13 and 0.12 for control and CLL, respectively. The mean values for the samples incubated with CXCL2 are higher than for their corresponding counterparts. However, the scatter plot illustrates fluctuations with some mean values reaching negative chemotactic indices. None of the differences in the chemotactic indices are significantly changed.

Directed distance

Directed distance is measured through the cumulative distance of migration during the recording time. The mean values are illustrated in Figure 51B. The distance covered by control bone marrow neutrophils without CXCL2 is 42 µm and with CXCL2 52.5 µm. In contrast, CLL neutrophils without chemokine supplementation have migrated 35.3 µm on average whereas CXCL2 addition leads to 48 µm. The increase for stimulated control neutrophils mounts up to 25 %, while it adds up to a 37 % rise for CLL neutrophils incubated with CXCL2. There were no significant changes.

9.6.2.2. Random migration

The analysis of random migration includes the entity of cell motility independent of its direction. Thus, it is not relevant whether the cell is migrating towards or away from a chemokine gradient.

Track Displacement

Track displacement is a parameter, important to assess the migratory behaviour, based on the distance the cell has migrated compared to its initial spatial point. For this, the exact trajectory is not considered at all. The end point is compared to the point of origin. Track displacement does not change for control neutrophils is 38 µm with and without CXCL2 (Figure 51C). However, there is a surge from 29.6 µm in the absence of CXCL2 for CLL neutrophils to 40.7 µm for stimulated CLL neutrophils. Hence, CLL neutrophils migrate farer away from their point of origin which is only slightly increased to the control group. The changes are not significant.

Velocity

As illustrated in Figure 51D, non-stimulated neutrophils of control and CLL mice are similar: 6.8 µm/min and 6.9 µm/min, respectively. Stimulation with CXCL2 leads to a surge up to 8.0 µm/min for both groups. Consequently, the incubation with CXCL2 does not change, neither for control nor for CLL neutrophils in the absence and presence of CXCL2. The mean values scatter for all groups, with the largest fluctuation present in the stimulated CLL group. The smallest standard deviation has been observed for stimulated control neutrophils. None of the differences were significant.

In conclusion, 3D-cell migration experiments suggest that neutrophil migration is not altered in CLL when tested in this experimental approach.

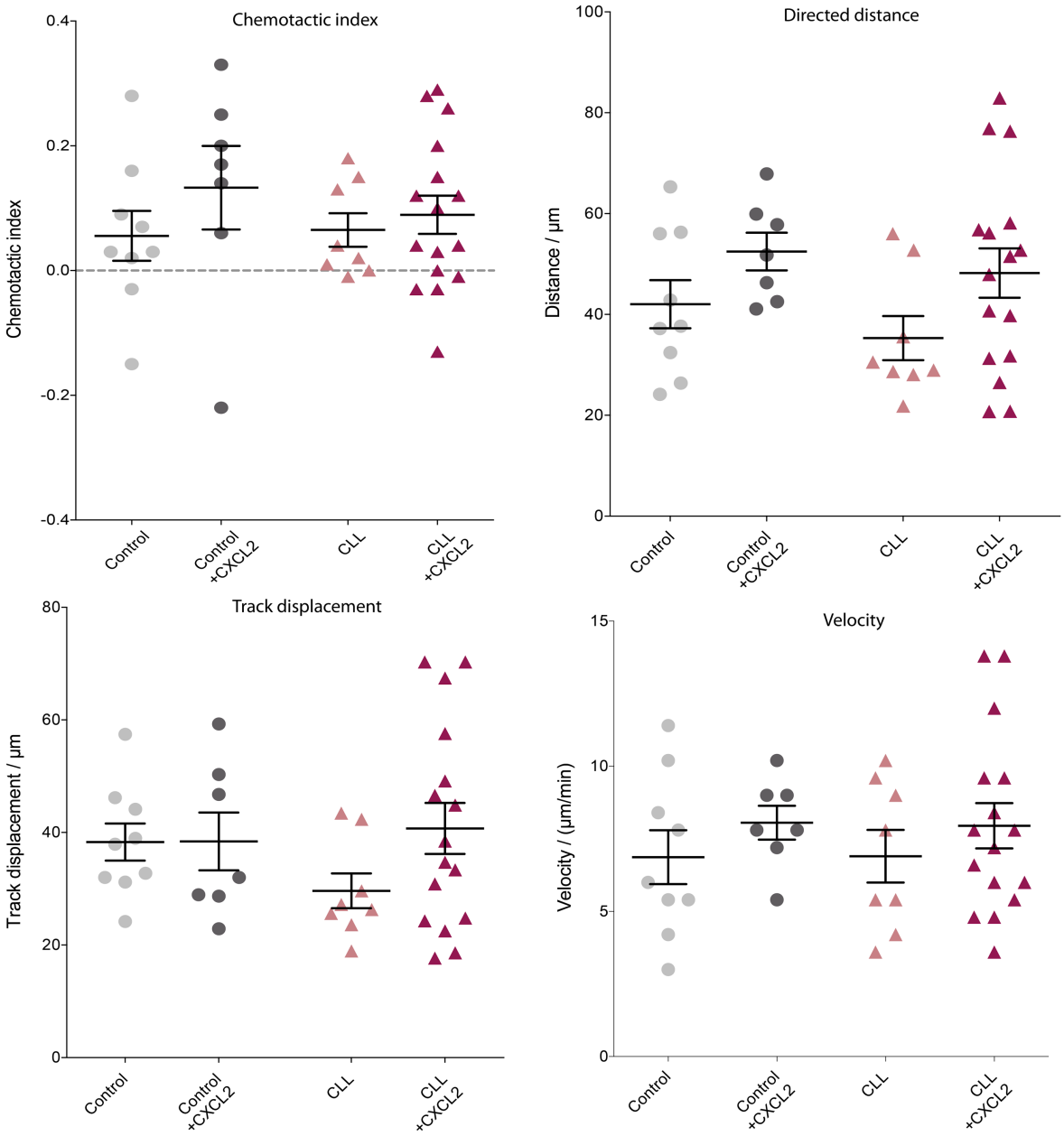

Figure 51. Migration parameters of BM neutrophils from control and CLL mice in a 3D-migration assay.

Bone marrow neutrophils from control and CLL mice were embedded in a 3D-migration assay and incubated ± 200 ng/ml CXCL2. Migration was recorded every 30s for 30 min and parameters for directed and random migration were calculated as previously described. Each point represents the mean value of the analysed parameter of 200-300 individual cell tracks per group (n=8). (A) The mean velocities for each group and their corresponding SD are: Control mean= 0.056, SD= 0.12; Control + CXCL2 mean= 0.133, SD= 0.177; CLL mean= 0.065, SD= 0.076; CLL + CXCL2 mean= 0.089, SD= 0.123. (B) Control mean = 42.0 µm, SD= 14.3; Control + CXCL2 mean= 52.5 µm, SD= 9.9; CLL mean= 35.3 µm, SD= 12.4; CLL + CXCL2 mean= 48.2 µm, SD= 19.6. (C) Control mean= 38.3 µm, SD= 9.9; Control + CXCL2 mean= 3.4 µm, SD= 13.6; CLL mean= 29.6 µm, SD= 8.8; CLL + CXCL2 mean= 40.7 µm, SD= 18.14. (D) Control mean= 6.8 µm/min, SD= 2.8 µm/min; Control + CXCL2 mean= 8.0 µm/min, SD= 1.6 µm/min; CLL mean= 6.9 µm/min, SD= 2.6 µm/min; CLL + CXCL2 mean= 8.0 µm/min, SD= 3.1 µm/min. Statistical test: Ordinary one-way ANOVA with Bonferroni post-hoc.

9.7. NETosis capacity of CLL plasma

9.7.1. Modification of the human NETosis assay

A NETosis assay was already developed at the Institute of Experimental Immunology and Imaging [287]. This protocol was established to study NETs of human neutrophils. In order to study the impact of CLL microenvironment on human neutrophils, the protocol had to integrate human plasma. In addition to PMA, the stimulating agent of NETosis, neutrophils were incubated with various concentrations of human plasma. The concentration that led to the biggest cumulative NETosis effect was chosen. For this, human neutrophils from healthy donors were incubated with RPMI medium supplemented with 0.2 (0.04 %), 1 (0.2 %), 5 (1 %), 25 µl (5 %) or no human plasma (0 %) and 25 nM PMA for 3 h. After the staining, the quantification of the NETosis capacity of each treatment was based on the DNA mask as described in 8.2.9. Notably, circular DNA signals and background noise were excluded and only DNA signals bigger than 10 pixels were chosen (Figure 52).

The induction of NETosis scatters in stimulated samples in the absence of human plasma (0 %; mean: $8.8x10^6$ µm^2), while no PMA and no human plasma led to a small, spontaneous NET area formation (mean: $1.8x10^6$ µm^2; Figure 53). Furthermore, a volume concentration of 0.2 % human plasma with 25 nM PMA led to an increased NET formation (mean: $9.2x10^6$ µm^2) which is comparable to the PMA only stimulated control sample (0 %). In the absence of PMA, human neutrophils incubated with 0.2 % human plasma induced a mean NETosis area of 7.0 $x10^5$ µm^2. An equivalent, but weak induction of NETosis occurred in response to 0.04 % human plasma with (mean: $1.3x10^6$ µm^2) and without PMA (mean: $1.2x10^6$ µm^2). The fluctuation in NET area formation is similar between control (0 %) and 0.2 % stimulated samples. At the same time, 1 % (mean: $4.5x10^6$ µm^2) and 5 % (mean: $5.2x10^6$ µm^2) human plasma supplementation and PMA incubation induced comparable levels of NET formation, while only few NETs were formed in the absence of PMA (1 % mean: $1.6x10^5$ µm^2; 5 % mean: $8.8x10^5$ µm^2). The only significant difference was observed in the 1 % human plasma group. Human neutrophils were also incubated with higher human plasma concentrations, such as 20% in addition to 25 nM PMA (data not shown). However, the incubation led to cell lysis and neutrophil signals were not retrieved.

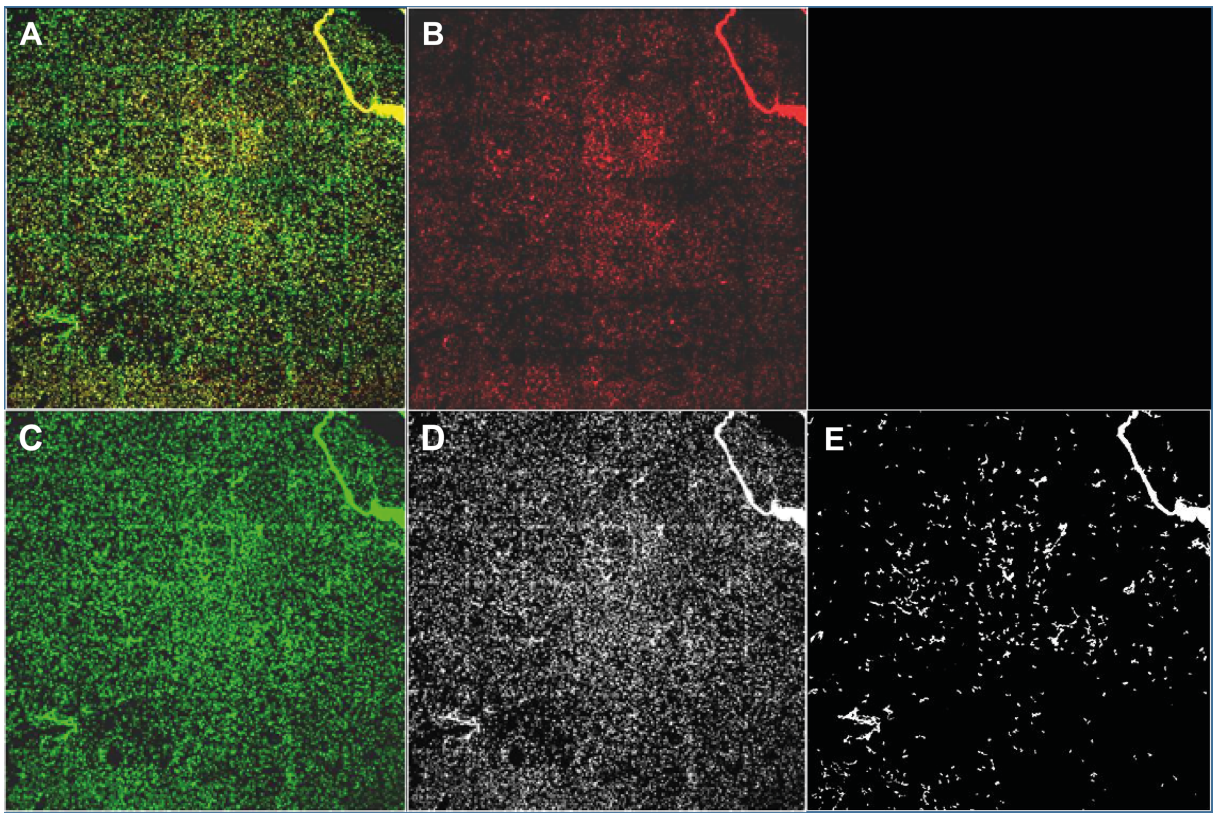

Figure 52. Multistep process via mask generation to quantify NETosis area.

The quantification of NETosis was based on differential staining of DNA (C; YOYO-1™) and neutrophils (B; CD66b-PE). The composite picture was used to generate a specific DNA mark (A-D). After increasing the values for circularity and size, a NETosis mask was created (E). Consequently, the area of NETs can be quantified to compare the capacity to induce NETosis during different treatments. Magnification: 100x; Field of view: 4926 µm x 4926 µm.

The results from the optimisation of the NETosis assay show that human plasma has an impact on the NET formation of human neutrophils (Figure 53). The most significant increase from unstimulated to stimulated neutrophils was recorded for 1 % supplementation of human plasma. This group of samples also reveal the smallest range of standard deviation. Consequently, 1 % (v/v %) human plasma concentration will be used during incubation for the study of the impact of CLL microenvironment on the NETosis capacity of human neutrophils.

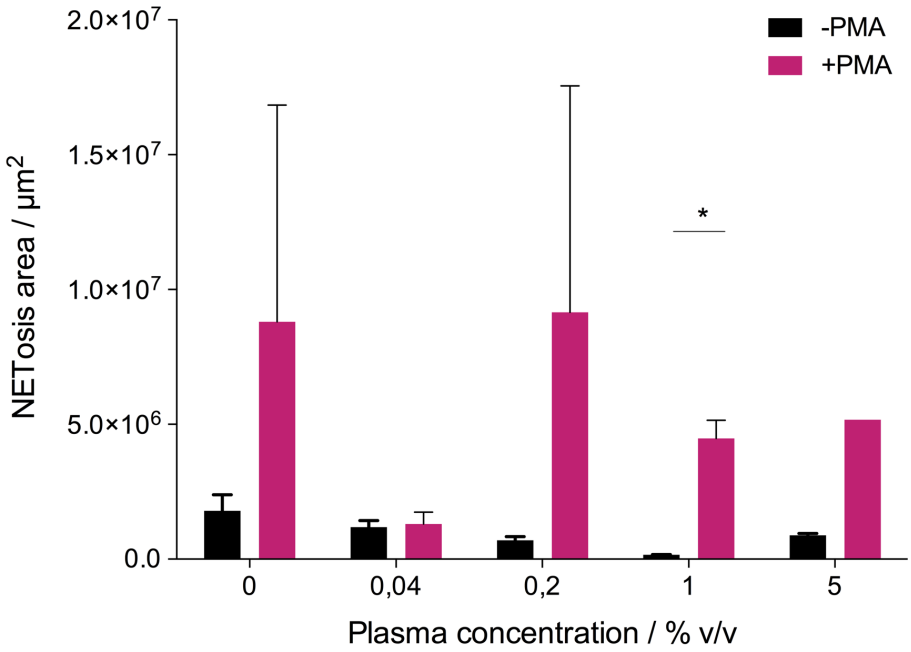

Figure 53. The optimisation of the NETosis assay with increasing CLL plasma concentration.

Neutrophils were incubated with PMA and human plasma in order to find the optimal human plasma concentration. A titration series is shown here. Even in the absence of human plasma, the induction of NETosis scatters in stimulated samples. Additionally, a concentration of 0.2 % human plasma led to an increased NET formation in the presence of PMA with similar fluctuations to the corresponding control (0%). While 1 % and 5 % human plasma supplementation and PMA incubation induces equal levels of NET formation, while almost no NETs were formed in the absence of human plasma. 0.04 % human plasma with PMA did not led to an increased NETosis capacity. Unstimulated human neutrophil induced small spontaneous NETs. Magnification: 40x. Statistical test: multiple t-tests.

9.7.2. Impact of CLL plasma on NETosis capacity of human neutrophils

The NET formation was measured after incubation of human neutrophils from one healthy donor with human plasma (1 %) of nine untreated CLL patients as described before (8.2.9). Human neutrophils were incubated in the absence and presence of 25 nM PMA. In addition to human CLL plasma, human plasma from the healthy donor was used for control samples. NETosis assays were performed in triplicates. Due to technical difficulties, some samples were only performed in singles (CLL1 +PMA; CLL2 +/-PMA; CLL3 -PMA) or duplicates (CLL3 +PMA; CLL4 +PMA; CLL5 +PMA; CLL8 +/-PMA; CLL9 +PMA). Representative images of this study are illustrated in Figure 55.

In general, unstimulated neutrophils (-PMA) have a limited dispersion of mean values between $5{,}9 \times 10^4$ µm² to $5{,}1 \times 10^5$ µm². In contrast, the scattering of mean values of stimulated samples (+PMA) vary between $5{,}4 \times 10^5$ µm² and $3{,}6 \times 10^6$ µm². The PMA

treatment has a significant impact on all samples. The treatment with different human CLL plasmas induces large scattering of data with no significant impact. Nonetheless, there are remarkable differences in the NETosis induction capacity of human CLL plasmas.

Some of the human CLL plasmas are able to induce a stronger NETosis than the control, treated with self-plasma. In detail, CLL 6, 8 and 9 have the strongest capacity to induce NET formation in stimulated samples, with a mean value of $3.62x10^6$ μm^2, $3.10x10^6$ μm^2 and $3.32x10^6$ μm^2, respectively. The stimulated control sample has an average NETosis area $2.09x10^6$ μm^2. On the contrary, the NET area induced in stimulated samples with human plasma from CLL patient 2, 3 and 7 mounted up to $6.72x10^5$ μm^2, $5.47x10^5$ μm^2 and $5.85x10^5$ μm^2, respectively. These human CLL plasma induced a lower NET formation compared to the stimulated control sample. Similarly, CLL1, 3 and 4 induced lower NET areas compared to the stimulated control sample (CLL1: $1.23x10^5$ μm^2; CLL3: $1.51x10^5$ μm^2; CLL4: $1.27x10^5$ μm^2). In the absence of PMA, the self-plasma treated sample induced an average NETosis area of $2.08x10^5$ μm^2. Only three unstimulated CLL plasma (-PMA) treated neutrophil samples formed less NETosis than the unstimulated control (CLL2: $5.96x10^4$ μm^2; CLL3: $1.26x10^5$ μm^2; CLL4: $1.75x10^5$ μm^2). The remaining six unstimulated CLL human plasma treated neutrophil samples (-PMA) have an increased power to induce NET formation compared to the self-plasma treated control, with CLL8 having the strongest NETosis capacity in the absence of PMA (CLL1: $4.29x10^5$ μm^2; CLL5: $4.00x10^5$ μm^2; CLL6: $3.04x10^5$ μm^2; CLL7: $3.51x10^5$ μm^2; CLL8: $5.16x10^5$ μm^2 and CLL9: $3.87x10^5$ μm^2).

The detailed composite images reveal early stages of NETosis in neutrophils incubated with CLL plasma only in Figure 55. Conversely, neutrophils incubated with self-plasma in the absence of PMA show no signs of NET formation. The stimulation with PMA leads to NETosis in neutrophils treated with self-plasma and CLL plasma. NET formation area of stimulated CLL plasma samples were decreased in comparison to the self-plasma treated and PMA-incubated controls (Figure 54 and Figure 55).

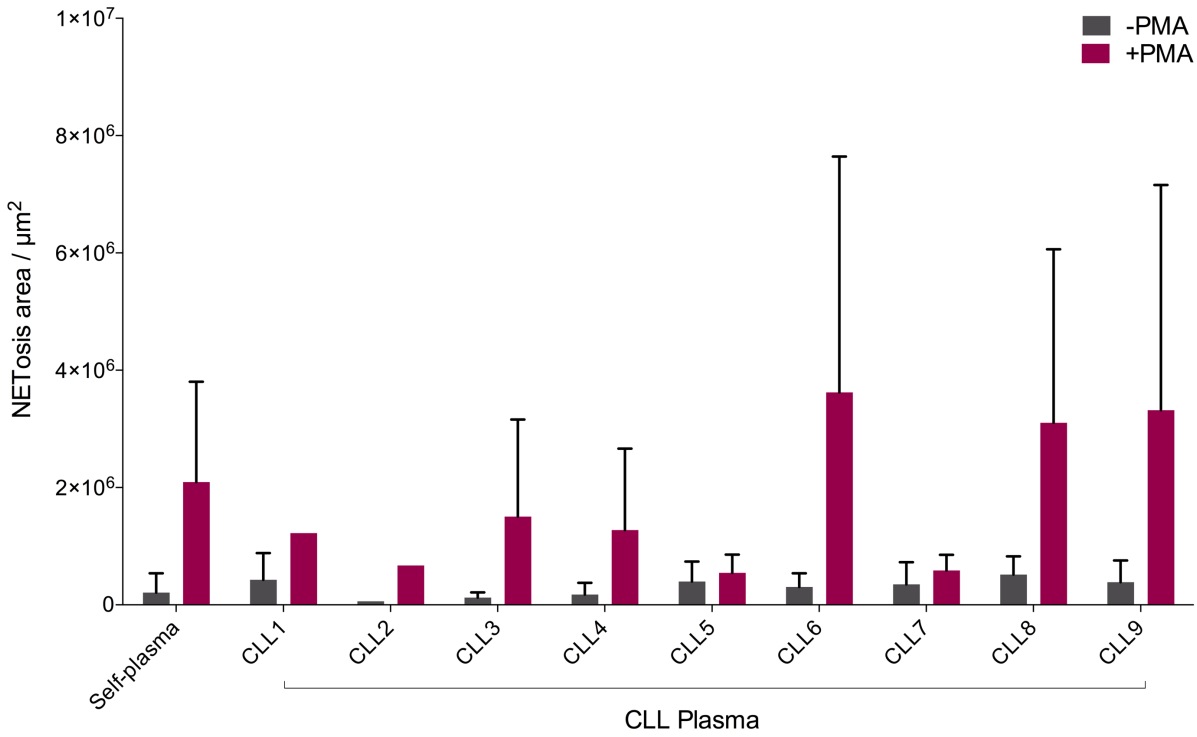

Figure 54. NETosis capacity of neutrophils treated with self-plasma and CLL plasma.

Individual mean values of NETosis area post-incubation with blood plasma derived from untreated CLL patients. Neutrophils of a healthy donor were incubated with self-plasma (1 %, v/v %) and CLL plasma (1 %, v/v %) and samples were additionally stimulated with 25 nM PMA. NETs were stained with YOYO-1 and CD66b and analysed by fluorescence microscopy. NETosis areas were quantified as previously described. The treatment with PMA is the only significant variation observed during this experiment (**). There are no significant differences among the different human CLL plasmas used during NET formation. Statistical test: Two-way ANOVA test with Bonferroni post-hoc.

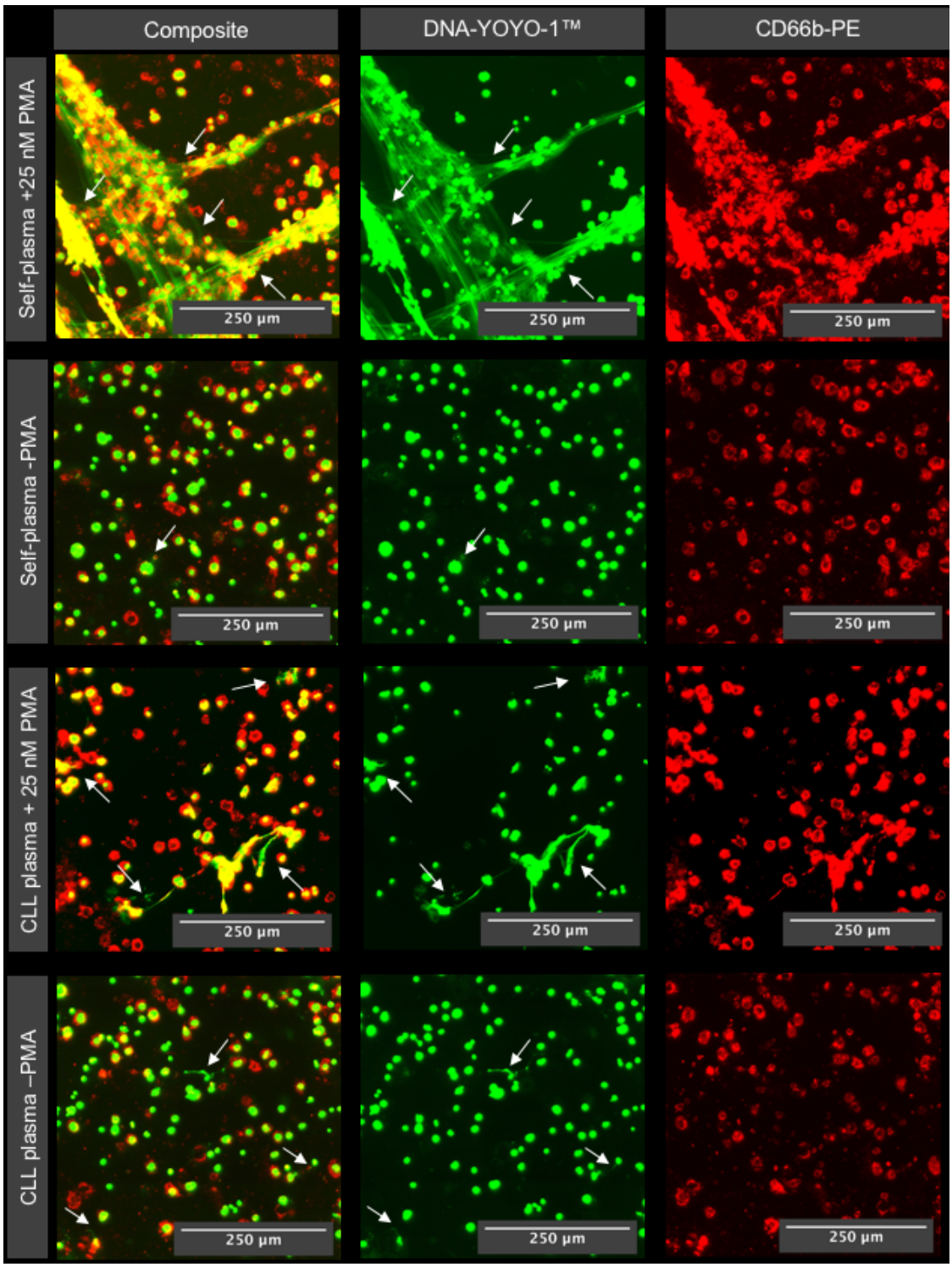

Figure 55. Overview of representative images of NETs post-stimulation with PMA, self- or CLL plasma.

Representative zoom-ins of NET formation during 400x magnification. Neutrophils of a healthy donor were incubated with self-plasma (1 %, v/v %) and CLL plasma (1 %, v/v %) and samples were additionally stimulated with 25 nM PMA. NETs were stained with YOYO-1 and CD66b and analysed by fluorescence microscopy. NETosis areas were quantified as previously described. White arrows indicate NET formation. Self-plasma treated, PMA-stimulated neutrophils led to higher NET formation compared to CLL plasma treated, PMA-stimulated neutrophils. In contrast, CLL plasma incubation only induced more NETosis than self-plasma treated neutrophils.

In order to validate whether CLL plasma has an altered capacity to induce NETosis, the quantification of the NETosis area has been summarized for all CLL patients and visualised in Figure 56. The NETosis activity is significantly increased in self-plasma and CLL plasma samples upon PMA stimulation. The difference between unstimulated and stimulated is higher for self-plasma compared to CLL plasma (CLL Plasma +PMA: $1{,}90x10^6$ μm^2 vs. CLL Plasma –PMA: $3{,}33x10^2$ μm^2; self-plasma –PMA: $1{,}23x10^2$ μm^2 vs. self-plasma +PMA: $2{,}86x10^6$ μm^2; Figure 56). Both stimulated groups have different NETosis capacities. Self-plasma (+PMA) is able to generate more NETosis than CLL plasma (+PMA). However, the dispersion of the data within the group of CLL plasma incubated with PMA is much higher. In contrast, the dispersion of data is limited in neutrophils treated with CLL plasma only. In regard to the unstimulated groups, CLL plasma was able to induce a slightly increased NETosis compared to the self-plasma treated neutrophil samples (Figure 54).

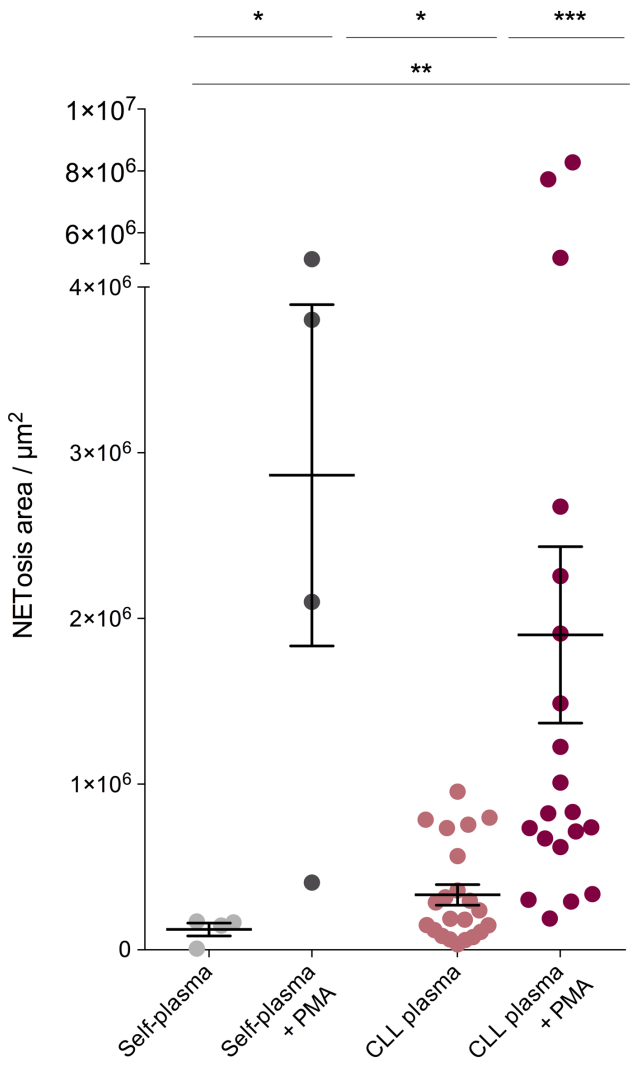

Figure 56. Summary of NETosis area quantification post-stimulation ±PMA, ±self-plasma or CLL plasma.

Summary of the NETosis assay. Neutrophils of a healthy donor were incubated with self-plasma (1 %, v/v %) and CLL plasma (1 %, v/v %) and samples were additionally stimulated with 25 nM PMA. NETs were stained with YOYO-1 and CD66b and analysed by fluorescence microscopy. NETosis areas were quantified as previously described. The comparison of four groups reveal that self-plasma treated neutrophils have the highest capacity to induce NETosis. CLL plasma in combination with PMA induced the second largest NET area. In contrast, both unstimulated groups generated smaller NETosis areas. However, unstimulated CLL plasma treated neutrophils are able to induce a slightly increased NET area compared to unstimulated self-plasma samples. Statistical test: Kruskal-Wallis test.

10. Discussion

The plethora of neutrophil functions in pathological contexts, such as atherosclerosis, rheumatoid diseases, diabetes, allergies, anaphylaxis, metabolic disorders and cancer has been studied previously (reviewed in [10]). However, the function of neutrophils during CLL has not been studied so far. This study has examined the neutrophil function during CLL and thus provides novel insights into the mechanism that might predispose CLL patients to recurrent and severe infections.

In regard to CLL, the study of neutrophils might focus on various aspects, such as the contribution to disease progression, development in the bone marrow, functional impairment during antimicrobial defence, migration, degranulation and NETosis. This study has specifically focused on these important aspects. Furthermore, the current study provides evidence that the clonal expansion of malignant B-cells is not limited to the BM, but also occurs in peripheral and non-lymphoid organs, such as the bladder and the lung. Interestingly, infections in CLL patients mainly occurring in these organs indicate that CLL B-cells contribute to the immunosuppression of the innate immune response. Beyond infiltration of the organs, CLL B-cells also affect neutrophils in a systematic manner. Studies on neutrophils during CLL are limited and only a few studies are available which have studied innate immune cell functions rather than their implication in tumours and as tumour-associated phenotypes [223, 224, 226, 288]. This thesis provides novel insights on how the neutrophil phenotype is altered during CLL. Furthermore, neutrophil phenotype and function were elucidated after UPEC infection in the presence of CLL. Also, important neutrophil effector functions, such as antibacterial response, migration and NETosis have been investigated. To this date, this study is the first comprehensive report that focuses on the alteration of neutrophil phenotype and effector function by CLL prior to and post-infection.

10.1. Phenotypical alterations on neutrophils in CLL

There is increasing literature on the role of neutrophils during tumorigenesis. So far, an altered neutrophil development and release from the BM, apoptotic resistance and even functional dichotomy in tumour-associated neutrophils (TAN) have been described previously [289]. In this context, the roles of N1 and N2 neutrophil subsets have been proposed to be similar to the classification of tumour-associated macrophages (TAM) [290, 291]. While the former displays an antitumour phenotype,

the latter demonstrated tumour-promoting capacities, such as improving angiogenesis, providing proliferation signals and reducing cellular senescence in tumour cells [292, 293]. The majority of these studies are based on solid cancer models [290, 294]. In the context of CLL, the majority of studies focused on phenotypic alterations of circulating monocyte and macrophage subsets in CLL patients due its tumorigenic role as NLC [295-297] and studies on phenotypical changes of neutrophils during CLL are missing. In fact, the impact of the CLL microenvironment on neutrophil development and maturation has not been studied so far. Even though a classification of N1 and N2 subsets exists in other cancer models, a complete phenotypical characterisation of neutrophils has not been performed until today.

This study provides novel insights about the phenotypical changes in neutrophils of untreated CLL patients as well as from the *in vivo* CLL model. Further characterisations have been conducted on neutrophils in the blood and bladder post-UTI of CLL mice. Firstly, phenotypical characterization of neutrophils in whole blood samples from untreated CLL patients revealed strong negative correlation for $CD10^+$, $CD62L^+$ and $CXCR4^+$ neutrophil frequencies with increasing tumour load in the circulation. In fact, CD10 serves as a stable marker to distinguish mature and immature neutrophils and has been shown to have T-cell suppressive capacity [298]. Based on this study, Brandau and Hartl have proposed to use CD10 as a stratification marker to evaluate the immunosuppressive potential in neutrophils and in myeloid-derived suppressor cells (MDSC) [299]. In the context of CLL, MDSC with monocytic and granulocytic origin have been described in patients connecting these findings to CLL tumorigenesis and identifying these cell populations as possible targets for therapeutic intervention [298, 300, 301]. Interestingly, as suggested by Marini *et al.* G-CSF treatment may lead to restoration of neutrophil functions. CLL patients with neutropenia receive G-CSF injections within their treatment regime. Nevertheless, a restoration of neutrophil effector functions via G-CSF application to increase the number of mature and functionally active neutrophils has not been successful in CLL [302]. In this context, the question remains as to how neutrophil functions can be restored by increasing CD10 expression in neutrophils. In regard to the decline of CD62L-expressing neutrophils in untreated CLL patients, further investigation is required to identify the activation status of neutrophils with decreased CD62L frequency through sCD62L quantification. However, neutrophils with a

decreased CD62L expression are described as functionally active cells and are in line with murine data obtained in this study [54, 303]. Declining frequencies of CXCR4-expressing neutrophils were also observed in the blood of untreated CLL patients. In contrast, a weak but positive correlation was observed for $ICAM1^+$ and $PDL1^+$ neutrophil subsets and lymphocyte numbers in blood. These findings suggest an activated, mature but rather immunosuppressed phenotype of neutrophils in untreated CLL patients. The functional marker PDL1 is well known for its immunosuppressive function on a wide variety of cells [304]. Additionally, has been extensively used as a marker to assess functional activity of neutrophils in infections as well as cancer [305, 306]. Therefore, PDL1 expression on neutrophils might be involved in the promotion of neutrophil differentiation into an immunosuppressive subset [307]. Furthermore, the results of the phenotyping of neutrophils from untreated CLL patients are partially corroborated by another phenotypic characterization conducted by Manukyan *et al.* [288]. However, neutrophil subsets were not correlated to CLL load in the circulation but compared to healthy age-matched samples which does not stratify neutrophil alterations during CLL disease progression. Moreover, a similar phenotype with enhanced ICAM1 expression in combination with low CD62L and CXCR4 expression on neutrophils was also described as tumour-promoting neutrophils during early-stage human lung cancer which might account for the impairment of neutrophil effector functions and subsequent risk of infections in CLL [308]. As this study was limited to five patients, further patient samples are necessary to provide more conclusive studies.

Secondly, higher frequencies of $CD11b^+$, $CXCR2^+$, $ICAM1^+$ and declined levels of $CXCR4^+$ and $CD62L^+$ subsets indicate a mature and activated phenotype in neutrophils in the blood of CLL mice. The combination of these surface molecules were particularly described for aged neutrophils in other disease contexts [309-311]. Interestingly, most of these surface molecules are implicated during neutrophil activation, recruitment and migration. Leukocyte recruitment is initiated by increased expression of CXCR2 and decreased expression of CXCR4 as previously described in 7.1.3 [44] and it depends on the presence of adhesion molecules, specifically on integrins and ICAM1. Specifically, CD11b has been shown to be upregulated on aged neutrophils post-LPS stimulation [309]. In CLL, neutrophils probably increase their CD11b in response to inflammatory conditions in the absence of an infection [312]. A positive correlation between CD11b and ICAM1 was also described for aged

neutrophils in this study. Further functional aspects of migration in regard to CXCR2, ICAM1 and CD62L will be discussed in the discussion chapter about migration (see 10.3). The most important question resulting from these findings is whether an enhanced activation of neutrophils in CLL contributes to an enhanced bacterial clearance. For this, phenotypical characterisation of neutrophils in the blood were found to be activated but functionally altered with decreased frequencies of CD62L and intracellular MPO, and an increased proportion of the ICAM1^{+} neutrophil subset in CLL. Conflicting reports exists about the role of the oxidative burst in CLL neutrophils [225, 288]. In this study, functional evidence through decreased MPO, phagocytosis activity and findings from the proteomic studies hints at an impairment of the oxidative burst in neutrophils during CLL which requires further investigation. Ceruloplasmin has been identified as a protein target which is higher abundant in CLL neutrophils and proposed to inhibit MPO function [275]. Targeting ceruloplasmin might help to restore MPO levels in neutrophils in CLL.

Neutrophils that are recruited into the bladder, the focus of infection, were mostly immature, immunosuppressed and less activated as shown through increased frequencies of TGF-βRI, CD62L, cKit and CXCR4 subsets in CLL. The functionality seems to cease upon stimulation via bacterial infection in CLL as suggested by the aggravated UPEC infection. Upregulation of CXCR4 has been particularly implied in homing and sequestration of neutrophils in the BM [43, 313] and is also a marker for aged neutrophils. In fact, increased CD62L expression is described as a marker for non-aged neutrophils, while increased CXCR4 is used to refer to aged neutrophils [309, 312]. Hence, the results of phenotypical characterization clash with the finding that ageing neutrophils decrease their CD62L surface expression and increase their CXCR4 expression to home back to the BM for disposal by BM macrophages, as CXCR4 and CD62L frequencies are not inversely correlated in this study [309, 310]. The constellation with cKit tilts the neutrophil phenotype towards immaturity after UTI and CLL. Furthermore, receptors required for neutrophil recruitment diminished and thus less mature neutrophils reach the site of infection with signs of immunosuppression revealed by TGF-βRI [310]. Counteraction of neutrophil recruitment of functionally active, aged neutrophils might be probably facilitated by TGF-β signalling as reported in a different context [314]. More interestingly, TGF-β signalling has been found to mediate neutrophil modulation in CLL [307]. Thus, targeting TGF-β might restore neutrophil phenotype into its functionally active state

and decrease risk of infection in CLL. These findings corroborate that aggravated bacterial burden in the urinary bladder of CLL mice during UTI were not controlled by neutrophil action. Thus, functionally active neutrophils do not reach the inflammation focus and different, functionally immature subsets are located in the bladder during UTI in CLL. To this end, this study shows novel insights about the impact of CLL on neutrophils and provide an extensive phenotypical characterization of neutrophils in CLL.

10.2. Antibacterial function of neutrophils in CLL

One of the prominent neutrophil effector functions is the antimicrobial defence which comprises a plethora of killing mechanisms. Neutropenia predisposes to an infection risk, while excessive neutrophil levels may lead to host tissue damage. Thus, an adequate number of neutrophils and their efficient antimicrobial activity is crucial for bacterial clearance. Infections are the leading cause of morbidity and mortality in CLL patients [1]. Our findings from the phenotypical characterisation and proteomic data suggest altered antibacterial responses by neutrophils in CLL. These findings were corroborated through diminished *ex vivo* phagocytosis activity and decreased intracellular levels of MPO in neutrophils during CLL. Cytoscape network analyses and individual protein targets, such as ceruloplasmin and ankyrin, verified that the antibacterial response is altered in neutrophils during CLL. During *in vivo* studies, bacterial burden was severely aggravated despite higher number of neutrophils in UPEC-infected CLL mice compared to control-infected CLL mice. However, the association between neutrophil levels at the site of infection and the bacterial burden was inversely correlated in CLL. Neutrophil effector functions are essential for UPEC clearance and to reduce the risk of recurrent infections [69, 263, 265, 266]. Thus, the results from this study clearly indicate that neutrophil effector functions and adequate levels of neutrophils were compromised which has not been described before. The increased risk of infection has predominantly been linked to hypogammaglobulinemia, B-cell and T-cell dysfunctions or even neutropenia but completely neglected neutrophil effector function [3, 212, 241, 315-318]. One particular study described haematopoietic alterations for all precursor subsets except granulocytes in the BM of untreated CLL patients [318]. Neutropenia is not a common clinical feature in CLL and only occurs in a small frequency of CLL patients mostly at advanced disease stages or due to chemotherapy [319]. Neutrophil counts

were not decreased in the CLL patient cohort tested during this study and are reported to be within the reference range in untreated CLL patients [221]. In this study, we provide evidence that neutropenia as neither been observed in CLL patients nor in the murine CLL models. Importantly, neutrophil levels did not increase with aggravating bacterial burden in the infected urinary bladder.

In order to kill the pathogen, neutrophils have to recognize microbial patterns to distinguish them from host tissue. Subsequently, they take up the pathogen and kill it through ingestion and eventually during the formation of an acidic phagolysosome through the help of intracellular enzymatic digestion and antimicrobial peptides. The formation of NADPH oxidase and thus the generation of the respiratory burst has to be analysed during phagocytosis by neutrophils in CLL (7.1.5). As an initial approach to gain mechanistic insights about the elicitation of a respiratory burst, MPO^+ neutrophil frequencies were tested in the circulation before and after UPEC infection and also at the site of infection during CLL. Interestingly, MPO^+ neutrophils were decreased in the circulation of CLL mice. Regardless, equal levels were localised in the UPEC-infected bladder in both, control and CLL mice. MPO can employ its bactericidal activity through the production of antimicrobial molecules during the respiratory burst, but it also harbours its own antibacterial killing capacity [123]. Therefore, the antibacterial impairment is MPO-independent in neutrophils during UTI and CLL. The formation of the NADPH oxidase through $gp91^{phox}$, $p22^{phox}$, $p47^{phox}$, $p67^{phox}$, $p40^{phox}$, and the downstream products, e.g. superoxide, hydrogen peroxide, hypochlorous acid, will be subject to further investigation in regard of their concentration and killing capacity. Protein levels of the NADPH oxidase components can be verified through semi-quantification methods, e.g. western blotting and flow cytometry. At the same time, the quantification of the products during the respiratory burst can be measured as shown by Chen and Jungur or summarized by Elbim and Lizard [320, 321]. In addition, neutrophil enzymes, such as elastase, lysozyme, β-glucuronidase, have to be included in future functional studies of neutrophils in CLL to determine the degranulation efficiency.

Another interesting aspect in the modulation of neutrophil effector functions during CLL might be conferred by the ZAP70 signalling [174]. ZAP70 is a T-cell receptor component and relevant during antigen presentation and processing [174, 231]. The abnormal expression of ZAP70 in malignant B-cells indicate an unfavourable CLL progression through unknown signalling [322]. A study published by Wagner *et al.*

demonstrates how the ZAP70 signalling contributes to the CLL disease progression through the activation of Syk, implying stimulation pathways similar to the ones of the innate immune system [323, 324]. There are no studies published on how the unfavourable ZAP70 expression modulates neutrophil functions during the antibacterial response in CLL. Thus, targeting ZAP70 signalling might be beneficial to restore the neutrophil response to bacterial infection by controlling CLL progression. In this context, Püllmann and colleagues reported that a subset of neutrophils expresses a functionally active T-cell receptor based variable immunoreceptor, which hints at adaptive microbial recognition [325]. In detail, neutrophils in circulation have been shown to express components of the TCR, such as α- and β-chain, as well as ζ-chain of CD3, ZAP70 and LAT through IHC and FC [325]. Although these findings were described more than a decade ago, functional evidence has not been provided yet and thus this molecular target might be of particular importance when analysing neutrophil activation and crosstalk with CLL B-cells during antimicrobial defence in CLL.

In order to study neutrophil-specific target proteins, the Cre-*loxP* system can be used. The Cre-*lox*P system was established more than twenty years ago by Gu, Zou and Rajewsky [326]. This experimental method facilitates cell-specific deletion of any gene of interest and is highly valuable. For mechanistical studies of neutrophils in the CLL setting, a neutrophil-specific promoter, such as Ly6G-cre or Mrp8-cre must be used as the LysM-cre promoter targets dendritic cells, monocytes, 25 % of lung epithelial cells and macrophages in addition to neutrophils [327]. Hence, targeting monocytes and macrophages by the LysM-cre may cause decelerated CLL development and thus is unfit to be used to study CLL impact on neutrophils during disease progression. In summary, the antibacterial response by neutrophils has been shown to be defective and requires further investigation to reveal mechanistic insights into how the CLL microenvironment modulates neutrophil effector functions on a molecular level. By combining all proteomics, phenotyping and antimicrobial defence studies, top target genes/proteins can be chosen to create neutrophil-specific KO animal models via the Cre-*lox*P system to confirm the biological relevance *in vivo* during the antimicrobial response as well as revealing the mechanistic insights into the immunosuppression of neutrophils conferred by CLL.

10.3. Migratory capacity of neutrophils in CLL

One of the major characteristics of neutrophils is their migratory capacity during infection and is essential during the innate immune response. On one hand, excessive neutrophil responses lead to host tissue damage. On the other hand, decreased neutrophil recruitment to the site of inflammation may not contain the infection risking further dissemination. Thus, the migration of neutrophils is tightly regulated as described in 7.1.4. Recent technological improvements in *in vivo* imaging and *in vitro* assays enables the minute visualisation of neutrophil migration in physiological and pathological settings [41]. In order to study the migration of neutrophils of CLL mice, a 3D-*in vitro* set up has been established in this study. In this migration assay, collagen type I was used to mimic a natural microenvironment for neutrophils and has been partly adapted to protocols of Lämmermann and Friedl [115, 328]. Our findings show that neutrophil stimulation was achieved by supplementing the medium with 200 ng/ml CXCL2. Even though the reproducibility of the assay was limited, differences in the migratory behaviour were not detected for directed or random migration of neutrophils of CLL mice implicating the absence of any migratory defects *in vitro.* As it was shown in one of the previous chapters (10.1), neutrophil phenotypes are tissue-specific and thus, neutrophil recruitment and migration was analysed in CLL animals. First, G-CSF levels were enhanced in CLL, but increased bacterial burden in UPEC-infected CLL animals did not lead to enhanced neutrophil recruitment. We observed an inversely correlation for neutrophil numbers and UPEC burden at the site of infection. This finding is surprising as neutrophil levels increase with rising bacterial burden in UPEC-infected control mice and thus suggests an impaired antibacterial response by neutrophils in CLL. Consequently, the migratory behaviour is impaired during UTI and CLL *in vivo*. As implied by the phenotypical characterisation of neutrophils at the site of the infection, none of the surface markers that are implied in migration were upregulated upon infection. Instead, neutrophil subsets with TGF-βRI, CD62L, cKit and CXCR4 expression were increased 21 hpi indicating an immature and immunosuppressed phenotype. As mentioned earlier TGF-βRI was reported to be particularly involved in the decline of neutrophil recruitment [314]. Furthermore, reduced CD62L expression is usually associated with enhanced shedding during the initial stage of extravascular recruitment cascade [23]. As reported by Uhl *et al.*, increased levels of ICAM1 and CD11b are necessary for stronger affinity confirmation and thus enabling increased

extravasation of functionally active, aged neutrophils to the site of infection [312]. In addition, aged neutrophils with increased expression of ICAM1, CD11b and decreased CD62L expression are recruited quicker to the site of inflammation and lead the antibacterial response through enhanced phagocytosis [309, 312]. In the presence of UTI and CLL, neutrophil subsets that arrive at the site of infection are functionally impaired as indicated by the surface marker expression. Neutrophil recruitment is insufficient in UTI and CLL most probably because of inadequate expression of the integrins and adhesion molecules required for the migration to inflamed tissues. Therefore, a restoration of the adhesion molecules and integrins on neutrophils through additional stimulation might increase neutrophil migration as well as effector function during UTI and CLL. Potential targets that might account for the insufficient neutrophil recruitment during UTI and CLL were found through proteome analysis. Accordingly, platelet factor 4 (*PLF4)* acts a chemoattractant for CD11b/CD18 and is involved in the LFA1/ICAM1 interaction in neutrophils during inflammation [278, 329, 330], while arachidonate 15-lipoxygenase (*LOX15*) is associated with CXCR2-dependent neutrophil recruitment during acute lung injury [277]. PLF4 protein expression was decreased in BM neutrophils and was even reported to enhance neutrophil phagocytosis of *E.coli* [329]. In addition, LOX15 protein was decreased in both BM and blood neutrophils in CLL.

In summary, the migratory behaviour of neutrophils has been shown to be insufficient during UTI and CLL and further investigation is needed to unveil underlying molecular dysfunctions related to neutrophil recruitment and migration. By combining all proteomics, phenotyping and migration studies, top protein targets have been chosen to create neutrophil-specific KO animal models via the Cre-*lox*P system as previously described. These studies could validate the biological relevance *in vivo* during the neutrophil migration and recruitment as a response to infection.

10.4. NETosis activity of neutrophils in CLL

This study provides novel information about the impact of CLL plasma on the NETosis capacity of neutrophils of a healthy donor. The induction of NETosis has been implicated in various infectious as well as non-infectious disease contexts [158, 331]. Excessive NET formation leads to host tissue damage [147]. A recent study showed enhanced NETosis activity of neutrophils from CLL patients [225]. NETosis was reported to reveal underlying neutrophil dysfunction. However, mechanistic

insights were not given about how CLL stimulates neutrophils to eject their DNA into extracellular space. In order to investigate the NETosis capacity during CLL, a NETosis assay had to be established. Initially, we tried to create a NETosis assay with murine neutrophils. However, the NETosis rates of neutrophils from the murine circulation or BM were not sufficient for the study (data not shown). Consequently, a NETosis assay was generated to test plasma on neutrophils of a healthy donor. CLL plasma incubation combined with PMA stimulation led to NET formation of neutrophils of a healthy donor. This result indicates that the CLL microenvironment is able to stimulate neutrophils possible through a chronic inflammatory micromilieu as suggested by Podaza *et al.* [225]. In regard to the NETosis assay (9.7.2), the use of self-plasma on human neutrophils as a control is one of the critical aspects of this study. Plasma from age-matched healthy donors must be used in order to replicate the results and elucidate the impact of the systemic inflammatory CLL microenvironment on the NETosis activity of untreated CLL patients. A recent study has demonstrated a higher activity for NET formation in neutrophils from CLL patients compared to age-matched samples from healthy donors with an incubation time of 4 h while in this study an incubation time of 3 h was chosen [225]. This increased NETosis activity could not be linked to higher levels of neutrophil enzymes, such as elastase or MPO, or ROS. Furthermore, a similar approach was performed in which plasma derived from CLL patients was tested for NET induction in neutrophils from healthy donors. CLL plasma was able to induce increased NET formation post-stimulation. Although this study does not provide any mechanistic insights about the increased NETosis activity, it emphasizes on the ability of the CLL microenvironment to play a role in modulating NET formation. Therefore, future approaches need to include a more targeted approach. In regard to infections, concerns were raised whether NETosis is antimicrobial or if pathogens actually might benefit from an nutrient-rich DNA environment to generate biofilms [147]. With other effector functions being extensively studied and described, the mechanisms underlying NETosis activity is yet to be fully understood. Especially pathological settings seem to either contribute to the disease progression, e.g. in systemic autoimmune diseases, or to be beneficial for host defence against microbes [13, 30, 147, 331]. Thus, further investigation is required to elucidate how this increased NETosis activity contributes to an increased risk for infections and infection severity in CLL patients.

10.5. Immunosuppression in CLL

Quantitative and qualitative dysfunctions have been observed in innate and adaptive immune cells in CLL patients [203, 317]. CLL cells have been described to be nonresponsive to TGF-β, an immunoregulatory cytokine, in order to evade from immune surveillance [285, 286]. At the same time, the establishment of an immunosuppressive micromilieu was proposed as a survival mechanism of B-cells [192]. However, immunosuppressive cytokine signalling might affect other immune cells as CLL cells were found in every organ we tested. As shown by Schiwon *et al.*, the immune response might be orchestrated by resident and Ly6C+ macrophages, but the bacterial clearance depends largely on neutrophil action during UTI [69]. Therefore, functional impairment of neutrophils was hypothesised to be caused by immunosuppressive signals in CLL. Firstly, TGF-β2 levels were increased in plasma of CLL mice indicating a systemic immunosuppressive milieu. This particular finding was confirmed by Lotz *et al*. [332] but is opposed by Matveeva *et al.* stating that the TGF-β signalling is inactivated in CLL. Disease stratification might contribute to elucidate which proportion of CLL patients display inactive TGF-β signalling. In addition to TGF-β2 cytokine analysis, TGF-βRI was quantified in neutrophils of CLL mice. Notably, TGF-βRI-expressing neutrophils were increased at the site of infection in CLL indicating enhanced TGF-β signalling which is particularly intriguing as GDF15, a relative of TGF-β is implicated in neutrophil integrin inactivation via Cdc42 in a TGF-βRI and TGF-βRII-dependent manner [314]. Cdc42 is involved in the actin dynamics during chemotaxis and helps to steer neutrophils towards the focus of inflammation as previously described (7.1.4). Hence, increased levels of TGF-βRI-expressing neutrophils are probably unable to perform chemotaxis efficiently and might be responsible for the insufficient supply of neutrophils at the site of infection in CLL. Systemic intervention of TGF-β signalling [314] or the generation of neutrophil-specific TGF-βR KO animals must be generated through the Cre-*loxP* system as an attempt to restore neutrophil migration in response to UTI in CLL. Further evidence for possible sources of immunosuppression are provided in this thesis. PDL1-expressing neutrophils enhanced with increasing tumour load in untreated CLL patients and immune checkpoint blockade has been shown to be beneficial for $CD8^+$ T-cell functions [241]. Moreover, PD1, the corresponding receptor for PDL1, is

increased on CLL cells [333]. These findings corroborate the immunosuppressed capacity of neutrophils in CLL patients and might partially contribute to elucidate the increased risk of infection.

In fact, IL10 is a potent immunosuppressive cytokine produced by CLL B-cells and has also been found in the CLL microenvironment of *Eμ-TCL1* mice [170, 226, 238, 296, 334, 335]. T-cell proliferation was restored by IL10 intervention in CLL [335]. Similarly, neutrophil functions can be restored through systemic blocking approaches via small inhibitor intervention or antibody-based inactivation of IL10. Thus, IL10 serves as an attractive target to modulate immunosuppression in CLL and to rescue neutrophil functionality during infections and CLL. Additionally, a cytokine array must be performed to quantify and delineate further immunosuppressive cytokines in the CLL microenvironment.

In conclusion, this study provides a comprehensive understanding in regard to immunosuppression of neutrophils conferred by CLL. The immunosuppressive signalling has been shown to be increased in CLL and potential targets have been suggested to be tested during neutrophil migration and the antibacterial response to elucidate further mechanisms about the impairment of neutrophil effector function during CLL.

11. Conclusions

In this thesis, neutrophils were studied in Chronic Lymphocytic Leukaemia (CLL) as bacterial infections are the leading cause of death in CLL patients. We found that the phenotype and the function of neutrophils were altered during CLL indicating that the dysfunction of neutrophils are the cause for recurrent and severe infections in CLL. We also found CLL B-cells in non-lymphoid organs, such as the lung and the bladder, indicating that these cells establish a CLL-specific microenvironment that locally shape the immunosuppressive phenotype of neutrophils. This study also reveals increased TGF-β expression during CLL and TGF-β receptor expression on neutrophils indicating a potential mechanism for the immunosuppression of neutrophils. Finally, translational data confirmed the aberrant neutrophil phenotype in human subjects suggesting that therapeutic restoration of the canonical phenotype and function of neutrophils in CLL patients might reduce the risk of severe infections and mortality during CLL. Future experiments are required to identify and evaluate neutrophil-specific targets to restore neutrophil function to improve the antibacterial response during CLL.

12. Acknowledgements

Although I realise that this acknowledgement section cannot do as much justice as the people deserve, I attempt this to be an extended dedication to those who have been showing me incredible support throughout this journey. In terms of education, I have always been blessed and I consider this as a chance to express my gratitude. I thank all who in one way or another contributed in the completion of this thesis.

First and foremost, I am grateful for the endless support, love and encouragement of my parents and for always making sure I can fully concentrate on my studies. I thank Daniel for his incredible guidance throughout the project, giving me the confidence as well as the freedom to explore my research interests and teaching me the fine nuances of scientific writing. Thanks for being an easy-going supervisor!

Special and heartfelt thanks should be mentioned to the “Engel Lab”. There is no particular order when it comes to express my gratitude. I thank you girls and boys for continuously supporting our studies by open discussions, helping out in the lab, working together before deadlines and all the fun we have had in the last four years creating this lab a place of community and not competition. It has been a pleasure to work with you all. Special mention goes out to Kristina, my fellow PhD colleague since day 1 for your contagious enthusiasm, valuable scientific input and continuous encouragement, all of which is an understatement to what we have been going through together in the last four years. My heartfelt gratitude goes to Jenny, you deserve a special mention for your invaluable technical assistance as well as contributing so much contagious energy to this study as well as providing me with the much-needed encouragement in the lab and off work throughout these years. I am deeply grateful for Jule’s heartwarming nature, contribution to scientific discussions and unlimited care throughout the thesis. I surely know that you girls were my pillar of support no matter what, always prioritising each other’s needs and especially during the writing process. Sincere thanks to Steffi for your technical assistance and the much-needed pep-talks in regard to anything related in lab or life. I am grateful for Camille’s valuable technical assistance and patience especially with the IHC and proteome studies regardless of the many times I asked her. I would like to thank to Elena de Dios Panal for being a highly motivated master student, being incredibly ambitious and witty. You set up the bar for coming students.

I am grateful for Elke Mostler for making sure I could fully concentrate on writing the thesis, making sure that my general knowledge didn’t fade away during this time

through quiz challenges and enlighten my mood with her wittiness. You girls made sure that there was no problem big enough that could not be tackled. Thanks for giving me the confidence and making this place of work as nice as home.

Besides, I would like to extend my gratitude to Jan Dürig for providing us with excellent expertise in the field of CLL, granting access to clinical samples and his guidance throughout the study. My sincere thanks goes to MPC led by Barbara Sitek, and particularly to Thilo Bracht who has been incredibly supportive and patient with me and the proteome analyses as well as explaining me the fine nuances of the LS-MS/MS. Furthermore, I would like to thank Ralf Herrmann for his incredible support and lessons about proteomics. His sense of humour helped me to work through the immense set of data. Moreover, I am grateful for the scientific guidance and inspiration provided by Marc Schuster who has been an incredible mentor throughout the migration studies and also during the writing of the thesis. I also thank Alexandra Brenzel and Anthony Squire for their continuous technical assistance and input during imaging and sorting which has helped countless times to achieve the impossible. In addition, I would like to thank Matthias Gunzer, Mike Hasenberg, Juliane Weski, Bola Hanna and Martina Seiffert for their scientific input during this study. I recognize that this research would not have been possible without the financial assistance of the DFG, thus I express my gratitude to my supervisor for giving me the chance to co-write the funding paper and the DFG for granting it. I must also acknowledge the animal facility with special mention to the MFZ animal facility. Thanks to Jule, Marc, Jenny, Kristina, Saiyani and Ragavi who participated in the many proof-reading sessions during their spare time!

In this last paragraph, I want to thank a special set of amazing people in my life. Thank you Christina and Laavannya for always making me feel like I can achieve anything! You both have been my pillar of strength. Importantly, I would like to thank my siblings for always being proud of whatever I do (professionally) despite their fear of listening to my lab work. Thank you Nethel for your heartwarming support and culinary care throughout this time and Ragavi for your endless encouragement and love that was much needed during all ups and downs. Last but not least, I would like to thank my husband for ensuring that I received the needed Excel expertise, for prioritizing my studies and my goals and trying to stay engaged in any conversations that had to do with “mouse”.

13. Bibliography

1. Wadhwa, P.D. and V.A. Morrison, *Infectious complications of chronic lymphocytic leukemia.* Semin Oncol, 2006. **33**(2): p. 240-9.

2. Morrison, V.A., *Infectious complications of chronic lymphocytic leukaemia: pathogenesis, spectrum of infection, preventive approaches.* Best Pract Res Clin Haematol, 2010. **23**(1): p. 145-53.

3. Morrison, V.A., *Infections in patients with leukemia and lymphoma.* Cancer Treat Res, 2014. **161**: p. 319-49.

4. Morrison, V.A., *Infectious complications in patients with chronic lymphocytic leukemia: pathogenesis, spectrum of infection, and approaches to prophylaxis.* Clin Lymphoma Myeloma, 2009. **9**(5): p. 365-70.

5. Dearden, C., *Disease-specific complications of chronic lymphocytic leukemia.* Hematology Am Soc Hematol Educ Program, 2008: p. 450-6.

6. Kay, A.B., *Paul Ehrlich and the Early History of Granulocytes.* Microbiol Spectr, 2016. **4**(4).

7. Amulic, B., et al., *Neutrophil function: from mechanisms to disease.* Annu Rev Immunol, 2012. **30**: p. 459-89.

8. Sionov, R.V., Z.G. Fridlender, and Z. Granot, *The Multifaceted Roles Neutrophils Play in the Tumor Microenvironment.* Cancer Microenviron, 2015. **8**(3): p. 125-58.

9. O'Connell, K.E., et al., *Practical murine hematopathology: a comparative review and implications for research.* Comp Med, 2015. **65**(2): p. 96-113.

10. Nicolas-Avila, J.A., J.M. Adrover, and A. Hidalgo, *Neutrophils in Homeostasis, Immunity, and Cancer.* Immunity, 2017. **46**(1): p. 15-28.

11. Sadik, C.D., N.D. Kim, and A.D. Luster, *Neutrophils cascading their way to inflammation.* Trends Immunol, 2011. **32**(10): p. 452-60.

12. Nathan, C., *Neutrophils and immunity: challenges and opportunities.* Nat Rev Immunol, 2006. **6**(3): p. 173-82.

13. Brinkmann, V., et al., *Neutrophil extracellular traps kill bacteria.* Science, 2004. **303**(5663): p. 1532-5.

14. Fuchs, T.A., et al., *Novel cell death program leads to neutrophil extracellular traps.* J Cell Biol, 2007. **176**(2): p. 231-41.

15. Mocsai, A., *Diverse novel functions of neutrophils in immunity, inflammation, and beyond.* J Exp Med, 2013. **210**(7): p. 1283-99.

16. Pillay, J., et al., *In vivo labeling with 2H2O reveals a human neutrophil lifespan of 5.4 days.* Blood, 2010. **116**(4): p. 625-7.

17. Tak, T., et al., *What's your age again? Determination of human neutrophil half-lives revisited.* J Leukoc Biol, 2013. **94**(4): p. 595-601.

18. Galli, S.J., N. Borregaard, and T.A. Wynn, *Phenotypic and functional plasticity of cells of innate immunity: macrophages, mast cells and neutrophils.* Nat Immunol, 2011. **12**(11): p. 1035-44.

19. Tofts, P.S., et al., *Doubts concerning the recently reported human neutrophil lifespan of 5.4 days.* Blood, 2011. **117**(22): p. 6050-2; author reply 6053-4.

20. Li, K.W., et al., *Deuterium and neutrophil kinetics.* Blood, 2011. **117**(22): p. 6052-3; author reply 6053-4.

21. Summers, C., et al., *Neutrophil kinetics in health and disease.* Trends Immunol, 2010. **31**(8): p. 318-24.

22. Colotta, F., et al., *Modulation of granulocyte survival and programmed cell death by cytokines and bacterial products.* Blood, 1992. **80**(8): p. 2012-20.

23. Kolaczkowska, E. and P. Kubes, *Neutrophil recruitment and function in health and inflammation.* Nat Rev Immunol, 2013. **13**(3): p. 159-75.

24. Nauseef, W.M. and N. Borregaard, *Neutrophils at work.* Nat Immunol, 2014. **15**(7): p. 602-11.

25. Hartenstein, V., *Blood cells and blood cell development in the animal kingdom.* Annu Rev Cell Dev Biol, 2006. **22**: p. 677-712.

26. Palis, J. and M.C. Yoder, *Yolk-sac hematopoiesis: the first blood cells of mouse and man.* Exp Hematol, 2001. **29**(8): p. 927-36.

27. Leiding, J.W., *Neutrophil Evolution and Their Diseases in Humans.* Front Immunol, 2017. **8**: p. 1009.

28. Ding, L., et al., *Endothelial and perivascular cells maintain haematopoietic stem cells.* Nature, 2012. **481**(7382): p. 457-62.

29. Orkin, S.H. and L.I. Zon, *Hematopoiesis: an evolving paradigm for stem cell biology.* Cell, 2008. **132**(4): p. 631-44.

30. Bardoel, B.W., et al., *The balancing act of neutrophils.* Cell Host Microbe, 2014. **15**(5): p. 526-36.

31. Gorgens, A., et al., *New relationships of human hematopoietic lineages facilitate detection of multipotent hematopoietic stem and progenitor cells.* Cell Cycle, 2013. **12**(22): p. 3478-82.

32. Hoppe, P.S., et al., *Early myeloid lineage choice is not initiated by random PU.1 to GATA1 protein ratios.* Nature, 2016. **535**(7611): p. 299-302.

33. Arinobu, Y., et al., *Reciprocal activation of GATA-1 and PU.1 marks initial specification of hematopoietic stem cells into myeloerythroid and myelolymphoid lineages.* Cell Stem Cell, 2007. **1**(4): p. 416-27.

34. Borregaard, N., *Neutrophils, from marrow to microbes.* Immunity, 2010. **33**(5): p. 657-70.

35. Lieschke, G.J., et al., *Mice lacking granulocyte colony-stimulating factor have chronic neutropenia, granulocyte and macrophage progenitor cell deficiency, and impaired neutrophil mobilization.* Blood, 1994. **84**(6): p. 1737-46.

36. Bjerregaard, M.D., et al., *The in vivo profile of transcription factors during neutrophil differentiation in human bone marrow.* Blood, 2003. **101**(11): p. 4322-32.

37. Fiedler, K. and C. Brunner, *The role of transcription factors in the guidance of granulopoiesis.* Am J Blood Res, 2012. **2**(1): p. 57-65.

38. Sheshachalam, A., et al., *Granule protein processing and regulated secretion in neutrophils.* Front Immunol, 2014. **5**: p. 448.

39. Mayadas, T.N., X. Cullere, and C.A. Lowell, *The multifaceted functions of neutrophils.* Annu Rev Pathol, 2014. **9**: p. 181-218.

40. Shiohara, M., et al., *Phenotypic and functional alterations of peripheral blood monocytes in neutrophil-specific granule deficiency.* J Leukoc Biol, 2004. **75**(2): p. 190-7.

41. de Oliveira, S., E.E. Rosowski, and A. Huttenlocher, *Neutrophil migration in infection and wound repair: going forward in reverse.* Nat Rev Immunol, 2016. **16**(6): p. 378-91.

42. Wang, J., et al., *Visualizing the function and fate of neutrophils in sterile injury and repair.* Science, 2017. **358**(6359): p. 111-116.

43. Suratt, B.T., et al., *Role of the CXCR4/SDF-1 chemokine axis in circulating neutrophil homeostasis.* Blood, 2004. **104**(2): p. 565-71.

44. Eash, K.J., et al., *CXCR2 and CXCR4 antagonistically regulate neutrophil trafficking from murine bone marrow.* J Clin Invest, 2010. **120**(7): p. 2423-31.

45. Bachelerie, F., et al., *International Union of Basic and Clinical Pharmacology. [corrected]. LXXXIX. Update on the extended family of chemokine receptors and introducing a new nomenclature for atypical chemokine receptors.* Pharmacol Rev, 2014. **66**(1): p. 1-79.

46. Arancibia, S.A., et al., *Toll-like receptors are key participants in innate immune responses.* Biol Res, 2007. **40**(2): p. 97-112.

47. Zeytun, A., et al., *Induction of cytokines and chemokines by Toll-like receptor signaling: strategies for control of inflammation.* Crit Rev Immunol, 2010. **30**(1): p. 53-67.

48. Ley, K., et al., *Getting to the site of inflammation: the leukocyte adhesion cascade updated.* Nat Rev Immunol, 2007. **7**(9): p. 678-89.

49. Phillipson, M. and P. Kubes, *The neutrophil in vascular inflammation.* Nat Med, 2011. **17**(11): p. 1381-90.

50. Nourshargh, S. and R. Alon, *Leukocyte migration into inflamed tissues.* Immunity, 2014. **41**(5): p. 694-707.

51. Petri, B., M. Phillipson, and P. Kubes, *The physiology of leukocyte recruitment: an in vivo perspective.* J Immunol, 2008. **180**(10): p. 6439-46.

52. Yago, T., et al., *E-selectin engages PSGL-1 and CD44 through a common signaling pathway to induce integrin alphaLbeta2-mediated slow leukocyte rolling.* Blood, 2010. **116**(3): p. 485-94.

53. Mueller, H., et al., *Tyrosine kinase Btk regulates E-selectin-mediated integrin activation and neutrophil recruitment by controlling phospholipase C (PLC) gamma2 and PI3Kgamma pathways.* Blood, 2010. **115**(15): p. 3118-27.

54. Ivetic, A., *A head-to-tail view of L-selectin and its impact on neutrophil behaviour.* Cell Tissue Res, 2018. **371**(3): p. 437-453.

55. Zarbock, A., et al., *Leukocyte ligands for endothelial selectins: specialized glycoconjugates that mediate rolling and signaling under flow.* Blood, 2011. **118**(26): p. 6743-51.

56. Ramachandran, V., et al., *Dynamic alterations of membrane tethers stabilize leukocyte rolling on P-selectin.* Proc Natl Acad Sci U S A, 2004. **101**(37): p. 13519-24.

57. Sundd, P., et al., *Quantitative dynamic footprinting microscopy reveals mechanisms of neutrophil rolling.* Nat Methods, 2010. **7**(10): p. 821-4.

58. Schmidtke, D.W. and S.L. Diamond, *Direct observation of membrane tethers formed during neutrophil attachment to platelets or P-selectin under physiological flow.* J Cell Biol, 2000. **149**(3): p. 719-30.

59. Williams, M.R., et al., *Emerging mechanisms of neutrophil recruitment across endothelium.* Trends Immunol, 2011. **32**(10): p. 461-9.

60. Pruenster, M., et al., *The Duffy antigen receptor for chemokines transports chemokines and supports their promigratory activity.* Nat Immunol, 2009. **10**(1): p. 101-8.

61. Horuk, R., et al., *The Duffy antigen receptor for chemokines: structural analysis and expression in the brain.* J Leukoc Biol, 1996. **59**(1): p. 29-38.

62. Campbell, J.J., et al., *Chemokines and the arrest of lymphocytes rolling under flow conditions.* Science, 1998. **279**(5349): p. 381-4.

63. Gorina, R., et al., *beta2 integrin-mediated crawling on endothelial ICAM-1 and ICAM-2 is a prerequisite for transcellular neutrophil diapedesis across the inflamed blood-brain barrier.* J Immunol, 2014. **192**(1): p. 324-37.

64. Goldfinger, L.E., et al., *Spatial restriction of alpha4 integrin phosphorylation regulates lamellipodial stability and alpha4beta1-dependent cell migration.* J Cell Biol, 2003. **162**(4): p. 731-41.

65. Xu, J., et al., *Divergent signals and cytoskeletal assemblies regulate self-organizing polarity in neutrophils.* Cell, 2003. **114**(2): p. 201-14.

66. Gautam, N., et al., *Signaling via beta(2) integrins triggers neutrophil-dependent alteration in endothelial barrier function.* J Exp Med, 2000. **191**(11): p. 1829-39.

67. McDonald, B., et al., *Intravascular danger signals guide neutrophils to sites of sterile inflammation.* Science, 2010. **330**(6002): p. 362-6.

68. Wang, S., et al., *Venular basement membranes contain specific matrix protein low expression regions that act as exit points for emigrating neutrophils.* J Exp Med, 2006. **203**(6): p. 1519-32.

69. Schiwon, M., et al., *Crosstalk between sentinel and helper macrophages permits neutrophil migration into infected uroepithelium.* Cell, 2014. **156**(3): p. 456-68.

70. Carman, C.V. and T.A. Springer, *A transmigratory cup in leukocyte diapedesis both through individual vascular endothelial cells and between them.* J Cell Biol, 2004. **167**(2): p. 377-88.

71. Phillipson, M., et al., *Endothelial domes encapsulate adherent neutrophils and minimize increases in vascular permeability in paracellular and transcellular emigration.* PLoS One, 2008. **3**(2): p. e1649.

72. Barreiro, O., et al., *Dynamic interaction of VCAM-1 and ICAM-1 with moesin and ezrin in a novel endothelial docking structure for adherent leukocytes.* J Cell Biol, 2002. **157**(7): p. 1233-45.

73. Petri, B., et al., *Endothelial LSP1 is involved in endothelial dome formation, minimizing vascular permeability changes during neutrophil transmigration in vivo.* Blood, 2011. **117**(3): p. 942-52.

74. Feng, D., et al., *Neutrophils emigrate from venules by a transendothelial cell pathway in response to FMLP.* J Exp Med, 1998. **187**(6): p. 903-15.

75. Sage, P.T. and C.V. Carman, *Settings and mechanisms for trans-cellular diapedesis.* Front Biosci (Landmark Ed), 2009. **14**: p. 5066-83.

76. Wisse, E., et al., *The liver sieve: considerations concerning the structure and function of endothelial fenestrae, the sinusoidal wall and the space of Disse.* Hepatology, 1985. **5**(4): p. 683-92.

77. Wong, J., et al., *A minimal role for selectins in the recruitment of leukocytes into the inflamed liver microvasculature.* J Clin Invest, 1997. **99**(11): p. 2782-90.

78. McDonald, B., et al., *Interaction of CD44 and hyaluronan is the dominant mechanism for neutrophil sequestration in inflamed liver sinusoids.* J Exp Med, 2008. **205**(4): p. 915-27.

79. Menezes, G.B., et al., *Selective down-regulation of neutrophil Mac-1 in endotoxemic hepatic microcirculation via IL-10.* J Immunol, 2009. **183**(11): p. 7557-68.

80. Carvalho-Tavares, J., et al., *A role for platelets and endothelial selectins in tumor necrosis factor-alpha-induced leukocyte recruitment in the brain microvasculature.* Circ Res, 2000. **87**(12): p. 1141-8.

81. McDonald, B. and P. Kubes, *Interactions between CD44 and Hyaluronan in Leukocyte Trafficking.* Front Immunol, 2015. **6**: p. 68.

82. Alam, C.A., et al., *The inhibition of neutrophil-endothelial cell adhesion by hyaluronan independent of CD44.* Inflammopharmacology, 2005. **12**(5-6): p. 535-50.

83. Ng, L.G., et al., *Visualizing the neutrophil response to sterile tissue injury in mouse dermis reveals a three-phase cascade of events.* J Invest Dermatol, 2011. **131**(10): p. 2058-68.

84. Futosi, K., S. Fodor, and A. Mocsai, *Reprint of Neutrophil cell surface receptors and their intracellular signal transduction pathways.* Int Immunopharmacol, 2013. **17**(4): p. 1185-97.

85. Zhang, Q., et al., *Circulating mitochondrial DAMPs cause inflammatory responses to injury.* Nature, 2010. **464**(7285): p. 104-7.

86. Raoof, M., et al., *Mitochondrial peptides are potent immune activators that activate human neutrophils via FPR-1.* J Trauma, 2010. **68**(6): p. 1328-32; discussion 1332-4.

87. Li, L., et al., *New development in studies of formyl-peptide receptors: critical roles in host defense.* J Leukoc Biol, 2016. **99**(3): p. 425-35.

88. Russo, R.C., et al., *The CXCL8/IL-8 chemokine family and its receptors in inflammatory diseases.* Expert Rev Clin Immunol, 2014. **10**(5): p. 593-619.

89. Kobayashi, Y., *The role of chemokines in neutrophil biology.* Front Biosci, 2008. **13**: p. 2400-7.

90. Stephens, L., et al., *A novel phosphoinositide 3 kinase activity in myeloid-derived cells is activated by G protein beta gamma subunits.* Cell, 1994. **77**(1): p. 83-93.

91. Yoo, S.K., et al., *Lyn is a redox sensor that mediates leukocyte wound attraction in vivo.* Nature, 2011. **480**(7375): p. 109-12.

92. Klyubin, I.V., K.M. Kirpichnikova, and I.A. Gamaley, *Hydrogen peroxide-induced chemotaxis of mouse peritoneal neutrophils.* Eur J Cell Biol, 1996. **70**(4): p. 347-51.

93. Niethammer, P., et al., *A tissue-scale gradient of hydrogen peroxide mediates rapid wound detection in zebrafish.* Nature, 2009. **459**(7249): p. 996-9.

94. Yoo, S.K., et al., *Differential regulation of protrusion and polarity by PI3K during neutrophil motility in live zebrafish.* Dev Cell, 2010. **18**(2): p. 226-36.

95. Beerman, R.W., et al., *Direct In Vivo Manipulation and Imaging of Calcium Transients in Neutrophils Identify a Critical Role for Leading-Edge Calcium Flux.* Cell Rep, 2015. **13**(10): p. 2107-17.

96. Weiner, O.D., *Regulation of cell polarity during eukaryotic chemotaxis: the chemotactic compass.* Curr Opin Cell Biol, 2002. **14**(2): p. 196-202.

97. Kolsch, V., P.G. Charest, and R.A. Firtel, *The regulation of cell motility and chemotaxis by phospholipid signaling.* J Cell Sci, 2008. **121**(Pt 5): p. 551-9.

98. Afonso, P.V. and C.A. Parent, *PI3K and chemotaxis: a priming issue?* Sci Signal, 2011. **4**(170): p. pe22.

99. Charest, P.G. and R.A. Firtel, *Big roles for small GTPases in the control of directed cell movement.* Biochem J, 2007. **401**(2): p. 377-90.

100. Lam, P.Y. and A. Huttenlocher, *Interstitial leukocyte migration in vivo.* Curr Opin Cell Biol, 2013. **25**(5): p. 650-8.

101. Yang, H.W., S.R. Collins, and T. Meyer, *Locally excitable Cdc42 signals steer cells during chemotaxis.* Nat Cell Biol, 2016. **18**(2): p. 191-201.

102. Hirsch, E., et al., *Central role for G protein-coupled phosphoinositide 3-kinase gamma in inflammation.* Science, 2000. **287**(5455): p. 1049-53.

103. Sasaki, T., et al., *Function of PI3Kgamma in thymocyte development, T cell activation, and neutrophil migration.* Science, 2000. **287**(5455): p. 1040-6.

104. Lacalle, R.A., et al., *Type I phosphatidylinositol 4-phosphate 5-kinase controls neutrophil polarity and directional movement.* J Cell Biol, 2007. **179**(7): p. 1539-53.

105. Lokuta, M.A., et al., *Type Igamma PIP kinase is a novel uropod component that regulates rear retraction during neutrophil chemotaxis.* Mol Biol Cell, 2007. **18**(12): p. 5069-80.

106. Srinivasan, S., et al., *Rac and Cdc42 play distinct roles in regulating PI(3,4,5)P3 and polarity during neutrophil chemotaxis.* J Cell Biol, 2003. **160**(3): p. 375-85.

107. Hind, L.E., W.J. Vincent, and A. Huttenlocher, *Leading from the Back: The Role of the Uropod in Neutrophil Polarization and Migration.* Dev Cell, 2016. **38**(2): p. 161-9.

108. Wong, K., A. Van Keymeulen, and H.R. Bourne, *PDZRhoGEF and myosin II localize RhoA activity to the back of polarizing neutrophil-like cells.* J Cell Biol, 2007. **179**(6): p. 1141-8.

109. Liu, X., et al., *Moesin and myosin phosphatase confine neutrophil orientation in a chemotactic gradient.* J Exp Med, 2015. **212**(2): p. 267-80.

110. Kumar, S., et al., *Cdc42 regulates neutrophil migration via crosstalk between WASp, CD11b, and microtubules.* Blood, 2012. **120**(17): p. 3563-74.

111. Szczur, K., Y. Zheng, and M.D. Filippi, *The small Rho GTPase Cdc42 regulates neutrophil polarity via CD11b integrin signaling.* Blood, 2009. **114**(20): p. 4527-37.

112. Hyun, Y.M., et al., *Uropod elongation is a common final step in leukocyte extravasation through inflamed vessels.* J Exp Med, 2012. **209**(7): p. 1349-62.

113. Smith, L.A., et al., *Neutrophil traction stresses are concentrated in the uropod during migration.* Biophys J, 2007. **92**(7): p. L58-60.

114. Cera, M.R., et al., *JAM-A promotes neutrophil chemotaxis by controlling integrin internalization and recycling.* J Cell Sci, 2009. **122**(Pt 2): p. 268-77.

115. Lammermann, T., et al., *Rapid leukocyte migration by integrin-independent flowing and squeezing.* Nature, 2008. **453**(7191): p. 51-5.

116. Thomas, C.J. and K. Schroder, *Pattern recognition receptor function in neutrophils.* Trends Immunol, 2013. **34**(7): p. 317-28.

117. Broz, P., M.B. Ohlson, and D.M. Monack, *Innate immune response to Salmonella typhimurium, a model enteric pathogen.* Gut Microbes, 2012. **3**(2): p. 62-70.

118. Kennedy, A.D., et al., *Dectin-1 promotes fungicidal activity of human neutrophils.* Eur J Immunol, 2007. **37**(2): p. 467-78.

119. Nordenfelt, P. and H. Tapper, *Phagosome dynamics during phagocytosis by neutrophils.* J Leukoc Biol, 2011. **90**(2): p. 271-84.

120. Soehnlein, O., *An elegant defense: how neutrophils shape the immune response.* Trends Immunol, 2009. **30**(11): p. 511-2.

121. Segal, A.W., J. Dorling, and S. Coade, *Kinetics of fusion of the cytoplasmic granules with phagocytic vacuoles in human polymorphonuclear leukocytes. Biochemical and morphological studies.* J Cell Biol, 1980. **85**(1): p. 42-59.

122. VanderVen, B.C., R.M. Yates, and D.G. Russell, *Intraphagosomal measurement of the magnitude and duration of the oxidative burst.* Traffic, 2009. **10**(4): p. 372-8.

123. Winterbourn, C.C., A.J. Kettle, and M.B. Hampton, *Reactive Oxygen Species and Neutrophil Function.* Annu Rev Biochem, 2016. **85**: p. 765-92.

124. Volpp, B.D., W.M. Nauseef, and R.A. Clark, *Two cytosolic neutrophil oxidase components absent in autosomal chronic granulomatous disease.* Science, 1988. **242**(4883): p. 1295-7.

125. Nunoi, H., et al., *Two forms of autosomal chronic granulomatous disease lack distinct neutrophil cytosol factors.* Science, 1988. **242**(4883): p. 1298-301.

126. Kwong, C.H., et al., *Regulation of the human neutrophil NADPH oxidase by rho-related G-proteins.* Biochemistry, 1993. **32**(21): p. 5711-7.

127. Babior, B.M., J.D. Lambeth, and W. Nauseef, *The neutrophil NADPH oxidase.* Arch Biochem Biophys, 2002. **397**(2): p. 342-4.

128. Segal, A.W., *The function of the NADPH oxidase of phagocytes and its relationship to other NOXs in plants, invertebrates, and mammals.* Int J Biochem Cell Biol, 2008. **40**(4): p. 604-18.

129. Babior, B.M., R.S. Kipnes, and J.T. Curnutte, *Biological defense mechanisms. The production by leukocytes of superoxide, a potential bactericidal agent.* J Clin Invest, 1973. **52**(3): p. 741-4.

130. Makino, R., et al., *Stoichiometric conversion of oxygen to superoxide anion during the respiratory burst in neutrophils. Direct evidence by a new method for measurement of superoxide anion with diacetyldeuteroheme-substituted horseradish peroxidase.* J Biol Chem, 1986. **261**(25): p. 11444-7.

131. Furtmuller, P.G., U. Burner, and C. Obinger, *Reaction of myeloperoxidase compound I with chloride, bromide, iodide, and thiocyanate.* Biochemistry, 1998. **37**(51): p. 17923-30.

132. Johansson, A., et al., *Different subcellular localization of cytochrome b and the dormant NADPH-oxidase in neutrophils and macrophages: effect on the production of reactive oxygen species during phagocytosis.* Cell Immunol, 1995. **161**(1): p. 61-71.

133. Karlsson, A. and C. Dahlgren, *Assembly and activation of the neutrophil NADPH oxidase in granule membranes.* Antioxid Redox Signal, 2002. **4**(1): p. 49-60.

134. Taylor, W.R., D.T. Jones, and A.W. Segal, *A structural model for the nucleotide binding domains of the flavocytochrome b-245 beta-chain.* Protein Sci, 1993. **2**(10): p. 1675-85.

135. Hampton, M.B., A.J. Kettle, and C.C. Winterbourn, *Involvement of superoxide and myeloperoxidase in oxygen-dependent killing of Staphylococcus aureus by neutrophils.* Infect Immun, 1996. **64**(9): p. 3512-7.

136. Imlay, J.A., *Pathways of oxidative damage.* Annu Rev Microbiol, 2003. **57**: p. 395-418.

137. Jiang, Q. and J.K. Hurst, *Relative chlorinating, nitrating, and oxidizing capabilities of neutrophils determined with phagocytosable probes.* J Biol Chem, 1997. **272**(52): p. 32767-72.

138. Green, J.N., A.J. Kettle, and C.C. Winterbourn, *Protein chlorination in neutrophil phagosomes and correlation with bacterial killing.* Free Radic Biol Med, 2014. **77**: p. 49-56.

139. Painter, R.G., et al., *The role of chloride anion and CFTR in killing of Pseudomonas aeruginosa by normal and CF neutrophils.* J Leukoc Biol, 2008. **83**(6): p. 1345-53.

140. Rosen, H., et al., *Methionine oxidation contributes to bacterial killing by the myeloperoxidase system of neutrophils.* Proc Natl Acad Sci U S A, 2009. **106**(44): p. 18686-91.

141. Naik, E. and V.M. Dixit, *Mitochondrial reactive oxygen species drive proinflammatory cytokine production.* J Exp Med, 2011. **208**(3): p. 417-20.

142. Brinkmann, V., et al., *Neutrophil extracellular traps: how to generate and visualize them.* J Vis Exp, 2010(36).

143. Miralda, I., S.M. Uriarte, and K.R. McLeish, *Multiple Phenotypic Changes Define Neutrophil Priming.* Front Cell Infect Microbiol, 2017. **7**: p. 217.

144. Kuhns, D.B., et al., *Residual NADPH oxidase and survival in chronic granulomatous disease.* N Engl J Med, 2010. **363**(27): p. 2600-10.

145. Klebanoff, S.J., et al., *Myeloperoxidase: a front-line defender against phagocytosed microorganisms.* J Leukoc Biol, 2013. **93**(2): p. 185-98.

146. Takei, H., et al., *Rapid killing of human neutrophils by the potent activator phorbol 12-myristate 13-acetate (PMA) accompanied by changes different from typical apoptosis or necrosis.* J Leukoc Biol, 1996. **59**(2): p. 229-40.

147. Yipp, B.G. and P. Kubes, *NETosis: how vital is it?* Blood, 2013. **122**(16): p. 2784-94.

148. Urban, C.F., et al., *Neutrophil extracellular traps contain calprotectin, a cytosolic protein complex involved in host defense against Candida albicans.* PLoS Pathog, 2009. **5**(10): p. e1000639.

149. Hakkim, A., et al., *Activation of the Raf-MEK-ERK pathway is required for neutrophil extracellular trap formation.* Nat Chem Biol, 2011. **7**(2): p. 75-7.

150. Bianchi, M., et al., *Restoration of NET formation by gene therapy in CGD controls aspergillosis.* Blood, 2009. **114**(13): p. 2619-22.

151. Patel, S., et al., *Nitric oxide donors release extracellular traps from human neutrophils by augmenting free radical generation.* Nitric Oxide, 2010. **22**(3): p. 226-34.

152. Keshari, R.S., et al., *Reactive oxygen species-induced activation of ERK and p38 MAPK mediates PMA-induced NETs release from human neutrophils.* J Cell Biochem, 2013. **114**(3): p. 532-40.

153. Papayannopoulos, V., et al., *Neutrophil elastase and myeloperoxidase regulate the formation of neutrophil extracellular traps.* J Cell Biol, 2010. **191**(3): p. 677-91.

154. Wang, Y., et al., *Human PAD4 regulates histone arginine methylation levels via demethylimination.* Science, 2004. **306**(5694): p. 279-83.

155. Murthy, A.R., et al., *In vitro candidastatic properties of the human neutrophil calprotectin complex.* J Immunol, 1993. **151**(11): p. 6291-301.

156. Pilsczek, F.H., et al., *A novel mechanism of rapid nuclear neutrophil extracellular trap formation in response to Staphylococcus aureus.* J Immunol, 2010. **185**(12): p. 7413-25.

157. McDonald, B., et al., *Intravascular neutrophil extracellular traps capture bacteria from the bloodstream during sepsis.* Cell Host Microbe, 2012. **12**(3): p. 324-33.

158. Yipp, B.G., et al., *Infection-induced NETosis is a dynamic process involving neutrophil multitasking in vivo.* Nat Med, 2012. **18**(9): p. 1386-93.

159. Saitoh, T., et al., *Neutrophil extracellular traps mediate a host defense response to human immunodeficiency virus-1.* Cell Host Microbe, 2012. **12**(1): p. 109-16.

160. Jenne, C.N., et al., *Neutrophils recruited to sites of infection protect from virus challenge by releasing neutrophil extracellular traps.* Cell Host Microbe, 2013. **13**(2): p. 169-80.

161. Hirsch, J.G., *Bactericidal action of histone.* J Exp Med, 1958. **108**(6): p. 925-44.

162. Harwood, N.E., P. Barral, and F.D. Batista, *Neutrophils--the unexpected helpers of B-cell activation.* EMBO Rep, 2012. **13**(2): p. 93-4.

163. Balazs, M., et al., *Blood dendritic cells interact with splenic marginal zone B cells to initiate T-independent immune responses.* Immunity, 2002. **17**(3): p. 341-52.

164. Scapini, P., et al., *G-CSF-stimulated neutrophils are a prominent source of functional BLyS.* J Exp Med, 2003. **197**(3): p. 297-302.

165. Schwaller, J., et al., *Neutrophil-derived APRIL concentrated in tumor lesions by proteoglycans correlates with human B-cell lymphoma aggressiveness.* Blood, 2007. **109**(1): p. 331-8.

166. Puga, I., et al., *B cell-helper neutrophils stimulate the diversification and production of immunoglobulin in the marginal zone of the spleen.* Nat Immunol, 2011. **13**(2): p. 170-80.

167. Kipps, T.J., et al., *Chronic lymphocytic leukaemia.* Nat Rev Dis Primers, 2017. **3**: p. 17008.

168. Hamblin, T., *Historical aspects of chronic lymphocytic leukaemia.* Br J Haematol, 2000. **111**(4): p. 1023-34.

169. Fabbri, G. and R. Dalla-Favera, *The molecular pathogenesis of chronic lymphocytic leukaemia.* Nat Rev Cancer, 2016. **16**(3): p. 145-62.

170. Forconi, F. and P. Moss, *Perturbation of the normal immune system in patients with CLL.* Blood, 2015. **126**(5): p. 573-81.

171. Siegel, R.L., K.D. Miller, and A. Jemal, *Cancer statistics, 2018.* CA Cancer J Clin, 2018. **68**(1): p. 7-30.

172. Yang, S.M., et al., *The mystery of chronic lymphocytic leukemia (CLL): Why is it absent in Asians and what does this tell us about etiology, pathogenesis and biology?* Blood Rev, 2015. **29**(3): p. 205-13.

173. Hallek, M., et al., *iwCLL guidelines for diagnosis, indications for treatment, response assessment, and supportive management of CLL.* Blood, 2018. **131**(25): p. 2745-2760.

174. Durig, J., et al., *ZAP-70 expression is a prognostic factor in chronic lymphocytic leukemia.* Leukemia, 2003. **17**(12): p. 2426-34.

175. Fu, S.M., R.J. Winchester, and H.G. Kunkel, *Occurrence of surface IgM, IgD, and free light chains of human lymphocytes.* J Exp Med, 1974. **139**(2): p. 451-6.

176. Preud'homme, J.L., et al., *Surface IgD in immunoproliferative disorders.* Scand J Immunol, 1974. **3**(6): p. 853-8.

177. Nowell, P.C. and D.A. Hungerford, *Chromosome studies on normal and leukemic human leukocytes.* J Natl Cancer Inst, 1960. **25**: p. 85-109.

178. Dohner, H., et al., *Genomic aberrations and survival in chronic lymphocytic leukemia.* N Engl J Med, 2000. **343**(26): p. 1910-6.

179. Austen, B., et al., *Mutations in the ATM gene lead to impaired overall and treatment-free survival that is independent of IGVH mutation status in patients with B-CLL.* Blood, 2005. **106**(9): p. 3175-82.

180. Zenz, T., et al., *From pathogenesis to treatment of chronic lymphocytic leukaemia.* Nat Rev Cancer, 2010. **10**(1): p. 37-50.

181. Grever, M.R., et al., *Comprehensive assessment of genetic and molecular features predicting outcome in patients with chronic lymphocytic leukemia: results from the US Intergroup Phase III Trial E2997.* J Clin Oncol, 2007. **25**(7): p. 799-804.

182. Hallek, M., *Chronic lymphocytic leukemia: 2017 update on diagnosis, risk stratification, and treatment.* Am J Hematol, 2017. **92**(9): p. 946-965.

183. Rush, L.J., et al., *Epigenetic profiling in chronic lymphocytic leukemia reveals novel methylation targets.* Cancer Res, 2004. **64**(7): p. 2424-33.

184. Cimmino, A., et al., *miR-15 and miR-16 induce apoptosis by targeting BCL2.* Proc Natl Acad Sci U S A, 2005. **102**(39): p. 13944-9.

185. Eisemann, N., M. Schnoor, and A. Katalinic, *Prediction of chronic lymphocytic leukaemia incidence in Germany and of patients ineligible for standard chemotherapy.* Hematol Oncol, 2016. **34**(2): p. 93-101.

186. Binet, J.L., et al., *A new prognostic classification of chronic lymphocytic leukemia derived from a multivariate survival analysis.* Cancer, 1981. **48**(1): p. 198-206.

187. Landgren, O., et al., *B-cell clones as early markers for chronic lymphocytic leukemia.* N Engl J Med, 2009. **360**(7): p. 659-67.

188. Marti, G., et al., *Overview of monoclonal B-cell lymphocytosis.* Br J Haematol, 2007. **139**(5): p. 701-8.

189. Rawstron, A.C., et al., *Inherited predisposition to CLL is detectable as subclinical monoclonal B-lymphocyte expansion.* Blood, 2002. **100**(7): p. 2289-90.

190. Rawstron, A.C., et al., *Monoclonal B-cell lymphocytosis and chronic lymphocytic leukemia.* N Engl J Med, 2008. **359**(6): p. 575-83.

191. Klein, U. and R. Dalla-Favera, *Germinal centres: role in B-cell physiology and malignancy.* Nat Rev Immunol, 2008. **8**(1): p. 22-33.

192. Burger, J.A. and N. Chiorazzi, *B cell receptor signaling in chronic lymphocytic leukemia.* Trends Immunol, 2013. **34**(12): p. 592-601.

193. Gaidano, G., R. Foa, and R. Dalla-Favera, *Molecular pathogenesis of chronic lymphocytic leukemia.* J Clin Invest, 2012. **122**(10): p. 3432-8.

194. Ghiotto, F., et al., *Remarkably similar antigen receptors among a subset of patients with chronic lymphocytic leukemia.* J Clin Invest, 2004. **113**(7): p. 1008-16.

195. Damle, R.N., et al., *Ig V gene mutation status and CD38 expression as novel prognostic indicators in chronic lymphocytic leukemia.* Blood, 1999. **94**(6): p. 1840-7.

196. Kikushige, Y., et al., *Self-renewing hematopoietic stem cell is the primary target in pathogenesis of human chronic lymphocytic leukemia.* Cancer Cell, 2011. **20**(2): p. 246-59.

197. Damle, R.N., et al., *B-cell chronic lymphocytic leukemia cells express a surface membrane phenotype of activated, antigen-experienced B lymphocytes.* Blood, 2002. **99**(11): p. 4087-93.

198. Seifert, M. and R. Kuppers, *Molecular footprints of a germinal center derivation of human IgM+(IgD+)CD27+ B cells and the dynamics of memory B cell generation.* J Exp Med, 2009. **206**(12): p. 2659-69.

199. Burger, J.A., et al., *Blood-derived nurse-like cells protect chronic lymphocytic leukemia B cells from spontaneous apoptosis through stromal cell-derived factor-1.* Blood, 2000. **96**(8): p. 2655-63.

200. Lagneaux, L., et al., *Chronic lymphocytic leukemic B cells but not normal B cells are rescued from apoptosis by contact with normal bone marrow stromal cells.* Blood, 1998. **91**(7): p. 2387-96.

201. Burger, J.A., et al., *High-level expression of the T-cell chemokines CCL3 and CCL4 by chronic lymphocytic leukemia B cells in nurselike cell cocultures and after BCR stimulation.* Blood, 2009. **113**(13): p. 3050-8.

202. Francis, S., et al., *The effect of immunoglobulin VH gene mutation status and other prognostic factors on the incidence of major infections in patients with chronic lymphocytic leukemia.* Cancer, 2006. **107**(5): p. 1023-33.

203. Ravandi, F. and S. O'Brien, *Immune defects in patients with chronic lymphocytic leukemia.* Cancer Immunol Immunother, 2006. **55**(2): p. 197-209.

204. Hudson, R.P. and S.J. Wilson, *Hypogammaglobulinemia and chronic lymphatic leukemia.* Cancer, 1960. **13**: p. 200-4.

205. Sampalo, A., et al., *Chronic lymphocytic leukemia B cells inhibit spontaneous Ig production by autologous bone marrow cells: role of CD95-CD95L interaction.* Blood, 2000. **96**(9): p. 3168-74.

206. Itala, M., O. Vainio, and K. Remes, *Functional abnormalities in granulocytes predict susceptibility to bacterial infections in chronic lymphocytic leukaemia.* Eur J Haematol, 1996. **57**(1): p. 46-53.

207. Rozman, C., E. Montserrat, and N. Vinolas, *Serum immunoglobulins in B-chronic lymphocytic leukemia. Natural history and prognostic significance.* Cancer, 1988. **61**(2): p. 279-83.

208. Sinisalo, M., et al., *Vaccination against infections in chronic lymphocytic leukemia.* Leuk Lymphoma, 2003. **44**(4): p. 649-52.

209. Sinisalo, M., et al., *Similar humoral immunity parameters in chronic lymphocytic leukemia patients independent of VH gene mutation status.* Leuk Lymphoma, 2004. **45**(12): p. 2451-4.

210. Widhopf, G.F., 2nd, et al., *Chronic lymphocytic leukemia B cells of more than 1% of patients express virtually identical immunoglobulins.* Blood, 2004. **104**(8): p. 2499-504.

211. Chiorazzi, N., et al., *T cell helper defect in patients with chronic lymphocytic leukemia.* J Immunol, 1979. **122**(3): p. 1087-90.

212. Platsoucas, C.D., et al., *Abnormal T lymphocyte subpopulations in patients with B cell chronic lymphocytic leukemia: an analysis by monoclonal antibodies.* J Immunol, 1982. **129**(5): p. 2305-12.

213. Kay, N.E., *Abnormal T-cell subpopulation function in CLL: excessive suppressor (T gamma) and deficient helper (T mu) activity with respect to B-cell proliferation.* Blood, 1981. **57**(3): p. 418-20.

214. Gorgun, G., et al., *Chronic lymphocytic leukemia cells induce changes in gene expression of CD4 and CD8 T cells.* J Clin Invest, 2005. **115**(7): p. 1797-805.

215. Ramsay, A.G., et al., *Chronic lymphocytic leukemia T cells show impaired immunological synapse formation that can be reversed with an immunomodulating drug.* J Clin Invest, 2008. **118**(7): p. 2427-37.

216. Fust, G., et al., *C1 and C4 abnormalities in chronic lymphocytic leukaemia and their significance.* Immunol Lett, 1987. **14**(3): p. 255-9.

217. Middleton, O., et al., *Complement deficiencies limit CD20 monoclonal antibody treatment efficacy in CLL.* Leukemia, 2015. **29**(1): p. 107-14.

218. Pedersen, D.V., et al., *Functional and structural insight into properdin control of complement alternative pathway amplification.* EMBO J, 2017. **36**(8): p. 1084-1099.

219. Schlesinger, M., I. Broman, and G. Lugassy, *The complement system is defective in chronic lymphatic leukemia patients and in their healthy relatives.* Leukemia, 1996. **10**(9): p. 1509-13.

220. Varga, L., et al., *Low activity of the classical complement pathway predicts short survival of patients with chronic lymphocytic leukaemia.* Clin Exp Immunol, 1995. **99**(1): p. 112-6.

221. Nosari, A., *Infectious complications in chronic lymphocytic leukemia.* Mediterr J Hematol Infect Dis, 2012. **4**(1): p. e2012070.

222. Boggs, D.R., *The cellular composition of inflammatory exudates in human leukemias.* Blood, 1960. **15**: p. 466-75.

223. Zeya, H.I., et al., *Monocyte and granulocyte defect in chronic lymphocytic leukemia.* Am J Pathol, 1979. **95**(1): p. 43-54.

224. Kontoyiannis, D.P., et al., *Impaired bactericidal but not fungicidal activity of polymorphonuclear neutrophils in patients with chronic lymphocytic leukemia.* Leuk Lymphoma, 2013. **54**(8): p. 1730-3.

225. Podaza, E., et al., *Neutrophils from chronic lymphocytic leukemia patients exhibit an increased capacity to release extracellular traps (NETs).* Cancer Immunol Immunother, 2017. **66**(1): p. 77-89.

226. Gatjen, M., et al., *Splenic Marginal Zone Granulocytes Acquire an Accentuated Neutrophil B-Cell Helper Phenotype in Chronic Lymphocytic Leukemia.* Cancer Res, 2016. **76**(18): p. 5253-65.

227. Deniset, J.F., et al., *Splenic Ly6G(high) mature and Ly6G(int) immature neutrophils contribute to eradication of S. pneumoniae.* J Exp Med, 2017. **214**(5): p. 1333-1350.

228. Ciccone, M., et al., *SnapShot: chronic lymphocytic leukemia.* Cancer Cell, 2014. **26**(5): p. 770-770 e1.

229. Bichi, R., et al., *Human chronic lymphocytic leukemia modeled in mouse by targeted TCL1 expression.* Proc Natl Acad Sci U S A, 2002. **99**(10): p. 6955-60.

230. Simonetti, G., et al., *Mouse models in the study of chronic lymphocytic leukemia pathogenesis and therapy.* Blood, 2014. **124**(7): p. 1010-9.

231. Herling, M., et al., *TCL1 shows a regulated expression pattern in chronic lymphocytic leukemia that correlates with molecular subtypes and proliferative state.* Leukemia, 2006. **20**(2): p. 280-5.

232. Hofbauer, J.P., et al., *Development of CLL in the TCL1 transgenic mouse model is associated with severe skewing of the T-cell compartment homologous to human CLL.* Leukemia, 2011. **25**(9): p. 1452-8.

233. Gorgun, G., et al., *E(mu)-TCL1 mice represent a model for immunotherapeutic reversal of chronic lymphocytic leukemia-induced T-cell dysfunction.* Proc Natl Acad Sci U S A, 2009. **106**(15): p. 6250-5.

234. Chen, S.S., et al., *Epigenetic alterations in a murine model for chronic lymphocytic leukemia.* Cell Cycle, 2009. **8**(22): p. 3663-7.

235. Kern, C., et al., *Involvement of BAFF and APRIL in the resistance to apoptosis of B-CLL through an autocrine pathway.* Blood, 2004. **103**(2): p. 679-88.

236. Nishio, M., et al., *Nurselike cells express BAFF and APRIL, which can promote survival of chronic lymphocytic leukemia cells via a paracrine pathway distinct from that of SDF-1alpha.* Blood, 2005. **106**(3): p. 1012-20.

237. Cols, M., et al., *Stromal endothelial cells establish a bidirectional crosstalk with chronic lymphocytic leukemia cells through the TNF-related factors BAFF, APRIL, and CD40L.* J Immunol, 2012. **188**(12): p. 6071-83.

238. DiLillo, D.J., et al., *Chronic lymphocytic leukemia and regulatory B cells share IL-10 competence and immunosuppressive function.* Leukemia, 2013. **27**(1): p. 170-82.

239. Enzler, T., et al., *Chronic lymphocytic leukemia of Emu-TCL1 transgenic mice undergoes rapid cell turnover that can be offset by extrinsic CD257 to accelerate disease progression.* Blood, 2009. **114**(20): p. 4469-76.

240. Hanna, B.S., et al., *Depletion of CLL-associated patrolling monocytes and macrophages controls disease development and repairs immune dysfunction in vivo.* Leukemia, 2016. **30**(3): p. 570-9.

241. McClanahan, F., et al., *PD-L1 checkpoint blockade prevents immune dysfunction and leukemia development in a mouse model of chronic lymphocytic leukemia.* Blood, 2015. **126**(2): p. 203-11.

242. ten Hacken, E., et al., *Targeting the LYN/HS1 signaling axis in chronic lymphocytic leukemia.* Blood, 2013. **121**(12): p. 2264-73.

243. Wu, Q.L., et al., *Tumoricidal effects of activated macrophages in a mouse model of chronic lymphocytic leukemia.* J Immunol, 2009. **182**(11): p. 6771-8.

244. Abraham, S.N. and Y. Miao, *The nature of immune responses to urinary tract infections.* Nat Rev Immunol, 2015. **15**(10): p. 655-63.

245. Wu, X.R., et al., *Uroplakins in urothelial biology, function, and disease.* Kidney Int, 2009. **75**(11): p. 1153-1165.

246. Flores-Mireles, A.L., et al., *Urinary tract infections: epidemiology, mechanisms of infection and treatment options.* Nat Rev Microbiol, 2015. **13**(5): p. 269-84.

247. Foxman, B., *Urinary tract infection syndromes: occurrence, recurrence, bacteriology, risk factors, and disease burden.* Infect Dis Clin North Am, 2014. **28**(1): p. 1-13.

248. Ronald, A., *The etiology of urinary tract infection: traditional and emerging pathogens.* Am J Med, 2002. **113 Suppl 1A**: p. 14S-19S.

249. Ragnarsdottir, B., et al., *Genetics of innate immunity and UTI susceptibility.* Nat Rev Urol, 2011. **8**(8): p. 449-68.

250. Wright, K.J. and S.J. Hultgren, *Sticky fibers and uropathogenesis: bacterial adhesins in the urinary tract.* Future Microbiol, 2006. **1**(1): p. 75-87.

251. Hadjifrangiskou, M., et al., *Transposon mutagenesis identifies uropathogenic Escherichia coli biofilm factors.* J Bacteriol, 2012. **194**(22): p. 6195-205.

252. Martinez, J.J. and S.J. Hultgren, *Requirement of Rho-family GTPases in the invasion of Type 1-piliated uropathogenic Escherichia coli.* Cell Microbiol, 2002. **4**(1): p. 19-28.

253. Rice, J.C., et al., *Pyelonephritic Escherichia coli expressing P fimbriae decrease immune response of the mouse kidney.* J Am Soc Nephrol, 2005. **16**(12): p. 3583-91.

254. Schwartz, D.J., et al., *Population dynamics and niche distribution of uropathogenic Escherichia coli during acute and chronic urinary tract infection.* Infect Immun, 2011. **79**(10): p. 4250-9.

255. Hannan, T.J., et al., *Host-pathogen checkpoints and population bottlenecks in persistent and intracellular uropathogenic Escherichia coli bladder infection.* FEMS Microbiol Rev, 2012. **36**(3): p. 616-48.

256. Blango, M.G., et al., *Forced resurgence and targeting of intracellular uropathogenic Escherichia coli reservoirs.* PLoS One, 2014. **9**(3): p. e93327.

257. Ashkar, A.A., et al., *FimH adhesin of type 1 fimbriae is a potent inducer of innate antimicrobial responses which requires TLR4 and type 1 interferon signalling.* PLoS Pathog, 2008. **4**(12): p. e1000233.

258. Agace, W.W., et al., *Interleukin-8 and the neutrophil response to mucosal gram-negative infection.* J Clin Invest, 1993. **92**(2): p. 780-5.

259. Abraham, S., J. Shin, and R. Malaviya, *Type 1 fimbriated Escherichia coli-mast cell interactions in cystitis.* J Infect Dis, 2001. **183 Suppl 1**: p. S51-5.

260. Haraoka, M., et al., *Neutrophil recruitment and resistance to urinary tract infection.* J Infect Dis, 1999. **180**(4): p. 1220-9.

261. Agace, W.W., et al., *Escherichia coli induces transuroepithelial neutrophil migration by an intercellular adhesion molecule-1-dependent mechanism.* Infect Immun, 1995. **63**(10): p. 4054-62.

262. Van den Steen, P.E., et al., *Biochemistry and molecular biology of gelatinase B or matrix metalloproteinase-9 (MMP-9).* Crit Rev Biochem Mol Biol, 2002. **37**(6): p. 375-536.

263. Zec, K., et al., *Neutrophil Migration into the Infected Uroepithelium Is Regulated by the Crosstalk between Resident and Helper Macrophages.* Pathogens, 2016. **5**(1).

264. Shahin, R.D., et al., *Neutrophil recruitment and bacterial clearance correlated with LPS responsiveness in local gram-negative infection.* J Immunol, 1987. **138**(10): p. 3475-80.

265. Jaillon, S., et al., *The humoral pattern recognition molecule PTX3 is a key component of innate immunity against urinary tract infection.* Immunity, 2014. **40**(4): p. 621-32.

266. Hannan, T.J., et al., *Inhibition of Cyclooxygenase-2 Prevents Chronic and Recurrent Cystitis.* EBioMedicine, 2014. **1**(1): p. 46-57.

267. Hasenberg, A., et al., *Catchup: a mouse model for imaging-based tracking and modulation of neutrophil granulocytes.* Nat Methods, 2015. **12**(5): p. 445-52.

268. Miltenyi, S., et al., *High gradient magnetic cell separation with MACS.* Cytometry, 1990. **11**(2): p. 231-8.

269. Abbitt, K.B., et al., *Antibody ligation of murine Ly-6G induces neutropenia, blood flow cessation, and death via complement-dependent and independent mechanisms.* J Leukoc Biol, 2009. **85**(1): p. 55-63.

270. Naboulsi, W., et al., *Quantitative Tissue Proteomics Analysis Reveals Versican as Potential Biomarker for Early-Stage Hepatocellular Carcinoma.* J Proteome Res, 2016. **15**(1): p. 38-47.

271. Seddigh, P., et al., *Quantitative Analysis of Proteome Modulations in Alveolar Epithelial Type II Cells in Response to Pulmonary Aspergillus fumigatus Infection.* Mol Cell Proteomics, 2017. **16**(12): p. 2184-2198.

272. Bracht, T., et al., *Analysis of disease-associated protein expression using quantitative proteomics-fibulin-5 is expressed in association with hepatic fibrosis.* J Proteome Res, 2015. **14**(5): p. 2278-86.

273. Wilhelmsen, K., K. Farrar, and J. Hellman, *Quantitative in vitro assay to measure neutrophil adhesion to activated primary human microvascular endothelial cells under static conditions.* J Vis Exp, 2013(78): p. e50677.

274. Fujimoto, H., et al., *Flow cytometric method for enumeration and classification of reactive immature granulocyte populations.* Cytometry, 2000. **42**(6): p. 371-8.

275. Chapman, A.L., et al., *Ceruloplasmin is an endogenous inhibitor of myeloperoxidase.* J Biol Chem, 2013. **288**(9): p. 6465-77.

276. Moffat, F.L., Jr., et al., *Involvement of CD44 and the cytoskeletal linker protein ankyrin in human neutrophil bacterial phagocytosis.* J Cell Physiol, 1996. **168**(3): p. 638-47.

277. Rossaint, J., et al., *Eliminating or blocking 12/15-lipoxygenase reduces neutrophil recruitment in mouse models of acute lung injury.* Crit Care, 2012. **16**(5): p. R166.

278. Kuijpers, T.W., et al., *The impact of platelet-activating factor (PAF)-like mediators on the functional activity of neutrophils: anti-inflammatory effects of human PAF-acetylhydrolase.* Clin Exp Immunol, 2001. **123**(3): p. 412-20.

279. Wang, Z., et al., *Regulation of innate immune responses by DAI (DLM-1/ZBP1) and other DNA-sensing molecules.* Proc Natl Acad Sci U S A, 2008. **105**(14): p. 5477-82.

280. Balajthy, Z., et al., *Tissue-transglutaminase contributes to neutrophil granulocyte differentiation and functions.* Blood, 2006. **108**(6): p. 2045-54.

281. Page, S.M., et al., *Stimulation of neutrophil interleukin-8 production by eosinophil granule major basic protein.* Am J Respir Cell Mol Biol, 1999. **21**(2): p. 230-7.

282. Shannon, P., et al., *Cytoscape: a software environment for integrated models of biomolecular interaction networks.* Genome Res, 2003. **13**(11): p. 2498-504.

283. Thomas, P.D., H. Mi, and S. Lewis, *Ontology annotation: mapping genomic regions to biological function.* Curr Opin Chem Biol, 2007. **11**(1): p. 4-11.

284. Ingersoll, M.A. and M.L. Albert, *From infection to immunotherapy: host immune responses to bacteria at the bladder mucosa.* Mucosal Immunol, 2013. **6**(6): p. 1041-53.

285. Schiemann, W.P., et al., *Transforming growth factor-beta (TGF-beta)-resistant B cells from chronic lymphocytic leukemia patients contain recurrent mutations in the signal sequence of the type I TGF-beta receptor.* Cancer Detect Prev, 2004. **28**(1): p. 57-64.

286. Douglas, R.S., et al., *Chronic lymphocytic leukemia B cells are resistant to the apoptotic effects of transforming growth factor-beta.* Blood, 1997. **89**(3): p. 941-7.

287. Stecher, M., *Visualisierung von NET assoziierten Proteinen und Strukturen mittels Superresolutionsmikroskopie*, in *Faculty of Biology*. 2014, Universität Duisburg-Essen: Essen.

288. Manukyan, G., et al., *Neutrophils in chronic lymphocytic leukemia are permanently activated and have functional defects.* Oncotarget, 2017. **8**(49): p. 84889-84901.

289. Coffelt, S.B., M.D. Wellenstein, and K.E. de Visser, *Neutrophils in cancer: neutral no more.* Nat Rev Cancer, 2016. **16**(7): p. 431-46.

290. Fridlender, Z.G., et al., *Polarization of tumor-associated neutrophil phenotype by TGF-beta: "N1" versus "N2" TAN.* Cancer Cell, 2009. **16**(3): p. 183-94.

291. Piccard, H., R.J. Muschel, and G. Opdenakker, *On the dual roles and polarized phenotypes of neutrophils in tumor development and progression.* Crit Rev Oncol Hematol, 2012. **82**(3): p. 296-309.

292. Yang, L., et al., *Expansion of myeloid immune suppressor Gr+CD11b+ cells in tumor-bearing host directly promotes tumor angiogenesis.* Cancer Cell, 2004. **6**(4): p. 409-21.

293. Di Mitri, D., et al., *Tumour-infiltrating Gr-1+ myeloid cells antagonize senescence in cancer.* Nature, 2014. **515**(7525): p. 134-7.

294. Powell, D.R. and A. Huttenlocher, *Neutrophils in the Tumor Microenvironment.* Trends Immunol, 2016. **37**(1): p. 41-52.

295. Gustafson, M.P., et al., *Association of an increased frequency of CD14+ HLA-DR lo/neg monocytes with decreased time to progression in chronic lymphocytic leukaemia (CLL).* Br J Haematol, 2012. **156**(5): p. 674-6.

296. Maffei, R., et al., *The monocytic population in chronic lymphocytic leukemia shows altered composition and deregulation of genes involved in phagocytosis and inflammation.* Haematologica, 2013. **98**(7): p. 1115-23.

297. Jitschin, R., et al., *CLL-cells induce IDOhi CD14+HLA-DRlo myeloid-derived suppressor cells that inhibit T-cell responses and promote TRegs.* Blood, 2014. **124**(5): p. 750-60.

298. Marini, O., et al., *Mature CD10(+) and immature CD10(-) neutrophils present in G-CSF-treated donors display opposite effects on T cells.* Blood, 2017. **129**(10): p. 1343-1356.

299. Brandau, S. and D. Hartl, *Lost in neutrophil heterogeneity? CD10!* Blood, 2017. **129**(10): p. 1240-1241.

300. Ferrer, F., Chiu, Vergani, Mazzarello, Palacios, Bagnara, Chen, Yancopoulos, Liu, Xochelli, Yan, Barrientos, E. Kolitz, Allen, Stamatopoulos, Rai, Sherry and Chiorazzi, *In CLL, Myeloid-Derived Suppressor Cells and Their Monocytic and Granulocytic Varieties Differ in T-Cell Subset Association and Polarization Induction.* Blood, 2016. **128**(22): p. 4350.

301. Brandau, S., et al., *Myeloid-derived suppressor cells in the peripheral blood of cancer patients contain a subset of immature neutrophils with impaired migratory properties.* J Leukoc Biol, 2011. **89**(2): p. 311-7.

302. Zarco, M.A., et al., *Phenotypic changes in neutrophil granulocytes of healthy donors after G-CSF administration.* Haematologica, 1999. **84**(10): p. 874-8.

303. Leliefeld, P.H.C., et al., *Differential antibacterial control by neutrophil subsets.* Blood Adv, 2018. **2**(11): p. 1344-1355.

304. Pardoll, D.M., *The blockade of immune checkpoints in cancer immunotherapy.* Nat Rev Cancer, 2012. **12**(4): p. 252-64.

305. Luo, Q., et al., *PD-L1-expressing neutrophils as a novel indicator to assess disease activity and severity of systemic lupus erythematosus.* Arthritis Res Ther, 2016. **18**: p. 47.

306. Cheng, Y., et al., *Cancer-associated fibroblasts induce PDL1+ neutrophils through the IL6-STAT3 pathway that foster immune suppression in hepatocellular carcinoma.* Cell Death Dis, 2018. **9**(4): p. 422.

307. Podaza, E., et al., *Chronic lymphocytic leukemia cells increase neutrophils survival and promote their differentiation into CD16(high) CD62L(dim) immunosuppressive subset.* Int J Cancer, 2018.

308. Eruslanov, E.B., et al., *Tumor-associated neutrophils stimulate T cell responses in early-stage human lung cancer.* J Clin Invest, 2014. **124**(12): p. 5466-80.

309. Zhang, D., et al., *Neutrophil ageing is regulated by the microbiome.* Nature, 2015. **525**(7570): p. 528-32.

310. Kolaczkowska, E., *The older the faster: aged neutrophils in inflammation.* Blood, 2016. **128**(19): p. 2280-2282.

311. Ferri, L.E., et al., *L-selectin shedding in sepsis limits leukocyte mediated microvascular injury at remote sites.* Surgery, 2009. **145**(4): p. 384-91.

312. Uhl, B., et al., *Aged neutrophils contribute to the first line of defense in the acute inflammatory response.* Blood, 2016. **128**(19): p. 2327-2337.

313. Casanova-Acebes, M., et al., *Rhythmic modulation of the hematopoietic niche through neutrophil clearance.* Cell, 2013. **153**(5): p. 1025-35.

314. Artz, A., S. Butz, and D. Vestweber, *GDF-15 inhibits integrin activation and mouse neutrophil recruitment through the ALK-5/TGF-betaRII heterodimer.* Blood, 2016. **128**(4): p. 529-41.

315. Mauro, F.R., et al., *Clinical relevance of hypogammaglobulinemia, clinical and biologic variables on the infection risk and outcome of patients with stage A chronic lymphocytic leukemia.* Leuk Res, 2017. **57**: p. 65-71.

316. Riches, J.C., et al., *T cells from CLL patients exhibit features of T-cell exhaustion but retain capacity for cytokine production.* Blood, 2013. **121**(9): p. 1612-21.

317. Tsiodras, S., et al., *Infection and immunity in chronic lymphocytic leukemia.* Mayo Clin Proc, 2000. **75**(10): p. 1039-54.

318. Manso, B.A., et al., *Bone marrow hematopoietic dysfunction in untreated chronic lymphocytic leukemia patients.* Leukemia, 2018.

319. Zent, C.S. and N.E. Kay, *Autoimmune complications in chronic lymphocytic leukaemia (CLL).* Best Pract Res Clin Haematol, 2010. **23**(1): p. 47-59.

320. Chen, Y. and W.G. Junger, *Measurement of oxidative burst in neutrophils.* Methods Mol Biol, 2012. **844**: p. 115-24.

321. Elbim, C. and G. Lizard, *Flow cytometric investigation of neutrophil oxidative burst and apoptosis in physiological and pathological situations.* Cytometry A, 2009. **75**(6): p. 475-81.

322. Gobessi, S., et al., *ZAP-70 enhances B-cell-receptor signaling despite absent or inefficient tyrosine kinase activation in chronic lymphocytic leukemia and lymphoma B cells.* Blood, 2007. **109**(5): p. 2032-9.

323. Maus, M.V., *Innate immune signaling in CLL.* Blood, 2016. **127**(4): p. 376-8.

324. Wagner, M., et al., *Integration of innate into adaptive immune responses in ZAP-70-positive chronic lymphocytic leukemia.* Blood, 2016. **127**(4): p. 436-48.

325. Puellmann, K., et al., *A variable immunoreceptor in a subpopulation of human neutrophils.* Proc Natl Acad Sci U S A, 2006. **103**(39): p. 14441-6.

326. Gu, H., Y.R. Zou, and K. Rajewsky, *Independent control of immunoglobulin switch recombination at individual switch regions evidenced through Cre-loxP-mediated gene targeting.* Cell, 1993. **73**(6): p. 1155-64.

327. McCubbrey, A.L., et al., *Promoter Specificity and Efficacy in Conditional and Inducible Transgenic Targeting of Lung Macrophages.* Front Immunol, 2017. **8**: p. 1618.

328. Friedl, P., et al., *New dimensions in cell migration.* Nat Rev Mol Cell Biol, 2012. **13**(11): p. 743-7.

329. Lishko, V.K., et al., *Leukocyte integrin Mac-1 (CD11b/CD18, alphaMbeta2, CR3) acts as a functional receptor for platelet factor 4.* J Biol Chem, 2018. **293**(18): p. 6869-6882.

330. Srivastava, K., et al., *Platelet factor 4 mediates inflammation in experimental cerebral malaria.* Cell Host Microbe, 2008. **4**(2): p. 179-87.

331. Gupta, S. and M.J. Kaplan, *The role of neutrophils and NETosis in autoimmune and renal diseases.* Nat Rev Nephrol, 2016. **12**(7): p. 402-13.

332. Lotz, M., E. Ranheim, and T.J. Kipps, *Transforming growth factor beta as endogenous growth inhibitor of chronic lymphocytic leukemia B cells.* J Exp Med, 1994. **179**(3): p. 999-1004.

333. Grzywnowicz, M., et al., *Programmed death-1 and its ligand are novel immunotolerant molecules expressed on leukemic B cells in chronic lymphocytic leukemia.* PLoS One, 2012. **7**(4): p. e35178.

334. Alhakeem, S.S., et al., *Chronic Lymphocytic Leukemia-Derived IL-10 Suppresses Antitumor Immunity.* J Immunol, 2018. **200**(12): p. 4180-4189.

335. Shaim, H., et al., *The CXCR4-STAT3-IL-10 Pathway Controls the Immunoregulatory Function of Chronic Lymphocytic Leukemia and Is Modulated by Lenalidomide.* Front Immunol, 2017. **8**: p. 1773.

Der Lebenslauf ist in der Online-Version aus Gründen des Datenschutzes nicht enthalten.